Aus dem

Institut für Prophylaxe und Epidemiologie der Kreislaufkrankheiten

Direktor: Prof. Dr. med. Christian Weber

G protein coupled receptors in inflammation

- from kinin to chemokine

Habilitationsschrift

vorgelegt von Dr. Johan Duchêne

München, 2023

In der vorliegenden kumulativen Habilitationsschrift werden die folgenden fünf Publikationen zusammenfassend beschreiben und im Kontext diskutiert:

(1) **Duchene J**, Lecomte F, Ahmed S, Cayla C, Pesquero J, Bader M, Perretti M, Ahluwalia A. A novel inflammatory pathway involved in leukocyte recruitment: role for the kinin B1 receptor and the chemokine CXCL5. *J Immunol*, 179(7):4849-56 (**2007**).

(2) **Duchene J**, Cayla C, Vessillier S, Scotland R, Yamashiro K, Lecomte F, Syed I, Vo P, Marrelli A, Pitzalis C, Cipollone F, Schanstra J, Bascands JL, Hobbs AJ, Perretti M, Ahluwalia A. Laminar shear stress regulates endothelial kinin B1 receptor expression and function: potential implication in atherogenesis. *Arterioscler Thromb Vasc Biol*, 29(11):1757-63 (**2009**).

(3) Rousselle A, Qadri F, Leukel L, Yilmaz R, Fontaine JF, Sihn G, Bader M, Ahluwalia A, **Duchene J**. CXCL5 limits macrophage foam cell formation in atherosclerosis. *J Clin Invest,* 123(3):1343-7 (**2013**).

(4) **Duchene J**, Novitzky-Basso I, Thiriot A, Casanova-Acebes M, Bianchini M, Etheridge SL, Hub E, Nitz K, Artinger K, Eller K, Caamaño J, Rülicke T, Moss P, Megens RTA, von Andrian UH, Hidalgo A, Weber C, Rot A. Atypical chemokine receptor 1 on nucleated erythroid cells regulates hematopoiesis. *Nat Immunol*. 18(7):753-761 (**2017**).

(5) Rot A, Gutjahr JC, Biswas A, Aslani M, Hub E, Thiriot A, von Andrian UH, Megens RTA, Weber C, **Duchene J**. Murine bone marrow macrophages and human monocytes do not express atypical chemokine receptor 1. *Cell Stem Cell.* 29 (7):1013-1015 **(2022).**

Table of contents

1. Summary

At the core of all noncommunicable diseases (NCDs) such as cancer and cardiovascular disease, is inflammation, a highly complexed process tightly orchestrating the action of multiple inflammatory molecules. Among the receptors expressed by the hematopoietic and non-hematopoietic cells, G protein-coupled receptors (GPCRs) play a key role in inflammation as they are activated by different inflammatory molecules such as amines, peptides, eicosanoids, and chemokines.

The first studies summarized here unveiled a novel pathway of inflammation involving the interconnection between two GPCRs, namely the kinin B1 receptor (B1R) and the CXC chemokine receptor 2 (CXCR2). The inflammatory cytokine, IL-1β, and proatherogenic factors were identified to induce the production of the CXCL5 chemokine in endothelial cells through a B1R-dependent mechanism in acute conditions. In turn, the release of CXCL5 at the surface of endothelial cells resulted in the recruitment of CXCR2$^+$ neutrophils into the inflamed tissue. The next study highlighted an unexpected role for the CXCL5 chemokine in chronic inflammatory disease. While CXCL5 was highly expressed by endothelial cells, its induction was protective in atherosclerotic conditions. CXCL5 was found to activate macrophages, increase the expression of ACBA1, a transporter that mediates cholesterol efflux, and consequently regulate foam cell formation. The last studies focused on a particular class of chemokine receptors, so-called atypical chemokine receptors (ACKRs) and more specifically on ACKR1, which is highly expressed by erythroblasts in the bone marrow. ACKR1 was identified as a regulator of homeostasis of haematopoietic stem and progenitor cells (HSPCs) and to control downstream hematopoiesis. Notably, erythroblasts were shown to directly interact with HSPCs in an ACKR1-dependent manner. In the absence of ACKR1, steady-state haematopoiesis was altered, bone marrow HSPCs localized remotely from erythroblasts and gave rise to phenotypically distinct neutrophils.

Altogether, the work presented here provides additional evidence that the chemokine system *via* its action on the classical but also the atypical chemokine receptors, plays a crucial role on hematopoietic cells and in inflammation. Moreover, this work highlights the complexity of chemokine targeting in NCDs, as the same chemokine may have distinct biological effects in different inflammatory diseases. Further research is therefore required to fully apprehend the contribution of GPCRs and especially ACKRs in NCDs, to elucidate pathological mechanisms, and to ultimately develop new drug therapies targeting these receptors.

2. Introduction

Noncommunicable diseases (NCDs) are pathologies that, in contrast to infectious diseases, are not transmitted from one person to another. It has been established that inflammation is at the root of all NCDs. Therefore, NCDs are also known as chronic inflammatory diseases.

2.1 What is inflammation?

Inflammation is classically described as a response of our immune system to infection or tissue injury. The primary functions of inflammation are to eliminate the culprit stimulus, remove infected/damaged tissue, and finally restore tissue homeostasis[1, 2, 3].

The Roman physician Celsus (-25BC – 50AD) was the first to recognize the major role of inflammation in maintaining tissue homeostasis[4]. He described four cardinal signs of inflammation, now known as the 'Celsus tetrad of inflammation', which is still a reference for physicians nowadays: *calor* (heat), *rubor* (redness), *tumor* (swelling) and *dolor* (pain) (**Figure 1**). These simple inflammation traits are in fact the direct consequences of the action of inflammatory mediators on the blood vessels and within the tissue. Vasodilation and increased vascular permeability during inflammation result in increased local blood flow and leakage of fluid into the tissue, which altogether are responsible for heat, redness and swelling[5]. The release of inflammatory mediators inside the tissue in turn activates sensory nerves and causes pain[6].

A controlled acute inflammatory response is considered as beneficial and essential as it preserves the integrity of the host tissues. However, when inflammatory response is dysregulated and persists, in a chronic state, it becomes detrimental and contributes to the pathogenesis of many NCDs such as atherosclerosis, kidney disease, diabetes, rheumatoid arthritis and cancer. 'Chronic inflammation' was characterized in the late 19th century by the German medical biologist Rudolf Virchow (1821-1902) who was the first to acknowledge the harmful side of inflammation[4]. Accordingly, he added a fifth cardinal sign to the Celsus tetrad of inflammation, namely "loss of tissue or organ function" (**Figure 1**).

During the same period (late 19th century), a new discipline, named 'Immunology' was founded which provided a novel dimension to the inflammation model. The discovery of leukocyte subsets by the German immunologist Paul Ehrlich (1854-1915)[7] and the phagocytic function of macrophages by the Russian immunologist Ilya Metchnikov (1845-1916)[4, 8] established the foundations of Immunology and the essential role of immune cells in the inflammatory response (**Figure 1**).

Figure 1. Inflammation and immunology. During the first century, Celsus characterized inflammation by four cardinal signs (heat, redness, swelling and pain) and described it as an essential biological response in maintaining homeostasis. Later, Virchow (1821-1902) added a fifth sign of inflammation: "loss of function" that he linked to an uncontrolled inflammatory response. Paul Ehrlich (1854-1915) and Ilya Metchnikov (1845-1916) established a new discipline in Biology so-called Immunology. Ilya Metchnikov is considered as the "father of innate immunity" as he discovered macrophages and described their phagocytic functions. Center : drawings from E. Mechnnikov. (1901) « L'immunité dans les maladies infectieuses ». Paris, Masson. Accessible on wellcomecollection.org.

2.2 An overview of the molecular and cellular mechanisms involved in inflammation

Based on these foundations, a multitude of research efforts have been able to describe more accurately the series of molecular and cellular events that are involved in the inflammatory process[3, 9, 10] (**Figure 2**). An inflammatory response initially involves the recognition of pathogens or tissue damage by tissue resident macrophages and mast cells. These cells express pattern recognition receptors (PRR) to sense stimuli called "danger signals"[11]. Such signals can be present on pathogens (e.g., LPS, DNA, mannose, or glucan) as in the case of pathogen-associated molecular pattern (PAMP) but also on endogenous tissue (e.g., HMGB1, ATP, DNA or hyaluronan) as for damage-associated molecular pattern (DAMP)[12, 13]. Distinct subtypes of PPRs that recognize specific patterns exist, such as transmembrane Toll-like receptors (TLRs), C-type lectin receptors (CLRs), cytoplasmic nucleotide binding domain, leucine-rich-repeat containing receptors (NOD-like receptors or NLRs), or retinoic acid-inducible gene-I-like receptors (RLRs)[12, 13]. Once resident macrophages and mast cells detect a "danger signal", they are activated and produce a variety of inflammatory mediators, such as cytokines (e.g., IL-1β and TNFα), chemokines (e.g., CXCL5, CXCL8 and CCL2), eicosanoids (e.g., prostaglandins and leukotrienes), vasoactive amines (e.g., histamine) and peptides (e.g., Substance P, kinins)[3]. Altogether, these mediators induce a local exudate which is composed of plasma proteins and

leukocytes. The main goal is to allow leukocytes (for instance neutrophils as they are the first and most abundant white blood cell type recruited during inflammation) to leave the blood vessels and migrate to the site of infection or injury. Immediately after their release, vasoactive amines and eicosanoids affect the vasculature causing vasodilation and increase vascular permeability which, in concert, facilitate the extravasation of leukocytes. In parallel, cytokines released in the tissue activate the endothelium of the blood vessels[14, 15]. Consequently, inflamed endothelial cells express high level of adhesion molecules (e.g., E and P selectins) that interact with glycosylated ligands (e.g., P-selectin glycoprotein ligand-1 and CD44) present at the surface of hematopoietic cells. Interaction of selectins with their ligands enables leukocytes to roll on the inflamed endothelium[9, 10, 14, 15]. The firm arrest of leukocytes is then triggered by chemokines[16].
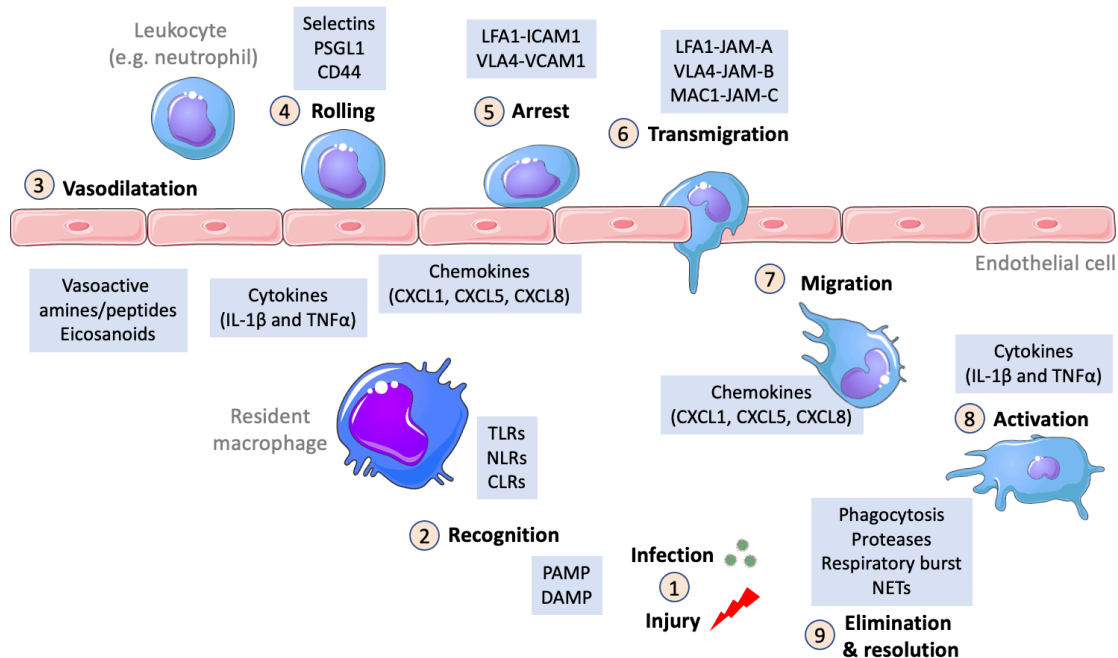

Figure 2. Cascade of events involved in inflammation. Following infection or tissue injury, tissue resident macrophages which recognize "danger signal" are activated. They then produce and release inflammatory mediators which induce vasodilation (vasoactive mediators) but also activate the endothelium (cytokines). Leukocytes then roll on the inflamed endothelium (mediated by selectins), are eventually activated by chemokines, and adhere firmly on the endothelium using integrins. Leukocytes can then transmigrate through the endothelium and migrate to the site of inflammation by following a chemokine gradient. Once they reach the site of infection or injury, leukocytes such as neutrophils are activated by cytokines and by pathogen directly and can eliminate the culprit by employing different molecular weapons.

Chemokines are produced by tissue resident macrophages during inflammation and in turn transported and presented by endothelial cells[17] (via the atypical chemokine receptor 1[18] - ACKR1- for instance, see section 1.3.c. for further details). Chemokine presentation at the endothelium luminal surface then activates leukocytes by increasing the affinity of the integrins[19]. The strong binding between the activated integrins such as CD18/CD11a, also known as Lymphocyte function-associate antigen 1 (LFA-1), with the intercellular adhesion molecule 1 (ICAM1) that is highly expressed at the surface of inflamed endothelium results in leukocyte arrest[20, 21, 22]. Moreover, activated endothelial cells may also produce chemokines and present them directly via glycosaminoglycans (GAGs),

amplifying the activation and adhesion of leukocytes[23, 24]. Ultimately, transmigration enables leukocytes to reach the inflamed tissue. At this stage, leukocytes migrate mainly at the junction between two adjacent endothelial cells[10]. This step involves the interactions between integrins (LFA1, VLA4 or MAC1) expressed by leukocytes and junctional adhesion molecules such as JAM-A, JAM-B and JAM-C present at the junctions between endothelial cells[25, 26, 27, 28]. Once leukocytes have passed through the vessel wall, they migrate to the site of inflammation following a chemokine gradient formed in the tissue, a process called chemotaxis[16, 29, 30]. Chemokines are indeed attractant molecules for leukocytes, which move towards the source of chemokine production, facilitating their recruitment at the right location[16, 29, 30]. Neutrophils that express CXCR2 at their surface are attracted by specific chemokines such as CXCL1, CXCL2, CXCL5 and CXCL8[31, 32]. Once they reach the site of inflammation, neutrophils become activated either by the action of cytokines or by direct contact with the pathogens. Upon activation, neutrophils utilize a wide range of weapons such as respiratory burst with reactive oxygen species (ROS) production , proteases release (e.g. proteinase 3, cathepsin G or elastase…), phagocytic activity, and neutrophil extracellular traps (NET) to kill the pathogens or eliminate the necrotic cells[33]. Neutrophils, however, do not distinguish between pathogens and host tissue, resulting in inevitable collateral damage to host tissue[2, 3, 33]. The inflammatory process can therefore not last too long and must enter the resolution phase, without which inflammation becomes chronic and may generate irreversible damage.

2.2 G-protein coupled receptors in inflammation

It emerges that inflammation is a highly complexed process involving the tightly orchestrated action of multiple inflammatory molecules. Among the receptors expressed by the hematopoietic and non-hematopoietic cells, G protein-coupled receptors (GPCRs) represent a key target in inflammation as they are activated by different inflammatory molecules such as amines, peptides, eicosanoids, and chemokines[34, 35]. But what are GPCRs?

GPCRs are in fact the largest family of membrane receptors in eukaryote and are involved in a wide variety of physiological processes spanning from senses of vision taste and smell, to mood and immune response. It may therefore not be surprising that GPCRs are targets for nearly 35% of the drugs currently on the market[36, 37]. GPCRs are characterized by their seven-transmembrane domains but their actual name comes from the common signaling pathway used by the different receptors upon activation (**Figure 3**). Following the binding of a specific ligand, GCPR activation causes conformational change in the receptor that leads to the activation of the heterotrimeric GTP-binding proteins (also known as G proteins)[38, 39]. In a non-stimulated status, G proteins are formed by an α-subunit which binds GDP and βγ dimers. Once activated, an exchange of GDP by GTP in Gα results in

the dissociation of Gα from Gβγ. Subsequently, Gα-GTP and Gβγ may activate a number of effector proteins (e.g. adenyl cyclase, phospholipase C, phospholipase A2, Ca^{2+} and K^+ channels). Eventually, the GTPase activity in the Gα subunit leads to GTP hydrolysis and formation of the Gα-GDP, triggering re-association with βγ dimers. In addition to the classical G-protein signaling pathways, it has now become clear that GPCRs can also utilize G-protein-independent signaling pathways to mediate their biological effects. Following its activation, a GPCR may for instance be phosphorylated by G-protein-coupled receptor kinases (GRKs) which leads to the recruitment of β-arrestin. Not only does binding of β-arrestin impede G-protein binding to its receptor but also results in receptor desensitization as well as activation of alternative signaling pathways.
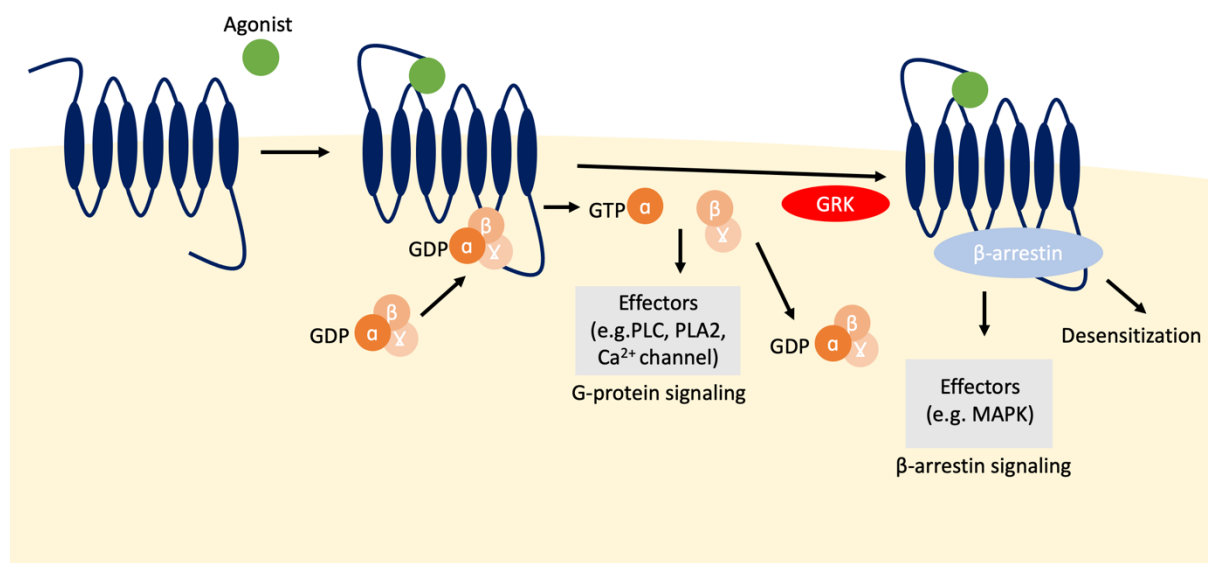

Figure 3. GPCR signaling. Following the binding of an agonist, the GPCR changes its conformation. The activated receptor binds heterotrimeric G proteins formed of α, β and γ -subunits. This coupling leads to an exchange of GDP by GTP on Gα protein and subsequently the dissociation of the heterotrimeric complex and the activation of G protein signaling pathways. GTPase activity of Gα subunit leads to the reformation of the heterotrimeric G proteins and ultimately the arrest of the G protein signaling. Activated GPCRs can also be phosphorylated by G-protein-coupled receptor kinases (GRKs). Phosphorylated GPCRs recruit β-arrestins which are involved in the activation of G-protein independent signaling pathways as well as the desensitization of the receptor.

We will now briefly discuss two systems that activate GPCRs and play a crucial role in the inflammatory response: the kinins and the chemokines.

a. Kinins and kinin receptors

Kinins are peptides, which are synthetized at sites of inflammation. They act through activation of two GPCRs: B1 and B2 receptors (B1R and B2R)[40]. While B2R is constitutively expressed in steady state conditions, B1R is expressed only in the context of inflammation[41]. Cytokines such as IL-1β and TNFα, which are produced during inflammation, were shown to induce B1R expression[42, 43]. Bradykinin (BK) results from the degradation of kininogen precursor by enzymes called kallikreins. BK is a short-lived peptide and is rapidly catabolized by carboxypeptidases, also termed kininases, into the metabolite des-Arg9-BK, which has a significantly higher half-life[40, 41]. While BK binds the B2R, des-Arg9-BK

activates B1R[41]. The pro-inflammatory properties of BK had already been described back in 1960 as injection of pure bradykinin induced the four cardinal signs (rubor, calor, tumor and dolor) of inflammation described by Celsus[44]. Because the activation of endothelial B2R mediates the release of nitric oxide and prostaglandins[41], the inflammatory function of BK was mainly attributed to its potent vasodilatation function[45]. In the last two decades, it has become clear however, that kinins and especially the B1R plays a more direct role in leukocyte recruitment as its stimulation induces the production of key inflammatory mediators such as histamine and cytokines[40, 46].

 As mentioned above, leukocyte recruitment at the site of infection or issue injury is a critical facet of inflammation. Among diverse signals involved in this process, the cytokine IL-1β plays a key role in cell recruitment. Interestingly, IL-1β was also shown to be a crucial signal that induces a strong expression of B1R. A first report describing the role of B1R activation in leukocyte recruitment established that following IL-1β treatment, B1R activation with an agonist induced neutrophil migration[47]. This also suggested that B1R plays an important role in mediating IL-1β-induced leukocyte recruitment. The generation of the knock-out B1R mouse model confirmed the central role of B1R in inflammation[48]. It was indeed shown that the absence of B1R reduced leukocyte infiltration[48] and conferred a strong protection in several experimental models of inflammatory disease [49, 50, 51, 52].

b. Chemokines and chemokine receptors

Chemokines, also known as chemotactic cytokines, play a key role in controling immune cell migration in the context of inflammation. Inflammatory chemokines are produced in high concentrations in response to infection or injury and bind to 20 different GPCRs[29, 30, 31, 32]. These chemokine receptors are expressed on all immune cells and their activation by chemokines mediate leukocyte recruitment. Briefly, after a chemokine binds to its receptor, G protein is activated and causes the subsequent activation of phospholipase C (PLC)[53, 54]. PLC cleaves a molecule called phosphatidylinositol (4,5)-bisphosphate (PIP2) into two second messenger molecules known as Inositol triphosphate (IP3) and diacylglycerol (DAG)[53, 54]. While IP3 triggers the release of calcium from intracellular stores, DAG activates protein kinase C (PKC)[53, 54]. These events promote the activation of different signaling pathways such Ras-MAP kinase pathways that are crucial to generate cell adhesion and cell movement within the cell harboring the chemokine receptor[53, 54]. On one hand, this induces the activation of integrins, and consequently leads to the arrest of leukocytes on the inflamed endothelium[53, 54]. On the other hand, chemokines produced in the tissue form a gradient that guides leukocytes to the site of inflammation, a process called chemotaxis[53, 54]. In this process, actin filaments are rearranged and polymerized at the leading edge of the leukocyte to form a pseudopod with polarised cell morphology leading to cell movement[53, 54].

Chemokines are classified in four groups based on their amino acid composition, especially the first two cysteine residues of a conserved tetra-cysteine motif. The CC and CXC chemokines form the two largest groups[31, 32]. The chemokine receptors expressed on the surface of a leukocyte then determine the subset that migrates into the inflamed tissue. CXCL8[55] and CCL2[56, 57] were the first chemokines to be isolated and identified to attract neutrophils and monocytes, respectively. Neutrophils express high level of chemokine receptor CXCR2 at their surface while monocytes express CCR2. The chemokine CXCL8 as well as CXCL1 and CXCL5 which are produced in the tissue and presented at the surface of the endothelium bind specifically to CXCR2 and thus induce arrest and migration of neutrophils[58, 59]. CCL2 binds to CCR2 and thus attracts monocytes to the site of inflammation[60, 61]. Nevertheless, in addition to their function in cell migration, it is now clear that chemokines can also modulate other inflammatory functions such as cytokine release and phagocytosis[29, 30].

c. Atypical chemokine receptors

Conventional chemokine receptors are not the only receptors that bind chemokines. Indeed, a group of four receptors referred to atypical chemokine receptors (ACKRs) can also bind chemokines[62, 63, 64]. It must be noted that a fifth receptor, so far known as GPR182, has been deorphanized[65, 66] and may soon join the ACKR family as ACKR5. In contrast to conventional chemokine receptors, ACKRs are mainly expressed by non-haematopoietic cells such as lymphatic and vascular endothelial cells or erythrocytes, with the exception of ACKR2 and ACKR3, which are also expressed by some specific leukocyte subsets. ACKRs are structurally similar to GPCRs, but they do not couple with G proteins due to the absence of the canonical Asp-Arg-Tyr-Leu-Ala-Ile-Val (DRYLAIV) motif usually found at the junction of the third transmembrane domain and the second intracellular loop (**Figure 4**). Thus, ACKRs fail to induce G protein-dependent signaling pathways and subsequent cellular responses, such as chemotaxis. Instead, the main feature of ACKRs is to regulate the bioavailability of chemokines[18, 67, 68, 69] and consequently to control chemokine signaling of conventional receptors. They do so by using two different mechanisms (Figure 4). First, ACKRs, such as ACKR2, ACKR3 and ACKR4, may still signal via G-protein-independent signaling pathways. Indeed, the NPxxYxF motif present in the seventh transmembrane domain in these ACKRs allows the recruitment of β-arrestin2[70, 71, 72]. By engaging β-arrestin pathway, these ACKRs are rapidly internalized with their bound chemokines, which are ultimately degraded in lysosomes[73]. As such, ACKRs are able to remove chemokines excess (aka scavenger function) and are therefore actively involved in the resolution phase of the inflammation. In contrast, ACKR1 (aka Duffy Antigen receptor for chemokines or DARC), which is expressed by erythrocytes and venular endothelial cells,[74] does not recruit β-arrestins as it lacks the NPxxYxF motif and thus utilizes other mechanisms to regulate chemokine bioavaibility[75] (**Figure 4**). On one hand, it was shown that endothelial ACKR1 regulates leukocyte trafficking by presenting chemokines[17, 18].

Indeed, chemokines that bound to endothelial ACKR1 are transported by a mechanism called transcytosis and are ultimately presented by ACKR1 on the apical surface of endothelial cells to leukocytes, which leads to their firm adhesion on the endothelium[18]. More recently, it was also showed that ACKR1 regulates leukocyte transendothelial migration[76]. Indeed, CXCL2 produced by neutrophils is deposited on ACKR1 at endothelial junctions, and ACKR1-presented CXCL2 facilitates unidirectional luminal-to-abluminal migration of neutrophils[76]. On the other hand, ACKR1 on red blood cells was described to function as a chemokine "sink"[77]. Indeed, it was shown that, by capturing chemokines, erythrocyte ACKR1 can buffer the levels of circulating inflammatory chemokines[78, 79, 80, 81], thus dampening systemic leukocyte activation[81, 82, 83]. Interestingly, it was also suggested that captured chemokines on erythrocyte ACKR1 could be released when their abundance is low[62].

In summary, ACKRs can transport, present, buffer, release, internalize and degrade chemokines. In other words, ACKRs are key receptors in regulating chemokines bioavaibility and consequently are pivotal players in controlling inflammation.
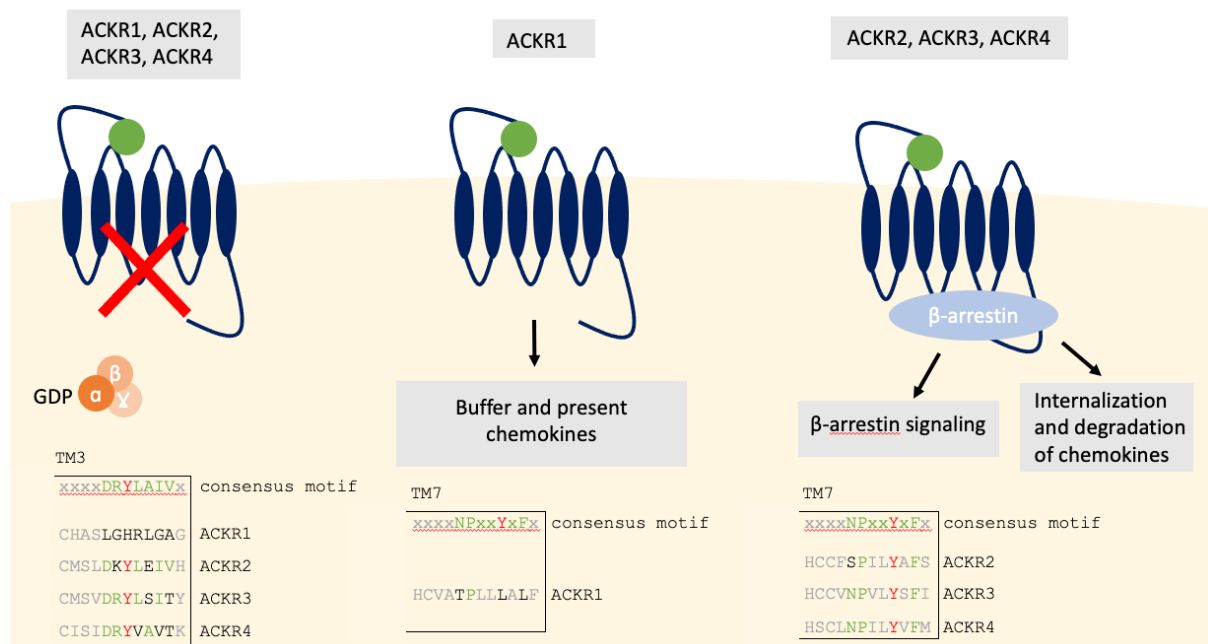

Figure 4. ACKR features. ACKRs are structurally like GPCRs but the lack the DRYLAIV motif and thus cannot recruit G-proteins. The main function of ACKRs is to regulate chemokines bioavailability by buffering, presenting or scavenging chemokines. TM3= 3rd transmembrane domain. TM7= 7th transmembrane domain.

2.4. Objectives

The main goal of this work was to investigate the molecular pathways of inflammation involving GPCRs and especially identifying novel mechanisms involved in resident cell activation and leukocyte recruitment. In particular, I have been interested in understanding how the kinin and chemokine systems regulate leukocyte migration and activation as well as defining their effects in acute and chronic inflammatory diseases.

3. Original research and discussion

3.1 Interplay between kinins and chemokines in inflammation

Duchene J, Lecomte F, Ahmed S, Cayla C, Pesquero J, Bader M, Perretti M, Ahluwalia A. A novel inflammatory pathway involved in leukocyte recruitment: role for the kinin B1 receptor and the chemokine CXCL5. *J Immunol*, 179(7):4849-56 (**2007**).

Duchene J, Cayla C, Vessillier S, Scotland R, Yamashiro K, Lecomte F, Syed I, Vo P, Marrelli A, Pitzalis C, Cipollone F, Schanstra J, Bascands JL, Hobbs AJ, Perretti M, Ahluwalia A. Laminar shear stress regulates endothelial kinin B1 receptor expression and function: potential implication in atherogenesis. *Arterioscler Thromb Vasc Biol*, 29(11):1757-63 (**2009**).

During inflammation, kinins are highly produced at the site of inflammation where they activate kinin receptors. The kinin B2 receptor (B2R) is rapidly desensitized and mainly mediates acute response. In contrast, the kinin B1 receptor (B1R), normally absent in steady state, is induced under inflammatory conditions and does not undergo desensitization upon activation[40]. It is well known that B1R activation is actively involved in the inflammation process and promotes leukocyte recruitment[46, 47]. The exact mechanism involved had however not been described previous to these studies.

Among the different cytokines released in inflammation that mediate leukocyte recruitment, IL-1β had been shown to induce a great elevation of B1R expression[46, 47]. Moreover, it had been demonstrated that blocking B1R, using antagonists, reduced IL-1β-mediated leukocyte recruitment[46]. In our study, using B1R-knockout (B1R$^{-/-}$) mice[48], we confirmed the crucial role of B1R in IL-1β-mediated leukocyte recruitment. Indeed, we demonstrated that IL-1β induced an augmentation of leukocytes rolling, adhesion, and emigration in wild-type mice and all these parameters were severely reduced in B1R$^{-/-}$ mice (**Figure 5, inset**). The near abolition of cell recruitment in B1R$^{-/-}$ mice suggested that previous studies using antagonists, had highly underestimated the magnitude of the cell recruitment response to IL-1β[46, 47]. This may have been due to the fact that the antagonists used were peptidic in nature and therefore prone to degradation[40]. Importantly, these data also suggested that inhibition of leukocyte recruitment was likely to play a major role in the apparent protection afforded by the absence of the B1R in experimental models of inflammatory disease in B1R$^{-/-}$ mice[49, 50, 51, 52].

In this study, we next showed that most tissue-infiltrated leukocytes of WT mice treated with IL-1β were actually neutrophils. Consequently, we hypothesized that CXCL chemokines (CXCL1, CXCL2 and CXCL5) that bind to CXCR2 and specifically attract neutrophils[31, 32, 84], could be involved in IL-1β-mediated cell recruitment regulated by B1R. Out of all other chemokines linked to B1R activation, CXCL5 was the most closely associated chemokine. Its production in B1R$^{-/-}$ mice was almost abolished, suggesting that CXCL5 predominantly mediated the effects of B1R activation. We next demonstrated

that immunoneutralisation of CXCL5 diminished IL-1β-induced neutrophil adhesion and emigration, whereas rolling remained unaffected. These findings suggested that, while CXCL5 plays a major role in the adhesion and emigration in response to B1R activation, other pathways were involved in the enhanced cell rolling consequent to receptor activation. It is likely that an early adhesion molecule pathway is involved in this process.

It was well known that endothelial cells also play a major role in the neutrophil recruitment process and can secrete chemokines[85, 86, 87]. Consequently, we assessed whether they could be involved in the leukocyte recruitment induced by B1R. We could indeed demonstrate that after its induction by IL-1β, stimulation of B1R with an agonist resulted in the production of CXCL5 in endothelial cells. In this context, this study unraveled a novel pathway of neutrophil recruitment centered on kinin B1 receptor activation of the CXCL5 chemokine (**Figure 5**).
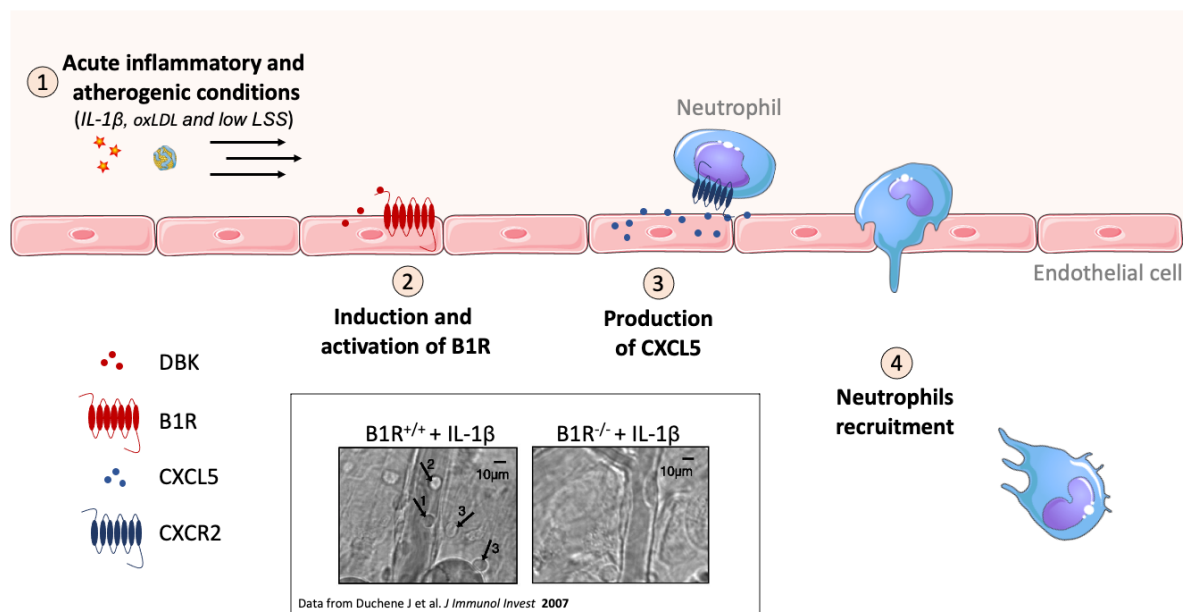

Figure 5. B1R-CXCL5 pathway involved in leukocyte recruitment. Inflammatory cyrokine (IL-1β) as well as proatherogenic factors (oxLDL and low laminar shear stress) induce the expression of B1R in endothelial cells. Kininogen and kallikrein that are necessary to produce B1R agonist (des-arg9-BK, DBK) are also expressed in endothelial cells during inflammation. The activation of B1R by DBK leads to the production of CXCL5 by the endothelial cells. In turn, CXCL5 is presented at the surface of the endothelium to facilitate the adhesion of neutrophils. Subsequently, neutrophils can transmigrate through the endothelium and migrate to the site of inflammation. (**Inset**) Representative intravital microscopy images showing leukocyte recruitment in mouse mesenteric postcapillary venules in vivo in response to IL-1β in B1R^{+/+} and B1R^{-/-} mice. The arrows show rolling (1), adherent (2), and emigrated (3) cells.

In the second study, we tested the relevance of this novel inflammatory pathway in a pathological context. Activation of endothelial cell is considered a hallmark of cardiovascular disease. It is known that alteration of the endothelial phenotype is involved in atherosclerosis development. Laminar shear stress (LSS), which is defined as the frictional force engendered by blood flow on the endothelium, is a well-recognized regulator of the endothelial phenotype[88, 89]. In large arteries, the unidirectional physiological levels of LSS are high and endow the endothelium with an anti-inflammatory phenotype, whereas low LSS levels found at sites of atheroma formation is

proinflammatory and pathogenic. In addition, the oxidation of LDL is also considered as a crucial atherogenic factor within the vascular wall as oxidized LDL (oxLDL) induce endothelial dysfunction[90]. We demonstrated in this study that, not only IL-1β but also proatherogenic conditions, namely low LSS and oxLDL, also modulated the expression of B1R in aortic endothelial cells. Of note, we showed that activation of B1R in these conditions also led to production of CXCL5. Although we described that endothelial cells were a major source of B1R-induced CXCL5, we cannot exclude that other cell types within the vasculature might also be sources of B1R-induced chemokine production.

In summary, these findings unveiled an unexpected pathway of inflammation where an inflammatory cytokine (IL-1β) and proatherogenic conditions (oxLDL and low LSS) were shown to induce CXCL5 chemokine production in endothelial cells through a B1R-dependent mechanism. The production and release of CXCL5 at the surface of endothelial cells led to adhesion of neutrophils on the endothelium and their subsequent recruitment into the inflamed tissue (**Figure 5**). This work identified the kinin B1 receptor and CXCL5 as potential therapeutic targets in inflammatory cardiovascular disease such as atherosclerosis.

3.2 Unexpected role of CXCL5 chemokine in atherosclerosis

Rousselle A, Qadri F, Leukel L, Yilmaz R, Fontaine JF, Sihn G, Bader M, Ahluwalia A, **Duchene J**. CXCL5 limits macrophage foam cell formation in atherosclerosis. *J Clin Invest,* 123(3):1343-7 (**2013**).

Atherosclerosis has long only been considered as a disorder of lipid deposition within the vessel wall of arteries. About two decades ago, a new and more complex paradigm has been proposed with the growing realization that inflammation played a pivotal role in both atherogenesis and its complications[91]. Since then, atherosclerosis has been considered as a chronic inflammatory disease of the arterial wall. Specifically, inflammatory cell recruitment has been identified to participate in all stages of atherosclerosis: from the initiation of atheromatous plaque formation and progression, through instability of the plaque, to plaque rupture and thrombotic complications, acute myocardial infarction or stroke[92].

Monocytes and macrophages are abundantly present in atherosclerotic plaques. As such chemokines that attract monocytes and activate macrophages were shown to be implicated in the pathogenesis of atherosclerosis[93, 94, 95]. Substantial evidence has incriminated CCL2 and CX_3CL1 in the development of atherosclerosis. Early studies, using CCR2-deficient[61] and CCL2-deficient mice[96], have proposed that CCL2-CCR2 axis plays a pivotal role in the recruitment of monocytes in the atherosclerotic plaques. It was later demonstrated however, that CCL2 was critical for monocyte mobilization from bone marrow [97]. The lesion phenotype observed in CCR2-deficient mice may therefore be ascribed to a reduction of the circulating monocyte numbers rather than a decrease of their recruitment[98]. Once in the atherosclerotic plaques, monocytes that differentiate into macrophages can also be activated by chemokines that modulate their fate. It has been demonstrated for instance, that absence of CX_3CL1[99] or CX_3CR1[100, 101] resulted in a reduction of atherosclerotic lesions. Later, it was shown that CX_3CL1/CX_3CR1 axis delivered an important survival signal for lesional macrophages[102]. Specifically, stimulation with CX_3CL1 rescued phagocytes from experimentally induced cell death and restored atherogenesis in CX_3CR1-deficent mice[102].

Although it is known that other chemokines and in particular ELR^+ CXCL chemokines, such as CXCL1 and CXCL2, are induced during atherosclerosis, their exact functional contribution to the development of the pathology has not been ascertained[92, 103, 104]. The ELR^+ CXCL chemokines are well-known to be potent and specific attractants of neutrophils in acute inflammation[29]. While the role of neutrophils in the pathogenesis of atherosclerosis has been described [105, 106]; it remains uncertain whether ELR^+ CXCL chemokines play a role in atherosclerosis by recruiting neutrophils within the plaques. It was also suggested that CXCR2, the receptor activated by ELR^+ CXCL chemokines, was involved in the accumulation of macrophages in advanced atherosclerotic plaques[107]. The fact that CXCL1 alone has

a similar but less pronounced effect points toward the implication of alternative CXCR2 ligands in the pathogenesis of atherosclerosis[108]. CXCL5, another ELR$^+$ CXCL chemokine, had received little attention in chronic inflammatory disease so far, which prompted us to investigate its expression and function in atherosclerosis.

We found that CXCL5 expression was upregulated in both aorta and plasma of atherosclerosis-prone ApoE-deficient (Apoe$^{-/-}$) mice fed a western diet. This rise in CXCL5 expression, unlike the rise in CXCL1 and CXCL2, was also evident in Apoe$^{-/-}$ mice fed a chow diet. The level of CXCL5 induction was similar with both diets in Apoe$^{-/-}$ mice, suggesting that CXCL5 expression was induced once cholesterol levels reached mild hypercholesterolemia but was not further increased above this cholesterol level threshold. Using a mouse model developing mild hypercholesterolemia-induced endothelial dysfunction without atherosclerotic plaque formation (C57/Bl6 mice fed a western diet), we found that CXCL5 expression was also increased in the aortas. This data suggested that CXCL5 was produced by altered endothelial cells rather than the atheromatous plaque. This is in accordance with our previous findings (see section 3.1) that CXCL5 was produced by endothelial cells under atherogenic conditions (low laminar shear stress and oxLDL).

Next, we investigated the function of CXCL5 in atheroprone-mice, using a neutralizing anti-CXCL5 antibody. Blocking CXCL5 in Apoe$^{-/-}$ mice fed a western diet did not reduce lesion size or infiltration of neutrophils and monocytes. Unexpectedly, we found an accumulation of foam cells in atherosclerotic plaques which we identified as macrophages with increased lipid storage capacity (**Figure 6, inset**). Using Apoe$^{-/-}$ B1R$^{-/-}$ mice, we confirmed that the reduction of CXCL5 was associated with an accumulation of macrophage foam cells in atherosclerotic plaques. Importantly, blocking CXCL5 did not affect monocytosis or plasma cholesterol levels. Together, these data suggested that CXCL5 may directly activate macrophage activity. To test this hypothesis, mice fed a western diet were treated with exogenous CXCL5. We observed that administration of CXCL5 limited peritoneal macrophage foam cell formation. Moreover, we showed that this was due to a direct effect of CXCL5 on macrophages as stimulation of cholesterol-loaded peritoneal macrophages with CXCL5 *in vitro* was also able to reduce intracellular lipid accumulation. Thus, we concluded that CXCL5 activated macrophage and regulated the formation of foam cell.

We then postulated that CXCL5 could limit foam cell formation by modulating cholesterol uptake (decrease) and/or cholesterol efflux (increase). Interestingly, in macrophages, CXCL5 treatment significantly upregulated the expression of ABCA1[109], a transporter that mediates the efflux of cholesterol, while the expression of other cholesterol trafficking genes, such as Msr1, CD36 and Abcg1 was not affected. CXCL5 binds to CXCR2 typically known to be expressed by neutrophils. We could show that activated macrophages also expressed CXCR2. Importantly, the induction of ABCA1 by

CXCL5 could be reversed, either by blocking CXCL5 or CXCR2 and CXCL5 treatment produced an increase of cholesterol efflux in macrophages. Altogether these data demonstrated that CXCL5 induced ABCA1 expression and reduced the cholesterol content of macrophages.
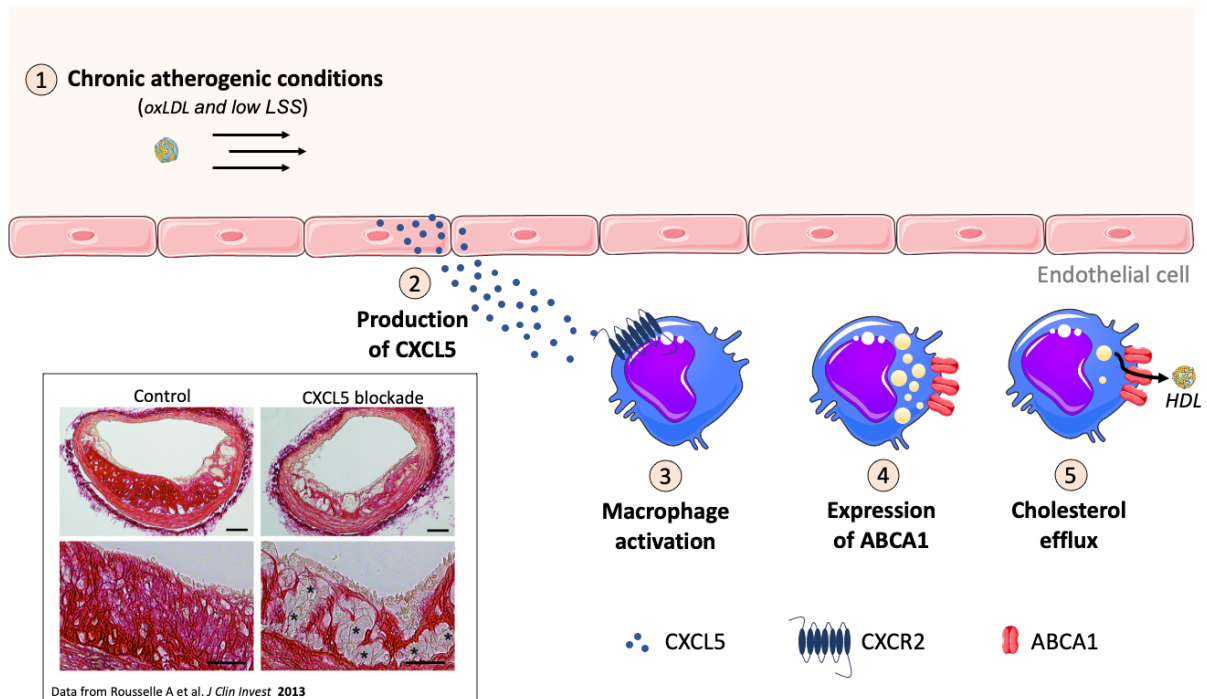

Figure 6. CXCL5 limits macrophage foam cell formation in atherosclerosis. Proatherogenic conditions induce the production of CXCL5 by aortic endothelial cells. Activation of macrophages expressing CXCR2 by CXCL5 leads to the expression of ABCA1 that controls the cholesterol efflux and reduces the formation of foam cells in atherosclerotic plaques. **(Inset)** Representative images from brachiocephalic artery lesions from Apoe$^{-/-}$ mice treated with isotype control or anti-CXCL5 antibodies. Black asterisks indicate the presence of foam cells in the atherosclerotic plaques.

In conclusion, our study highlighted a new role for an ELR$^+$ CXCL chemokine in chronic inflammatory disease. We and others have previously shown that, CXCL5 is released by endothelial cells during acute inflammation and plays a key role in attracting neutrophils at the site of inflammation[83, 110, 111]. Here, we demonstrated that in atherosclerosis, CXCL5 was also highly expressed by endothelial cells, but that surprisingly its induction was associated with a protective role (**Figure 6**). Of note, a clinical study also identified a negative correlation between circulating CXCL5 levels and the severity of coronary artery disease (CAD)[112], which is consistent with a protective role of CXCL5 in atherosclerosis. Our study provides a potential mechanism for this beneficial effect as we showed that CXCL5 limited the cholesterol content of macrophages and thus foam cell formation which may ultimately reduce the risk of plaque rupture. In atherosclerotic conditions, CX$_3$CL1 has been shown to modulate macrophage activity[102]. Our data strengthened the emerging concept that chemokines can also regulate foam cell formation, as proposed for CXCL4[113]. Additionally, our findings highlighted the complex interplay between inflammation and atherosclerosis and support the notion that proinflammatory mediators of acute immune responses are not necessarily harmful in chronic inflammatory diseases.

3.3 Regulation of hematopoiesis by the atypical chemokine receptor 1

Duchene J, Novitzky-Basso I, Thiriot A, Casanova-Acebes M, Bianchini M, Etheridge SL, Hub E, Nitz K, Artinger K, Eller K, Caamaño J, Rülicke T, Moss P, Megens RTA, von Andrian UH, Hidalgo A, Weber C, Rot A. Atypical chemokine receptor 1 on nucleated erythroid cells regulates hematopoiesis. *Nat Immunol*. 18(7):753-761 (**2017**).

Rot A, Gutjahr JC, Biswas A, Aslani M, Hub E, Thiriot A, von Andrian UH, Megens RTA, Weber C, **Duchêne J**. Murine bone marrow macrophages and human monocytes do not express atypical chemokine receptor 1. *Cell Stem Cell.* 29 (7):1013-1015 **(2022).**

Chemokines and their receptors are amply documented to play a key role in inflammation. Until now, the focus had been set on elucidating leukocyte migration during homeostatic and pathological immune responses. Classical chemokine receptors that are expressed at the surface of leukocytes have typically been therapeutic targets of choice. Another class of chemokine receptor, so-called atypical chemokine receptor (ACKR) family, can also bind chemokines[63, 64]. ACKRs are structurally similar to GPCR but do not couple to G proteins due to the absence of the DRYLAIV motif in the second intracellular loop. As a result, ACKRs fail to induce G-protein-dependent signalling pathways and subsequent cellular responses, such as chemotaxis. Instead, this family of receptors fine-tunes chemokine activity by regulating chemokine availability and cellular presentation. In contrast to 'classical' receptors, ACKRs are mainly expressed by non-haematopoietic cells, such as lymphatic and vascular endothelial cells. Although the essential role in development as well as in inflammatory and immune responses of ACKRs, make them potential therapeutic targets, they have remained largely unexplored. Therefore, investigating the molecular and biological functions of the ACKR system may open new avenues for therapeutic targets.

ACKR1, also known as Duffy Antigen, binds more than 20 different inflammatory CC and CXC (including CXCL5) chemokines and has been ascribed a unique expression profile in erythrocytes[114], venular endothelial cells[18, 74] and cerebellar Purkinje neurons[75] (**Figure 7**). This well-established pattern of cell expression, characteristic and unique among all chemokine receptors, has however been challenged. Indeed, two studies reported ACKR1 expression in myeloid cells, by macrophages as well as monocytes[115, 116]. The findings have been particularly provocative as, despite extensive literature, these were the first reports of ACKR1 expression by any leukocyte type and subset. If correct, this would profoundly change the accepted concepts of ACKR1 involvement in chemokine pathophysiology and its role in health and disease. The broad potential implications of these reports combined with uncertainties about the specificity of the antibodies used therein, prompted us to validate a panel of anti-mouse and anti-human ACKR1 antibodies to either confirm or refute ACKR1 expression in myeloid cells. As respective negative controls, the specificity of antibodies was verified

using tissues of ACKR1-deficient mice[81] and blood of Duffy-negative individuals, who naturally lack ACKR1 on erythrocytes due to a prevalent polymorphism[117]. Our analysis revealed that two antibodies, 6B7 and 2C3, were highly specific for mouse and human ACKR1, respectively. Using these antibodies, we could demonstrate in mouse and human that ACKR1 was neither expressed in macrophages, nor in monocytes. The two anti-ACKR1 antibody clones used to detect ACKR1 in mouse macrophages and human monocytes[115, 116] were not specific, as they detected epitope(s) unrelated to ACKR1 on myeloid cells. The propensity of myeloid cells to complex with other cells such as erythroid cells means that staining with specific anti-ACKR1 antibodies might also lead to an erroneous ascription of ACKR1 immunoreactivity to cells devoid of it. When complexed to erythroid cells, macrophages may appear ACKR1+ although they do not express the receptor (**Figure 7, inset**), a phenomenon also described with other circulating cell types[118]. In summary, we concluded that monocytes and macrophages did not express ACKR1 and only erythroid, venular endothelial cells and Purkinje neurons express ACKR1 (**Figure 7**).
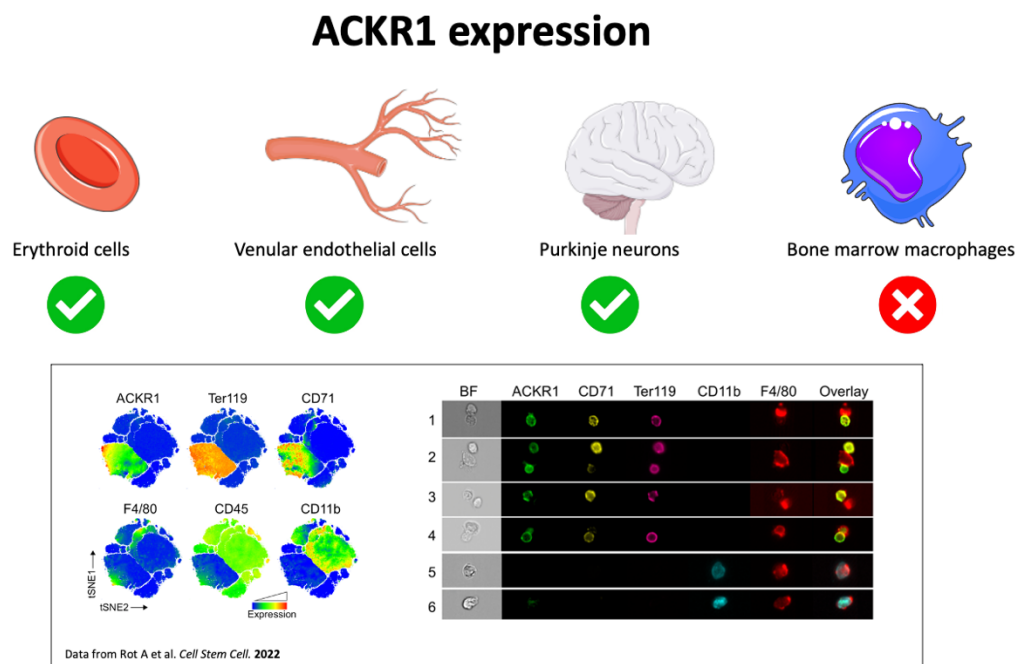

Figure 7. ACKR1 expression profile. ACKR1 has been ascribed a unique expression profile in erythroid, venular endothelial and purkinje cells. A study proposed that macrophages could also express ACKR1. We tested several anti-ACKR1 antibodies, validated their specificity using deficient organisms, and demonstrated that myeloid cells do not express ACKR1. **(Inset)** Left, BM cells of WT mice in t-SNE dimensional reduction based on the expression of 13 immunomarker assessed by flow cytometry. Right, gallery of representative images of F4/80pos ACKR1pos events visualized by imaging flow cytometry. Images highlight the presence of cell-cell complexes between F4/80pos macrophage and ACKR1pos erythroblast.

The role of ACKR1 on the venular endothelium has been extensively studied. It has been demonstrated that endothelial ACKR1 can internalize and transport inflammatory chemokines from the tissue onto the luminal endothelial cell surface[17, 18]. This machinery not only protects soluble chemokines from degradation but also allows their presentation at the surface of endothelial cells and consequently

leads to the firm adhesion of circulating leukocytes[76]. On circulating red blood cells, ACKR1 has been proposed to function as a chemokine buffer as it could scavenge chemokines that are highly produced during inflammation and release them when their abundance decrease[62]. Since red blood cells are terminally differentiated anuclear cells with no transcription and limited translation[119], the expression of ACKR1 might first occur during the earlier stages of erythropoiesis in the bone marrow. The expression and function of ACKR1 on erythroblasts has however never been studied prior to this study.

We found that ACKR1 was indeed highly expressed in erythroblasts. Its expression was detected initially in pro-erythroblasts, found to peak in early normoblasts and to gradually decline to the lowest amounts in mature erythrocytes. Importantly, among all hematopoietic BM cells, ACKR1 was expressed only in cells of the erythroid lineage. The high level of ACKR1 expression on erythroblasts, as compared to those in mature erythrocytes, suggested that ACKR1 might have a physiological role in the bone marrow. To evaluate the contribution of ACKR1 expression to bone marrow homeostasis, we compared parameters of hematopoiesis in ACKR1-deficient and wild-type mice. We found that ACKR1 expression had effects on the hematopoietic stem and progenitor cells (HSPCs). The absence of ACKR1 resulted in numeric changes and shifts in equilibria of HSPC subpopulations and led to characteristic changes in the expression of effector molecules such as CD34 on their cell surface. In addition, the analysis of the transcriptome of HSPC revealed that some of the transcripts of genes encoding neutrophil-specific effector molecules (e.g. CRAMP and NGP) were increased in HSPC from the BM of ACKR1 deficient mice compared to WT mice. Altogether, these data indicated that ACKR1 expression can regulate bone marrow homeostasis of HSPCs.

Next, we investigated whether the HSPC changes observed in ACKR1-deficient mice were due to the lack of ACKR1 expression in endothelial cells, erythroblasts or both. First, the characteristics for the ACKR1-deficient mice shifts in the HSPC populations were observed in chimeric mice, which lacked ACKR1 expression in the hematopoietic but not stromal compartment. These data indicated that ACKR1 expression in erythroid cells is the regulator of HSPC homeostasis. Next, experiments using parabiotic wild-type and ACKR1-deficient mouse pairs, which shared a common blood circulation but maintained their distinct tissue microenvironments, including in the BM, showed that ACKR1 on wild-type circulating erythrocytes failed to reverse the characteristic parameters of HSPC populations in the BM of ACKR1-deficient parabionts. Altogether, these findings in the reciprocal BM chimeric and parabiotic mice demonstrated that ACKR1 expressed on bone marrow erythroblasts regulated the homeostasis of HSPCs.

Using two-photon microscopy analysis of whole-mount bone marrows, we then showed that erythroblasts formed contacts with HSCs present in the bone marrow from wild-type mice. In the absence of ACKR1, most of these contacts between erythroblasts and HSC were lost (**Figure 8, inset**). These findings described a previously unknown direct interaction between erythroblasts and HSPCs in the bone marrow and uncovered the unexpected role of ACKR1 in the formation of such contacts. To explore how the absence of ACKR1 in the erythroid lineage might affect HSPC-derived cells, we studied the neutrophil phenotype of ACKR1-deficient mice. Neutrophils that developed from the altered HSPCs in the bone marrow of ACKR1-deficient mice carried a characteristic molecular signature, which notably included overexpression of Fcγ receptors (FcγRs; CD16/CD32), key molecules involved in neutrophil antimicrobial defense[120].
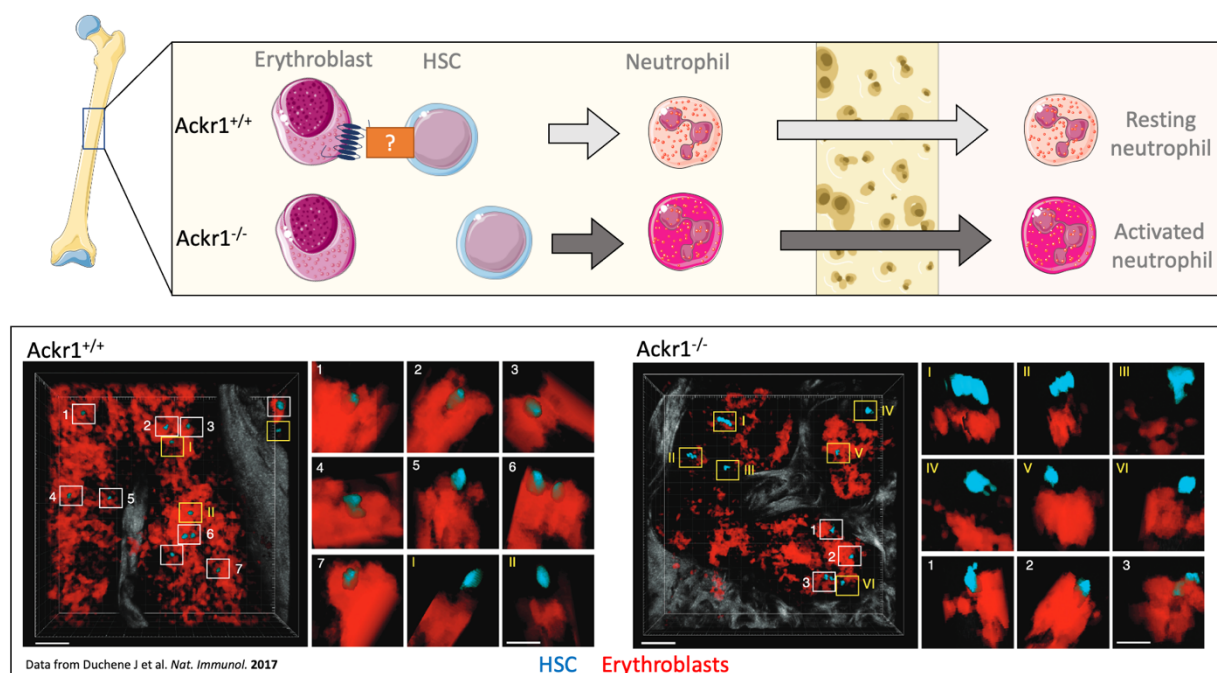

Figure 8. ACKR1 regulates hematopoiesis. In bone marrow, erythroblasts that expressed ACKR1 mediates interaction with hematopoietic stem cells (HSC) and enables a physiological hematopoiesis, resulting in the production of neutrophils with a resting phenotype. In the absence of ACKR1, an alternative hematopoiesis occurs, leading to the production of activated neutrophils. **(Inset)** Bone marrow localization of HSCs (blue) and NECs (red) in representative 3D recontructed images from whole-mounted femurs of WT and ACKR1-deficient mice. White squares with arabic numerals mark cell contacts between a HSC and NECs; yellow squares with Roman numerals indicate HSCs that do not interact with NECs.

In conclusion, this study demonstrated that ACKR1 was highly expressed by erythroblasts in the bone marrow where it regulates the homeostasis of haematopoietic stem and progenitor cells (HSPCs) and controls downstream hematopoiesis. Our findings showed that erythroblasts directly interacted with HSPCs in an ACKR1-dependent manner. In the absence of ACKR1, the steady-state haematopoiesis was altered, bone marrow HSPCs localized remotely from erythroblasts and gave rise to phenotypically distinct neutrophils (**Figure 8**). We then established that, in addition to the other described bone marrow niches[121, 122, 123], erythroid cells also regulate hematopoiesis.

4. Perspectives

Despite enormous progress in medical treatments, NCDs such as inflammatory pathologies, autoimmune disorders, cardiovascular diseases and cancer, remain major threats for human health. Since many GPCRs are activated by different inflammatory molecules (e.g. as amines, peptides, eicosanoids and chemokines), the GPCR family has represented a key target for the development of anti-inflammatory therapies. It is then not surprising that GPCRs constitute the largest family of proteins targeted by approved drugs[37]. It is estimated that 35% of approved drugs target GPCRs, which represent approximatively 700 drugs that modify the activity of 135 different receptors. What about future therapies? Should the GPCR family still be investigated for future drug target development?

4.1 Medications targeting chemokine receptors

Leukocytes express many chemokine receptors, making the chemokine system a promising drug target. Indeed, inhibitory molecules targeting chemokine receptors for hematopoietic stem cells transplantation (Plerixafor), HIV infection (Maraviroc) and T-cell lymphoma (Mogamulizumab) have been approved by FDA.

Plerixafor (aka AMD3100) is an antagonist for CXCR4[124, 125]. It was originally intended to be used as an anti-HIV agent as AMD3100 was shown to inhibit HIV replication in CD4 T cells *in vitro*[124, 125]. Rapidly, it emerged that AMD3100 targeted and blocked CXCR4. During phase I clinical trials, it appeared that Plerixafor promoted HSC mobilization very efficiently. AMD3100 blocks the interaction of CXCL12 with CXCR4, that is involved in HSC retention in the bone marrow. Plerixafor was approved by the FDA in 2008 and is now used to collect HSCs for treating myeloma by autologous stem cell transplantation[124]. It was recently proposed that patients with WHIM syndrome, an immunodeficient disorder involving leukopenia that is caused by an autosomal gain-of-function mutation in CXCR4, could also be treated with Plerixafor[126].

Maraviroc is an antagonist for CCR5[127]. It was developed to block CCR5-tropic HIV infection[127]. Indeed, CCR5 is an essential co-receptor for some HIV strains and an entry site for the virus in CD4 T cells. By binding to CCR5, Maraviroc then blocks HIV infection in CCR5$^+$ CD4 T cells. Maraviroc was approved by the FDA in 2007 and is now used in combination with other antiretroviral medications[127].

Mogamulizumab is monoclonal antibody targeting CCR4[128]. Mogamulizumab selectively binds to and blocks the activity of CCR4, which then inhibits CCR4-mediated signaling pathways[128]. Consequently, cellular migration and proliferation of T cells are inhibited by Mogamulizumab. Mogamulizumab was approved by the FDA in 2018 to treat adult T-cell lymphoma patients whose T cells typically overexpress CCR4[128].

Despite the success of chemokine receptor therapeutics, no small molecule antagonists (or other agents) have yet been licensed for therapeutic chemokine receptor blockade in inflammatory diseases. Targeting chemokine receptors for NCDs without adverse effects, may however represent a complex enterprise. The findings presented in section 3.1 and section 3.2 are good examples of this. The first studies (section 3.1) revealed a novel pathway of inflammation in which activation of the kinin B1 receptor induced CXCL5 chemokine production in endothelial cells involved in leukocytes recruitment at the site of inflammation (**Figure 5**) making CXCL5 a promising therapeutic target to dampen the inflammatory response in NCDs. In the next study (section 3.2) however, we highlighted that such an approach could have dramatic effects as blocking CXCL5 did not result in the reduction of atherosclerotic plaque formation but augmentation of foam cell formation instead (**Figure 6**). Moreover, blocking the chemokine receptors for a prolonged period would be expected to dramatically reduce leukocyte recruitment, and thus to decrease pathogens clearance and increase the risk of infection diseases. Although the chemokine axis remains an important therapeutic target to be further investigated, blocking it in NCDs may have a high cost. Alternative approaches are therefore needed to address this unmet clinical opportunity.

4.2. Targeting ACKRs to treat inflammatory diseases

So far, the focus of therapeutic targeting has been set on "classical" chemokine receptors. ACKRs may represent equally efficient targets, but have remained largely unexplored, partly because their roles in inflammation are still poorly understood[129]. The ability of ACKRs to control chemokine availability[62, 63], make their targeting particularly attractive to modulate the levels but not the entire function of chemokines[129]. Such an example is ACKR3, which regulates the extracellular levels of CXCL12 by binding and scavenging it[62, 63]. Administration of the ACKR3 antagonist ACT-1004-1239 led to an elevation of plasma CXCL12[130], and reduced leukocyte infiltration in an experimental autoimmune encephalomyelitis (EAE) mouse model[131]. Augmentation of CXCL12 levels in the plasma is thought to disturb the migration of leukocytes by modifying the chemokine gradient and thus reduce tissue-infiltration of inflammatory cells[131]. ACT-1004-1239 was also shown to directly enhance myelin repair, which can be explained by the neuroregenerative capacity of CXCL12[132, 133]. ACT-1004-1239 may then be considered as a fine-tuning drug that modulates both plasma and cerebrospinal fluid CXCL12 to reduce neuroinflammation and enhance myelin repair. ACT-1004-1239 is now in phase II clinical trial. The promising effect of ACKR3 targeting in inflammatory disease sheds light on the interest of targeting ACKRs in NCDs, paving the way towards identifying new therapeutic targets.

4.3. Studying ACKR1 polymorphism in inflammation

Not only ACKRs merit to be the focus of future drug development but understanding their functions in disease should also drive further investigation. The studies presented in section 3.3 pointed out to the key role of ACKR1 expressed by erythroid cells in modulating hematopoiesis. These findings are highly relevant for human health, as Duffy-negative individuals of African ancestry selectively lack ACKR1 expression in the cells of the erythroid lineage only[134, 135]. Indeed, sub-Saharan Africans and 70% of African Americans carry the variant rs2814778(G) in the gene encoding ACKR1 (**Figure 9A**). This variant corresponds to a single A to G substitution in the promoter region of ACKR1, which disrupts the binding site for the GATA1 erythroid transcription factor[117] (**Figure 9C**). Consequently, individuals who are homozygous for the allele, specifically lack ACKR1 expression on RBCs but still express ACKR1 on endothelium and neurons (**Figure 9B**), causing a Duffy-negative or FyB(ES) phenotype. To specifically assess the role of ACKR1 in the erythroid compartment, we developed a new mouse model. Using CRISPR/Cas9 genome editing system, we generated a mouse strain (*Ackr1*^GATA1-G) with the nucleotide substitution equivalent to that in the human rs2814778(G) ACKR1 polymorphism (**Figure 9D**). Such A to G substitution in the GATA1-binding motif was possible as the domain is 100% conserved in mouse and human (**Figure 9D**). Thus, this new FyB(ES)-like mouse model phenocopies Duffy-negative individuals carrying the rs2814778-G variant and provides a new experimental tool for studying the downstream effects of ACKR1 polymorphism in homeostasis and NCDs.
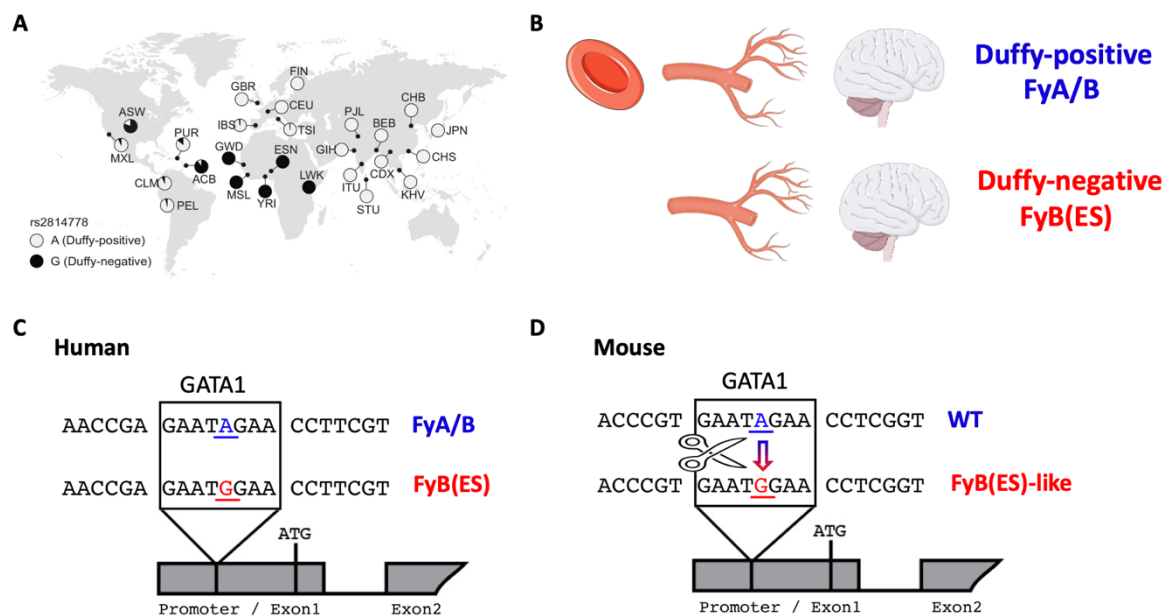

Figure 9. ACKR1 regulates hematopoiesis. (A) Global distribution of rs2814778 ACKR1 variant. **(B)** Individuals carrying the rs2814778-G (red) variant do not express ACKR1 in the erythroid compartment. This phenotype is called Duffy-negative of FyB(ES). **(C)** Human rs2814778-A (blue) and rs2814778-G (red) variants in the GATA1 region of the promoter of ACKR1, **(D)** Using CRISPR-Cas9 editing system, a single point substitution in the GATA1 motif (red) was created to generate FyB(ES)-like mice.

In conclusion, the work presented in this habilitation thesis provides evidence that GPCRs, and in particular the classical and atypical chemokine receptors, play a crucial role in inflammation. Further research is needed to fully apprehend the contribution of ACKRs in NCDs, elucidate pathological mechanisms and ultimately develop new drug therapies targeting these receptors.

5. References

1. Okin, D. & Medzhitov, R. Evolution of inflammatory diseases. *Curr Biol* **22**, R733-740 (2012).

2. Medzhitov, R. The spectrum of inflammatory responses. *Science* **374**, 1070-1075 (2021).

3. Medzhitov, R. Origin and physiological roles of inflammation. *Nature* **454**, 428-435 (2008).

4. Rocha e Silva, M. A brief survey of the history of inflammation. 1978. *Agents Actions* **43**, 86-90 (1994).

5. Williams, T.J. & Peck, M.J. Role of prostaglandin-mediated vasodilatation in inflammation. *Nature* **270**, 530-532 (1977).

6. Ji, R.R., Chamessian, A. & Zhang, Y.Q. Pain regulation by non-neuronal cells and inflammation. *Science* **354**, 572-577 (2016).

7. Strebhardt, K. & Ullrich, A. Paul Ehrlich's magic bullet concept: 100 years of progress. *Nat Rev Cancer* **8**, 473-480 (2008).

8. Gordon, S. Elie Metchnikoff: father of natural immunity. *Eur J Immunol* **38**, 3257-3264 (2008).

9. Nourshargh, S. & Alon, R. Leukocyte migration into inflamed tissues. *Immunity* **41**, 694-707 (2014).

10. Ley, K., Laudanna, C., Cybulsky, M.I. & Nourshargh, S. Getting to the site of inflammation: the leukocyte adhesion cascade updated. *Nat Rev Immunol* **7**, 678-689 (2007).

11. Matzinger, P. The danger model: a renewed sense of self. *Science* **296**, 301-305 (2002).

12. Chen, G.Y. & Nunez, G. Sterile inflammation: sensing and reacting to damage. *Nat Rev Immunol* **10**, 826-837 (2010).

13. Seong, S.Y. & Matzinger, P. Hydrophobicity: an ancient damage-associated molecular pattern that initiates innate immune responses. *Nat Rev Immunol* **4**, 469-478 (2004).

14. Pober, J.S. & Sessa, W.C. Evolving functions of endothelial cells in inflammation. *Nat Rev Immunol* **7**, 803-815 (2007).

15. Butcher, E.C. Leukocyte-endothelial cell recognition: three (or more) steps to specificity and diversity. *Cell* **67**, 1033-1036 (1991).

16. Rot, A. & von Andrian, U.H. Chemokines in innate and adaptive host defense: basic chemokinese grammar for immune cells. *Annu Rev Immunol* **22**, 891-928 (2004).

17. Middleton, J. *et al.* Transcytosis and surface presentation of IL-8 by venular endothelial cells. *Cell* **91**, 385-395 (1997).

18. Pruenster, M. *et al.* The Duffy antigen receptor for chemokines transports chemokines and supports their promigratory activity. *Nat Immunol* **10**, 101-108 (2009).

19. Laudanna, C., Kim, J.Y., Constantin, G. & Butcher, E. Rapid leukocyte integrin activation by chemokines. *Immunol Rev* **186**, 37-46 (2002).

20. Astrof, N.S., Salas, A., Shimaoka, M., Chen, J. & Springer, T.A. Importance of force linkage in mechanochemistry of adhesion receptors. *Biochemistry* **45**, 15020-15028 (2006).

21. Sigal, A. *et al.* The LFA-1 integrin supports rolling adhesions on ICAM-1 under physiological shear flow in a permissive cellular environment. *J Immunol* **165**, 442-452 (2000).

22. Chesnutt, B.C. *et al.* Induction of LFA-1-dependent neutrophil rolling on ICAM-1 by engagement of E-selectin. *Microcirculation* **13**, 99-109 (2006).

23. Johnson, Z., Proudfoot, A.E. & Handel, T.M. Interaction of chemokines and glycosaminoglycans: a new twist in the regulation of chemokine function with opportunities for therapeutic intervention. *Cytokine Growth Factor Rev* **16**, 625-636 (2005).

24. Graham, G.J., Handel, T.M. & Proudfoot, A.E.I. Leukocyte Adhesion: Reconceptualizing Chemokine Presentation by Glycosaminoglycans. *Trends Immunol* **40**, 472-481 (2019).

25. Dejana, E. Endothelial cell-cell junctions: happy together. *Nat Rev Mol Cell Biol* **5**, 261-270 (2004).

26. Nourshargh, S., Krombach, F. & Dejana, E. The role of JAM-A and PECAM-1 in modulating leukocyte infiltration in inflamed and ischemic tissues. *J Leukoc Biol* **80**, 714-718 (2006).

27. Muller, W.A. Leukocyte-endothelial-cell interactions in leukocyte transmigration and the inflammatory response. *Trends Immunol* **24**, 327-334 (2003).

28. Carman, C.V. & Springer, T.A. A transmigratory cup in leukocyte diapedesis both through individual vascular endothelial cells and between them. *J Cell Biol* **167**, 377-388 (2004).

29. Viola, A. & Luster, A.D. Chemokines and their receptors: drug targets in immunity and inflammation. *Annu Rev Pharmacol Toxicol* **48**, 171-197 (2008).

30. Griffith, J.W., Sokol, C.L. & Luster, A.D. Chemokines and chemokine receptors: positioning cells for host defense and immunity. *Annu Rev Immunol* **32**, 659-702 (2014).

31. Zlotnik, A. & Yoshie, O. Chemokines: a new classification system and their role in immunity. *Immunity* **12**, 121-127 (2000).

32. Zlotnik, A. & Yoshie, O. The chemokine superfamily revisited. *Immunity* **36**, 705-716 (2012).

33. Burn, G.L., Foti, A., Marsman, G., Patel, D.F. & Zychlinsky, A. The Neutrophil. *Immunity* **54**, 1377-1391 (2021).

34. Sun, L. & Ye, R.D. Role of G protein-coupled receptors in inflammation. *Acta Pharmacol Sin* **33**, 342-350 (2012).

35. Lammermann, T. & Kastenmuller, W. Concepts of GPCR-controlled navigation in the immune system. *Immunol Rev* **289**, 205-231 (2019).

36. Hauser, A.S., Attwood, M.M., Rask-Andersen, M., Schioth, H.B. & Gloriam, D.E. Trends in GPCR drug discovery: new agents, targets and indications. *Nat Rev Drug Discov* **16**, 829-842 (2017).

37. Sriram, K. & Insel, P.A. G Protein-Coupled Receptors as Targets for Approved Drugs: How Many Targets and How Many Drugs? *Mol Pharmacol* **93**, 251-258 (2018).

38. Hilger, D., Masureel, M. & Kobilka, B.K. Structure and dynamics of GPCR signaling complexes. *Nat Struct Mol Biol* **25**, 4-12 (2018).

39. Weis, W.I. & Kobilka, B.K. The Molecular Basis of G Protein-Coupled Receptor Activation. *Annu Rev Biochem* **87**, 897-919 (2018).

40. Leeb-Lundberg, L.M., Marceau, F., Muller-Esterl, W., Pettibone, D.J. & Zuraw, B.L. International union of pharmacology. XLV. Classification of the kinin receptor family: from molecular mechanisms to pathophysiological consequences. *Pharmacol Rev* **57**, 27-77 (2005).

41. Regoli, D. & Barabe, J. Pharmacology of bradykinin and related kinins. *Pharmacol Rev* **32**, 1-46 (1980).

42. Duchene, J. & Ahluwalia, A. The kinin B(1) receptor and inflammation: new therapeutic target for cardiovascular disease. *Curr Opin Pharmacol* **9**, 125-131 (2009).

43. Zhou, X., Polgar, P. & Taylor, L. Roles for interleukin-1beta, phorbol ester and a post-transcriptional regulator in the control of bradykinin B1 receptor gene expression. *Biochem J* **330 (Pt 1)**, 361-366 (1998).

44. Elliott, D.F., Horton, E.W. & Lewis, G.P. Actions of pure bradykinin. *J Physiol* **153**, 473-480 (1960).

45. Madeddu, P. *et al.* Cardiovascular phenotype of a mouse strain with disruption of bradykinin B2-receptor gene. *Circulation* **96**, 3570-3578 (1997).

46. McLean, P.G., Ahluwalia, A. & Perretti, M. Association between kinin B(1) receptor expression and leukocyte trafficking across mouse mesenteric postcapillary venules. *J Exp Med* **192**, 367-380 (2000).

47. Ahluwalia, A. & Perretti, M. Involvement of bradykinin B1 receptors in the polymorphonuclear leukocyte accumulation induced by IL-1 beta in vivo in the mouse. *J Immunol* **156**, 269-274 (1996).

48. Pesquero, J.B. *et al.* Hypoalgesia and altered inflammatory responses in mice lacking kinin B1 receptors. *Proc Natl Acad Sci U S A* **97**, 8140-8145 (2000).

49. Gabra, B.H., Berthiaume, N., Sirois, P., Nantel, F. & Battistini, B. The kinin system mediates hyperalgesia through the inducible bradykinin B1 receptor subtype: evidence in various

experimental animal models of type 1 and type 2 diabetic neuropathy. *Biol Chem* **387**, 127-143 (2006).

50.   Westermann, D. *et al.* Gene deletion of the kinin receptor B1 attenuates cardiac inflammation and fibrosis during the development of experimental diabetic cardiomyopathy. *Diabetes* **58**, 1373-1381 (2009).

51.   Souza, D.G. *et al.* Role of bradykinin B2 and B1 receptors in the local, remote, and systemic inflammatory responses that follow intestinal ischemia and reperfusion injury. *J Immunol* **172**, 2542-2548 (2004).

52.   Austinat, M. *et al.* Blockade of bradykinin receptor B1 but not bradykinin receptor B2 provides protection from cerebral infarction and brain edema. *Stroke* **40**, 285-293 (2009).

53.   Friedl, P. & Weigelin, B. Interstitial leukocyte migration and immune function. *Nat Immunol* **9**, 960-969 (2008).

54.   Wu, D. Signaling mechanisms for regulation of chemotaxis. *Cell Res* **15**, 52-56 (2005).

55.   Yoshimura, T. *et al.* Purification of a human monocyte-derived neutrophil chemotactic factor that has peptide sequence similarity to other host defense cytokines. *Proc Natl Acad Sci U S A* **84**, 9233-9237 (1987).

56.   Yoshimura, T. *et al.* Purification and amino acid analysis of two human glioma-derived monocyte chemoattractants. *J Exp Med* **169**, 1449-1459 (1989).

57.   Matsushima, K., Larsen, C.G., DuBois, G.C. & Oppenheim, J.J. Purification and characterization of a novel monocyte chemotactic and activating factor produced by a human myelomonocytic cell line. *J Exp Med* **169**, 1485-1490 (1989).

58.   Cacalano, G. *et al.* Neutrophil and B cell expansion in mice that lack the murine IL-8 receptor homolog. *Science* **265**, 682-684 (1994).

59.   Shuster, D.E., Kehrli, M.E., Jr. & Ackermann, M.R. Neutrophilia in mice that lack the murine IL-8 receptor homolog. *Science* **269**, 1590-1591 (1995).

60.   Kurihara, T., Warr, G., Loy, J. & Bravo, R. Defects in macrophage recruitment and host defense in mice lacking the CCR2 chemokine receptor. *J Exp Med* **186**, 1757-1762 (1997).

61.   Boring, L., Gosling, J., Cleary, M. & Charo, I.F. Decreased lesion formation in CCR2-/- mice reveals a role for chemokines in the initiation of atherosclerosis. *Nature* **394**, 894-897 (1998).

62.   Nibbs, R.J. & Graham, G.J. Immune regulation by atypical chemokine receptors. *Nat Rev Immunol* **13**, 815-829 (2013).

63.   Bachelerie, F. *et al.* International Union of Basic and Clinical Pharmacology. [corrected]. LXXXIX. Update on the extended family of chemokine receptors and introducing a new nomenclature for atypical chemokine receptors. *Pharmacol Rev* **66**, 1-79 (2014).

64.   Bachelerie, F. *et al.* New nomenclature for atypical chemokine receptors. *Nat Immunol* **15**, 207-208 (2014).

65.   Torphy, R.J. *et al.* GPR182 limits antitumor immunity via chemokine scavenging in mouse melanoma models. *Nat Commun* **13**, 97 (2022).

66.   Le Mercier, A. *et al.* GPR182 is an endothelium-specific atypical chemokine receptor that maintains hematopoietic stem cell homeostasis. *Proc Natl Acad Sci U S A* **118** (2021).

67.   Ulvmar, M.H. *et al.* The atypical chemokine receptor CCRL1 shapes functional CCL21 gradients in lymph nodes. *Nat Immunol* **15**, 623-630 (2014).

68.   Lee, K.M. *et al.* The chemokine receptors ACKR2 and CCR2 reciprocally regulate lymphatic vessel density. *EMBO J* **33**, 2564-2580 (2014).

69.   Cruz-Orengo, L. *et al.* CXCR7 influences leukocyte entry into the CNS parenchyma by controlling abluminal CXCL12 abundance during autoimmunity. *J Exp Med* **208**, 327-339 (2011).

70.   Watts, A.O. *et al.* beta-Arrestin recruitment and G protein signaling by the atypical human chemokine decoy receptor CCX-CKR. *J Biol Chem* **288**, 7169-7181 (2013).

71.   Coggins, N.L. *et al.* CXCR7 controls competition for recruitment of beta-arrestin 2 in cells expressing both CXCR4 and CXCR7. *PLoS One* **9**, e98328 (2014).

72.   Ragnarsson, L., Andersson, A., Thomas, W.G. & Lewis, R.J. Mutations in the NPxxY motif stabilize pharmacologically distinct conformational states of the alpha1B- and beta2-adrenoceptors. *Sci Signal* **12** (2019).

73.   Ray, P. *et al.* Carboxy-terminus of CXCR7 regulates receptor localization and function. *Int J Biochem Cell Biol* **44**, 669-678 (2012).

74.   Thiriot, A. *et al.* Differential DARC/ACKR1 expression distinguishes venular from non-venular endothelial cells in murine tissues. *BMC Biol* **15**, 45 (2017).

75.   Novitzky-Basso, I. & Rot, A. Duffy antigen receptor for chemokines and its involvement in patterning and control of inflammatory chemokines. *Front Immunol* **3**, 266 (2012).

76.   Girbl, T. *et al.* Distinct Compartmentalization of the Chemokines CXCL1 and CXCL2 and the Atypical Receptor ACKR1 Determine Discrete Stages of Neutrophil Diapedesis. *Immunity* **49**, 1062-1076 e1066 (2018).

77.   Darbonne, W.C. *et al.* Red blood cells are a sink for interleukin 8, a leukocyte chemotaxin. *J Clin Invest* **88**, 1362-1369 (1991).

78.   Jilma-Stohlawetz, P. *et al.* Fy phenotype and gender determine plasma levels of monocyte chemotactic protein. *Transfusion* **41**, 378-381 (2001).

79.   Schnabel, R.B. *et al.* Duffy antigen receptor for chemokines (Darc) polymorphism regulates circulating concentrations of monocyte chemoattractant protein-1 and other inflammatory mediators. *Blood* **115**, 5289-5299 (2010).

80. Fukuma, N. *et al.* A role of the Duffy antigen for the maintenance of plasma chemokine concentrations. *Biochem Biophys Res Commun* **303**, 137-139 (2003).

81. Dawson, T.C. *et al.* Exaggerated response to endotoxin in mice lacking the Duffy antigen/receptor for chemokines (DARC). *Blood* **96**, 1681-1684 (2000).

82. Reutershan, J., Harry, B., Chang, D., Bagby, G.J. & Ley, K. DARC on RBC limits lung injury by balancing compartmental distribution of CXC chemokines. *Eur J Immunol* **39**, 1597-1607 (2009).

83. Mei, J. *et al.* CXCL5 regulates chemokine scavenging and pulmonary host defense to bacterial infection. *Immunity* **33**, 106-117 (2010).

84. Rovai, L.E., Herschman, H.R. & Smith, J.B. The murine neutrophil-chemoattractant chemokines LIX, KC, and MIP-2 have distinct induction kinetics, tissue distributions, and tissue-specific sensitivities to glucocorticoid regulation in endotoxemia. *J Leukoc Biol* **64**, 494-502 (1998).

85. Imaizumi, T. *et al.* Human endothelial cells synthesize ENA-78: relationship to IL-8 and to signaling of PMN adhesion. *Am J Respir Cell Mol Biol* **17**, 181-192 (1997).

86. Chandrasekar, B. *et al.* Chemokine-cytokine cross-talk. The ELR+ CXC chemokine LIX (CXCL5) amplifies a proinflammatory cytokine response via a phosphatidylinositol 3-kinase-NF-kappa B pathway. *J Biol Chem* **278**, 4675-4686 (2003).

87. Beck, G.C., Yard, B.A., Breedijk, A.J., Van Ackern, K. & Van Der Woude, F.J. Release of CXC-chemokines by human lung microvascular endothelial cells (LMVEC) compared with macrovascular umbilical vein endothelial cells. *Clin Exp Immunol* **118**, 298-303 (1999).

88. Chatzizisis, Y.S. *et al.* Role of endothelial shear stress in the natural history of coronary atherosclerosis and vascular remodeling: molecular, cellular, and vascular behavior. *J Am Coll Cardiol* **49**, 2379-2393 (2007).

89. Malek, A.M., Alper, S.L. & Izumo, S. Hemodynamic shear stress and its role in atherosclerosis. *JAMA* **282**, 2035-2042 (1999).

90. Ludewig, B. *et al.* Linking immune-mediated arterial inflammation and cholesterol-induced atherosclerosis in a transgenic mouse model. *Proc Natl Acad Sci U S A* **97**, 12752-12757 (2000).

91. Ross, R. Atherosclerosis--an inflammatory disease. *N Engl J Med* **340**, 115-126 (1999).

92. Weber, C., Zernecke, A. & Libby, P. The multifaceted contributions of leukocyte subsets to atherosclerosis: lessons from mouse models. *Nat Rev Immunol* **8**, 802-815 (2008).

93. Drechsler, M., Duchene, J. & Soehnlein, O. Chemokines control mobilization, recruitment, and fate of monocytes in atherosclerosis. *Arterioscler Thromb Vasc Biol* **35**, 1050-1055 (2015).

94. Gautier, E.L., Jakubzick, C. & Randolph, G.J. Regulation of the migration and survival of monocyte subsets by chemokine receptors and its relevance to atherosclerosis. *Arterioscler Thromb Vasc Biol* **29**, 1412-1418 (2009).

95. Weber, C. & Noels, H. Atherosclerosis: current pathogenesis and therapeutic options. *Nat Med* **17**, 1410-1422 (2011).

96. Gu, L. *et al.* Absence of monocyte chemoattractant protein-1 reduces atherosclerosis in low density lipoprotein receptor-deficient mice. *Mol Cell* **2**, 275-281 (1998).

97. Serbina, N.V. & Pamer, E.G. Monocyte emigration from bone marrow during bacterial infection requires signals mediated by chemokine receptor CCR2. *Nat Immunol* **7**, 311-317 (2006).

98. Tsou, C.L. *et al.* Critical roles for CCR2 and MCP-3 in monocyte mobilization from bone marrow and recruitment to inflammatory sites. *J Clin Invest* **117**, 902-909 (2007).

99. Teupser, D. *et al.* Major reduction of atherosclerosis in fractalkine (CX3CL1)-deficient mice is at the brachiocephalic artery, not the aortic root. *Proc Natl Acad Sci U S A* **101**, 17795-17800 (2004).

100. Combadiere, C. *et al.* Decreased atherosclerotic lesion formation in CX3CR1/apolipoprotein E double knockout mice. *Circulation* **107**, 1009-1016 (2003).

101. Lesnik, P., Haskell, C.A. & Charo, I.F. Decreased atherosclerosis in CX3CR1-/- mice reveals a role for fractalkine in atherogenesis. *J Clin Invest* **111**, 333-340 (2003).

102. Landsman, L. *et al.* CX3CR1 is required for monocyte homeostasis and atherogenesis by promoting cell survival. *Blood* **113**, 963-972 (2009).

103. Zernecke, A. & Weber, C. Chemokines in atherosclerosis: proceedings resumed. *Arterioscler Thromb Vasc Biol* **34**, 742-750 (2014).

104. Yan, Y., Thakur, M., van der Vorst, E.P.C., Weber, C. & Doring, Y. Targeting the chemokine network in atherosclerosis. *Atherosclerosis* **330**, 95-106 (2021).

105. Soehnlein, O., Steffens, S., Hidalgo, A. & Weber, C. Neutrophils as protagonists and targets in chronic inflammation. *Nat Rev Immunol* **17**, 248-261 (2017).

106. Zernecke, A. *et al.* Protective role of CXC receptor 4/CXC ligand 12 unveils the importance of neutrophils in atherosclerosis. *Circ Res* **102**, 209-217 (2008).

107. Boisvert, W.A., Santiago, R., Curtiss, L.K. & Terkeltaub, R.A. A leukocyte homologue of the IL-8 receptor CXCR-2 mediates the accumulation of macrophages in atherosclerotic lesions of LDL receptor-deficient mice. *J Clin Invest* **101**, 353-363 (1998).

108. Boisvert, W.A. *et al.* Up-regulated expression of the CXCR2 ligand KC/GRO-alpha in atherosclerotic lesions plays a central role in macrophage accumulation and lesion progression. *Am J Pathol* **168**, 1385-1395 (2006).

109. Bodzioch, M. *et al.* The gene encoding ATP-binding cassette transporter 1 is mutated in Tangier disease. *Nat Genet* **22**, 347-351 (1999).

110. Duchene, J. *et al.* A novel inflammatory pathway involved in leukocyte recruitment: role for the kinin B1 receptor and the chemokine CXCL5. *J Immunol* **179**, 4849-4856 (2007).

111. Madalli, S. *et al.* Sex-specific regulation of chemokine Cxcl5/6 controls neutrophil recruitment and tissue injury in acute inflammatory states. *Biol Sex Differ* **6**, 27 (2015).

112. Ravi, S. *et al.* Clinical Evidence Supports a Protective Role for CXCL5 in Coronary Artery Disease. *Am J Pathol* **187**, 2895-2911 (2017).

113. Gleissner, C.A., Shaked, I., Little, K.M. & Ley, K. CXC chemokine ligand 4 induces a unique transcriptome in monocyte-derived macrophages. *J Immunol* **184**, 4810-4818 (2010).

114. Cutbush, M., Mollison, P.L. & Parkin, D.M. A New Human Blood Group. *Nature* **165**, 188-189 (1950).

115. Hur, J. *et al.* CD82/KAI1 Maintains the Dormancy of Long-Term Hematopoietic Stem Cells through Interaction with DARC-Expressing Macrophages. *Cell Stem Cell* **18**, 508-521 (2016).

116. Kim, E.Y. *et al.* Interleukin-22 Induces the Infiltration of Visceral Fat Tissue by a Discrete Subset of Duffy Antigen Receptor for Chemokine-Positive M2-Like Macrophages in Response to a High Fat Diet. *Cells* **8** (2019).

117. Tournamille, C., Colin, Y., Cartron, J.P. & Le Van Kim, C. Disruption of a GATA motif in the Duffy gene promoter abolishes erythroid gene expression in Duffy-negative individuals. *Nat Genet* **10**, 224-228 (1995).

118. Burel, J.G. *et al.* Circulating T cell-monocyte complexes are markers of immune perturbations. *Elife* **8** (2019).

119. Doss, J.F. *et al.* A comprehensive joint analysis of the long and short RNA transcriptomes of human erythrocytes. *BMC Genomics* **16**, 952 (2015).

120. Fossati, G., Moots, R.J., Bucknall, R.C. & Edwards, S.W. Differential role of neutrophil Fcgamma receptor IIIB (CD16) in phagocytosis, bacterial killing, and responses to immune complexes. *Arthritis Rheum* **46**, 1351-1361 (2002).

121. Itkin, T. *et al.* Distinct bone marrow blood vessels differentially regulate haematopoiesis. *Nature* **532**, 323-328 (2016).

122. Morrison, S.J. & Scadden, D.T. The bone marrow niche for haematopoietic stem cells. *Nature* **505**, 327-334 (2014).

123. Mendelson, A. & Frenette, P.S. Hematopoietic stem cell niche maintenance during homeostasis and regeneration. *Nat Med* **20**, 833-846 (2014).

124. De Clercq, E. Mozobil(R) (Plerixafor, AMD3100), 10 years after its approval by the US Food and Drug Administration. *Antivir Chem Chemother* **27**, 2040206619829382 (2019).

125. De Clercq, E. The bicyclam AMD3100 story. *Nat Rev Drug Discov* **2**, 581-587 (2003).

126. McDermott, D.H. *et al.* Plerixafor for the Treatment of WHIM Syndrome. *N Engl J Med* **380**, 163-170 (2019).

127. Kuritzkes, D., Kar, S. & Kirkpatrick, P. Maraviroc. *Nature Reviews Drug Discovery* **7**, 15-16 (2008).

128. Hutchings, C.J., Koglin, M., Olson, W.C. & Marshall, F.H. Opportunities for therapeutic antibodies directed at G-protein-coupled receptors. *Nature Reviews Drug Discovery* **16**, 787-810 (2017).

129. Gencer, S. *et al.* Atypical Chemokine Receptors in Cardiovascular Disease. *Thromb Haemost* **119**, 534-541 (2019).

130. Richard-Bildstein, S. *et al.* Discovery of the Potent, Selective, Orally Available CXCR7 Antagonist ACT-1004-1239. *J Med Chem* **63**, 15864-15882 (2020).

131. Pouzol, L. *et al.* ACT-1004-1239, a first-in-class CXCR7 antagonist with both immunomodulatory and promyelinating effects for the treatment of inflammatory demyelinating diseases. *FASEB J* **35**, e21431 (2021).

132. Patel, J.R., McCandless, E.E., Dorsey, D. & Klein, R.S. CXCR4 promotes differentiation of oligodendrocyte progenitors and remyelination. *Proc Natl Acad Sci U S A* **107**, 11062-11067 (2010).

133. Williams, J.L., Patel, J.R., Daniels, B.P. & Klein, R.S. Targeting CXCR7/ACKR3 as a therapeutic strategy to promote remyelination in the adult central nervous system. *J Exp Med* **211**, 791-799 (2014).

134. Peiper, S.C. *et al.* The Duffy antigen/receptor for chemokines (DARC) is expressed in endothelial cells of Duffy negative individuals who lack the erythrocyte receptor. *J Exp Med* **181**, 1311-1317 (1995).

135. Howes, R.E. *et al.* The global distribution of the Duffy blood group. *Nat Commun* **2**, 266 (2011).

6. Appendix

6.1   A novel inflammatory pathway involved in leukocyte recruitment: role for the kinin B1 receptor and the chemokine CXCL5.

Duchene J, Lecomte F, Ahmed S, Cayla C, Pesquero J, Bader M, Perretti M, Ahluwalia A.

A Novel Inflammatory Pathway Involved in Leukocyte Recruitment: Role for the Kinin B$_1$ Receptor and the Chemokine CXCL5[1]

Johan Duchene,* Florence Lecomte,* Saleh Ahmed,* Cecile Cayla,* Joao Pesquero,[†] Michael Bader,[‡] Mauro Perretti,* and Amrita Ahluwalia[2]*

The kinin B$_1$ receptor is an inducible receptor not normally expressed but induced by inflammatory stimuli and plays a major role in neutrophil recruitment, particularly in response to the cytokine IL-1β. However, the exact mechanism involved in this response is unclear. The aim of this study was to dissect the molecular mechanism involved, in particular to determine whether specific ELR-CXCL chemokines (specific neutrophil chemoattractants) played a role. Using intravital microscopy, we demonstrated that IL-1β-induced leukocyte rolling, adherence, and emigration in mesenteric venules of wild-type (WT) mice, associated with an increase in B$_1$ receptor mRNA expression, were substantially attenuated (>80%) in B$_1$ receptor knockout mice (B1KO). This effect in B1KO mice was correlated with a selective down-regulation of IL-1β-induced CXCL5 mRNA and protein expression compared with WT mice. Furthermore a selective neutralizing CXCL5 Ab caused profound suppression of leukocyte emigration in IL-1β-treated WT mice. Finally, treatment of human endothelial cells with IL-1β enhanced mRNA expression of the B$_1$ receptor and the human (h) CXCL5 homologues (hCXCL5 and hCXCL6). This response was suppressed by ~50% when cells were pretreated with the B$_1$ receptor antagonist des-Arg^9-[Leu^8]-bradykinin while treatment with des-Arg^9-bradykinin, the B$_1$ receptor agonist, caused a concentration-dependent increase in hCXCL5 and hCXCL6 mRNA expression. This study unveils a proinflammatory pathway centered on kinin B$_1$ receptor activation of CXCL5 leading to leukocyte trafficking and highlights the B$_1$ receptor as a potential target in the therapeutics of inflammatory disease. *The Journal of Immunology,* 2007, 179: 4849–4856.

L eukocyte recruitment at sites of tissue injury is an important facet of an inflammatory response (1). Polymorphonuclear neutrophils (PMNs)[3] are the first cells recruited to the inflammatory site and their uncontrolled accumulation is thought to contribute to organ dysfunction (2). One of the integral cytokines involved in cell recruitment is IL-1β (3). IL-1β brings about its effects by activating a number of proinflammatory pathways. In particular, this cytokine induces the expression of several acute response proteins, one of which is the kinin B$_1$ receptor. Our previous work demonstrates that this receptor plays an important role in mediating IL-1β-induced leukocyte recruitment (4, 5).

The kinins are commonly recognized as a family of inflammatory peptides (6–8), the effects of which are mediated by the endogenous agonists bradykinin (BK) and one of the main metabolites of BK, des-Arg^9-BK (DABK). The biological effects of the

kinins are brought about by their interaction with specific G protein-coupled receptors. At present, there are two clearly defined and cloned kinin receptors: B$_1$ and B$_2$. The B$_2$ receptor, which is activated by BK, is constitutively expressed, suffers rapid desensitization following activation, and mediates many of the acute actions of the kinins including edema, increased blood flow, and pain (6–8). In contrast the B$_1$ receptor, activated by DABK, is normally absent but is induced under inflammatory conditions, often hand-in-hand with an enhancement of the circulating levels of the endogenous B$_1$ agonist, DABK, and does not undergo desensitization upon activation (6–8). This receptor is induced during inflammation by certain immunostimulants, the optimal inducer being IL-1β (5, 7–9). In addition to a number of the inflammatory functions exhibited by B$_2$ receptor activation (6–8), B$_1$ receptor activation also stimulates leukocyte recruitment by promoting interaction between leukocytes and the endothelium, resulting in increased rolling, adhesion, and migration of PMNs (4, 5). Significantly, antagonism of B$_1$ receptors in vivo attenuates IL-1β-induced leukocyte accumulation (5), and inflammatory responses dependent upon leukocyte recruitment are attenuated in kinin B$_1$ receptor knockout (B1KO) mice (10); however, the exact downstream mechanisms involved in this response have yet to be determined.

Chemokines are proinflammatory cytokines that stimulate leukocyte chemoattraction and are produced in response to infectious and other inflammatory stimuli by a number of different cell types, including endothelial cells (11). That endothelial cells produce chemokines is of particular significance because within the vasculature the endothelial cell is the site for leukocyte recruitment, and expression of chemokines on the endothelial cell surface plays a pivotal role in leukocyte migration by facilitating the direct interaction of endothelial cells with leukocytes (1). More than 50

chemokines have been identified to date and have been classified into four groups according to the location of the conserved cysteine residues: CXCL, CCL, CL, and CX3CL (12). These chemokines play differential roles in specifically recruiting different cell types to an inflammatory site. With respect to neutrophil recruitment, the presence of a trio of amino acids, glutamate-leucine-arginine (ELR), before the CXCL motif appears to confer selectivity for promoting neutrophil migration (13). The most well described ELR-CXCL chemokines in mice include CXCL1 (also called keratinocyte-derived chemokine or KC), CXCL2 (also called macrophage inflammation protein-2 or MIP-2), CXCL5 (also called LPS-inducible CXC chemokine or LIX), and CXCL7 (also called neutrophil activating peptide-2 or NAP-2). Although good evidence supports a role for the kinin B$_1$ receptor in neutrophil recruitment (4, 5, 10), whether this is dependent upon ELR-CXCL chemokine expression and activity is unknown.

In this report, we demonstrate that the kinin B$_1$ receptor plays an essential role in IL-1β-induced neutrophil recruitment by using kinin B$_1$ receptor knockout (B1KO) mice (10). Moreover, we show that this effect is associated with the expression of a number of chemokines, in particular CXCL5, that are likely produced by endothelial cells following direct activation of endothelial kinin B$_1$ receptor. Because kinin B$_1$ receptor expression is raised in inflammatory disease (6–8) and leukocyte recruitment is proposed to play an important role in the innate immune response associated with a wide range of inflammatory diseases from traditional inflammatory conditions such as rheumatoid arthritis or sepsis to the more recently appreciated inflammatory disease of atherosclerosis (1), our findings highlight the B$_1$ receptor-CXCL5 pathway as a novel therapeutic target.

Materials and Methods

Animals

All experiments were conducted according to the Animals (Scientific Procedures) Act of 1986 (United Kingdom). Male C57BL/6J wild-type (WT) or B1KO (10) mice (C57BL/6 background) at 5 wk of age (10–15 g) were used in all experiments.

Intravital microscopy

Male WT and B1KO mice received either murine IL-1β (5 ng/mouse, i.p.; PeproTech) or a saline vehicle. After 4 h mice were anesthetized with diazepam (60 mg/kg, s.c.) and Hypnorm (0.7 mg/kg fentanyl citrate and 20 mg/kg fluanisone, i.m.), and the mesenteric vascular bed was prepared for viewing by intravital microscopy. Mesenteries were superfused with bicarbonate-buffered solution (132 mM NaCl, 4.7 mM KCl, 1.2 mM MgSO$_4$, 17.9 mM NaHCO$_3$, and 2.0 mM CaCl$_2$ (pH 7.4), gassed with 5% CO$_2$ and 95% N$_2$) at 37°C at a rate of 2 ml/min. The temperature of the stage was maintained at 37°C. The extent of the inflammatory response elicited by IL-1β was analyzed by counting the number of white blood cells rolling per minute. Cell adhesion was quantified by counting, for each vessel, the number of adherent neutrophils in a 100-μm length, and leukocyte emigration from the microcirculation into the tissue was quantified by counting the number of cells that had emigrated up to 50 μm away from the wall of 100-μm vessel segments. Venular blood flow was calculated from the product of mean RBC velocity (V_{mean} = centerline velocity/1.6) and microvascular cross-sectional area, assuming a cylindrical geometry. Wall shear rate was calculated by the Newtonian definition: shear rate = 8,000 × (V_{mean}/diameter). A minimum of three postcapillary venules (diameter between 20 and 40 μm; length of at least 100 μm) were observed for each mouse. To evaluate the role of CXCL5 in regulating leukocyte recruitment, a selective neutralizing mAb or control IgG (20 μg per animal, i.p.) was injected into the tail vein 30 min before IL-1β treatment. After 4 h, leukocyte rolling, adhesion, and emigration were measured as described above.

Myeloperoxidase (MPO) assay

MPO activity was determined in mesenteric tissue as an index of neutrophil accumulation (14). Mesenteric tissue, collected 4 h after IL-1β treatment, was homogenized in 1 ml of a 0.5% hexadecyltrimethylammonium bromide in MOPS buffer (10 mM, pH 7). After homogenization, samples were centrifuged at 4000 × g for 20 min at 4°C and the supernatant was collected for

determination of MPO levels as previously described (15). Data are expressed as units per gram of total protein content in the tissue as determined by Bradford assay.

Real-time quantitative RT-PCR of murine mesenteric tissue

Chemokine mRNA expression was determined by real-time quantitative RT-PCR. Briefly, mesenteric tissue was removed from saline or IL-1β-treated (for 2 h) mice as described above, snap frozen in liquid nitrogen, and stored at −80°C until use. Samples were homogenized and total RNA was isolated using a NucleoSpin RNA II purification kit (Macherey-Nagel) and then stored at −80°C until use. cDNA was synthesized from 1 μg of total RNA with Moloney murine leukemia virus reverse transcriptase (Promega) using oligo(dT) nucleotides. The following primers were used for mouse: CXCL1, 5′-TGAGCTGCGCTGTCAGTGCCT-3′ and 5′-AGAA GCCAGCGTTCACCAGA-3′; CXCL2, 5′-GAGCTTGAGTGTGACGCC CCCAGG-3′ and 5′-GTTAGCCTTGCCTTTGTTCAGTATC-3′; CXCL5, 5′-GCATTTCTGTTGCTGTTCACGCTG-3′ and 5′-CCTCCTTCTGGTTT TTCAGTTTAGC-3′; CXCL7, 5′-TGGGCCTGATCCTTGTTGCGC-3′ and 5′-GCACCGTTTTTTGTCCATTCTTCAG-3′; B$_1$ receptor, 5′-TGGA GTTGAACGTTTTGGGTTT-3′ and 5′-GTGAGGATCAGCCCCATT GT-3′; and β-actin, 5′-GAAATCGTGCGTGACATCAAAG-3′ and 5′-TG TAGTTTCATGGATGCCACAG-3′. Standard curves for these molecules were generated to determine the amplification efficiencies of target and reference genes. Quantitative PCR was performed on an ABI Prism 7900 sequence detection system with 100 nM primers and 20 ng of cDNA. Chemokine/receptor expression was normalized to β-actin and expressed as a relative value using the comparative threshold cycle (Ct) method ($2^{-\Delta\Delta Ct}$) according to the manufacturer's instructions. The levels of mRNA expression of genes of interest were normalized to saline control.

Measurement of CXCL5 protein expression

Mesenteric tissue of saline and IL-1β-treated (for 4 h) WT and B1KO mice was collected and homogenized and supernatants were collected. Mouse CXCL5 protein levels were determined by ELISA (Duoset; R&D Systems) according to the manufacturer's protocol. CXCL5 levels were expressed relative to total protein concentration of the supernatant samples.

HUVEC culture

HUVECs were cultured to passage 3 in EGM-2 endothelial cell medium (Cambrex/Lonza). Confluent cells were treated with vehicle (saline) or IL-1β (1 ng/ml for 0–24 h). In some experiments, the B$_1$ antagonist Lys-[-Leu^8]-des-Arg^9-BK (10 μM) was added to the medium 15 min before IL-1β treatment and the reaction was stopped after 8 h. In a further series of experiments, cells were incubated with the B$_1$ agonist Lys-des-Arg^9-BK (1–10,000 nM) for 4 h either directly or following a 24-h pretreatment with IL-1β.

Real-time quantitative RT-PCR of endothelial cells

HUVECs from the above experiments were washed with sterile PBS and collected by scraping, and samples were kept at −80°C until mRNA extraction. The human (h) CXCL5 homologues hCXCL5 and hCXCL6 and kinin B$_1$ receptor mRNA expression were determined as described above. The following primers were used: hCXCL5, 5′-GAGAGCTGCGTTGCGT TTG-3′ and 5′-TTTCCTTGTTTCCACCGTCCA-3′; hCXCL6 5′-GGTC CTGTCTCTGCTGTGC-3′ and 5′-GGGAGGCTACCACTTCCA-3′; hB$_1$ receptor, 5′-ACGCCTTCATTTTCTGCCTG-3′ and 5′-GCTGGCTCTG GTTGGAGGAT-3′; kininogen, 5′-AGACACGGCATTCAGTACTTTAA CA-3′ and 5′-TGGGCCCGTTTTACTTCATT-3′; kallikrein, 5′-GGGTCG CCACAACTTGTTTG-3′ and 5′-GCTGTAGTCCTCGTCTGCTT-3′; and GAPDH, 5′-CATGTTCGTCATGGGTGTGAA-3′ and 5′-ATGGACTG TGGTCATGAGTCCTT-3′.

Western blotting of endothelial cells

Following the treatment outlined above, cells were washed with ice-cold PBS, scraped, and lysed in ice-cold lysis buffer (20 mM Tris-HCl (pH 7.4), 50 mM NaCl, 50 mM NaF, 5 mM EDTA, and 20 mM Na$_4$P$_2$O$_7$·10H$_2$O). Supernatants were collected and protein concentration was determined by Bradford assay. Samples (20 μg) were subjected to electrophoresis using an 8% polyacrylamide gel followed by electrotransfer to a nitrocellulose membrane. To detect B$_1$ receptor, nitrocellulose were incubated with the polyclonal B$_1$ receptor Ab (A15C (16), a gift of Dr. J.-L. Bascands; dilution 1/5000) overnight at 4°C and then with a secondary peroxidase-coupled goat anti-rabbit Ab (dilution 1/2000; DakoCytomation). Visualization of bands was achieved by chemiluminescence (ECL kit; Amersham Biosciences). Selectivity of the Ab was determined by preadsorption of the Ab to its corresponding peptide at a concentration of 10 μg/ml at 4°C overnight. The autoradiographic bands were semiquantified and normalized to α-tubulin levels.
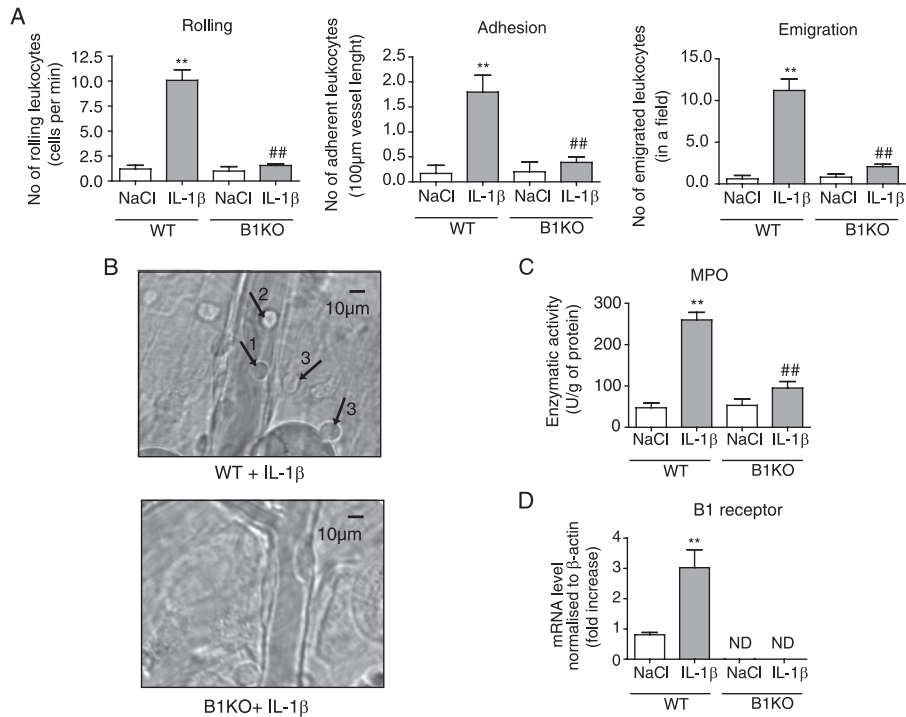
FIGURE 1. IL-1β-induced PMN recruitment is abolished in B1KO mice. *A*, Leukocyte-endothelial cell interactions in mouse mesenteric postcapillary venules in vivo in response to IL-1β (5 ng, i.p.) in WT and B1KO mice were measured by intravital microscopy. The different parameters of rolling, adhesion, and emigration of leukocytes were measured in WT and B1KO mice 4 h after treatment with saline (i.p.) or IL-1β. *B*, The arrows show rolling (point 1), adherent (point 2), and emigrated (points 3) cells. *C*, PMN accumulation was determined by measurement of MPO activity. Mesenteric tissue were removed from WT and B1KO mice 4 h following treatment with saline or IL-1β (5 ng, i.p.), and 25 ng of protein extract from each animal was used to measure MPO activity. The data are expressed as the unit of MPO per gram of total protein. *D*, The inducibility of B_1 receptor mRNA expression in mesenteric tissue in response to IL-1β (5 ng, i.p.) was assessed in WT and B1KO mice by quantitative real-time RT-PCR. The data are expressed as fold increase compared with control (WT NaCl) normalized to β-actin. Data are mean ± SEM for $n = 6$ animals per group. **, $p < 0.01$, saline vs treated values; ##, $p < 0.01$, WT vs B1KO values.

Statistical analysis

Values are given as means ± SE where n represents the number of animals or the number of experiments conducted for cells. Statistical comparisons were conducted using paired or unpaired Student's t test for two groups or one-way ANOVA for more than two groups. Differences were considered significant when $p < 0.05$.

Results

IL-1β-induced PMN recruitment is absent in B1KO mice

IL-1β caused a significant increase of mesenteric B_1 receptor mRNA expression (Fig. 1*D*) that was associated with a pronounced cellular recruitment in WT mice as indicated by the augmentation of leukocyte rolling, adhesion, and emigration (Fig. 1, *A* and *B*). All parameters of IL-1β-induced leukocyte recruitment were profoundly suppressed in B1KO mice, and this was likewise associated with a complete absence of B_1 receptor mRNA expres-

Table I. *Hemodynamic parameters in animals used for intravital microscopy studies[a]*

Genotype	Treatment	No. of Venules	Venule Diameter (μm)	Shear Rate (s⁻¹)
WT	Saline (4 h)	12	32.2 ± 3.3	254 ± 31
WT	IL-1β (4 h)	18	31.1 ± 2.9	276 ± 27
B1KO	Saline (4 h)	10	29.7 ± 4.2	235 ± 34
B1KO	IL-1β (4 h)	16	31.8 ± 3.7	287 ± 25

[a] Mice received either saline (100 μl, i.p.) or IL-1β (5 ng, i.p). Data are mean ± SEM.

sion (Fig. 1*D*). These differences were not due to changes in venular hemodynamics, because there were no significant differences in venule diameter or blood flow between WT and B1KO animals (see Table I). IL-1β-induced cellular recruitment in WT animals was associated with a ~3-fold increase in MPO activity that was markedly attenuated in B1KO mice (Fig. 1*C*).
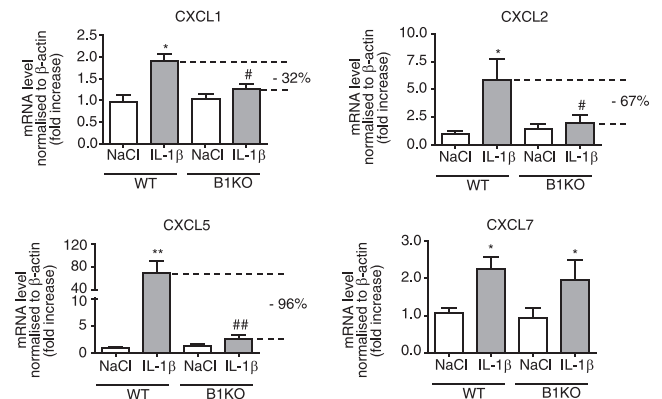

FIGURE 2. IL-1β-induced ELR-CXCL chemokine mRNA expression is attenuated in B1KO mice. mRNA expression of CXCL1, CXCL7, CXCL2, and CXCL5 was assessed using quantitative real-time RT-PCR of mesenteric tissue from WT and B1KO mice treated with saline or IL-1β (5 ng, i.p.; 2 h). The data are expressed as fold increase above control (WT NaCl) normalized to β-actin. Data shown are mean ± SEM for $n = 6$ animals per group. **, $p < 0.01$, saline vs treated values; ##, $p < 0.01$, WT vs B1KO values; *, $p < 0.05$, saline vs treated values; #, $p < 0.05$ WT vs B1KO values.
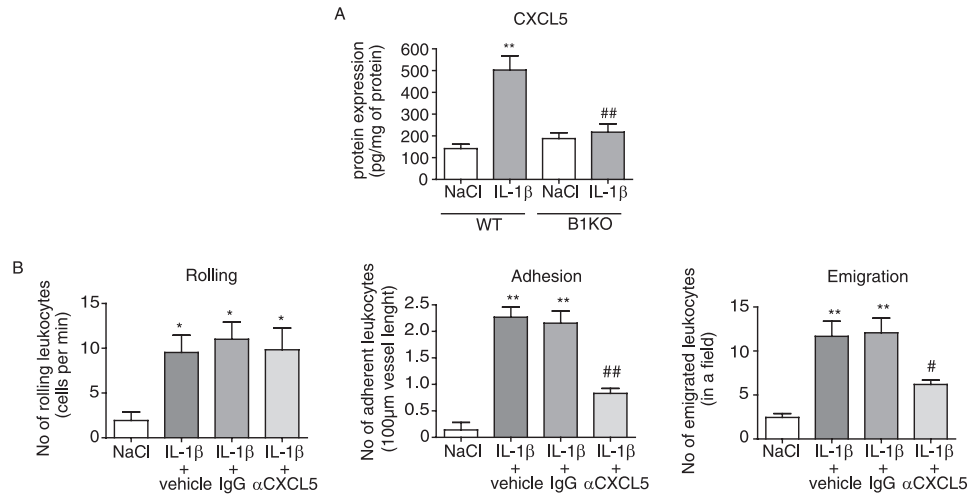
FIGURE 3. CXCL5 plays a major role in IL-1β-induced leukocyte recruitment. *A*, CXCL5 protein was measured by ELISA in mesenteric tissue removed from WT and B1KO mice 4 h after treatment with saline or IL-1β (5 ng, i.p.). The data are expressed as CXCL5 per milligram of total protein (pg/mg protein). Data shown are mean $\pm$ SEM for $n = 6$ animals per group. $**$, $p < 0.01$, saline vs treated values; ##, $p < 0.01$ WT vs B1KO values. *B*, Leukocyte-endothelial cell interactions in WT mouse mesenteric postcapillary venules were measured by intravital microscopy in vivo 4 h following treatment with IL-1β (5 ng, i.p.) in mice preinjected (30 min before IL-1β) with saline, control IgG, or anti-CXCL5 Ab (20 μg/mice, i.p.). Rolling, adhesion, and emigration of leukocytes were measured. Data shown are mean $\pm$ SEM for $n = 6$ animals per group. $**$, $p < 0.01$, saline vs treated values; ##, $p < 0.01$, WT vs treated values; $*$, $p < 0.05$, saline vs treated values; #, $p < 0.05$, WT vs treated values.

CXCL5 expression is abolished in B1KO mice

Quantitative PCR of the mesenteric tissue of IL-1β-treated WT animals revealed significant mRNA expression of the CXCL1, CXCL2, CXCL5, and CXCL7 chemokines above that measured in saline-treated controls (Fig. 2). However, this IL-1β-induced chemokine elevation was profoundly suppressed in tissues of B1KO mice with respect specifically to CXCL1 ($\sim$32% inhibition), CXCL2 ($\sim$67% inhibition), and CXCL5 (>95% inhibition). In contrast, CXCL7, which was up-regulated in WT mice, was not changed in B1KO mice.

Because CXCL5 appeared to be the most profoundly suppressed ELR-CXCL chemokine in B1KO mice (Fig. 2), we sought to as-

certain whether the changes in mRNA were reflected in protein expression. CXCL5 protein expression in the mesenteries of IL-1β-treated WT mice was substantially elevated compared with saline control (503 $\pm$ 66 pg/mg protein, $n = 6$ vs 142 $\pm$ 20 pg/mg protein, $n = 5$; $p < 0.01$ respectively). In contrast, this response to IL-1β was entirely absent in B1KO mice (218 $\pm$ 38 pg/mg protein, $n = 5$ vs 188 $\pm$ 27 pg/mg protein, $n = 6$; non significant) (Fig. 3A).

Neutralization of CXCL5 reduces IL-1β-induced leukocyte adhesion and emigration

Treatment of WT mice with a neutralizing anti-CXCL5 Ab inhibited IL-1β-induced cell adhesion and emigration by $\sim$50%, but no

FIGURE 4. Temporal relationship between endothelial kinin B$_1$ receptor, hCXCL5, hCXCL6, and kallikrein/kininogen expression in IL-β-treated endothelial cells. *A*, Time course (0, 4, 8, and 24h) of B$_1$ receptor, hCXCL5, and hCXCL6 mRNA expression in response to IL-1β (1 ng/ml) in HUVECs. Expression of B$_1$ receptor, hCXCL5, and hCXCL6 were measured by quantitative real-time RT-PCR. *B*, Protein expression of B$_1$ receptor in HUVECs after 8 h of IL-1β treatment by Western blotting. *C*, mRNA expression of kininogen and kallikrein in HUVECs after 4 h of IL-1β treatment was measured by quantitative real-time RT-PCR. The data are expressed as the fold increase above control (ctl; nontreated cells) normalized to GAPDH for mRNA and to tubulin for protein. Data shown are mean $\pm$ SEM for $n = 4$. $*$, $p < 0.05$, control vs treated values; $**$, $p < 0.01$, control vs treated values.
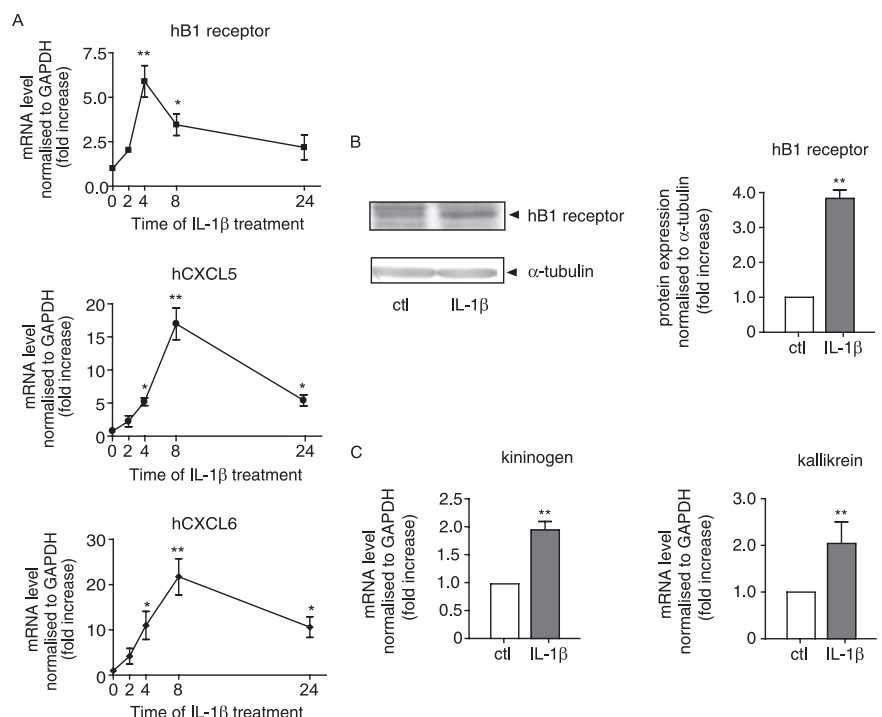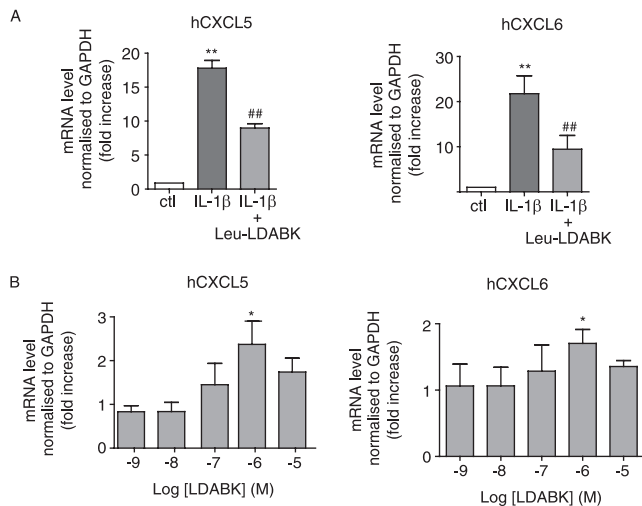
FIGURE 5. Kinin B_1 receptor-induced hCXCL5 and hCXCL6 expression in HUVEC. *A*, Effect of B_1 antagonist (Lys-[Leu^8]-des-Arg^9-BK at 10 μM;15-min pretreatment at $t = 0$) on IL-1β (1 ng/ml, 8 h)-induced hCXCL5 and hCXCL6 mRNA expression in HUVECs. *B*, Effect of B_1 agonist (Lys-des-Arg^9-BK, 4 h; 1–10,000 nM) on hCXCL5 and hCXCL6 mRNA expression. The data are expressed as the fold increase above control (ctl; nontreated cells) normalized to GAPDH for mRNA. Data are mean $\pm$ SEM for $n = 4$. **, $p < 0.01$, saline vs treated values; *, $p < 0.05$, saline vs treated values; ##, $p < 0.01$, IL-1β vs IL-1β plus Lys-[Leu^8]-des-Arg^9-BK values.

significant effect on cell rolling was observed at the 4-h time point (Fig. 3*B*). In contrast, control rabbit IgG had no significant effect on leukocyte recruitment.

Human CXCL5 homologues are regulated by B_1 receptor in human endothelial cells

Because previous evidence suggests that endothelial cells express B_1 receptor following exposure to inflammatory stimuli (5, 17–19) and because the endothelial cell is an important cellular source of chemoattractant (20–22), we investigated whether the endothelial cell might be an in vivo source of B_1 receptor-induced chemokine production. In HUVEC, kinin B_1 receptor mRNA was induced within 2 h of IL-1β treatment, peaked at 4 h ($\sim$5-fold increase), and remained significantly elevated at 8 h, returning to near basal levels by 24 h (Fig. 4*A*). This IL-1β-induced change in mRNA was associated with increases in kinin B_1 receptor protein expression (Fig. 4*B*). We also observed that IL-1β treatment induced an increase in the expression of the components of the kallikrein-kinin system, with an elevation in the levels of both kallikrein and kininogen (Fig. 4*C*). Basal levels of chemokines were low in unstimulated HUVECs; however, treatment with IL-1β caused a time-dependent increase in hCXCL5 homologue (hCXCL5 and hCXCL6) mRNA expression, peaking at 8 h but with a lag time of 2–4 h relative to kinin B_1 receptor expression (Fig. 4*A*). B_1 receptor blockade significantly suppressed IL-1β-induced hCXCL5 and hCXCL6 expression at the 8 h time point by $\sim$50% (Fig. 5*A*). Treatment of cells with a B_1 agonist produced concentration-dependent increases in hCXCL5 and hCXCL6 expression (Fig. 5*B*) in control cells. In addition, in cells pretreated with IL-1β for 24 h the application of a B_1 agonist produced a further 1.3 ± 0.07-fold increase ($n = 4$; $p < 0.05$, t test compared with IL-1β alone) in hCXCL5 expression above that induced by IL-1β alone.

Discussion

We have previously demonstrated that the kinin B_1 receptor plays an important role in mediating the recruitment of PMNs to a site of inflammation (4, 5), a finding that was supported by the recent observation that cell-dependent inflammation is reduced in B1KO mice (10). However, the exact mechanisms involved in this response were unclear. Our findings, in this report, support the thesis that B_1 receptor activation is essential for IL-1β-driven cell recruitment and, moreover, that neutrophil chemoattractant chemokines belonging to the ELR-CXCL family, most notably CXCL5, mediate this effect. In addition, we have established that the induction and subsequent endogenous activation of kinin B_1 receptors on endothelial cells is likely to play a major role in B_1 receptor-induced CXCL5 expression.

Treatment of WT mice with IL-1β induced a substantial elevation of mesenteric B_1 receptor mRNA expression. These observations are in accordance with our previous findings demonstrating low levels of B_1 receptor mRNA expression in control untreated murine mesenteric tissue but profound induction of expression following exposure to inflammatory stimuli (5). In contrast, no B_1 receptor mRNA expression was evident in the mesenteries of B1KO mice, either in the controls or following cytokine treatment. This absence of B_1 receptor expression in B1KO mice had a major impact on the magnitude of the inflammatory response to IL-1β treatment. Indeed, whereas in WT animals IL-1β produced a characteristic increase in leukocyte recruitment, in B1KO mice this response was abolished, an effect that was not due to inherent differences in venular hemodynamics because all hemodynamic parameters were similar between the two genotypes. We chose to use the mesenteric preparation with a 4-h IL-1β treatment because we have previously established that the B_1 receptor plays a major role in mediating leukocyte recruitment in the mouse mesentery at this time point and that this is associated with B_1 receptor mRNA expression (5). That the B_1 receptor is essential in this response is, of itself, an important observation because IL-1β is a pivotal regulator of cell activation in acute inflammation (23–25). It would be of interest to determine whether this phenomenon extends to other preparations of intravital microscopy, including the cremaster microcirculation.

The near abolition of cell recruitment in B1KO mice also suggests that our previous estimate of the magnitude of the kinin B_1 receptor-mediated component (using B_1 receptor antagonists) of the cell recruitment response to IL-1β, in the order of 50%, was a substantial underestimate (4, 5). This may have been due to the fact that the antagonists, des-Arg^9-[Leu^8]-BK and des-Arg^{10}-Hoe140, are peptidic in nature and therefore prone to degradation and express partial agonist activity (7, 8). Antagonists displaying no partial agonist activity and resistance to degradation, such as SSR240612 (26) or compound 11 (27), are likely to prove highly effective at inhibiting PMN recruitment. The essential role of the kinin B_1 receptor in leukocyte recruitment is highlighted by the observation that no compensatory mechanisms are activated in B1KO mice to maintain the inflammatory response to IL-1β. Our data also suggests that inhibition of leukocyte recruitment is likely to play a major role in the apparent protection afforded by the absence of the B_1 receptor in experimental models of inflammatory disease in B1KO mice, including diabetes (28), neuropathic pain (29), inflammatory hyperalgesia (10), and intestinal ischemia/reperfusion injury (30).

The innate immune response is a tightly orchestrated sequence of events; each stage is associated with the recruitment of a specific inflammatory cell type to the site of inflammation. The exact cell type recruited at each stage is determined by the sensitivity to and activity of distinct chemotactic factors (13). PMN recruitment is specifically dependent on the activity of ELR-CXCL chemokines. To date, four ELR-CXCL chemokines have been described in mice: CXCL1, CXCL2, CXCL5, and CXCL7 (also called KC,

MIP2, LIX, and NAP2, respectively) (31, 32). In the mouse, the ELR-CXCL chemokines bind to the chemokine receptor CXCR2, present on the neutrophil cell surface, to mediate cell migration (33). More recently, the mouse CXCR1 has been cloned (34); however, although the human chemokine hCXCL8 (also known as IL-8) binds this receptor, no specific endogenous murine chemokine ligand has been identified. IL-1β treatment of WT mice was associated with enhanced expression of all four murine of the CXCL chemokines measured. Moreover, our studies exposed a temporal and sequential relationship between kinin B$_1$ receptor expression, chemokine production, and cell recruitment. In contrast, the absence of cell recruitment in B1KO mice was associated with almost complete abrogation of IL-1β-induced transcription of CXCL5 and substantial inhibition of CXCL1 and CXCL2 expression with no effect on CXCL7 expression. The association between B$_1$ receptor activation and CXCL chemokine production is supported by previous work, albeit in different cells and with a different chemokine, where B$_1$ receptor activation of human fibroblasts stimulated hCXCL8 production (35).

Of the chemokines linked to B$_1$ receptor activation, CXCL5 appears to be the most closely associated because its production in B1KO mice was almost abolished, suggesting that perhaps it is this chemokine that predominantly mediates the effects of B$_1$ receptor activation. This is in accordance with previous publications identifying CXCL5 as the primary chemotactic agent underlying neutrophil recruitment in models of inflammatory disease, including myocardial ischemia-reperfusion injury (36), sepsis (37), and colitis (38). Indeed, in the present study we demonstrated that although basal levels of CXCL5 mRNA are very low in WT animals, IL-1β treatment causes a $\sim$70-fold increase in expression, a response inhibited by >95% in B1KO mice. This elevation in mRNA was associated with increases in protein expression that were likewise abolished in B1KO mice as evidenced by the measurement of CXCL5 by ELISA. The observation that the neutralizing Ab to CXCL5 significantly attenuated leukocyte recruitment to IL-1β supports the thesis that CXCL5 plays a major role in mediating the cellular response. However, the lack of effect of the Ab on leukocyte rolling suggests that perhaps the role of CXCL5 is centered on the adhesion and emigration steps of leukocyte recruitment. It is important to note, however, that although the CXCL5 Ab did not affect leukocyte rolling, IL-1β-induced rolling was abolished in B1KO mice. These findings suggest that B$_1$ receptor activation results in the stimulation of other pathways involved in cell rolling that are unrelated to chemokine synthesis. An obvious pathway that is likely to be implicated is the adhesion molecule pathway, specifically either at the level of the endothelial cell (such as P-selectin) or on the neutrophil itself (such as L-selectin). Further studies investigating this possibility are warranted to clarify this issue.

CXCL5, also called LIX in mice (39), is expressed in humans as ENA-78 (hCXCL5) and is also closely related to another human chemokine, GCP-2 (hCXCL6) (40). Indeed, it has been proposed that the human hCXCL5 and hCXCL6 genes are the result of an evolutionary gene duplication (40). CXCL5 was first cloned in mouse fibroblasts (39) and was subsequently shown to be expressed in a number of different tissues (31) in response to inflammatory cytokines, particularly IL-1β (20, 36). Because our previous studies excluded the possibility that B$_1$ receptor-induced cell recruitment is due to the direct activation of B$_1$ receptors on neutrophils (4), we hypothesized that the endothelial cell might be an important cellular source of B$_1$ receptor-induced CXCL5 production. However, in contrast to this thesis a recent publication has demonstrated that the direct activation of neutrophil B$_1$ receptors does cause neutrophil migration (41). This response was only ev-

ident in IL-1β pretreated cells in vitro and required a 24-h exposure to the B$_1$ agonist. Because we have shown that the B$_1$ receptor-dependent IL-1β-induced leukocyte recruitment response in vivo is evident after 2 h and peaks at 4 h (4, 5), it is unlikely that the slowly developing direct activation of neutrophil B$_1$ receptors contributes to the response evident in the current study. It is possible, however, that at later stages of the inflammatory response the direct activation of neutrophilic B$_1$ receptor may have a role to play in the ensuing activation of these cells.

The endothelial cell plays a major role in all steps of the neutrophil recruitment process (42), and endothelial cells are a major source of chemoattractant CXCL5 in mice (20), a characteristic also shared by human endothelial cells (21, 22). Analysis of HUVECs in the present study demonstrate that human endothelial cells express the B$_1$ receptor, as has been demonstrated previously (17, 19). In addition, like others (18, 43) we have shown that the elements of the kallikrein-kinin system necessary for endogenous B$_1$ agonist production are also present in these cells basally i.e., kallikrein and kininogen. However, we now also demonstrate that, following cytokine treatment, the expression of these factors is elevated in parallel with the elevation in expression of the B$_1$ receptor. These findings intimate that endogenous endothelial B$_1$ receptor activation might support the chemokine production evidenced in vivo.

Indeed, the treatment of human endothelial cells with IL-1β stimulated a time-dependent increase in B$_1$ receptor expression that was subsequently followed by a pronounced stimulation of hCXCL5 and hCXCL6 expression. This chemokine synthesis was likely to be a consequence of B$_1$ receptor activation, because the treatment of cells with the B$_1$ antagonist, Lys-[-Leu^8]-des-Arg^9-BK, significantly reduced this response. Moreover, this finding is supported by the observation that the treatment of endothelial cells with a B$_1$ agonist stimulated a concentration-dependent increase in hCXCL5 and hCXCL6 expression. The level of this enhanced expression, while significant, was at least 10-fold lower than that evident in vivo. This lower level of induction may have been related to the level of basal B$_1$ receptor expression in cells not stimulated with cytokine. Therefore, we investigated the activity of the B$_1$ agonist in IL-1β-treated cells. The relative increase in chemokine expression in B$_1$ agonist-treated cells vs cytokine-only treated cells, surprisingly, appeared similar to that in unstimulated cells. However, it is important to note that the 24 h following IL-1β-treatment chemokine expression is still significantly elevated and, therefore, the absolute potential for enhancement likely to be reduced. An alternative explanation for this apparent decreased potency in inducing chemokine expression in vitro over in vivo is simply that endothelial B$_1$ receptor activity synergizes/interacts with a blood-borne factor not present in these in vitro experiments. Finally, although it is clear that the endothelial cell is a major source of B$_1$-induced CXCL5/CXCL6, we cannot exclude the possibility that other cell types within the vasculature might also be sources of this B$_1$-induced chemokine production. In particular, both the fibroblast (44) and the mast cell (45) are cellular sources of CXCL5 and are cells that also express the B$_1$ receptor (7, 46).

The molecular mechanisms involved in this B$_1$ receptor-induced chemokine expression are uncertain; however, the transcription factor NF-κB, a pivotal transcriptional factor regulating inflammatory gene expression (47), has been identified as playing an essential role in IL-1β-induced hCXCL5 (48) or hCXCL6 (49) expression in human nonvascular cell types. Similarly, NFκB plays an essential role in mediating IL-1β-induced CXCL5 expression in mice (20). This regulation by NF-κB is of interest because B$_1$ receptor expression itself is also tightly regulated by a NF-κB-dependent pathway (16). This group demonstrated that

the application of a B_1 agonist to human fibroblasts enhanced B_1 receptor expression as a consequence of NF-κB activation, auto-regulation that is more pronounced in the presence of IL-1β (35). In addition, B_1 receptor activation itself also stimulates further IL-1β synthesis (50), suggesting a complex facilitatory interaction between the B_1 receptor and IL-1β that may play an important role in amplification of the inflammatory response especially because the kallikrein-kinin pathway is up-regulated at inflammatory sites, increasing endogenous B_1 agonist production (51). Together, these studies suggest that, during an inflammation following the initial induction of the kinin B_1 receptor by the appropriate inflammatory stimulus, the pathway may be continuously self-amplified to sustain the inflammatory response.

In summary, although the B_1 receptor has been proposed to play a role in inflammatory pathologies (7, 8, 10), its exact contribution to the inflammatory process has been uncertain. The findings from this study have allowed clarification of the key role of the kinin B_1 receptor in neutrophil recruitment at sites of inflammation and have determined that CXCL5 production plays a major role in this response. Moreover, endothelial cells have been described as a potential source for this novel B_1 receptor-CXCL5 pathway. These results, taken together with the observations that B_1 receptor expression is induced by inflammation in different diseases, endogenous B_1 agonist concentration increases at sites of inflammation, and B_1 receptor activation causes a range of cellular proinflammatory effects, highlights the B_1 receptor and, in particular, this novel B_1 receptor-CXCL5 pathway as potential therapeutic targets for inflammatory disease.

Disclosures

The authors have no financial conflict of interest.

References

1. Luster, A. D., R. Alon, and U. H. von Andrian. 2005. Immune cell migration in inflammation: present and future therapeutic targets. *Nat. Immunol.* 6: 1182–1190.
2. Brown, K. A., S. D. Brain, J. D. Pearson, J. D. Edgeworth, S. M. Lewis, and D. F. Treacher. 2006. Neutrophils in development of multiple organ failure in sepsis. *Lancet* 368: 157–169.
3. Tedgui, A., and Z. Mallat. 2006. Cytokines in atherosclerosis: pathogenic and regulatory pathways. *Physiol. Rev.* 86: 515–581.
4. Ahluwalia, A., and M. Perretti. 1996. Involvement of bradykinin B_1 receptors in the polymorphonuclear leukocyte accumulation induced by IL-1 β in vivo in the mouse. *J. Immunol.* 156: 269–274.
5. McLean, P. G., A. Ahluwalia, and M. Perretti. 2000. Association between kinin B_1 receptor expression and leukocyte trafficking across mouse mesenteric post-capillary venules. *J. Exp. Med.* 192: 367–380.
6. Marceau, F., J. F. Hess, and D. R. Bachvarov. 1998. The B_1 receptors for kinins. *Pharmacol. Rev.* 50: 357–386.
7. Leeb-Lundberg, L. M., F. Marceau, W. Muller-Esterl, D. J. Pettibone, and B. L. Zuraw. 2005. International union of pharmacology, XLV, classification of the kinin receptor family: from molecular mechanisms to pathophysiological consequences. *Pharmacol. Rev.* 57: 27–77.
8. Marceau, F., and D. Regoli. 2004. Bradykinin receptor ligands: therapeutic perspectives. *Nat. Rev. Drug Discov.* 3: 845–852.
9. Zhou, X., P. Polgar, and L. Taylor. 1998. Roles for interleukin-1β, phorbol ester and a post-transcriptional regulator in the control of bradykinin B_1 receptor gene expression. *Biochem. J.* 330: 361–366.
10. Pesquero, J. B., R. C. Araujo, P. A. Heppenstall, C. L. Stucky, J. A. Silva, Jr., T. Walther, S. M. Oliveira, J. L. Pesquero, A. C. Paiva, J. B. Calixto, et al. 2000. Hypoalgesia and altered inflammatory responses in mice lacking kinin B_1 receptors. *Proc. Natl. Acad. Sci. USA* 97: 8140–8145.
11. Goebeler, M., T. Yoshimura, A. Toksoy, U. Ritter, E. B. Brocker, and R. Gillitzer. 1997. The chemokine repertoire of human dermal microvascular endothelial cells and its regulation by inflammatory cytokines. *J. Invest. Dermatol.* 108: 445–451.
12. Zlotnik, A., and O. Yoshie. 2000. Chemokines: a new classification system and their role in immunity. *Immunity* 12: 121–127.
13. Lukacs, N. W., C. Hogaboam, E. Campbell, and S. L. Kunkel. 1999. Chemokines: function, regulation, and alteration of inflammatory responses. *Chem. Immunol.* 72: 102–120.
14. Mullane, K. M., R. Kraemer, and B. Smith. 1985. Myeloperoxidase activity as a quantitative assessment of neutrophil infiltration into ischemic myocardium. *J. Pharmacol. Methods* 14: 157–167.
15. Cuzzocrea, S., A. Tailor, B. Zingarelli, A. L. Salzman, R. J. Flower, C. Szabo, and M. Perretti. 1997. Lipocortin 1 protects against splanchnic artery occlusion and reperfusion injury by affecting neutrophil migration. *J. Immunol.* 159: 5089–5097.
16. Schanstra, J. P., E. Bataille, M. E. Marin Castano, Y. Barascud, C. Hirtz, J. B. Pesquero, C. Pecher, F. Gauthier, J. P. Girolami, and J. L. Bascands. 1998. The B_1-agonist des-Arg^{10}-kallidin activates transcription factor NF-κB and induces homologous up-regulation of the bradykinin B_1-receptor in cultured human lung fibroblasts. *J. Clin. Invest.* 101: 2080–2091.
17. Wohlfart, P., J. Dedio, K. Wirth, B. A. Scholkens, and G. Wiemer. 1997. Different B1 kinin receptor expression and pharmacology in endothelial cells of different origins and species. *J. Pharmacol. Exp. Ther.* 280: 1109–1116.
18. Yayama, K., N. Kunimatsu, Y. Teranishi, M. Takano, and H. Okamoto. 2003. Tissue kallikrein is synthesized and secreted by human vascular endothelial cells. *Biochim. Biophys. Acta* 1593: 231–238.
19. McLean, P. G., M. Perretti, and A. Ahluwalia. 2000. Kinin B_1 receptors and the cardiovascular system: regulation of expression and function. *Cardiovasc. Res.* 48: 194–210.
20. Chandrasekar, B., P. C. Melby, H. M. Sarau, M. Raveendran, R. P. Perla, F. M. Marelli-Berg, N. O. Dulin, and I. S. Singh. 2003. Chemokine-cytokine cross-talk: the ELR$^+$CXC chemokine LIX (CXCL5) amplifies a proinflammatory cytokine response via a phosphatidylinositol 3-kinase-NF-κB pathway. *J. Biol. Chem.* 278: 4675–4686.
21. Imaizumi, T., K. H. Albertine, D. L. Jicha, T. M. McIntyre, S. M. Prescott, and G. A. Zimmerman. 1997. Human endothelial cells synthesize ENA-78: relationship to IL-8 and to signaling of PMN adhesion. *Am. J. Respir. Cell Mol. Biol.* 17: 181–192.
22. Beck, G. C., B. A. Yard, A. J. Breedijk, K. Van Ackern, and F. J. Van Der Woude. 1999. Release of CXC-chemokines by human lung microvascular endothelial cells (LMVEC) compared with macrovascular umbilical vein endothelial cells. *Clin. Exp. Immunol.* 118: 298–303.
23. Dinarello, C. A. 2000. The role of the interleukin-1-receptor antagonist in blocking inflammation mediated by interleukin-1. *N. Engl. J. Med.* 343: 732–734.
24. Dinarello, C. A. 2004. Therapeutic strategies to reduce IL-1 activity in treating local and systemic inflammation. *Curr. Opin. Pharmacol.* 4: 378–385.
25. Dinarello, C. A., and S. M. Wolff. 1993. The role of interleukin-1 in disease. *N. Engl. J. Med.* 328: 106–113.
26. Gougat, J., B. Ferrari, L. Sarran, C. Planchenault, M. Poncelet, J. Maruani, R. Alonso, A. Cudennec, T. Croci, F. Guagnini, et al. 2004. SSR240612 [(2R)-2-[((3R)-3-(1,3-benzodioxol-5-yl)-3-[(6-methoxy-2-naphthyl)sulfonyl]amino] propanoyl)amino]-3-(4-[2R,6S)-2,6-dimethylpiperidinyl]methyl]phenyl)-*N*-isopropyl-*N*-methylpropanamide hydrochloride], a new nonpeptide antagonist of the bradykinin B_1 receptor: biochemical and pharmacological characterization. *J. Pharmacol. Exp. Ther.* 309: 661–669.
27. Su, D. S., M. K. Markowitz, R. M. DiPardo, K. L. Murphy, C. M. Harrell, S. S. O'Malley, R. W. Ransom, R. S. Chang, S. Ha, F. J. Hess, et al. 2003. Discovery of a potent, nonpeptide bradykinin B_1 receptor antagonist. *J. Am. Chem. Soc.* 125: 7516–7517.
28. Gabra, B. H., N. Berthiaume, P. Sirois, F. Nantel, and B. Battistini. 2006. The kinin system mediates hyperalgesia through the inducible bradykinin B_1 receptor subtype: evidence in various experimental animal models of type 1 and type 2 diabetic neuropathy. *Biol. Chem.* 387: 127–143.
29. Ferreira, J., A. Beirith, M. A. Mori, R. C. Araujo, M. Bader, J. B. Pesquero, and J. B. Calixto. 2005. Reduced nerve injury-induced neuropathic pain in kinin B_1 receptor knock-out mice. *J. Neurosci.* 25: 2405–2412.
30. Souza, D. G., E. S. Lomez, V. Pinho, J. B. Pesquero, M. Bader, J. L. Pesquero, and M. M. Teixeira. 2004. Role of bradykinin B_2 and B_1 receptors in the local, remote, and systemic inflammatory responses that follow intestinal ischemia and reperfusion injury. *J. Immunol.* 172: 2542–2548.
31. Rovai, L. E., H. R. Herschman, and J. B. Smith. 1998. The murine neutrophil-chemoattractant chemokines LIX, KC, and MIP-2 have distinct induction kinetics, tissue distributions, and tissue-specific sensitivities to glucocorticoid regulation in endotoxemia. *J. Leukocyte Biol.* 64: 494–502.
32. Oda, M., H. Haruta, M. Nagao, and Y. Nagata. 2002. Isolation and characterization of mouse homolog of the neutrophil activating peptide-2. *Biochem. Biophys. Res. Comm.* 290: 865–868.
33. Zhang, X. W., Q. Liu, Y. Wang, and H. Thorlacius. 2001. CXC chemokines, MIP-2, and KC induce P-selectin-dependent neutrophil rolling and extravascular migration in vivo. *Br. J. Pharmacol.* 133: 413–421.
34. Fu, W., Y. Zhang, J. Zhang, and W. F. Chen. 2005. Cloning and characterization of mouse homolog of the CXC chemokine receptor CXCR1. *Cytokine* 31: 9–17.
35. Phagoo, S. B., S. Poole, and L. M. Leeb-Lundberg. 1999. Autoregulation of bradykinin receptors: agonists in the presence of interleukin-1β shift the repertoire of receptor subtypes from B_2 to B_1 in human lung fibroblasts. *Mol. Pharmacol.* 56: 325–333.
36. Chandrasekar, B., J. B. Smith, and G. L. Freeman. 2001. Ischemia-reperfusion of rat myocardium activates NF-κB and induces neutrophil infiltration via lipopolysaccharide-induced CXC chemokine. *Circulation* 103: 2296–2302.
37. Madorin, W. S., T. Rui, N. Sugimoto, O. Handa, G. Cepinskas, and P. R. Kvietys. 2004. Cardiac myocytes activated by septic plasma promote neutrophil transendothelial migration: role of platelet-activating factor and the chemokines LIX and KC. *Circ. Res.* 94: 944–951.
38. Kwon, J. H., A. C. Keates, P. M. Anton, M. Botero, J. D. Goldsmith, and C. P. Kelly. 2005. Topical antisense oligonucleotide therapy against LIX, an enterocyte-expressed CXC chemokine, reduces murine colitis. *Am. J. Physiol.* 289: G1075–G1083.
39. Smith, J. B., and H. R. Herschman. 1995. Glucocorticoid-attenuated response genes encode intercellular mediators, including a new CXC chemokine. *J. Biol. Chem.* 270: 16756–16765.

40. Smith, J. B., L. E. Rovai, and H. R. Herschman. 1997. Sequence similarities of a subgroup of CXC chemokines related to murine LIX: implications for the interpretation of evolutionary relationships among chemokines. *J. Leukocyte Biol.* 62: 598–603.

41. Ehrenfeld, P., C. Millan, C. E. Matus, J. E. Figueroa, R. A. Burgos, F. Nualart, K. D. Bhoola, and C. D. Figueroa. 2006. Activation of kinin B$_1$ receptors induces chemotaxis of human neutrophils. *J. Leukocyte Biol.* 80: 117–124.

42. McIntyre, T. M., S. M. Prescott, A. S. Weyrich, and G. A. Zimmerman. 2003. Cell-cell interactions: leukocyte-endothelial interactions. *Curr. Opin. Hematol.* 10: 150–158.

43. Nolly, H., and A. Nolly. 1998. Release of endothelial-derived kallikrein, kininogen, and kinins. *Biol. Res.* 31: 169–174.

44. Lafontant, P. J., A. R. Burns, E. Donnachie, S. B. Haudek, C. W. Smith, and M. L. Entman. 2006. Oncostatin M differentially regulates CXC chemokines in mouse cardiac fibroblasts. *Am. J. Physiol.* 291: C18–C26.

45. Lukacs, N. W., C. M. Hogaboam, S. L. Kunkel, S. W. Chensue, M. D. Burdick, H. L. Evanoff, and R. M. Strieter. 1998. Mast cells produce ENA-78, which can function as a potent neutrophil chemoattractant during allergic airway inflammation. *J. Leukocyte Biol.* 63: 746–751.

46. Dlamini, Z., and K. D. Bhoola. 2005. Up-regulation of tissue kallikrein, kinin B$_1$ receptor, and kinin B$_2$ receptor in mast and giant cells infiltrating oesophageal squamous cell carcinoma. *J. Clin. Pathol.* 58: 915–922.

47. Pahl, H. L. 1999. Activators and target genes of Rel/NF-κB transcription factors. *Oncogene* 18: 6853–6866.

48. Catley, M. C., M. B. Sukkar, K. F. Chung, B. Jaffee, S. M. Liao, A. J. Coyle, el-B. Haddad, P. J. Barnes, and R. Newton. 2006. Validation of the anti-inflammatory properties of small-molecule IκB Kinase (IKK)-2 inhibitors by comparison with adenoviral-mediated delivery of dominant-negative IKK1 and IKK2 in human airways smooth muscle. *Mol. Pharmacol.* 70: 697–705.

49. Zhu, Y. M., S. M. Bagstaff, and P. J. Woll. 2006. Production and up-regulation of granulocyte chemotactic protein-2/CXCL6 by IL-1β and hypoxia in small cell lung cancer. *Br. J. Cancer* 94: 1936–1941.

50. Tiffany, C. W., and R. M. Burch. 1989. Bradykinin stimulates tumor necrosis factor and interleukin-1 release from macrophages. *FEBS Lett.* 247: 189–192.

51. Schremmer-Danninger, E., A. Offner, M. Siebeck, and A. A. Roscher. 1998. B$_1$ bradykinin receptors and carboxypeptidase M are both up-regulated in the aorta of pigs after LPS infusion. *Biochem. Biophys. Res. Comm.* 243: 246–252.

6.2   Laminar shear stress regulates endothelial kinin B1 receptor expression and function: potential implication in atherogenesis.

44

Duchene J, Cayla C, Vessillier S, Scotland R, Yamashiro K, Lecomte F, Syed I, Vo P, Marrelli A, Pitzalis C, Cipollone F, Schanstra J, Bascands JL, Hobbs AJ, Perretti M, Ahluwalia A.

Laminar Shear Stress Regulates Endothelial Kinin B1 Receptor Expression and Function
Potential Implication in Atherogenesis

Johan Duchene, Cécile Cayla, Sandrine Vessillier, Ramona Scotland, Kazuo Yamashiro,
Florence Lecomte, Irfan Syed, Phuong Vo, Alessandra Marrelli, Costantino Pitzalis,
Francesco Cipollone, Joost Schanstra, Jean-Loup Bascands, Adrian J. Hobbs,
Mauro Perretti, Amrita Ahluwalia

Objective—The proinflammatory phenotype induced by low laminar shear stress (LSS) is implicated in atherogenesis. The kinin B1 receptor (B1R), known to be induced by inflammatory stimuli, exerts many proinflammatory effects including vasodilatation and leukocyte recruitment. We investigated whether low LSS is a stimulus for endothelial B1R expression and function.

Methods and Results—Human and mouse atherosclerotic plaques expressed high level of B1R mRNA and protein. In addition, B1R expression was upregulated in the aortic arch (low LSS region) of ApoE$^{-/-}$ mice fed a high-fat diet compared to vascular regions of high LSS and animals fed normal chow. Of interest, a greater expression of B1R was noticed in endothelial cells from regions of low LSS in aortic arch of ApoE$^{-/-}$ mice. B1R was also upregulated in human umbilical vein endothelial cells (HUVECs) exposed to low LSS (0 to 2 dyn/cm^2) compared to physiological LSS (6 to 10 dyn/cm^2): an effect similarly evident in murine vascular tissue perfused ex vivo. Functionally, B1R activation increased prostaglandin and CXCL5 expression in cells exposed to low, but not physiological, LSS. IL-1β and ox-LDL induced B1R expression and function in HUVECs, a response substantially enhanced under low LSS conditions and inhibited by blockade of NFκB activation.

Conclusion—Herein, we show that LSS is a major determinant of functional B1R expression in endothelium. Furthermore, whereas physiological high LSS is a powerful repressor of this inflammatory receptor, low LSS at sites of atheroma is associated with substantial upregulation, identifying this receptor as a potential therapeutic target. (*Arterioscler Thromb Vasc Biol*. 2009;29:1757-1763.)

Key Words: atherosclerosis ■ laminar shear stress ■ inflammation ■ kinin B1 receptor

Cardiovascular disease (CVD) is the leading cause of death in developed countries with a major component of these deaths directly related to the consequences of atherogenesis (according to WHO statistics, 17 million people die of CVD each year, http://www.who.int). The past two decades has seen a growing appreciation that inflammatory mechanisms underlie the initiation and progressive development of an atheroma, and it is clear that the inner lining of the blood vessel wall, the endothelium, is a pivotal site at which these inflammatory events occur.[1] In particular, there is recognition that alteration of the phenotype of the endothelium, from protective (and maintaining homeostasis) to damaging, is likely to precipitate the atherogenic process.[2]

One of the major determinants of endothelial phenotype is laminar shear stress (LSS), defined as the frictional force engendered by blood flow on the endothelium. Indeed, variation in LSS has been identified as determining susceptibility of particular vascular sites to atheroma formation[2–4] and has been proposed to predominate above sex and dietary fat as a risk factor for atherosclerosis.[5,6] The levels of LSS vary throughout the circulation, however in large arteries (such as the aorta) the net unidirectional physiological levels of LSS are high (6 to 20 dyn/cm^2 in conduit vessels) and endow the endothelium with an antiinflammatory phenotype, whereas low LSS (<4 dyn/cm^2) levels found at sites of atheroma formation (ie, at

bifurcations and curvatures such as the aortic arch) is thought to be proinflammatory and pathogenic in atherosclerosis.[2] However, the exact mechanisms stimulated by LSS that predispose a site to atheroma formation remain unclear.

Of particular relevance to the present study has been the finding that an inducible and proinflammatory G protein–coupled receptor (GPCR), the kinin B1 receptor (B1R), is localized to sites of human aortic atheroma,[7] although the functional significance of this expression has not been explored. The kinins are a family of inflammatory peptides, including bradykinin (BK) or Lys-BK and their metabolites, des-Arg^{9}BK (DBK) and Lys-DBK (LDBK), that interact with 2 specific GPCRs: B1 receptor (B1R) and B2 receptor.[8] Whereas the B2R, activated by BK and Lys-BK, is constitutively expressed, the B1R, activated by DBK or Lys-DBK, is weakly expressed normally but is induced under inflammatory conditions.[8] Functionally, B1R activation induces a number of proinflammatory effects, therefore we investigated whether low (atherogenic) LSS might be a stimulus for B1R expression and inflammatory function in the blood vessel wall; these data were complemented by an analysis of the mechanisms involved in endothelial B1R expression and function in atherosclerosis.

Materials and Methods

Full details of all methods can be found in the supplemental materials (available online at http://atvb.ahajournals.org).

Cell Culture and Application of Shear Stress

Steady unidirectional LSS of 10, 6, 2, or 0 dyn/cm^2 was applied on human umbilical vein (HUVECs) or aortic (HAECs) endothelial cells using a cone and plate viscometer.[9,10] Cells were left untreated or treated with B1R agonist (Lys-des-Arg^9-BK; 10 μMol/L), IL-1β (10 ng/mL) or with oxidized LDL (oxLDL, 20 μg/mL[12–14]) in the absence or presence of the B1R antagonist SSR240612[11] (1 μMol/L: 15 minutes before IL-1β application) or with the NFκB inhibitor BAY 11-7082[15] (20 μMol/L: 15 minutes before IL-1β application).

Perfused Mouse Mesentery Preparations

The mesentery was mounted in a 37°C water-jacketed organ bath and perfused with warmed physiological salt solution with varying amounts of dextran to achieve high (6 dyn/cm^2) or low (2 dyn/cm^2) levels of LSS.

Atherosclerosis in ApoE$^{-/-}$ Mice

Male atherosclerosis-prone ApoE$^{-/-}$ mice were fed a high-fat or chow diet. The whole aorta was removed, and in some instances the aortic arch separated from the thoracic aorta for separate analysis of regions subjected to low LSS and high physiological LSS, respectively. Blood was collected for lipid analysis.

Immunohistochemical Analysis

The aortic arches of ApoE$^{-/-}$ mice were embedded in paraffin and immunohistochemistry analysis performed.

Prostaglandin and Nitric Oxide Measurement in Endothelial Cell Culture Supernatant

Concentrations of prostaglandin (PG)I$_2$ and PGE$_2$ were measured using enzyme immunoassay kits. Nitrite production, as a measure of endothelial NO generation, was measured as previously described.[16]
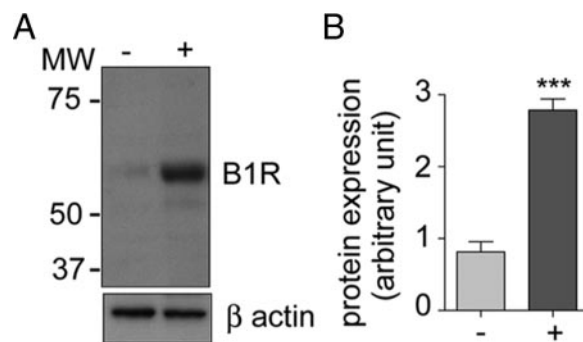

Figure 1. B1 receptor is induced in regions of atheroma in humans. A, Representative Western blot of B1R protein expression in human carotid endarterectomy tissue: sections: with (+; n=4) or without (−; n=4) plaque. B, Quantification of B1R expression normalized to β-actin. Data are shown as mean±SEM. ***$P<0.001$.

Quantitative Real-Time PCR

Total RNA was extracted from cells or tissue, cDNA synthesized, and quantitative real-time PCR conducted.

Western Blotting

Western blotting for B1R was determined in human carotid endarterectomy tissue and HUVEC samples using a selective antibody for B1R.[17] Samples were divided into sections containing lesion (+) and regions devoid of plaque (−) (supplemental Figure I).

Radioligand Binding Assay

In HUVECs, total B1R binding was determined by adding B1R agonist [^{3}H]-LDBK at 0.75 nmol/L, with nonspecific binding performed by cotreatment with LDBK in excess (10 μmol/L, 1 hour) on ice. Cells were dissolved and the radioactivity determined by liquid β-scintillation count.

Results

B1R Is Induced In Vivo in Vascular Regions Predisposed to Atheroma Formation

In tissue from human carotid endarterectomy B1R expression was more pronounced in regions of atheromatous plaque compared to regions devoid of plaque (Figure 1). B1R mRNA expression was also upregulated in a time-dependent fashion in aorta of ApoE$^{-/-}$ mice fed a high-fat diet ($P<0.05$; supplemental Figure IIA), an effect that was temporally associated with a rise in serum triglyceride level (supplemental Figure IIB). Mice fed a normal chow diet for 12 weeks had normal levels of both serum triglyceride and LDL cholesterol levels (supplemental Figure IIC through IID) and no change in B1R mRNA expression (Figure 2A). Further analysis of the different regions of the aorta (ie, regions of low LSS versus regions of high LSS), demonstrated that in ApoE$^{-/-}$ mice fed a high-fat diet a >3-fold increase in expression was evident in the arch region compared to the thoracic aorta (Figure 2B). Immunohistochemical assessment localised B1R to both smooth muscle and endothelial cells in sections of the inner curvature (ie, regions of low LSS, Figure 2C), with less intense expression evident in sections of the outer curvature.
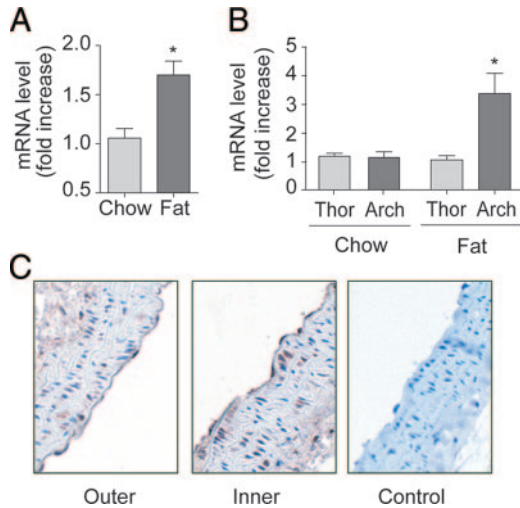
Figure 2. B1R is induced in regions of vessel curvature predisposed to atheroma formation in ApoE$^{-/-}$ mice. A through C, ApoE$^{-/-}$ mice fed a high-fat or normal chow diet for 12 weeks. B1R mRNA expression in whole aorta (A) or in aortic arch and thoracic aorta sections (B). C, B1R imunohistochemical expression in outer and inner curvatures of aortic arch of ApoE$^{-/-}$ mice fed a chow diet. Data are mean±SEM for n=9. *$P<0.05$. Arch indicates aortic arch; Thor, thoracic aorta.
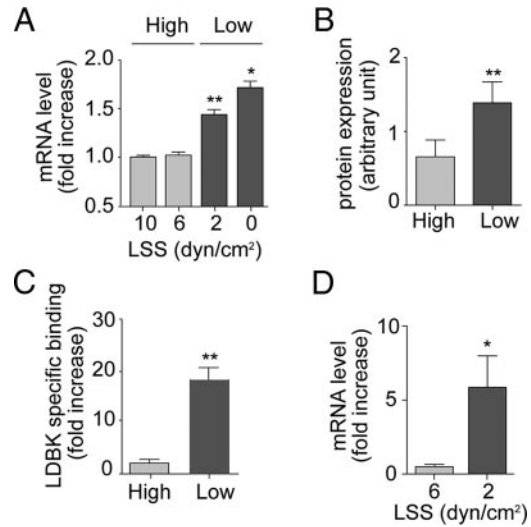

Figure 3. Low LSS induces B1R expression. B1R (A) mRNA expression, (B) protein expression, and (C) agonist binding in HUVECs subjected to low LSS or high LSS. Data are mean±SEM for n=6. **$P<0.01$, *$P<0.05$ high vs low values. D, B1R mRNA expression in mesenteric tissue from WT mice perfused at high (6 dyn/cm²) or low (2 dyn/cm²) LSS for 4 hours. Data are mean±SEM for n=5. *$P<0.05$.

Low LSS Induces Kinin B1R Expression in Endothelial Cells and in Mesenteric Tissue Ex Vivo

Exposure of HUVECs to physiological (high) LSS but not low LSS resulted in a time-dependent alignment of cells (supplemental Figure IIIA). Low LSS was also associated with decreased nitrite production reflecting endothelial dysfunction (supplemental Figure IIIB). Under high LSS a suppression of B1R mRNA expression relative to static HUVECs occurred that was maximal at 8 hours (by ≈50%) and sustained for up to 16 hours (supplemental Figure IVA). Comparison between cells exposed to high and low LSS for 8 hours exposed a ≈2-fold increase in B1R mRNA expression in cells under low LSS conditions (Figure 3A). In contrast in HAECs, B1R mRNA was undetectable in both conditions (data not shown, n=4). All further cell experiments were conducted after 8 hours of LSS exposure, and using physiological (high) LSS as a reference control.

Western blotting of cell lysates demonstrated upregulated expression after low but not high LSS (Figure 3B and supplemental Figure IVC). Confirmation of antibody selectivity was achieved in preadsorption experiments in HEK-293 (supplemental Figure IVB). In addition [³H]-LDBK binding was increased 20-fold ($P<0.01$) in cells exposed to low LSS (Figure 3C). HUVECs treated with IL-1β displayed binding with [³H]-LDBK, which was displaced by increasing concentrations of cold LDBK confirming the validity of [³H]-LDBK as tracer for these assays (supplemental Figure IVD).

LSS-induced regulation of B1R expression was also demonstrated in intact blood vessels; B1R mRNA was expressed at a very low level in mouse mesenteries exposed to physiological levels of LSS ex vivo, however exposure to low LSS caused a >5-fold elevation ($P<0.05$; Figure 3D).

Low LSS Increases B1R Functionality

Both PGI$_2$ and PGE$_2$ release and endothelial CXCL5 mRNA expression were significantly enhanced in response to LDBK in HUVECs exposed to low LSS but not high LSS (Figure 4). Neither COX-1 nor COX-2 expression were altered by LSS (supplemental Figure VA and VB). CXCL5 mRNA was also upregulated in aortic arch of ApoE$^{-/-}$ mice compared to thoracic aorta (>8-fold increase; data not shown, n=6).

Additive Effects of Low LSS and Inflammation on B1R Expression and Function

IL-1β caused a pronounced elevation of B1R mRNA expression in HUVECs under low LSS; an effect that peaked at 1
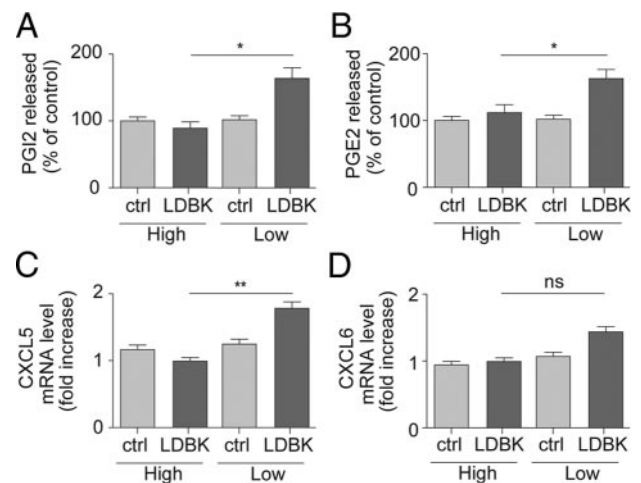

Figure 4. B1R activation stimulates PGE2, PGI2, and CXCL5 production only under low LSS. HUVECs were subjected to high or low LSS and stimulated or not with B1R agonist Lys-des-Arg⁹-Bradykinin (LDBK, 10 μmol/L) and (A) PGI2 or (B) PGE2 release and endothelial (C) CXCL5 and (D) CXCL6 mRNA expression measured. Data are mean±SEM for n=6. ns indicates nonsignificant. *$P<0.05$, **$P<0.01$.
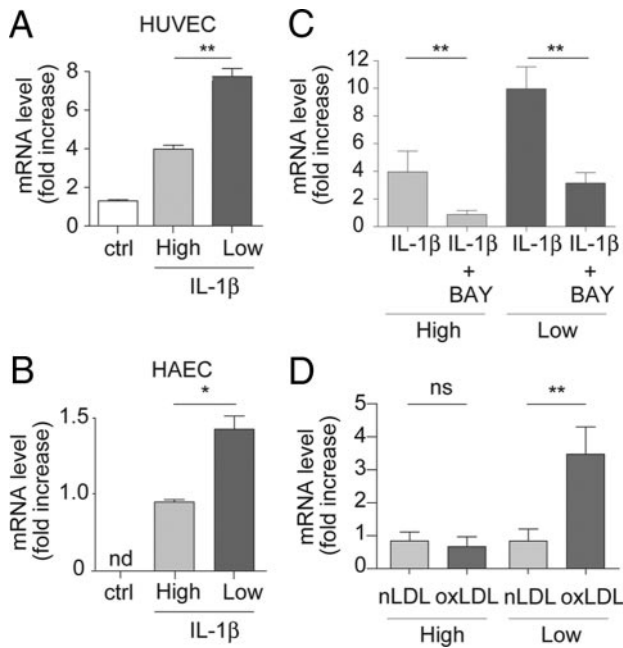
Figure 5. IL-1β–induced B1R expression is enhanced under low LSS conditions. B1R mRNA expression in (A) HUVECs (n=6) or (B) HAECs (n=6) subjected to varying LSS (0 to 10 dyn/cm², 12 hours), then stimulated or not with IL-1β (10 ng/mL, 4 hours) before or not treatment with (C) the NFκB inhibitor (BAY 11-7082, 20 μmol/L, n=6). D, After LSS HUVECs were treated with native LDL (nLDL, 20 μg/mL) or oxidized LDL (oxLDL, 20 μg/mL, 3 hour, n=3). *P<0.01, **P<0.05. nd indicates nondetermined; ns, nonsignificant.

Figure 6. IL-1β–induced CXCL5 and CXCL6 expression is mediated by B1R activation and enhanced under low LSS conditions. HUVECs were subjected to low LSS for 12 hours and treated with IL-1β (10 ng/mL) for 4 hours in the absence or presence of the B1R antagonist SSR240612 (1 μmol/L, 15 minutes before IL-1β application). CXCL5 (A) or CXCL6 (B) mRNA expression was measured levels normalized to GAPDH. Data are mean±SEM for n=6. **P<0.01.

hour and returned to basal by 8 hours (supplemental Figure VIA). In addition, although IL-1β (4 hour) caused ≈5-fold increase in B1R mRNA expression under low LSS conditions, this effect was substantially reduced (≈50%) under high LSS (Figure 5A). This enhanced expression in HUVECs exposed to low LSS was similarly evident in HAECs (Figure 5B), associated with enhanced LDBK-specific binding (supplemental Figure VIB and VIC) and inhibited by the NFκB inhibitor BAY 11-7082 (Figure 5C).

Confirmation that IL-1β-induced B1R expression was associated with enhanced B1R function was demonstrated by the finding that the elevated CXCL5 and CXCL6 mRNA expression evident in response to IL-1β under low LSS was suppressed by ≈50% by the B1R antagonist, SR240612 (Figure 6A-B). Finally, oxLDL caused a >3-fold increase in B1R mRNA expression compared to treatment with native LDL under low but not high LSS conditions (Figure 5D).

Discussion

LSS, the unidirectional frictional hemodynamic force, imposed on the endothelial cell surface as a result of blood flow plays a major role in maintaining homeostasis. Herein, we show that low LSS induces expression and functionality of the proinflammatory kinin B1R. Moreover, we demonstrate in vitro that inflammatory stimuli and low LSS, combined to mimic the atherogenic environment, synergize to enhance both expression and function of this receptor; a phenomenon also evident at sites of atheroma in both humans and a mouse mode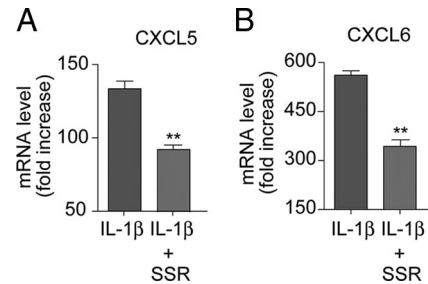l of atherosclerosis. Because activation of B1R is a pivotal step in promoting leukocyte recruitment and endothelial permeability in inflammatory responses[9,18] and elevated B1R expression is evident at sites of human atheroma,[7] we propose that the targeting of this receptor represents an exciting prospect for atherosclerotic disease.

Previous evidence has demonstrated that kinin B1R expression is evident in human blood vessels and may be associated with atherosclerosis.[7] In this study, Western blotting of segments of human carotid artery, collected from individuals undergoing endarterectomy, demonstrated a ≈3-fold elevation of kinin B1R in those areas associated with substantial atheromatous plaque only. Analysis of the aorta of ApoE$^{-/-}$ mice fed a high-fat diet exposed a similar selectivity in localization of B1R expression. Although B1R expression was evident basally expression increased over time, with a near doubling of expression by 12 weeks; an effect not evident in mice fed a chow diet. Comparison of the levels of expression in the aortic arch (a region of substantial atheroma formation) with the longitudinal section of the thoracic aorta (a region of no significant atheroma formation) demonstrated a clear localization of B1R to regions of atheromatous plaque formation and, interestingly, at a similar level of intensity evident in human blood vessels (ie, ≈3-fold increase). Immunohistochemical analysis suggested that expression was particularly evident in endothelial cells, the site of LSS sensing in the blood vessel wall (expression was also evident in smooth muscle and diffuse within the intima likely reflecting inflammatory cell recruitment,[7] as previously reported).

Indeed, subjecting endothelial cells in culture to low (atherogenic) LSS raised kinin B1R expression above that measured in cells exposed to physiological levels of LSS. That the levels of LSS used accurately reflect atherogenic and physiological levels of LSS was demonstrated by the presence of "endothelial dysfunction" under low LSS, as evidenced by decreased endothelial NO synthesis; a key indicator of this phenomenon in CVD.[18] Similarly, in the arterial circulation of the mesentery, subjected ex vivo to varying LSS, minimal B1R expression was observed under physiological LSS but a >5-fold increase in expression occurred after exposure to atherogenic LSS. Together,

these findings imply a selective upregulation of B1R expression by low atherogenic LSS. An alternative interpretation of these findings, however, is that high LSS represses B1R expression. Indeed, physiological LSS, through specific transcription factor dependent pathways, represses expression of a number of proinflammatory proteins in endothelial cells in culture.[19] However, in the present study B1R expression was suppressed after inhibition of the proinflammatory transcription factor NF-κB, implying an induction by low LSS rather than an inhibition by high LSS.

To investigate whether enhanced expression was associated with enhanced function we measured the expression of downstream inflammatory molecules. Prostaglandins released during inflammation produce local vasodilatation, increasing regional blood flow and microvascular permeability, together facilitating leukocyte infiltration.[20] Prostaglandins have also been implicated in mediating, at least in part, B1R-induced increases in vascular permeability and blood flow in several different vascular beds.[8,21] PGE_2 and PGI_2, in particular, are prominent prostaglandins involved in mediating these effects, but are also molecules that have been implicated in atherogenesis.[22–24] We demonstrated that although B1R agonist treatment did not alter PGE_2 and PGI_2 production by endothelial cells exposed to physiological LSS, both were elevated under low LSS. This effect likely relates to an increase in enzymatic activity because no changes in expression of the principal vascular COX enzymes, COX-1 and COX-2, were evident. More recently, we have also reported that B1R-induced inflammatory leukocyte recruitment is, at least in part, attributable to endothelial chemoattractant cytokine ELR-CXCL chemokine, CXCL5/6, synthesis.[17] In the current study B1R agonist also induced CXCL5 production in cells subjected to low LSS while having no effect under high LSS. Indeed, in support of this finding we measured elevated levels of CXCL5 at sites of atheroma formation in ApoE$^{-/-}$ mice. Collectively, these findings intimate that the enhanced expression of B1R under low LSS conditions directly correlates with the enhanced inflammatory phenotype of endothelial cells exposed to B1R agonists.

The kinin B1R promoter possesses several potential shear stress response elements (SSRE) with consensus sequence GAGACC,[25] Barbie box (CTTT motif), and GAGA (GAGAG motif)[26] sites for binding of specific transcription factors, particularly noteworthy being the transcription factor NFκB that binds to GAGACC.[27] NF-κB has been implicated in mediating the enhanced expression of a number of proteins dually regulated by both inflammation and low LSS, including adhesion molecules (E-selectin, VCAM-1)[5,6] and chemokines (MCP1, IL8).[28–30] In the present study we demonstrate that inhibition of NF-κB activation using BAY 11-7082, a selective inhibitor of cytokine-inducible I-κBα phosphorylation,[15,31] inhibited B1R expression in response to IL-1β under both high and low LSS conditions implicating NF-κB in both low LSS and IL-1β–induced B1R expression and low LSS alike.

As mentioned previously, inflammation plays a pivotal role in all stages of the atherosclerotic disease process:

initiation, progression, and plaque rupture.[1,32] An increasing body of evidence suggests that the prevailing hemodynamic conditions not only alters the expression of inflammatory genes within the endothelium but also determines the magnitude of the inflammatory response to pathogenic stimuli. Evidence suggests that low LSS is associated with an inflamed phenotype and enhanced responsiveness to diverse inflammatory stimuli including the cytokines IL-1β and TNFα, leading to enhanced expression of adhesion molecules and chemokines (eg, IL-8 and MCP-1)[5,29,33–36] as well as augmented inflammatory cell recruitment.[33,36] In line with these findings, in the current study, IL-1β produced a greater elevation of B1R expression, reflected by enhanced mRNA expression and agonist binding, and enhanced function in terms of prostaglandin and chemokine CXCL5 synthesis in cells subjected to low LSS compared to high LSS.

This enhanced activity was not limited solely to inflammatory cytokines but also to the molecule currently perceived to be the primary inflammatory stimulus in atherosclerosis: oxLDL.[37,38] At a concentration in line with those found in patients with CVD, and shown to be proinflammatory in endothelial cells,[12–14] oxLDL substantially elevated kinin B1R expression only in endothelial cells exposed to low LSS. In addition, our studies exposed the existence of a positive loop centered on B1R, whereby the effects produced by the cytokine in combination with low LSS were significantly attenuated by B1R blockade using SR240612. Equally interesting, SR240612 significantly inhibited IL-1β–induced CXCL6 as well as CXCL5 expression in cells subjected to low LSS, although the B1R agonist did not induce CXCL6 expression in HUVECs. This demonstrates that B1R expression and function were optimal when endothelial cells under low LSS were in a context of inflammation. SR240612 is a selective nonpeptidic antagonist with a Ki of 0.48 nmol/L at B1R and has an estimated pA_2 of 9.4 using standard organ bath assays for measurement of antagonist potency.[11] This antagonist has been tested against >100 other receptors and shows no or negligible activity at concentrations up to 1 μmol/L (the concentration we used for our experiments) and is at least 1000 times less potent at the kinin B2R. Thus, these findings clearly demonstrate the proinflammatory nature of B1R activation in endothelial cells and are in agreement with our previously published findings in B1R knockout mice,[17] demonstrating the essential role of the B1/CXCL5 pathway in inflammatory cell recruitment. Together, our data suggest that the contribution of the kinin B1R at sites of inflammation, in terms of both prostaglandins, CXCL5 and CXCL6 expression, is substantially enhanced at sites of low LSS and intimates a potential role for this pathway in the inflammatory events associated with atherogenesis.

A limitation of this work is that most of these data were produced with venular endothelium. However, to mitigate against this criticism, we investigated whether varying LSS could influence B1R expression in HAECs (cells relevant to clinical disease as demonstrated by the high prevalence of aortic lesions in patients, ie, ≈60%[39,40]). Indeed, although no expression was evident under basal

conditions, high LSS was a powerful suppressor of the raised expression under inflammatory conditions (ie, after IL-1β treatment). These findings intimate that the effect of LSS on endothelial B1R is likely a generalized feature of this cell type irrespective of vessel type.

Recent studies have implicated neutrophil recruitment in atherosclerosis.[41,42] Depletion of neutrophils, using an anti-PMN antibody, in ApoE$^{-/-}$ mice fed a high-fat diet significantly reduced plaque development.[42] Separate studies have also implicated neutrophil infiltration in promoting erosion and rupture of unstable plaque.[43,44] Studies investigating the pathways involved in the recruitment of this cell type clearly demonstrate that the interaction between neutrophils and endothelial cells in vivo occurs predominantly at sites of low shear.[34] Our previous studies have demonstrated an essential role for the kinin B1R in neutrophil recruitment to sites of inflammation, in particular we have demonstrated that Il-1β–induced neutrophil recruitment to the inflamed microvasculature was greatly diminished in B1R knockout mice.[17,45] Collectively, these data prompt us to speculate that a pathway centered on B1R expression and activation may underlie the neutrophil recruitment recently implicated in the process of atherogenesis in mouse models of disease,[41,42] although further studies are required to investigate this possibility more fully.

In conclusion, our data suggest that endothelial kinin B1R expression and function are tightly regulated by LSS, with expression being induced by low atherogenic levels of LSS, an effect substantially exacerbated under inflammatory conditions. Furthermore, we have identified a possible role for the kinin B1R in the pathogenesis of inflammatory CVD, particularly atherosclerosis; such findings imply that targeting the B1R pathway may prove beneficial in the therapeutic management of atherosclerotic disease.

Acknowledgments

Sources of Funding

Disclosures

References

1. Libby P. Inflammation in atherosclerosis. *Nature*. 2002;420:868–874.
2. Malek A, Alper SL, Izumo S. Hemodynamic shear stress and its role in atherosclerosis. *JAMA*. 1999;282:2035–2042.
3. Chien S. Effects of disturbed flow on endothelial cells. *Ann Biomed Eng*. 2008;36:554–562.
4. Chatzizisis YS, Coskun AU, Jonas M, Edelman ER, Feldman CL, Stone PH. Role of endothelial shear stress in the natural history of coronary atherosclerosis and vascular remodeling: molecular, cellular, and vascular behavior. *J Am Coll Cardiol*. 2007;49:2379–2393.
5. Passerini AG, Polacek DC, Shi C, Francesco NM, Manduchi E, Grant GR, Pritchard WF, Powell S, Chang GY, Stoeckert CJ Jr, Davies PF. Coexisting proinflammatory and antioxidative endothelial transcription profiles in a disturbed flow region of the adult porcine aorta. *Proc Natl Acad Sci U S A*. 2004;101:2482–2487.
6. Passerini AG, Shi C, Francesco NM, Chuan P, Manduchi E, Grant GR, Stoeckert CJ Jr, Karanian JW, Wray-Cahen D, Pritchard WF, Davies PF. Regional determinants of arterial endothelial phenotype dominate the impact of gender or short-term exposure to a high-fat diet. *Biochem Biophys Res Commun*. 2005;332:142–148.
7. Raidoo DM, Ramsaroop R, Naidoo S, Muller-Esterl W, Bhoola KD. Kinin receptors in human vascular tissue: their role in atheromatous disease. *Immunopharmacology*. 1997;36:153–160.
8. Leeb-Lundberg LM, Marceau F, Muller-Esterl W, Pettibone DJ, Zuraw BL. International union of pharmacology. XLV. Classification of the kinin receptor family: from molecular mechanisms to pathophysiological consequences. *Pharmacol Rev*. 2005;57:27–77.
9. Bussolari SR, Dewey CF Jr, Gimbrone MA Jr. Apparatus for subjecting living cells to fluid shear stress. *Rev Sci Instrum*. 1982;53:1851–1854.
10. Dewey CF Jr, Bussolari SR, Gimbrone MA Jr, Davies PF. The dynamic response of vascular endothelial cells to fluid shear stress. *J Biomech Eng*. 1981;103:177–185.
11. Gougat J, Ferrari B, Sarran L, Planchenault C, Poncelet M, Maruani J, Alonso R, Cudennec A, Croci T, Guagnini F, Urban-Szabo K, Martinolle JP, Soubrie P, Finance O, Le Fur G. SSR240612 [(2R)-2-[((3R)-3-(1,3-Benzodioxol-5-yl)-3-{[(6-methoxy-2-naphthyl)sulfonyl]amino}propanoyl)amino]-3-(4-{[2R,6S]-2,6-dimethylpiperidinyl]methyl}phenyl)-N-isopropyl-N-methylpropanamide Hydrochloride], a New nonpeptide antagonist of the bradykinin b1 receptor: biochemical and pharmacological characterization. *J Pharmacol Exp Ther*. 2004;309:661–669.
12. Itabe H, Ueda M. Measurement of Plasma Oxidized Low-Density Lipoprotein and its Clinical Implications. *J Atheroscler Thromb*. 2007;14:1–11.
13. Niemann B, Rohrbach S, Catar RA, Muller G, Barton M, Morawietz H. Native and oxidized low-density lipoproteins stimulate endothelin-converting enzyme-1 expression in human endothelial cells. *Biochem Biophy Res Comm*. 2005;334:747–753.
14. Thum T, Borlak J. LOX-1 Receptor blockade abrogates oxLDL-induced oxidative DNA damage and prevents activation of the transcriptional repressor oct-1 in human coronary arterial endothelium. *J Biol Chem*. 2008;283:19456–19464.
15. Pierce JW, Schoenleber R, Jesmok G, Best J, Moore SA, Collins T, Gerritsen ME. Novel inhibitors of cytokine-induced ikappa balpha phosphorylation and endothelial cell adhesion molecule expression show anti-inflammatory effects in vivo. *J Biol Chem*. 1997;272:21096–21103.
16. Ignarro LJ, Fukuto JM, Griscavage JM, Rogers NE, Byrns RE. Oxidation of nitric oxide in aqueous solution to nitrite but not nitrate: comparison with enzymatically formed nitric oxide from L-arginine. *Proc Natl Acad Sci U S A*. 1993;90:8103–8107.
17. Duchene J, Lecomte F, Ahmed S, Cayla C, Pesquero J, Bader M, Perretti M, Ahluwalia A. A novel inflammatory pathway involved in leukocyte recruitment: role for the kinin B1 receptor and the chemokine CXCL5. *J Immunol*. 2007;178:4849–4856.
18. Gimbrone MA Jr, Topper JN, Nagel T, Anderson KR, Garcia-Cardena G. Endothelial dysfunction, hemodynamic forces, and atherogenesis. *Ann N Y Acad Sci*. 2000;902:230–240.
19. Fledderus JO, van Thienen JV, Boon RA, Dekker RJ, Rohlena J, Volger OL, Bijnens AP, Daemen MJAP, Kuiper J, van Berkel TJC, Pannekoek H, Horrevoets AJG. Prolonged shear stress and KLF2 suppress constitutive proinflammatory transcription through inhibition of ATF2. *Blood*. 2007;109:4249–4257.
20. Williams TJ, Peck MJ. Role of prostaglandin-mediated vasodilatation in inflammation. *Nature*. 1977;270:530–532.
21. McLean PG, Perretti M, Ahluwalia A. Kinin B$_1$ receptors and the cardiovascular system: regulation of expression and function. *Cardiovasc Res*. 2000;48:194–210.
22. Cipollone F, Cicolini G, Bucci M. Cyclooxygenase and prostaglandin synthases in atherosclerosis: Recent insights and future perspectives. *Pharmacol Therap*. 2008;118:161–180.
23. McClelland S, Gawaz M, Kennerknecht E, Konrad CS, Sauer S, Schuerzinger K, Massberg S, Fitzgerald DJ, Belton O. Contribution of cyclooxygenase-1 to thromboxane formation, platelet-vessel wall interactions and atherosclerosis in the ApoE null mouse. *Atherosclerosis*. 2009;202:84–91.
24. Samuelsson B, Morgenstern R, Jakobsson PJ. Membrane prostaglandin E synthase-1: a novel therapeutic target. *Pharmacol Rev*. 2007;59:207–224.

25. Resnick N, Collins T, Atkinson W, Bonthron DT, Dewey CF, Gimbrone MA. Platelet-derived growth factor B chain promoter contains a cis-acting fluid shear-stress-responsive element. *Proc Natl Acad Sci U S A*. 1993;90:7908–7900.

26. Miyakawa AA, Lourdes Junqueira M, Krieger JE. Identification of two novel shear stress responsive elements in rat angiotensin I converting enzyme promoter. *Physiol Genomics*. 2004;17:107–113.

27. Khachigian LM, Resnick N, Gimbrone MA, Collins T. Nuclear factor-kappa B interacts functionally with the platelet-derived growth factor B-chain shear-stress response element in vascular endothelial cells exposed to fluid shear stress. *J Clin Invest*. 1995;96:1169–1175.

28. Chiu JJ, Chen LJ, Chang SF, Lee PL, Lee CI, Tsai MC, Lee DY, Hsieh HP, Usami S, Chien S. Shear stress inhibits smooth muscle cell-induced inflammatory gene expression in endothelial cells: role of NF-kappaB. *Arterioscler Thromb Vasc Biol*. 2005;25:963–969.

29. Partridge J, Carlsen H, Enesa K, Chaudhury H, Zakkar M, Luong L, Kinderlerer A, Johns M, Blomhoff R, Mason JC, Haskard DO, Evans PC. Laminar shear stress acts as a switch to regulate divergent functions of NF-{kappa}B in endothelial cells. *FASEB J*. 2007;21:3553–3561.

30. Chappell DC, Varner SE, Nerem RM, Medford RM, Alexander RW. Oscillatory shear stress stimulates adhesion molecule expression in cultured human endothelium. *Circ Res*. 1998;82:532–539.

31. Keller SA, Schattner EJ, Cesarman E. Inhibition of NF-kappa B induces apoptosis of KSHV-infected primary effusion lymphoma cells. *Blood*. 2000;96:2537–2542.

32. Ross R. Atherosclerosis – an inflammatory disease. *N Engl J Med*. 1999;340:115–126.

33. Sheikh S, Rahman M, Gale Z, Luu NT, Stone PC, Matharu NM, Rainger GE, Nash GB. Differing mechanisms of leukocyte recruitment and sensitivity to conditioning by shear stress for endothelial cells treated with tumour necrosis factor-alpha or interleukin-1beta. *Br J Pharmacol*. 2005;145:1052–1061.

34. Sheikh S, Rainger GE, Gale Z, Rahman M, Nash GB. Exposure to fluid shear stress modulates the ability of endothelial cells to recruit neutrophils in response to tumor necrosis factor-alpha: a basis for local variations in vascular sensitivity to inflammation. *Blood*. 2003;102:2828–2834.

35. Cheng C, Tempel D, van Haperen R, de Boer HC, Segers D, Huisman M, van Zonneveld AJ, Leenen PJ, van der SA, Serruys PW, de Crom R, Krams R. Shear stress-induced changes in atherosclerotic plaque composition are modulated by chemokines. *J Clin Invest*. 2007;117:616–626.

36. Shyy YJ, Hsieh HJ, Usami S, Chien S. Fluid shear stress induces a biphasic response of human monocyte chemotactic protein 1 gene expression in vascular endothelium. *Proc Natl Acad Sci U S A*. 1994;91:4678–4682.

37. Braunwald E. Shattuck lecture–cardiovascular medicine at the turn of the millennium: triumphs, concerns, and opportunities. *N Engl J Med*. 1997;337:1360–1369.

38. Ludewig B, Freigang S, Jaggi M, Kurrer MO, Pei YC, Vlk L, Odermatt B, Zinkernagel RM, Hengartner H. Linking immune-mediated arterial inflammation and cholesterol-induced atherosclerosis in a transgenic mouse model. *Proc Natl Acad Sci U S A*. 2000;97:12752–12757.

39. Mendel T, Popow J, Hier DB, Czlonkowska A. Advanced atherosclerosis of the aortic arch is uncommon in ischemic stroke: an autopsy study. *Neurol Res*. 2002;24:491–494.

40. Meissner I, Khandheria BK, Sheps SG, Schwartz GL, Wiebers DO, Whisnant JP, Covalt JL, Petterson TM, Christianson TJH, Agmon Y. Atherosclerosis of the aorta: Risk factor, risk marker, or innocent bystander? A prospective population-based transesophageal echocardiography study. *J Am Coll Cardiol*. 2004;44:1018–1024.

41. van Leeuwen M, Gijbels MJ, Duijvestijn A, Smook M, van de Gaar MJ, Heeringa P, de Winther MP, Tervaert JW. Accumulation of myeloperoxidase-positive neutrophils in atherosclerotic lesions in LDLR-/- mice. *Arterioscler Thromb Vasc Biol*. 2008;28:84–89.

42. Zernecke A, Bot I, Djalali-Talab Y, Shagdarsuren E, Bidzhekov K, Meiler S, Krohn R, Schober A, Sperandio M, Soehnlein O, Bornemann J, Tacke F, Biessen EA, Weber C. Protective role of CXC receptor 4/CXC ligand 12 unveils the importance of neutrophils in atherosclerosis. *Circ Res*. 2008;102:209–217.

43. Buffon A, Biasucci LM, Liuzzo G, D'Onofrio G, Crea F, Maseri A. Widespread coronary inflammation in unstable angina. *N Engl J Med*. 2002;347:5–12.

44. Naruko T, Ueda M, Haze K, van der Wal AC, van der Loos CM, Itoh A, Komatsu R, Ikura Y, Ogami M, Shimada Y, Ehara S, Yoshiyama M, Takeuchi K, Yoshikawa J, Becker AE. Neutrophil infiltration of culprit lesions in acute coronary syndromes. *Circulation*. 2002;106:2894–2900.

45. McLean P, Ahluwalia A, Perretti M. Association between kinin B1 receptor expression and leukocyte trafficking across mouse mesenteric post-capillary venules. *J Exp Med*. 2000;192:367–380.

SUPPLEMENT MATERIAL

Laminar shear stress regulates endothelial kinin B1 receptor expression and function:

potential implication in atherogenesis

Johan Duchene[1], Cécile Cayla[1], Sandrine Vessillier[1], Ramona Scotland[1], Kazuo Yamashiro[1], Florence Lecomte[1], Irfan Syed[1], Phuong Vo[1], Alessandra Marrelli[1], Costantino Pitzalis[1], Francesco Cipollone[2], Joost Schanstra[3], Jean-Loup Bascands[3], Adrian J Hobbs[4], Mauro Perretti[1], Amrita Ahluwalia[1]

[1]William Harvey Research Institute, Barts and The London School of Medicine & Dentistry, Charterhouse Square, London EC1M 6BQ, UK. [2]Italian Society For The Study of Atherosclerosis, Abruzzo Section, Italy,[3]Inserm, U858/I2MR, Department of Renal and Cardiac Remodelling, team #5, 1 avenue Jean Poulhès, BP 84225/Université Toulouse III Paul Sabatier, Institut de Médecine Moléculaire de Rangueil, Toulouse, F-31000 France. [4]Pharmacology, University College London, Medical Sciences Building, Gower Street, London WC1E 5JJ, UK.

MATERIALS AND METHODS

Human carotid endarterectomy

We studied four, not previously examined, surgical in-patients enlisted to undergo carotid endarterectomy for extracranial high-grade internal carotid artery stenosis. Carotid endarterectomy was performed in patients and tissue was immediately snap-frozen at -80°C until analysis of protein expression (see below). The study was approved by local Italian ethics review committees. Written informed consent was obtained from all patients before each examination.

Atherosclerosis in ApoE$^{-/-}$ mice

Male atherosclerosis-prone ApoE$^{-/-}$ mice (bred in-house, breeding pairs Jackson Labs USA) were fed a high fat diet (21% fat, 0.5% cholesterol, Harlan,UK) for 0, 3, 6 and 12 weeks or with chow diet for 12 weeks. Mice were killed by cervical dislocation the aorta was removed, snap frozen in liquid nitrogen and stored at -80ºC until use. In some experiments the aortic arch was separated from the longitudinal section of the thoracic aorta for separate analysis of regions of the aorta subjected to low (atherogenic) levels of LSS and high physiological levels of LSS respectively.

Cell culture and application of shear stress

Human Umbilical Vein Endothelial Cells (HUVECs; pooled donors, Lonza, UK) and Human Artery Endothelial Cells (HAEC, Lonza, UK) were cultured in EGM-2 endothelial growth

medium (Lonza, UK) at 37^oC , 5% CO_2 in Falcon 6-well plates. Cells at passage 4 and 80-90% confluency were used in all experiments. Steady unidirectional LSS of 10, 6, 2 or 0 dyn/cm^2 was applied, using a cone and plate viscometer as previously described[1,2]. Calculated values of LSS in large blood vessels suggest that physiological levels range from 5-20dyn/cm^2, thus for our studies cells were exposed to both 6 and 10 dyn/cm^2 to simulate physiological conditions. In order to mimic the levels of low LSS thought to be present at sites of atheroma cells were subjected to 2dyn/cm^2 or 0dyn/cm^2 (static). Evidence clearly link levels of unidirectional shear stress with alterations in endothelial phenotype supporting the use of this technique in our measurements[3,4]. Since we demonstrated that steady expression levels of B1R were achieved only after 8h and sustained up until 16h following application all analyses were conducted on cells exposed to shear stress for 16h unless stated otherwise. Since interleukin-1β (IL-1β) is the optimal inflammatory stimulus for kinin B1 receptor expression, to simulate an inflammatory stress cells were treated with IL-1β (10ng/ml, Preprotech EC, UK) for 4h (i.e at 12h following initiation of LSS) in the absence or presence of the B1R antagonist SSR240612[5] (1μM, 15 min prior to IL-1β application, kindly provided and synthesised by Jerini AG). Cells were also treated with oxidized LDL (oxLDL, 20μg/ml, 8h)[6-8] being introduced 8h into the LSS stimulus. Native LDL (nLDL) was used as control. After shear exposure and/or IL-1β/oxLDL treatment cells were rinsed twice in PBS and frozen at -80°C until analysis of mRNA or protein expression (see below).

Transfected HEK-293

cDNA for the human wild-type B1 receptor cloned into pcDNA3.1 (Invitrogen) was obtained from Missouri S&T cDNA Resource Center. HEK-293 cells were transiently transfected with

JetPEI as described by the manufacter (Polyplus-transfection). Briefly 3ng of the plasmid was incubated with 6µL of JetPEI for 30min at room temperature. The mix was then added to HEK-293 cultured in 6wells-plate (200,000-300,000 cells per wells) for 24h with RPMI medium (Lonza,Uk). The cells were rinsed in PBS and frozen at $-80^{o}C$ until analysis protein expression (see below)

Serum triglyceride and cholesterol analysis

Triglyceride and LDL cholesterol levels were determined in serum of ApoE-/- mice as described by the manufacturers (TR0100 Serum Triglyceride Determination Kit; Sigma and LDL/VLDL Cholesterol ELISA Kit (Abcam, UK).

Perfused mouse mesentery preparations

All experiments were conducted according to the Animals (Scientific Procedures) Act of 1986 (United Kingdom). Male C57BL/6 mice were killed by cervical dislocation, the superior mesenteric artery cannulated and the mesentery isolated and then mounted in a 37ºC water-jacketed organ bath and perfused with warmed (37ºC), oxygenated (5% CO_2 in O_2) physiological salt solution (PSS) of the following composition (in mM): NaCl 119, KCl 4.7, CaCl2.2H2O 2.5, MgSO4·7H2O 1.2, NaHCO3 25, KH2PO4 1.2, glucose 5.5, containing 1% Dextran (MW=64,000-76,000). Perfusion pressure was measured through an in-line transducer (P23XL, Becton Dickinson). The mesenteric bed was perfused at either physiological (1ml/min equivalent to an LSS of 6dyn/cm^2 within the superior mesenteric artery) or low (0.5ml/min equivalent to 2dyn/cm^2) flow rate. Decreases in flow rate below

4

0.5ml/min had profoundly depressed vascular constrictor responses to KCL and therefore was not used for experimentation. Neither flow rate significantly altered basal vasoactive responses. Constrictor responses to KCl (125mM) in PSS (equimolar substitution for NaCl) were unaffected by flow rate (37 ± 10.5mmHg, n=6 and 43 ± 11.1mmHg, n=5 for 1ml/min and 0.5ml/min, respectively) indicating no significant alteration in smooth muscle reactivity under these conditions of flow. Flow rate did not affect basal perfusion pressure (12±1.7, n=6; and 12±4.4 mmHg, n=5 for 1ml/min and 0.5ml/min, respectively). Each preparation was perfused for 4h, snap frozen in liquid N_2, and RNA extracted for real-time quantitative PCR.

Assessment of kinin B1-receptor-induced functionality: measurement of prostaglandin and chemokine synthesis

After exposure to shear stress or IL-1β cells were treated with the selective B1 agonist: Lys-des-Arg[9]-BK (LDBK, 10µM, Bachem). For prostaglandin measurement medium was collected 30 min after LDBK application, centrifuged for 20 min at 16000 rpm, 4ºC and the supernatant stored at -80ºC. Concentrations of 6-keto-PGF$_{1\alpha}$ (the stable hydrolysis product of PGI$_2$) and PGE$_2$ were measured using enzyme immunoassay kits (Cayman Chemical Co) according to the manufacturer's protocol. For PGE$_2$ measurement, prostaglandins were extracted with Sep-pak cartridges by solid phase extraction (Sep-Pak ® Vac C18, Waters Corporation) prior to assay. 6-keto-PGF$_{1\alpha}$ and PGE$_2$ concentrations were expressed relative to the cell protein concentration measured by Bradford assay. The effects of B1R activation on prostaglandin levels were expressed as a percentage of the level without agonist treatment for each condition. For assessment of B1-induced chemokine synthesis cells were collected, by scraping, at 4h

following treatment with Lys-DABK, snap frozen and stored at -80ºC until mRNA extraction and assessment of CXCL5 and CXCL6 mRNA expression as described below**.**

Ozone chemiluminescence for determination of nitrite

After exposure to shear stress medium was collected centrifuged for 20 min at 16000 rpm, 4ºC and the supernatant stored at -80ºC. Samples were analysed for nitrite using chemiluminescence as described previously[9]. Briefly, samples and standards containing nitrite were first reduced to NO, which was then quantified using a NO analyser (NOA 280, Sievers). Nitrite concentrations were determined by addition of samples to 1.5 % potassium iodide in glacial acetic acid under nitrogen at room temperature.

Quantitative real time PCR

Total RNA was extracted, cDNA synthesised and subjected to quantitative RT-PCR using SYBR green reagents (ABgene, UK). To quantify B1 receptor and CXCL5/CXCL6 chemokine mRNA expression, the following primers were used:

human B1 sense: 5'-ACG CCT TCA TTT TCT GCC TG-3', antisense: 5'-GCT GGC TCT GGT TGG AGG AT-3',

murine B1 sense: 5'-TGG AGT TGA ACG TTT TGG GTT T-3', antisense: 5'-GTG AGG ATC AGC CCC ATT GT-3',

human CXCL5 sense: 5'-GAG AGC TGC GTT GCG TTT G-3' and antisense: 5'- TTT CCT TGT TTC CAC CGT CCA-3',

human CXCL6 sense: 5'-GGT CCT GTC TCT GCT GTG C-3' and antisense: 5'-GGG AGG CTA CCA CTT CCA-3',

human GAPDH sense primer: 5'-CAT GTT CGT CAT GGG TGT GAA-3'; antisense primer: 5'-ATG GAC TGT GGT CAT GAG TCC TT-3',

murine β-actin: sense 5'-GAA ATC GTG CGT GAC ATC AAA G-3' and antisense 5'-TGT AGT TTC ATG GAT GCC ACA G-3'.

In HUVEC/HAEC B1 mRNA expression was normalised for each sample with respect to the corresponding (GAPDH) mRNA expression which is unaffected by alterations in fluid shear stress and in murine tissue the comparison was made to actin. The comparative Ct method of Livak and Schmittgen[10] was applied to compare gene expression levels between samples. Using the AB SDS2.1™ system software, the amplification threshold cycle values (CT) were obtained. The data were analysed using the equation $2^{-\Delta\Delta Ct}$ where ΔΔCt=(CtB1 or CXCL5/6-CtGAPDH)Treated-(CtB1 or CXCL5/6- CtGAPDH)Control.

Western blotting

Lysates were prepared from human carotid endarterectomy tissue or cells (HUVEC subjected to LSS and HEK-293 transfected with pcDNA3.1-B1R) and protein concentration determined as previously described[11] Lysate samples were subjected to western blotting to detect B1 receptor expression. Blots were probed with with the following antibodies: the rabbit polyclonal anti-B1 receptor antibody (K21N[12] dilutions of 1/2000 or 1/5000 in 2% milk were used for tissue or cell samples respectively). Secondary peroxidase-coupled sheep anti-rabbit

antibody (dilution 1/10000; Prepotech) or goat anti-rabbit antibody (dilution 1/2000; DakoCytomation) were used for tissue or cell samples respecively. 1/5000 of purified rabbit antiserum directed against a segment of the C-terminal sequence of the B1 receptor (termed K21N)[12]. For quantification of protein expression all blots were reprobed for β-actin or α-tubulin expression using rabbit anti-β-actin (Sigma-Aldrich, UK, 1/500 dilution) or 1/5000 dilution of mouse monoclonal anti-α-tubulin antibody (Sigma-Aldrich, UK) for tissue or cell samples respectively. The specificity of the B1R band was determined in pcDNA3.1-B1R transfected HEK-293 cells and HUVEC by pre-incubating the K21N antibody with the immunizing peptide prior to reaction with the membrane. Densitometric analysis was performed on scanned images (Hewlett Packard) and analyzed using TotalLab™.

Immunohistochemistry

Immunohistochemistry for B1R was performed on 3-µm-thick paraffin-embedded sections of aortic arch from ApoE-/- mice. Following rehydration, antigen was unmasked for 45 minutes at 95°C using Dako Target retrieval solution (pH 6; Dako). Endogenous peroxidase was blocked for 10 minutes with Dako peroxidase blocking reagent, and nonspecific binding was blocked for 20 minutes with Dako protein block. The primary antibody anti-B1R (K21N, 1/250 dilution) was added and incubated for 1 hour at room temperature. Following 3 washes with Tris buffered saline, slides were incubated with biotinylated anti-rabbit IgG (1/10000 dilution; Dako) was used as a secondary antibody for 60 minutes at room temperature. Omission of primary antibody and staining with isotype-matched control immunoglobulins served as negative control. After 3 washes with PBS-Tween, we treated individual sections with horseradish

peroxidase-labeled streptavidin (Dako) for 30 minutes, washed the sections 3 times with PBS-Tween, and determined peroxidase activity with 3,3-diaminobenzidine tetrahydrochloride (Dako). The slides were lightly counterstained with hematoxylin before dehydration and mounting in DePex (VWR International,Uk).

Radioligand binding assay

Radioligand binding was performed on whole cells exposed to 0-2 dyn/cm^2 or 6-10dyn/cm^2 (for 8h) treated or not with IL-1β (10ng/mL, 4h). In each experiment, total binding was determined by adding B1 agonist [^{3}H]-LDBK at 0.75nM and non-specific binding was performed by co-treatment with LDBK in excess (10µM, 1h) on ice. Following two washes with ice-cold TRIS buffer, cells were dissolved with 0.3N NaOH and the radioactivity determined by liquid β-scintillation count (1900TR, Packard). All measurements were conducted in triplicate in each experiment i.e. 3 separate wells, each containing 350,000 cells for each n. Specific binding was calculated by subtracting the non-specific binding from the total binding and expressed as fold change compare to cells subjected to physiological LSS (6-10dyn/cm^2). The specificity of [^{3}H]-LDBK binding was confirmed by constructing a competitive binding curve with increasing concentration of cold ligand, LDBK.

Statistical analysis

Values are given as means ± SEM where n represents the number of animals or the number of experiments conducted for cells. Statistical comparisons were conducted using paired or unpaired Student's t test for 2 groups or one way ANOVA for more than 2 groups. Differences

were considered significant when p<0.05. All statistics were calculated using Graph Pad Prism™

4.1.

SUPPLEMENTAL FIGURE

Figure SI. Representative human carotid endarterectomy tissue divided in two sections: with (+) or without (-) plaque.

Figure SII. ApoE$^{-/-}$ mice fed either a high fat or normal chow diet for 0, 3, 6 and 12 weeks. B1 receptor mRNA expression was measured by qPCR in whole aorta (A) and (B) serum triglyceride levels were measured in serum. Comparison of (C) triglyceride and (D) LDL cholesterol levels in serum after 12 weeks normal chow or high fat diet fed ApoE-/- mice. . Data are mean ± SEM for n=9, ** P<0.01, * P<0.05 chow diet (Chow) vs fat diet (Fat).

Figure SIII. HUVECs subjected to low LSS (0 or 2 dyn/cm^2) or physiological levels of LSS (6 or 10 dyn/cm^2) for 8h. (A) Representative image of cell alignment and (B) levels of NO synthesis measured by chemiluminesence for nitrite in endothelial culture medium following exposure to low or high LSS. Data are mean ± SEM for n=6, ***P<0.001.

Figure SIV. (A) Time dependency of B1 receptor expression in response to a physiological LSS stimulus. HUVECs were subjected to physiological levels of LSS (6 dyn/cm^2) for 2, 4, 8 and 16h, (B) B1 receptor protein expression was assessed by western-blotting in HEK-293 transfected with pcDNA3-B1R and HUVEC subjected to antibody preadsorbed with (+) or without (-) the B1R peptide against which the antibody was raised. (C) Typical B1 receptor protein expression as assessed by western-blotting and (D) B1 receptor binding was measured with [^{3}H]-LDBK in cells subjected stimulated with IL-1β (10ng/mL, 4h). Data are mean ± SEM for n=6.

Figure SV. HUVECs were subjected to physiological (6-10 dyn/cm^2) or low LSS (0-2 dyn/cm^2) for 12h and (A) COX-1 and (B) COX-2 expression determined by western blotting. Data are mean ± SEM for n=6, protein expression was normalized to α-tubulin.

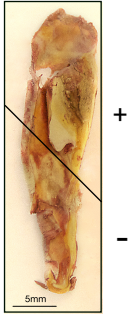**Figure SVI.** (A) HUVECs were subjected to low LSS (0-2 dyn/cm^2) for 12h and stimulated with IL-1β (10ng/mL) for different times (0, 1, 2, 4, 8 and 16h). HUVECs were subjected to varying LSS (0 to 10 dyn/cm^2) for 12h, then stimulated or not with IL-1β (10ng/mL) and (B) B1 receptor protein expression or (C) radioligand binding determined. Protein expression was normalized to α-tubulin. Data are mean ± SEM for n=6. * $P<0.01$, ** $P<0.05$, 6-10 dyn/cm^2 versus 0-2 dyn/cm^2 values or control versus treated value.
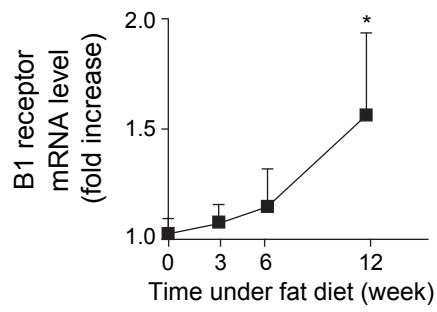
References

1. Bussolari SR, Dewey CF, Jr., Gimbrone MA, Jr. Apparatus for subjecting living cells to fluid shear stress. *Rev Sci Instrum* 1982;53:1851-1854.

2. Dewey CF, Jr., Bussolari SR, Gimbrone MA, Jr., Davies PF. The dynamic response of vascular endothelial cells to fluid shear stress. *J Biomech Eng* 1981;103:177-185.

3. Chien S. Mechanotransduction and endothelial cell homeostasis: the wisdom of the cell. *Am J Physiol Heart Circ Physiol* 2007;292:H1209-H1224.

4. Malek A, Alper SL, Izumo S. Hemodynamic shear stress and its role in atherosclerosis. *JAMA* 1999;282:2035-2042.

5. Gougat J, Ferrari B, Sarran L, Planchenault C, Poncelet M, Maruani J, Alonso R, Cudennec A, Croci T, Guagnini F, Urban-Szabo K, Martinolle JP, Soubrie P, Finance O, Le Fur G. SSR240612 [(2R)-2-[((3R)-3-(1,3-Benzodioxol-5-yl)-3-{[((6-methoxy-2-naphthyl)sulfonyl]amino}propanoyl)amino]-3-(4-{[2R,6S)-2,6-dimethylpiperidinyl]methyl}phenyl)-N-isopropyl-N-methylpropanamide Hydrochloride], a New Nonpeptide Antagonist of the Bradykinin B1 Receptor: Biochemical and Pharmacological Characterization. *J Pharmacol Exp Ther* 2004;309:661-669.

6. Itabe H, Ueda M. Measurement of Plasma Oxidized Low-Density Lipoprotein and its Clinical Implications. *Journal of Atherosclerosis and Thrombosis* 2007;14:1-11.

7. Niemann B, Rohrbach S, Catar RA, Muller G, Barton M, Morawietz H. Native and oxidized low-density lipoproteins stimulate endothelin-converting enzyme-1 expression in human endothelial cells. *Biochemical and Biophysical Research Communications* 2005;334:747-753.

8. Thum T, Borlak J. LOX-1 Receptor Blockade Abrogates oxLDL-induced Oxidative DNA Damage and Prevents Activation of the Transcriptional Repressor Oct-1 in Human Coronary Arterial Endothelium. *J Biol Chem* 2008;283:19456-19464.

9. Ignarro LJ, Fukuto JM, Griscavage JM, Rogers NE, Byrns RE. Oxidation of nitric oxide in aqueous solution to nitrite but not nitrate: comparison with enzymatically formed nitric oxide from L-arginine. *Proc Natl Acad Sci U S A* 1993;90:8103-8107.

10. Livak KJ, Schmittgen TD. Analysis of relative gene expression data using real-time quantitative PCR and the 2(-Delta Delta C(T)) Method. *Methods* 2001;25:402-408.

11. Duchene J, Lecomte F, Ahmed S, Cayla C, Pesquero J, Bader M, Perretti M, Ahluwalia A. A novel inflammatory pathway involved in leukocyte recruitment: role for the kinin B1 receptor and the chemokine CXCL5. *J Immunol* 2007;179:4849-4856.

12. Schanstra JP, Bataille E, Castano MEM, Barascud Y, Hirtz C, Pesquero JB, Pecher C, Gauthier F, Girolami J-P, Bascands J-L. The B_1 agonist [des-arg^{10}]-kallidin activates transcrition factor NF-kB and induces homologous upregulation of the bradykinin B_1-receptor in cultured human lung fibroblasts. *J Clin Invest* 1998;101:2080-2091.
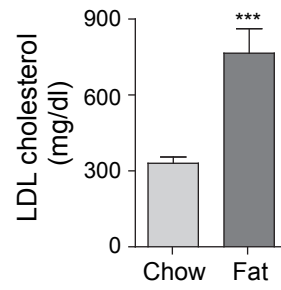
A

B

C

D

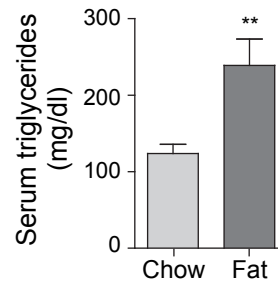FigIII Duchene J *et al*

A
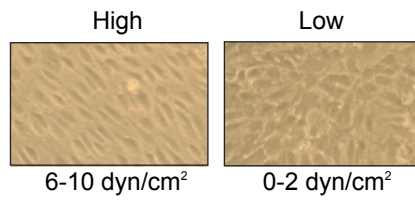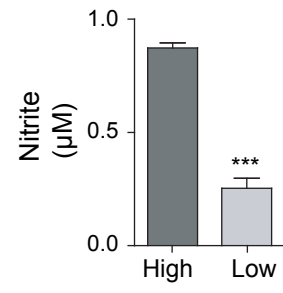
High

Low

6-10 dyn/cm²   0-2 dyn/cm²

B

Nitrite (µM)

***

FigIV Duchene J *et al*
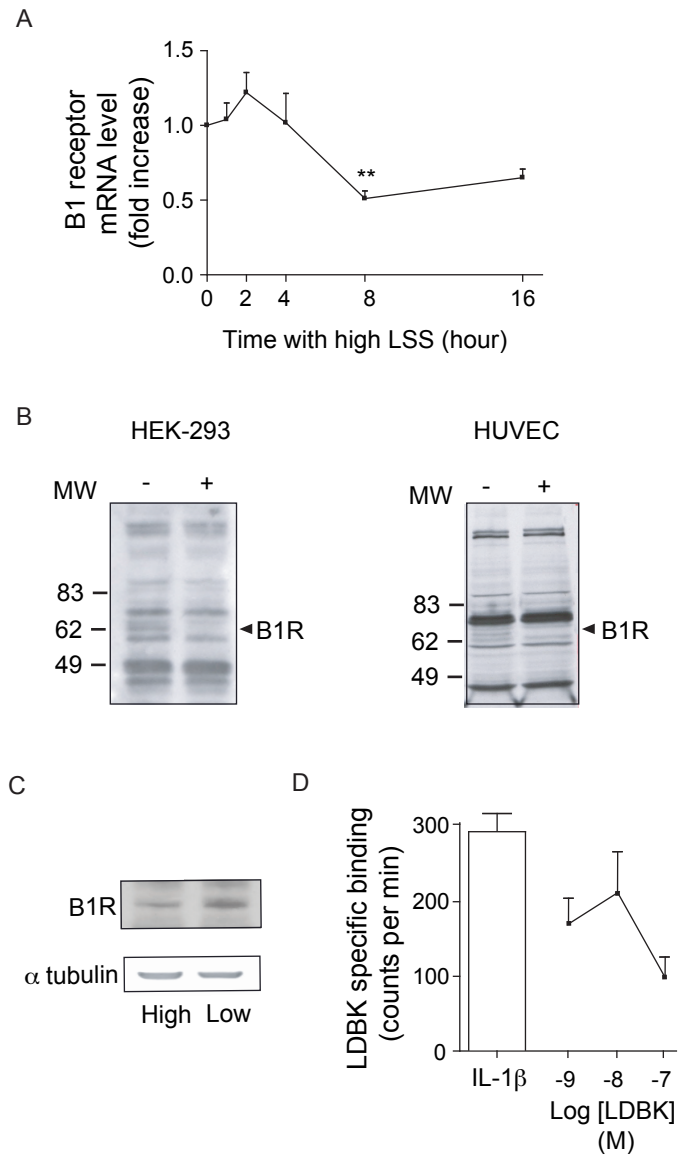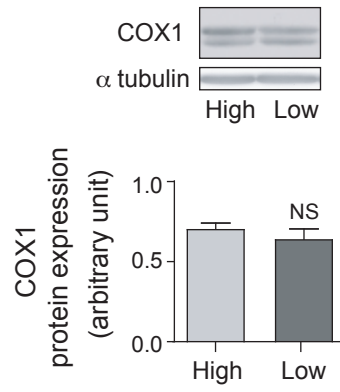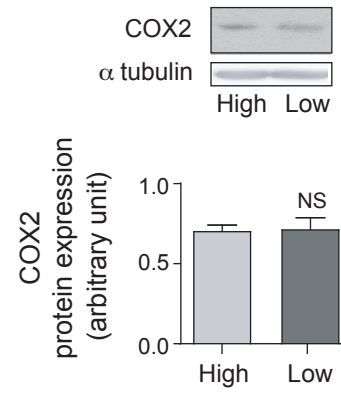
A

B

HEK-293   HUVEC
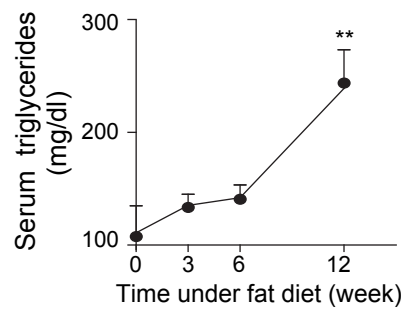

C   D

FigV Duchene J *et al*

A

COX1

α tubulin

High Low

B

COX2

α tubulin

High Low

A

B1 receptor
mRNA level
(fold increase)

Time of IL-1β incubation (hour)

B

B1 receptor
protein expression
(arbitrary unit)

ctrl   IL-1β

Low

C

LDBK specific binding
(fold increase)

ctrl   IL-1β

Low

6.3 CXCL5 limits macrophage foam cell formation in atherosclerosis.

Rousselle A, Qadri F, Leukel L, Yilmaz R, Fontaine JF, Sihn G, Bader M, Ahluwalia A, **Duchene J.**

CXCL5 limits macrophage foam cell formation in atherosclerosis

Anthony Rousselle,[1] Fatimunnisa Qadri,[1] Lisa Leukel,[1] Rüstem Yilmaz,[1] Jean-Fred Fontaine,[1] Gabin Sihn,[1] Michael Bader,[1] Amrita Ahluwalia,[2] and Johan Duchene[1]

[1]Max Delbrück Center for Molecular Medicine, Berlin, Germany. [2]William Harvey Research Institute, Queen Mary, University of London, Barts and The London, London, United Kingdom.

The ELR⁺-CXCL chemokines have been described typically as potent chemoattractants and activators of neutrophils during the acute phase of inflammation. Their role in atherosclerosis, a chronic inflammatory vascular disease, has been largely unexplored. Using a mouse model of atherosc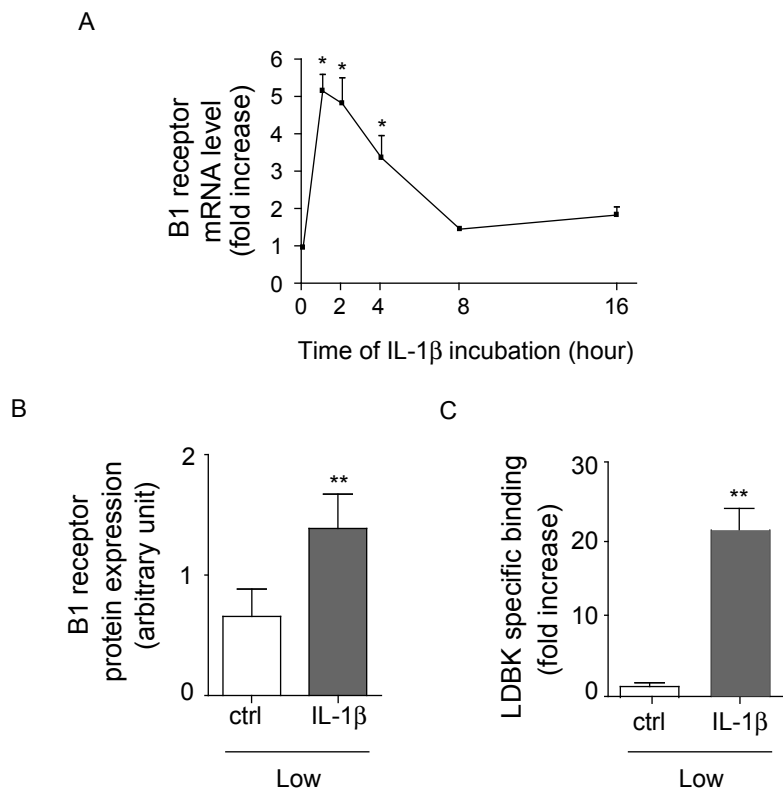lerosis, we found that CXCL5 expression was upregulated during disease progression, both locally and systemically, but was not associated with neutrophil infiltration. Unexpectedly, inhibition of CXCL5 was not beneficial but rather induced a significant macrophage foam cell accumulation in murine atherosclerotic plaques. Additionally, we demonstrated that CXCL5 modulated macrophage activation, increased expression of the cholesterol efflux regulatory protein ABCA1, and enhanced cholesterol efflux activity in macrophages. These findings reveal a protective role for CXCL5, in the context of atherosclerosis, centered on the regulation of macrophage foam cell formation.

Introduction

Atherosclerosis is a disease in which chronic inflammation plays a fundamental role. Activated macrophages accumulate in atherosclerotic lesions and contribute not only to the initiation phase but also to the development, progression, and the complication stages of the disease (1). Chemokines, cytokines that attract and activate leukocytes, are implicated in all stages of atherosclerosis and as such have been proposed as potential therapeutic targets (2). Substantial evidence has incriminated the CCL2 and CX3CL1 chemokines, which recruit and stimulate monocytes/macrophages, in the pathogenesis of atherosclerosis (1).

Although it is known that ELR⁺-CXCL chemokines, in particular CXCL1 and CXCL2, are induced during atherosclerosis (3–5), their exact functional contribution to the development of the pathology has not been ascertained. Indeed, while the ELR⁺-CXCL chemokines have been identified as potent and specific attractants of neutrophils in acute inflammation (2), whether this effect underlies their role in chronic diseases such as atherosclerosis is uncertain. One study, however, has put forward the hypothesis that the ELR⁺-CXCL receptor CXCR2 is involved in the accumulation of macrophages in advanced atherosclerotic plaques leading to lesion progression (6). The fact that CXCL1 alone has a similar but less pronounced effect (7) points toward the implication of alternative CXCR2 ligands in the pathogenesis of atherosclerosis. However, CXCL5, which has recently been shown to participate in obesity-induced insulin resistance (8), has received little attention in other obesity-related pathologies. We therefore set ourselves to investigate its expression and function in atherosclerosis.

Results and Discussion

Upregulation of CXCL5 in atherosclerosis. In atherosclerosis-prone *Apoe⁻/⁻* mice fed a Western diet (WD), CXCL5 expression was upregulated in both aorta and plasma and remained elevated up to 48 weeks

(Figure 1A). As previously observed (3, 5), expression of CXCL1 and CXCL2 was also increased as disease progressed (Supplemental Figure 1A; supplemental material available online with this article; doi:10.1172/JCI66580DS1). This rise in CXCL5 expression, unlike the rise in CXCL1 and CXCL2, was also evident in *Apoe⁻/⁻* mice fed a chow diet (CD) for 12 weeks (Figure 1, B and C), despite a lower elevation of plasma triglycerides and cholesterol levels (Supplemental Figure 1B). Of note, the level of CXCL5 induction (mRNA and protein) was similar with both diets in *Apoe⁻/⁻* mice, which suggests that CXCL5 expression is induced once the cholesterol levels reach a mild hypercholesterolemia but is not further increased if the cholesterol level goes above this threshold. Further analysis of the aortic arch region, which is more prone to develop atherosclerotic plaques, compared with the thoracic aortas of *Apoe⁻/⁻* mice fed a CD, confirmed that CXCL5, but not CXCL1 and CXCL2, expression was specifically upregulated in susceptible regions (9-fold increase) (Supplemental Figure 1C). These data suggest that the regulation of CXCL5 expression is distinct from that of CXCL1 and CXCL2 and that CXCL5 might play an essential role in atherosclerosis.

Endothelial cells are a source of CXCL5 in atherogenic conditions. Similar to what we observed in *Apoe⁻/⁻* mice, there was an increase of *Cxcl5* expression in the aortas of WT animals treated with a WD (Figure 1D), a mouse model that develops mild hypercholesterolemia-induced endothelial dysfunction but without monocyte infiltration, foam macrophage accumulation, and atherosclerotic plaque formation. This intimates that CXCL5 comes from endothelial cells rather than the atheromatous plaque. Accordingly, activated macrophages and cholesterol-loaded macrophages in vitro did not produce CXCL5 (data not shown). In human endothelial cells, in which the combinatory treatment of oxidized LDL or IL-1β and proatherogenic (low) laminar shear stress (LSS) leads to a similar dysfunction, an increase of expression of the human homolog of CXCL5, CXCL6 (9), was seen compared with that in endothelial cells subjected to physiological (high) LSS (Figure 1, E–G). The expression of CXCL8, the alleged ELR⁺-CXCL prototype chemokine in humans, remained unchanged (Figure 1, E and F).

Inhibition of CXCL5 is associated with macrophage foam cell accumulation in atherosclerotic plaques. Despite the potent neutrophil chemotaxis of
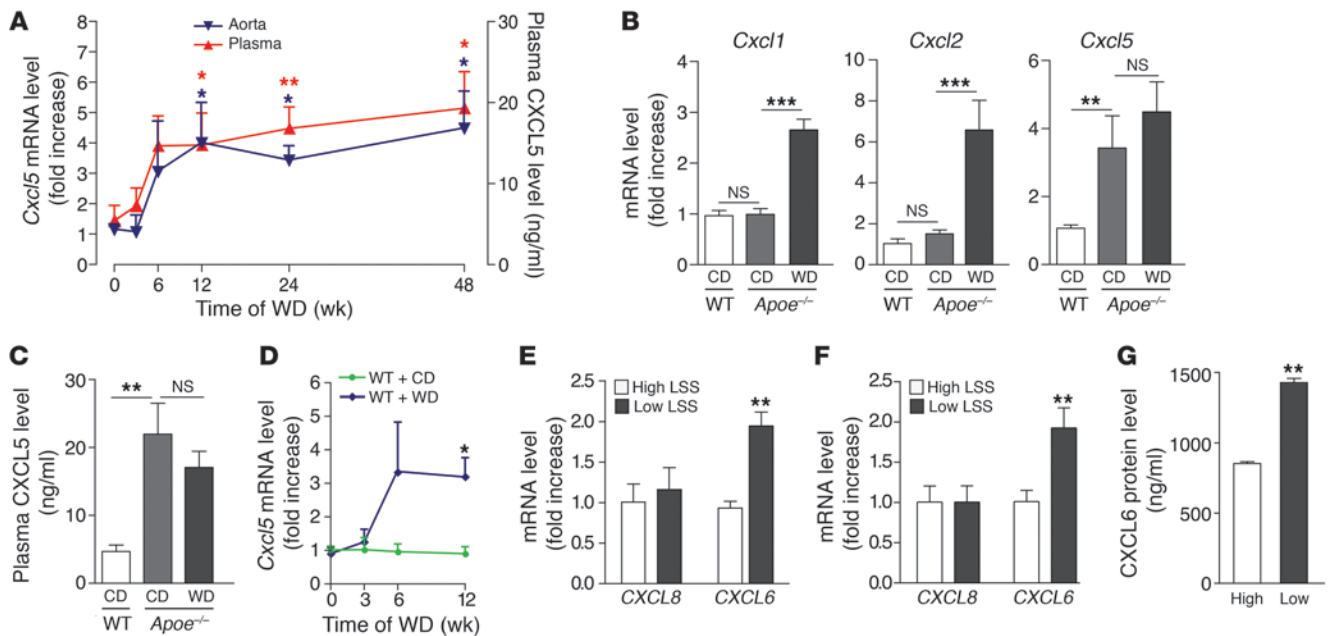

Figure 1
Upregulation of CXCL5 in atherosclerosis. (**A**) Assessment of *CXCL5* mRNA (blue triangles) and protein (red triangles) expression during the progression of atherosclerosis in aortas and plasma of *Apoe*$^{-/-}$ mice, respectively (*n* = 6–8 per time point), fed a WD for the indicated time. *Apoe*$^{-/-}$ mice fed a CD were used as controls. (**B**) Aortic *Cxcl1*, *Cxcl2*, and *Cxcl5* mRNA and (**C**) plasma CXCL5 protein expression was measured in *Apoe*$^{-/-}$ mice fed CD or WD for 12 weeks (*n* = 8 mice per group). WT mice fed CD for 12 weeks were used as controls. (**D**) Assessment of *Cxcl5* mRNA in aortas of WT mice (*n* = 6–8 per time point) fed WD. WT mice fed CD were used as controls. (**E**–**G**) HUVECs were subjected to high or low LSS and stimulated with (**E**) oxidized LDL (*n* = 3) or (**F** and **G**) IL-1β (*n* = 6). (**E** and **F**) *CXCL8* and *CXCL6* mRNA expression and (**G**) protein release were determined. (**A**–**G**) mRNA and protein levels were measured by qPCR and ELISA, respectively. Data are mean ± SEM. *P < 0.05, **P < 0.01, ***P < 0.001.

CXCL5 in acute inflammatory models (2, 10, 11), the rise in CXCL5 levels observed in *Apoe*$^{-/-}$ mice fed a WD was not accompanied by neutrophil infiltration within the atheromatous plaques (Supplemental Figure 1D). Moreover, blocking CXCL5 using a specific mAb did not diminish lesion size (Supplemental Figure 2, A and B) or the infiltration of monocytes/macrophages (Figure 2, E, G, and I, and Supplemental Figure 2C), as has been observed when blocking CXCL1 and CXCR2 in murine models of atherosclerosis (6, 7). Instead, we observed an accumulation of foam cells in both the brachiocephalic artery and the aortic root lesions (Figure 2B and Supplemental Figure 2E) corresponding to macrophages (Figure 2, C, E, G, and I, and Supplemental Figure 2C) with increased lipid storage capacity (Figure 2, C, F, H, and J, and Supplemental Figure 2D). This was accompanied by a significant reduction of collagen content (Figure 2, A and D, and Supplemental Figure 2, E and F), suggesting a role for CXCL5 in both macrophage activity and plaque stability. The kinin B1 receptor has been recently described to regulate CXCL5 expression (10). This specific CXCL5 reduction also could be observed in ApoE-B1R double-knockout mice (Supplemental Figure 3A) and was associated with higher macrophage foam cell accumulation in atherosclerotic plaques (Supplemental Figure 3, D–G). These observations corroborate the role of CXCL5 in atherosclerosis, without the use of blocking Abs, and in a more chronic state with mild hypercholesterolemia (after 60 weeks of CD). However, neither of the 2 models had a change in monocytosis or plasma cholesterol levels (Table 1 and Supplemental Figure 3, B and C), suggesting that CXCL5 limits macrophage foam cell accumulation through a different route. In the context of CXCL5

inhibition, it was recently described that a subsequential increase of CXCL1 and CXCL2 as well as their upstream regulator IL-17 could lead to a greater recruitment of leukocytes or leukocytosis (11, 12). Moreover, CXCL1 and CXCL2 have both been implicated in leukocyte mobilization (13, 14) and CXCL1 has been implicated as a potent monocyte chemoattractant in atherosclerosis (15). However, this indirect effect could not account for our results, since neither expression levels of CXCL1, CXCL2, and IL-17 nor monocytosis were affected here (Table 1, Supplemental Figure 3A, and Supplemental Figure 5). Importantly, we demonstrated that exogenous CXCL5 diminished peritoneal macrophage (PM) foam cell formation in vivo (Figure 3A and Supplemental Figure 4). Taken together, these findings intimate that CXCL5 can alter the phenotype of macrophages in atherosclerosis by preventing foam cell formation.

CXCL5 regulates macrophage activation. It is well described that the T cell–adaptive response participates in atherogenesis (1). Because T cells are known to modulate macrophages, we asked whether

Table 1

Anti-CXCL5 Ab does not change peripheral blood parameters in *Apoe*$^{-/-}$ mice

Models	Total cholesterol (mg/dl)	Monocytes (% of wbc)	CXCL1 (pg/ml)	CXCL2 (pg/ml)
Isotype IgG	739.2 ± 62.4	7.2 ± 0.7	1,154 ± 104	103 ± 24
CXCL5 Ab	840.1 ± 133.9	6.9 ± 0.4	1,033 ± 88	107 ± 12
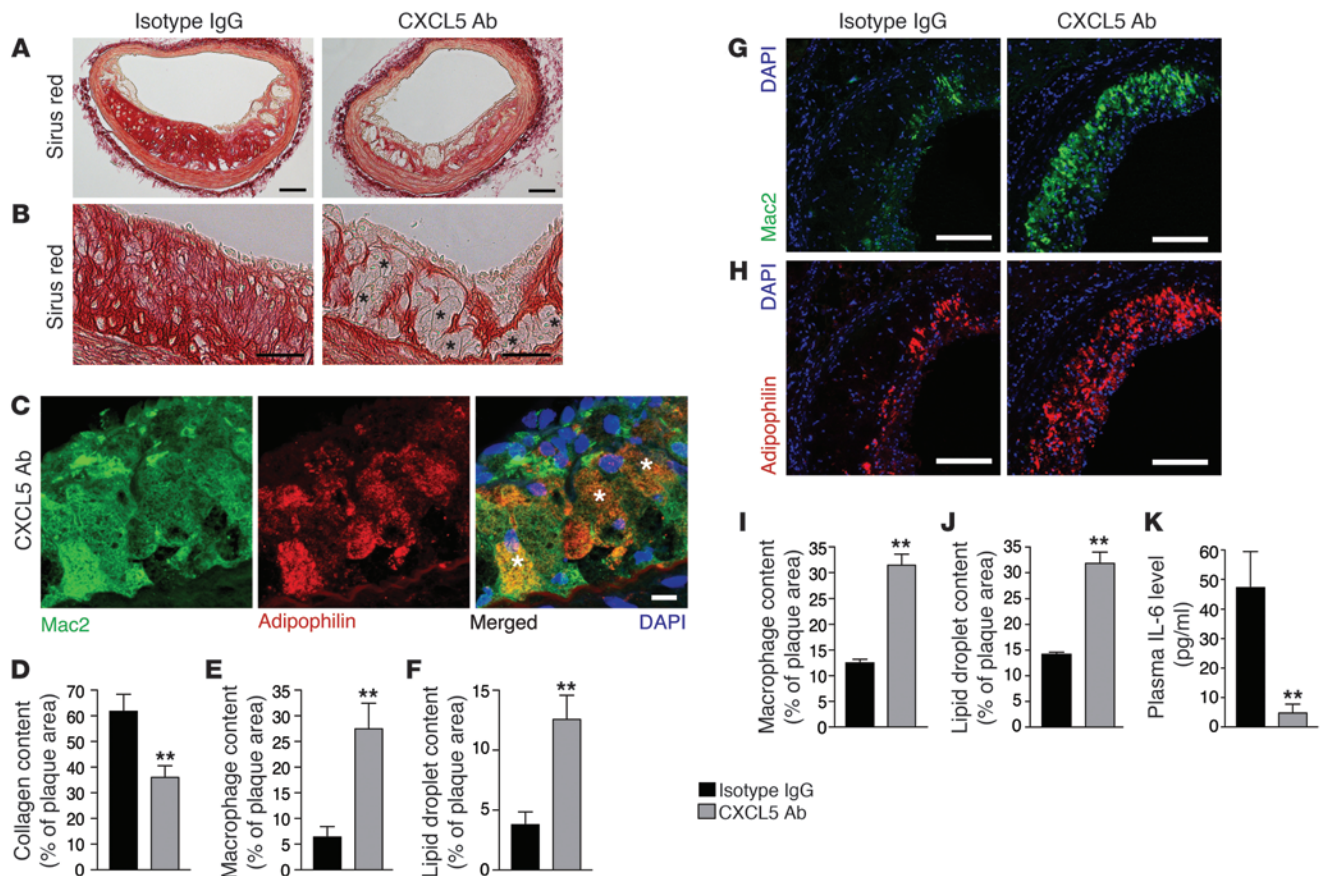
Figure 2

Blockade of CXCL5 is associated with macrophage foam cell accumulation in atherosclerotic plaques. *Apoe*−/− mice were fed a WD and treated with either IgG isotype control (IgG) or anti-CXCL5 Ab (CXCL5 Ab) for 12 weeks. (**A** and **B**) Representative images from brachiocephalic artery lesions of picrosirius red staining for collagen detection. Black asterisks indicate some foam cells. (**C**) Representative images of macrophages (Mac2 immunostaining) containing lipid droplets (adipophilin immunostaining) from anti-CXCL5 Ab-treated brachiocephalic artery lesions. White asterisks indicate double-positive cells. (**D**–**F**) Quantification of (**D**) sirius red staining, (**E**) Mac2, and (**F**) adipophilin immunostaining in brachiocephalic artery lesions. Representative images from aortic root lesions of (**G**) Mac2 and (**H**) adipophilin immunostaining. Quantification of (**I**) Mac2 and (**J**) adipophilin immunostaining in aortic root lesions. (**K**) Quantification of plasma IL-6 by ELISA. Data in **D**–**F** and **I**–**K** represent mean ± SEM. *n* =7–8. ****P* < 0.01. Scale bars: 100 μm (**A**, **G**, and **H**); 50 μm (**B**); 10 μm (**C**).

blocking CXCL5 in atherosclerotic mice could have affected the overall profile of cytokines typically secreted by T cells. Plasma levels of cytokines produced by Th1 (IFN-γ and IL-2), Th2 (IL-4), Th17 (IL-17), or Treg (IL-10) cells were unchanged (Supplemental Figure 5). However, circulating levels of IL-6, a cytokine mainly secreted by activated macrophages, were significantly lower in *Apoe*−/− mice treated with anti-CXCL5 Ab (Figure 2K). In addition, a gene expression correlation analysis, based upon a microarray data set of age-dependent aorta transcriptomes from WT and *Apoe*−/− mice, revealed that among all cytokines only IL-6 was positively and highly correlated with CXCL5 profile expression (*r* = 0.76) (Supplemental Table 1). Moreover, a biological functions analysis of these correlated genes revealed that, besides the expected immune function genes, the expression of CXCL5 in atherosclerosis was particularly associated with macrophage activation genes (Supplemental Table 2, *P* = 1.47 × 10⁻⁷). These observations strongly suggest that CXCL5 directly acts on macrophages rather than on the T cell–adaptive response. Indeed, stimulation of primary bone marrow–derived macrophages (BMDMs)

and PMs with CXCL5 induced an augmentation of *Il6* expression, an effect that was even greater in cholesterol-loaded macrophages (Figure 3B and Supplemental Figure 6, B and C). Thus, in addition to the well-described neutrophil arrest and recruitment-associated functions of ELR⁺-CXCL chemokines, herein we demonstrate that CXCL5 specifically modulates macrophage activation, particularly by upregulating IL-6 expression.

Activation of the CXCL5/CXCR2 pathway induces ABCA1 expression and cholesterol efflux in macrophages. Since in our experiments the primary target of CXCL5 appeared to be macrophages, we investigated whether the effects of CXCL5 on foam cell formation observed in vivo were due to a direct action. In vitro, CXCL5 was indeed able to reduce intracellular lipid accumulation in macrophages (Figure 3C). We speculated that this might be attributable to a decrease of cholesterol uptake or/and an increase of cholesterol efflux. In BMDMs and PMs, CXCL5 treatment significantly upregulated the expression of *Abca1*, a transporter that mediates the efflux of cholesterol (Figure 3, D and E, and Supplemental Figure 6D). In contrast, the expression of other cholesterol trafficking genes, such
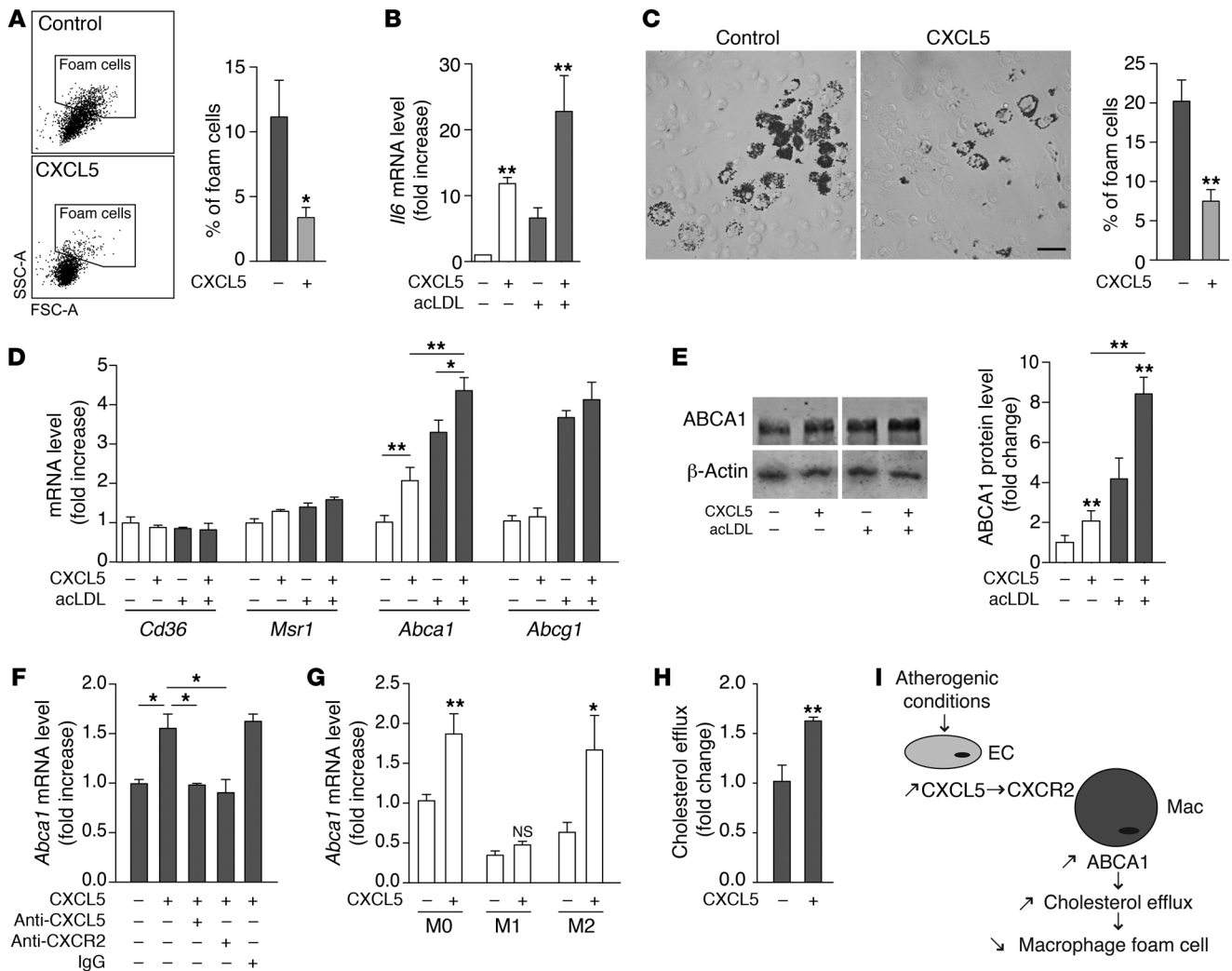
Figure 3

CXCL5 modulates macrophage activation and induces ABCA1 expression and cholesterol efflux in macrophages. (**A**) *Apoe*$^{-/-}$ mice were fed a WD and treated with CXCL5 for 12 days. By flow cytometry, PMs (CD11b$^+$CD115$^+$) were gated and foam cells were identified as high forward scatter (FSChi) and high side scatter (SSChi) cells. Data are mean ± SEM. *$P < 0.05$. $n = 3$ animals per group. (**B** and **D**–**G**) BMDMs or (**C** and **H**) PMs were cholesterol loaded (gray bars) or not (white bars) with acLDL and treated with or without CXCL5 in vitro. (**B**) Macrophage activation was determined by *Il6* mRNA expression in BMDMs using qPCR. $n = 6$. (**C**) Foam cell formation was assessed in cholesterol-loaded PMs as the percentage of Oil Red O–positive cells. Scale bar: 50 μm. $n = 4$. (**D**) Expression of genes involved in cholesterol trafficking was measured by qPCR in BMDMs. $n = 6$. (**E**) ABCA1 protein expression was measured by Western blotting in BMDMs. Lanes separated by a white line were run on the same gel but were noncontiguous. $n = 3$–5. (**F**) CXCL5-induced ABCA1 expression was blocked by anti-CXCL5 Ab and anti-CXCR2 Ab in cholesterol-loaded BMDMs. $n = 4$. (**G**) Expression of CXCL5-induced *Abca1* in naive (M0), classically activated (M1), and alternatively activated (M2) macrophages from BMDM was determined by qPCR. $n = 4$. (**H**) Cholesterol efflux was assessed in cholesterol-loaded PMs treated or not with CXCL5. $n = 6$. (**I**) Proposed mechanism of action for CXCL5 in atherosclerosis. EC, endothelial cell; Mac, macrophage. Data are mean ± SEM. *$P < 0.05$, **$P < 0.01$.

as *Msr1*, *Cd36*, and *Abcg1*, was not affected. Accordingly, in the in vivo gene expression correlation study mentioned earlier, *Abca1* was highly correlated with *CXCL5* expression ($r = 0.78$, Supplemental Table 1). ABCA1 upregulation was even more pronounced in cholesterol-loaded macrophages treated with CXCL5 (Figure 3, D and E, and Supplemental Figure 6D). Additionally, stimulation with CXCL5 induced ABCA1 expression in alternatively activated (M2) macrophages but not in classically activated (M1) macrophages (Figure 3G and Supplemental Figure 7, B and C). Accordingly, there is evidence to support that M2 macrophages are more sus-

ceptible to foam cell formation (16, 17). These observations suggest that in atherosclerotic lesions, in which macrophage heterogeneity is observed, several subtypes of macrophages can be targeted by CXCL5. Importantly, the induction of ABCA1 could be reversed, both by anti-CXCL5 Ab and by anti-CXCR2 Ab (Figure 3F, Supplemental Figure 6A, and Supplemental Figure 7C). Because IL-6 has been implicated in ABCA1 induction (18), we tested whether this was the case here. However, anti–IL-6 Ab treatment did not inhibit CXCL5-induced ABCA1 (Supplemental Figure 7A). Indeed, the fast induction of ABCA1 observed here does not support the implica-

tion of an indirect pathway through cytokine release but rather suggests that the CXCL5/CXCR2 pathway regulates ABCA1 in a direct manner. Finally, we demonstrated that CXCL5 treatment produced an increase of cholesterol efflux in macrophages (Figure 3H). Altogether these data demonstrate that CXCL5 induces ABCA1 expression and reduces the cholesterol content of macrophages.

To summarize, our findings show that, unlike other ELR$^+$-CXCL chemokines (6, 7), the induction of CXCL5 plays a protective role in atherosclerosis (Figure 3I). It does so by limiting the cholesterol content of macrophages and therefore foam cell formation, a function that we believe has never been attributed to an ELR$^+$-CXCL chemokine prior to this study. These findings strengthen the emerging concept that chemokines can regulate foam cell formation, as was recently proposed for CXCL4 (19). Additionally, these findings highlight the complex interplay between inflammation and atherosclerosis and support the notion that proinflammatory mediators of acute immune responses are not necessarily harmful in chronic inflammatory diseases (20, 21). This study encourages us to rethink ELR$^+$-CXCL chemokines as important players of chronic inflammatory diseases, especially in light of their newly described role in macrophage regulation.

Methods

See Supplemental Methods for details.

Animal procedure. All mice were males on a C57BL/6 background. 6-week-old Apoe$^{-/-}$ and WT mice were placed on a WD (21% fat, 0.2% cholesterol, Harlan Teklad) or remained on CD for the indicated time (see the legends for Figures 1 and 2). ELR$^+$-CXCL chemokines were quantified from the aorta mRNA by qPCR, and plasma CXCL5 concentration was assessed by ELISA.

Additionally, Apoe$^{-/-}$ mice fed a WD were treated with a mouse CXCL5 mAb (50 μg per mouse, i.p., every 72 hours, R&D Systems; ref. 22) or IgG isotype control for 12 weeks. Alternatively, Apoe$^{-/-}$B1R$^{-/-}$ and Apoe$^{-/-}$B1R$^{+/+}$ mice were fed a CD for 60 weeks. The brachiocephalic artery and heart were fixed with 4% PFA and embedded in paraffin for histology and immunostaining analysis. Blood was collected for measurement of leukocytes, lipids, cytokines, and chemokines.

In addition, Apoe$^{-/-}$ mice on WD were injected with CXCL5 (400 ng, i.p., every 72 hours, Peprotech). After 12 days, animals were sacrificed for peri-toneal cell isolation. Macrophage foam cell formation was determined by flow cytometry and by staining of lipids with Oil Red O.

Cell stimulation. Using a cone and plate viscometer, HUVECs were exposed to steady unidirectional high (10 dyn/cm²) or low (2 dyn/cm²) LSS for 24 hours. Oxidized LDL (20 μg/ml, BTI) or IL-1β (10 ng/ml, Peprotech) was added for the last 4 hours or an additional 24 hours for treatment.

PMs or BMDMs were stimulated with CXCL5 (100 ng/ml, Peprotech) and cholesterol loaded or not with acLDL (20 μg/ml, BTI). In some experiments, macrophages were also treated with CXCL5, CXCR2, IL-6, or control IgG Abs (20 μg/ml, 20 minutes prior to CXCL5 stimulation).

qPCR analysis was performed after 4 hours of treatment. ELISA and Western blotting were performed on supernatant collected at 24 to 48 hours and on cell lysate collected at 24 hours. Macrophage foam cells were stained for lipids with Oil Red O.

Statistics. Data are expressed as mean ± SEM. Results were analyzed by 2-tailed Student's *t* test or 1-way ANOVA with Bonferroni post-hoc test for multiple comparisons as appropriate using GraphPad Prism software. A *P* value of less than 0.05 was considered statistically significant.

Study approval. All experiments followed United Kingdom legislation for the protection of animals and were approved by the Ethical Review Process of Queen Mary, University of London.

Address correspondence to: Johan Duchene, Max Delbrück Center for Molecular Medicine, Robert-Rössle-Strasse 10, 13092 Berlin, Germany. Phone: 49.30.9406.3592; Fax: 49.30.9406.2110; E-mail: johan.duchene@mdc-berlin.de.

1. Weber C, Zernecke A, Libby P. The multifaceted contributions of leukocyte subsets to atherosclerosis: lessons from mouse models. *Nat Rev Immunol*. 2008;8(10):802–815.
2. Viola A, Luster AD. Chemokines and their receptors: Drug targets in immunity and inflammation. *Annu Rev Pharmacol Toxicol*. 2008;48(1):171–197.
3. Murphy N, et al. Hypercholesterolaemia and circulating levels of CXC chemokines in apoE*3 Leiden mice. *Atherosclerosis*. 2002;163(1):69–77.
4. Murphy N. Temporal relationships between circulating levels of cc and cxc chemokines and developing atherosclerosis in apolipoprotein E*3 Leiden mice. *Arterioscler Thromb Vasc Biol*. 2003;23(9):1615–1620.
5. Tabibiazar R. Proteomic profiles of serum inflammatory markers accurately predict atherosclerosis in mice. *Physiol Genomics*. 2006;25(2):194–202.
6. Boisvert WA, Santiago R, Curtiss LK, Terkeltaub RA. A leukocyte homologue of the IL-8 receptor CXCR-2 mediates the accumulation of macrophages in atherosclerotic lesions of LDL receptor-deficient mice. *J Clin Invest*. 1998;101(2):353–363.
7. Boisvert WA, et al. Up-regulated expression of the CXCR2 ligand KC/GRO-α in atherosclerotic lesions plays a central role in macrophage accumulation and lesion progression. *Am J Pathol*. 2006; 168(4):1385–1395.
8. Chavey C, et al. CXC ligand 5 is an adipose-tissue derived factor that links obesity to insulin resistance. *Cell Metab*. 2009;9(4):339–349.
9. Zlotnik A, Yoshie O. The chemokine superfamily revisited. *Immunity*. 2012;36(5):705–716.
10. Duchene J, et al. A novel inflammatory pathway involved in leukocyte recruitment: role for the kinin B1 receptor and the chemokine CXCL5. *J Immunol*. 2007;179(7):4849–4856.
11. Mei J, et al. CXCL5 regulates chemokine scavenging and pulmonary host defense to bacterial infection. *Immunity*. 2010;33(1):106–117.
12. Mei J, et al. Cxcr2 and Cxcl5 regulate the IL-17/G-CSF axis and neutrophil homeostasis in mice. *J Clin Invest*. 2012;122(3):974–86.
13. Wengner AM, Pitchford SC, Furze RC, Rankin SM. The coordinated action of G-CSF and ELR + CXC chemokines in neutrophil mobilization during acute inflammation. *Blood*. 2007;111(1):42–49.
14. Eash KJ, Greenbaum AM, Gopalan PK, Link DC. CXCR2 and CXCR4 antagonistically regulate neutrophil trafficking from murine bone marrow. *J Clin Invest*. 2010;120(7):2423–2431.
15. Huo Y. The chemokine KC, but not monocyte chemoattractant protein-1, triggers monocyte arrest on early atherosclerotic endothelium. *J Clin Invest*. 2001;108(9):1307–1314.
16. Oh J, et al. Endoplasmic reticulum stress controls M2 macrophage differentiation and foam cell formation. *J Biol Chem*. 2012;287(15):11629–11641.
17. Yakubenko VP, Bhattacharjee A, Pluskota E, Cathcart MK. M 2 Integrin activation prevents alternative activation of human and murine macrophages and impedes foam cell formation. *Circ Res*. 2011;108(5):544–554.
18. Frisdal E, et al. Interleukin-6 protects human macrophages from cellular cholesterol accumulation and attenuates the proinflammatory response. *J Biol Chem*. 2011;286(35):30926–30936.
19. Gleissner CA, Shaked I, Little KM, Ley K. CXC chemokine ligand 4 induces a unique transcriptome in monocyte-derived macrophages. *J Immunol*. 2010;184(9):4810–4818.
20. Alexander MR, et al. Genetic inactivation of IL-1 signaling enhances atherosclerotic plaque instability and reduces outward vessel remodeling in advanced atherosclerosis in mice. *J Clin Invest*. 2012;122(1):70–79.
21. Taleb S, et al. Loss of SOCS3 expression in T cells reveals a regulatory role for interleukin-17 in atherosclerosis. *J Exp Med*. 2009;206(10):2067–2077.
22. Jeyaseelan S. Induction of CXCL5 during inflammation in the rodent lung involves activation of alveolar epithelium. *Am J Respir Cell Mol Biol*. 2005; 32(6):531–539.

Cxcl5 limits macrophage foam cell formation in atherosclerosis

Anthony Rousselle, Fatimunnisa Qadri, Lisa Leukel, Rüstem Yilmaz, Jean-Fred Fontaine, Gabin Sihn, Michael Bader, Amrita Ahluwalia, Johan Duchene.

Online supplement

SUPPLEMENTAL METHODS

Experimental design. 6wks old ApoE$^{-/-}$ and WT mice were placed on a WD (21% fat, 0.2% cholesterol, Harlan Teklad) or remained on CD for the indicated time. ELR$^+$-CXCL chemokines were quantified from aorta tissue mRNA and plasma CXCL5 concentration was assessed by ELISA.

Additionally, ApoE$^{-/-}$ mice fed a WD were treated with a mouse CXCL5 mAb (50 µg/mouse, i.p., every 72h, R&D) or IgG isotype control for 12 wks. Alternatively, ApoE$^{-/-}$-B$_1$R$^{-/-}$ and ApoE$^{-/-}$-B$_1$R$^{+/+}$ mice were fed a CD for 60 wks. Brachiocephalic artery and heart were fixed with 4% PFA and embedded in paraffin for histology analysis. Blood was collected for leucocytes, lipids, cytokines and chemokines measurement.

Histology and immunostaining. Serial sections (5µm) of brachiocephalic artery and aortic root were stained with hematoxylin and eosin to determine lesion size. Collagen was detected using Sirius Red coloration. Sections were stained for macrophages (Mac-2 mAb, Acris, 1:200), neutrophils (Ly6G mAb, BioLegend, 1:100), lipid-droplet content (adipophilin mAb, Fitzgerald, 1:1000) and detected with secondary anti-rat Cy3- (1:300) or Alexa 488-(1:500) Ab. Quantification analysis was assessed with ImageJ software.

Chemokine and cytokine measurement. Plasma Cxcl1 (Peprotech), Cxcl2 and Cxcl5 (R&D) and supernatant CXCL6 and IL-6 (R&D) levels were determined by ELISA. Plasma IFNγ, IL-2, IL-4, IL-6, IL-10, IL-12p70 and IL-17 levels were measured using Milliplex technology (Millipore).

Lipids profile. Plasma cholesterol and triglyceride levels were determined with commercially available kits (Abcam and Sigma).

Blood monocyte counting. ApoE$^{-/-}$ mice fed a WD were treated with Cxcl5 mAb or control as above. Blood was collected after 2wks, red blood cell lysed (BD PharmLyse) and cells stained with CD11b (APC), CD115 (PE) and Ly6G (FITC) (all Biolegend). Total monocytes were identified as CD11b$^+$CD115$^+$Ly6G$^-$ cells. Data were acquired using BD LSR II flow cytometer and analysed with FlowJo software.

Real-time quantitative PCR. cDNA was synthesized from 1 μg total RNA with M-MLV reverse transcriptase (Promega) using random hexamer nucleotides. Real-time quantitative PCR was performed using SYBR Green PCR Master Mix (Applied Biosystems) on an ABI Prism 7900 sequence detection system with 10 ng of cDNA and 100 nM primers (sequences in Supplemental Table 3). Gene expression was normalized to β–actin (aorta) or HPRT (macrophage) or GAPDH (HUVEC) and expressed as a relative value to control group using the comparative threshold cycle method ($2^{-\Delta\Delta Ct}$).

Microarray analysis. Raw data (CEL files) from 18 mouse aorta samples of an Affymetrix microarray dataset of WT and ApoE$^{-/-}$ mice fed WD for 6, 32 and 78 wks was downloaded from the Gene Expression Omnibus database (identifier: GSE10000), processed and analysed using the R/Bioconductor statistical software. GCRMA normalisation method was applied on the 45101 probes. We filtered out probes with low variation in expression (at least 15% of the samples must have an expression value greater than the 10th percentile of all values in the dataset, and the inter quartile range must be greater than the median), probes having no annotated Entrez Gene identifier, and duplicated probes by keeping the one with the higher variance. There were a total of 19304 probes selected for further analysis. Pearson's correlation coefficients of gene probe expression profiles were computed between the Cxcl5 profile (Affymetrix probe identifier: 1419728_at) and profiles of the selected probes. P-values for significance were assessed using the distribution of all pairwise

probe correlation coefficients. 266 probes were significantly correlated to Cxcl5 (P<=0.01) and analysed for Biological Functions using Protein ANalysis THrough Evolutionary Relationships (www.pantherdb.org).

***In vivo* model of foam cell formation.** ApoE$^{-/-}$ mice on WD were injected with Cxcl5 (400ng, i.p., every 72h, Peprotech). After 12d, animals were sacrificed for peritoneal cells isolation. By flow cytometry, gated macrophages (CD11b^{+}CD115$^{+)}$ were identified as foam (FSc^{hi}SSc^{hi}). In parallel, macrophages were left to adhere (2h) in DMEM and lipids were stained with Oil-Red-O. Cells with over 1/3 of cytoplasm lipids were considered as foam.

Endothelial cell stimulation. Using a cone and plate viscometer, HUVECs were exposed to steady unidirectional high (10dyn/cm^2) or low (2 dyn/cm^2) LSS for 24h. Treatment with oxidized LDL (20µg/ml, BTI) or IL‑1β (10ng/ml, Preprotech) was added for the last 4h or an additional 24h. qPCR analysis was carried out from 4h cell lysate. CXCL6 ELISA was performed from 24h supernatant.

Primary macrophage culture. Mouse bone-marrow-derived macrophages (BMDM) flushed out from femur were seeded in 10% FBS DMEM with M-CSF (50ng/mL) for 5-7d. Peritoneal macrophages (PM) isolated 4d after injection of 3% thioglycollate (1mL, i.p.) were left to adhere (2h) in DMEM. Non-adherent cells were PBS washed and primary macrophages were placed in 1% FBS DMEM overnight before further treatment.

Macrophage stimulation. PMs or BMDMs were stimulated with Cxcl5 (100ng/mL) with (20µg/mL) or without acLDL. In some experiments, cells were also treated with either Cxcl5-, Cxcr2-, IL-6-, or control IgG antibodies (20µg/mL, 20min prior to Cxcl5 stimulation). In addition, some macrophages were polarised into classically-activated

macrophages (M1) with IFNY̌ (10ng/mL, 4h) or alternatively-activated macrophages (M2) with IL-4 (10ng/mL, 4h) and co-treated with Cxcl5. qPCR analysis was carried out from 4h cell lysate. ABCA1 Western Blotting and IL-6 ELISA were performed from 24h or 48h cell lysate or supernatant respectively.

***In vitro* model of foam cell formation.** acLDL-loaded (20µg/mL) PMs were treated (100ng/mL) or not with Cxcl5 for 24h in 2.5% serum containing medium. 4% PFA fixed macrophages were stained for lipids with 0.5% Oil-Red-O. Cells with over 1/3 of cytoplasm lipids were considered as foam.

Cholesterol efflux assay. PMs were incubated with acLDL (20µg/mL) with (100ng/mL) or without Cxcl5 for 48h. NDB cholesterol (1µg/mL) was added for 6h. Medium was then replaced by fresh serum-free medium containing ApoAI (10µg/mL, BTI) for 4h. Fluorescence-labelled cholesterol was measured from collected supernatant and cell lysate (0.1N NaOH). Cholesterol efflux was calculated by dividing supernatant fluorescence by the sum of fluorescence in the media and cells.

Western blotting. Proteins from macrophage lysate were separated on 10% SDS-polyacrylamide gel, transferred to PVDF membranes, blocked (Odyssey) and ABCA1 was detected by incubation with rabbit anti-mouse Ab (1/500, Novus) at 4°C overnight followed by donkey-anti-rabbit IgG (IRDyeTM 800CW, 1/10000, Odyssey, 30min).
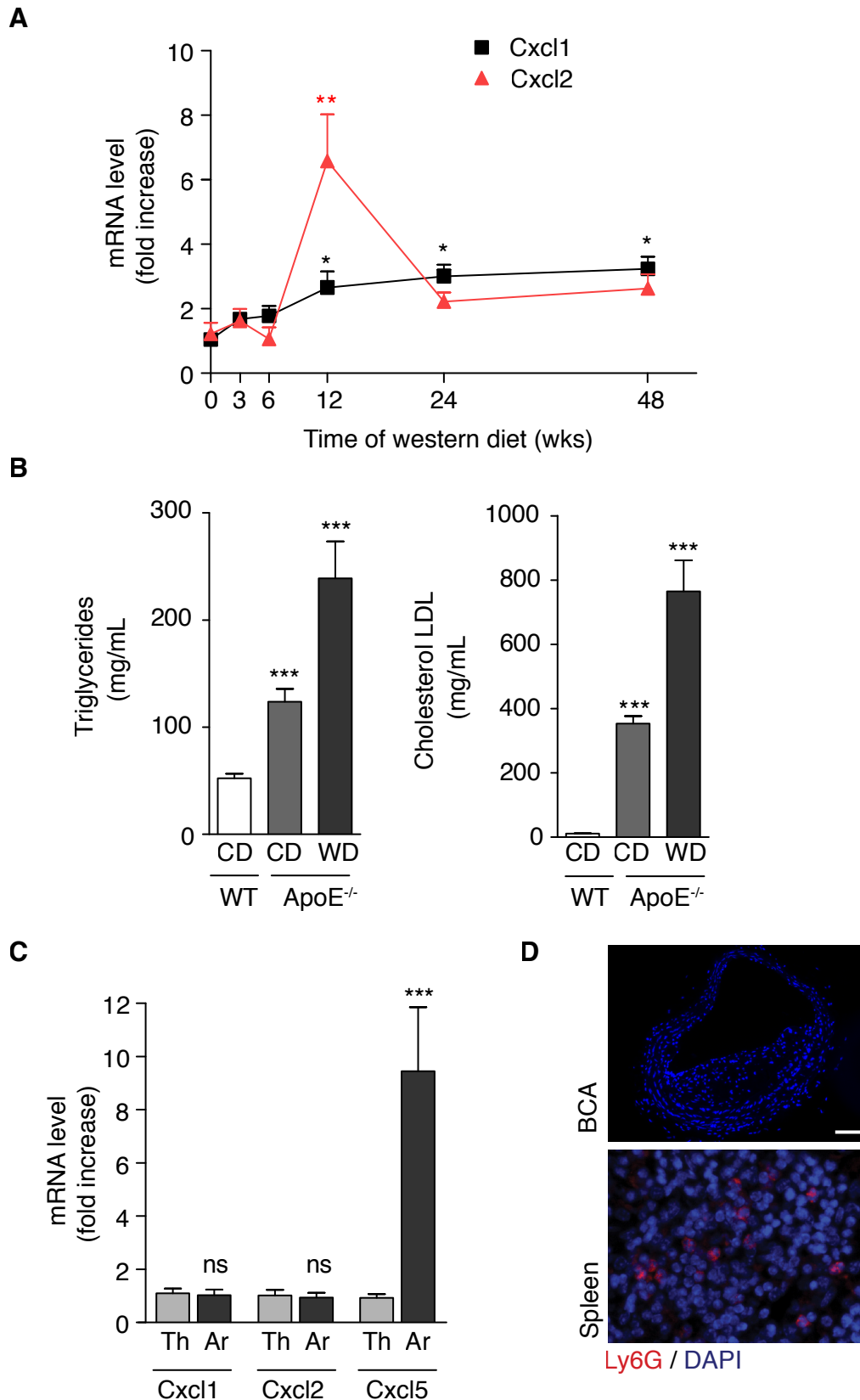
Supplemental Figure 1. Expression of ELR⁺-Cxcl chemokines in atherosclerosis.
(A) Assessment of Cxcl1 (■) and Cxcl2 (▲) mRNA during the progression of atherosclerosis in aorta of ApoE⁻/⁻
mice (n=6-8 per time point) fed a WD for the indicated time. (B) Triglycerides and LDL cholesterol were measured
in plasma of WT and ApoE⁻/⁻ mice fed either chow (CD) or western (WD) diet for 12wks (n=8 mice per group). (C)
Aortic Cxcl1, Cxcl2 and Cxcl5 mRNA expression was measured in ApoE⁻/⁻ mice under CD for 12wks in thoracic
aorta (Th) and aortic arch (Ar) (n=8 mice per group). Data are mean SEM. ***P<0.001, **P<0.01, *P<0.05. ns,
not significant. (D) Representative images of brachiocephalic artery (BCA) and spleen from ApoE⁻/⁻ mice fed a
WD for 12wks and stained with anti-Ly6G Ab for neutrophil detection. Spleen was used as a positive control for
Ly6G immunostaining. Scale bar= 75µm.
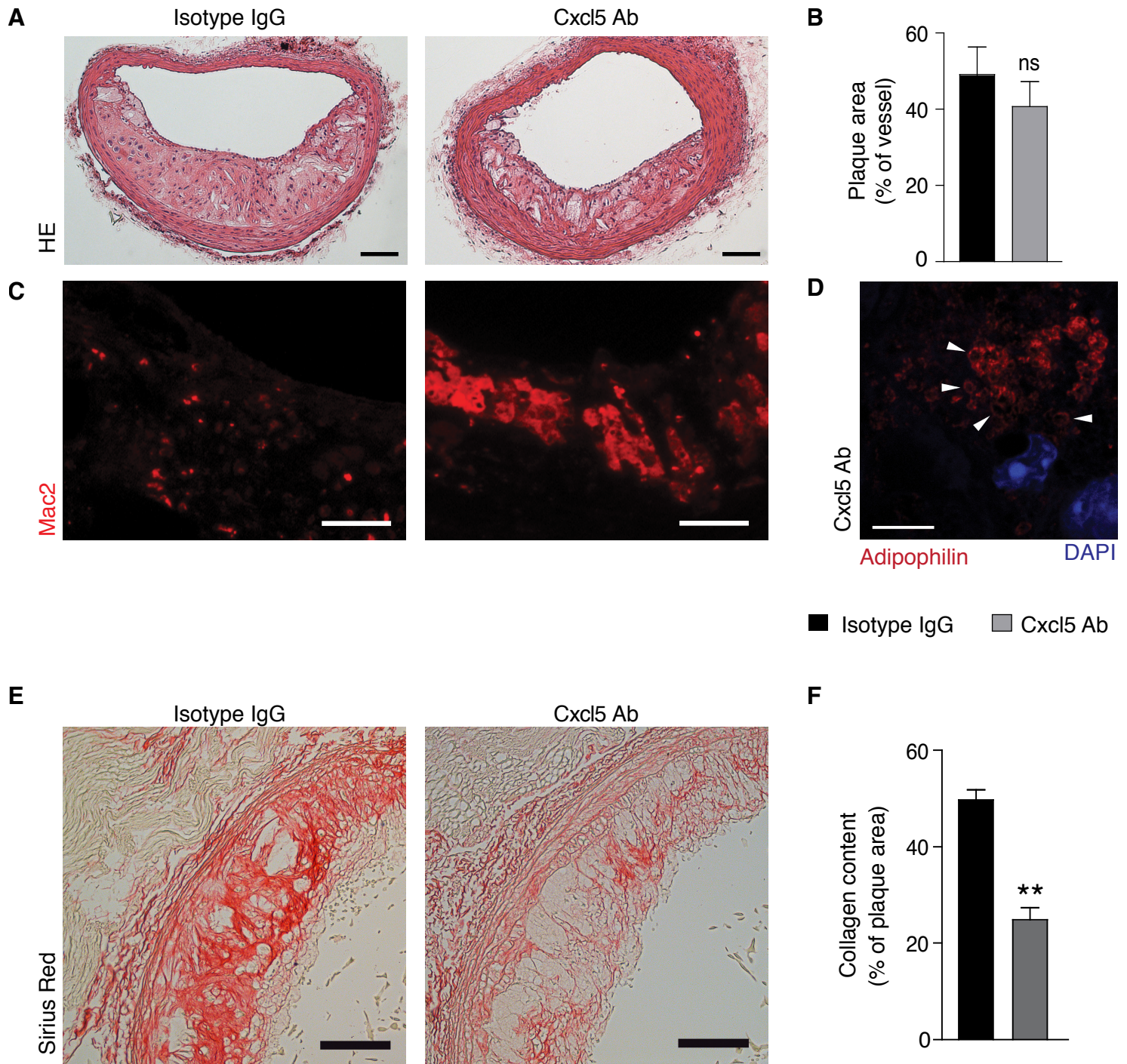
Supplemental Figure 2. Blockade of Cxcl5 augments macrophage foam cell formation.
ApoE$^{-/-}$ mice were fed a WD for 12wks and treated with either IgG isotype control (IgG) or anti-Cxcl5 Antibody (Cxcl5 Ab). Brachiocephalic artery and heart were removed, cut and stained. Representative images from brachiocephalic artery lesions of (A) hematoxylin-eosin staining (HE) and (C) Mac2 immunostaining for macrophage detection. (B) Quantification of plaque size in brachiocephalic artery lesions. (D) Representative image of brachiocephalic artery section from Cxcl5 Ab treated mice immunostained for adipophilin. White arrows indicate lipid-droplet. Representative images from aortic root lesions of (E) picosirius red staining for collagen detection. (F) Quantification of collagen content in aortic root lesions. (B and F) Data represent mean ± SEM. n =7- 8. **P<0.01. ns: not significant. Scale bars 100μm(A and E), 50μm (C), 10μm (D).
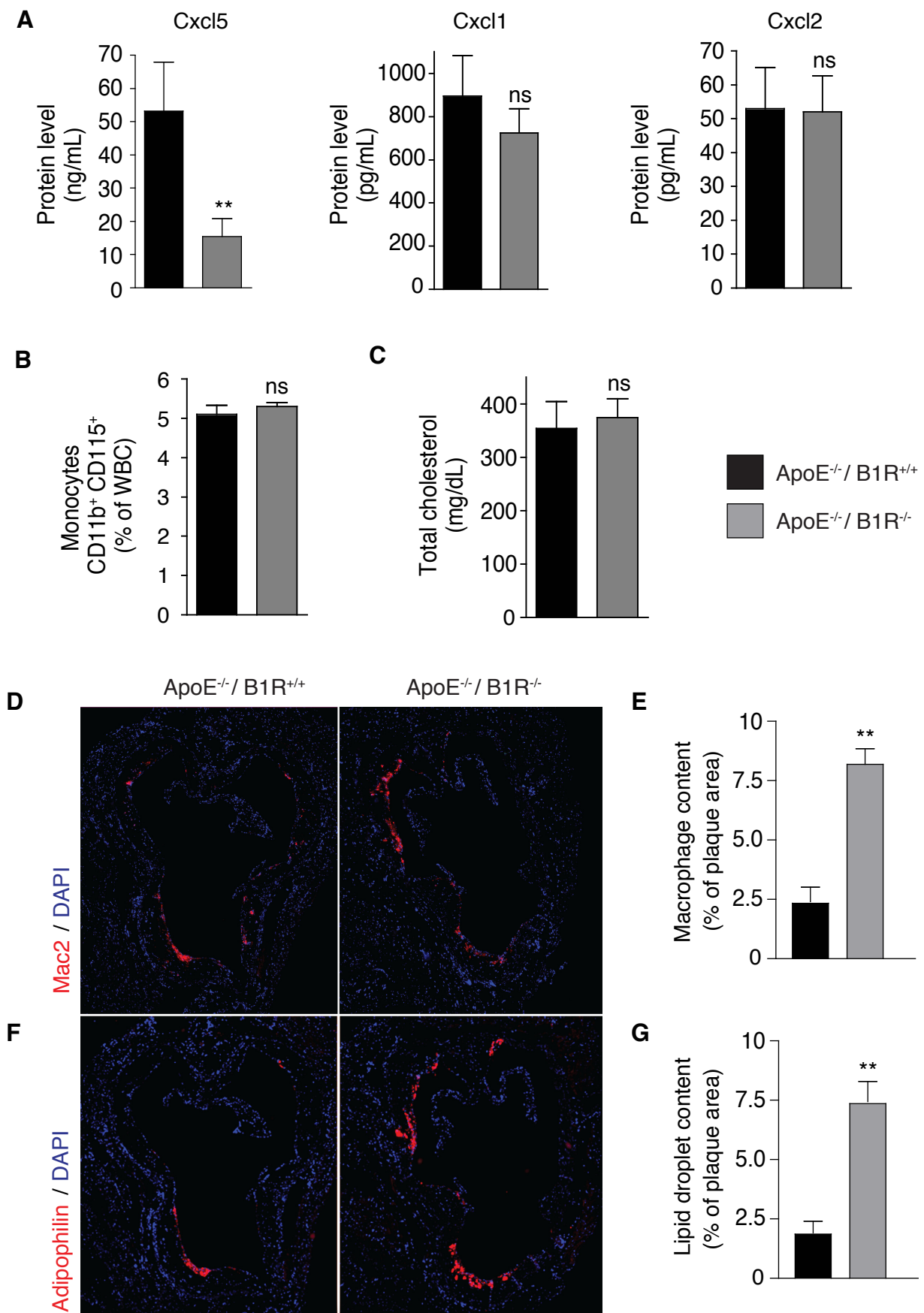
Supplemental Figure 3. Reduction of Cxcl5 in ApoE$^{-/-}$ B1R$^{-/-}$ mice is correlated with an increase of foam macrophage cells in atherosclerotic plaques.

ApoE$^{-/-}$ / B1R$^{+/+}$ and ApoE$^{-/-}$ / B1R$^{-/-}$ mice were fed a CD for 60wks. (A) Cxcl1, Cxcl2 and Cxcl5 levels were measured in plasma by ELISA. (B) Monocytes were measured in blood by flow cytometry analysis. (C) Cholesterol level was determined in plasma. (D-G) Heart was removed and aortic root section were analysed. Representative images of aortic root sections immunostained for Mac2 (D) and Adipophilin (F). Quantification of macrophage (E) and lipid-droplet (G) content in atherosclerotic plaque area within the aortic root. Data in A, B, C, E and G represent mean ± SEM. n = 8.**P<0.01. ns, not significant.

A

NaCl

Cxcl5

B
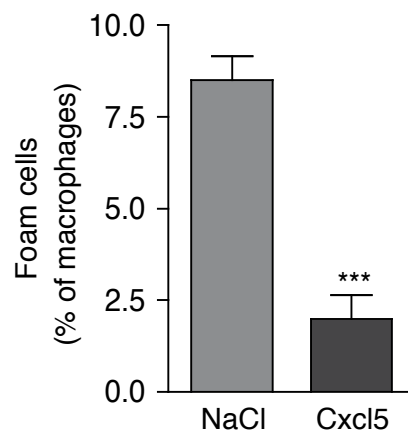
Supplemental Figure 4. Cxcl5 reduces macrophage foam cell formation in vivo.
ApoE^{-/-} mice were fed a WD and treated with either saline or Cxcl5 (i.p. 400ng, every 72h) for 12days. Peritoneal macrophages were isolated and stained with Oil-Red-O. (A) Representative images of peritoneal macrophages stained with Oil-Red-O. (B) Quantification of peritoneal foamy macrophages (Oil-Red-O positive). Data represent mean ± SEM. n = 3. ***P<0.001.
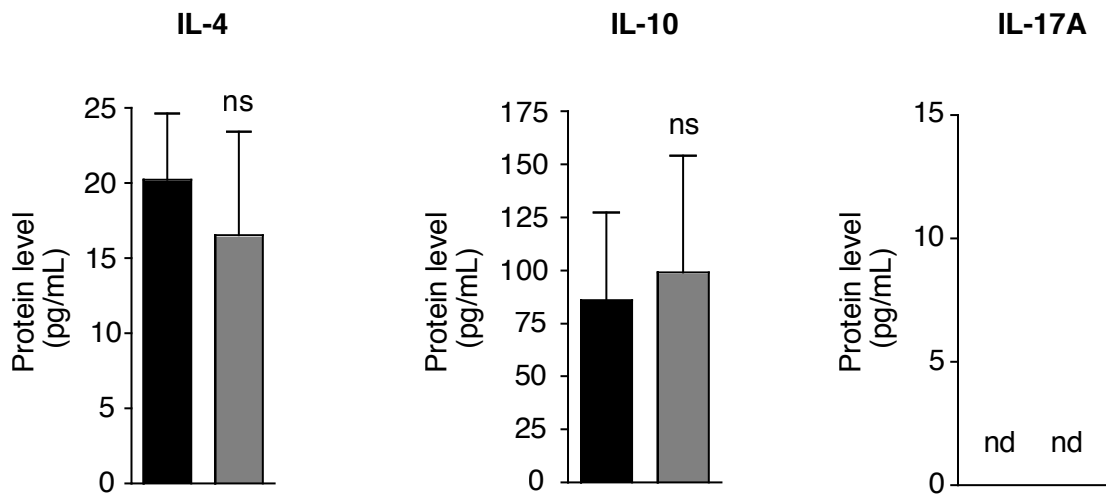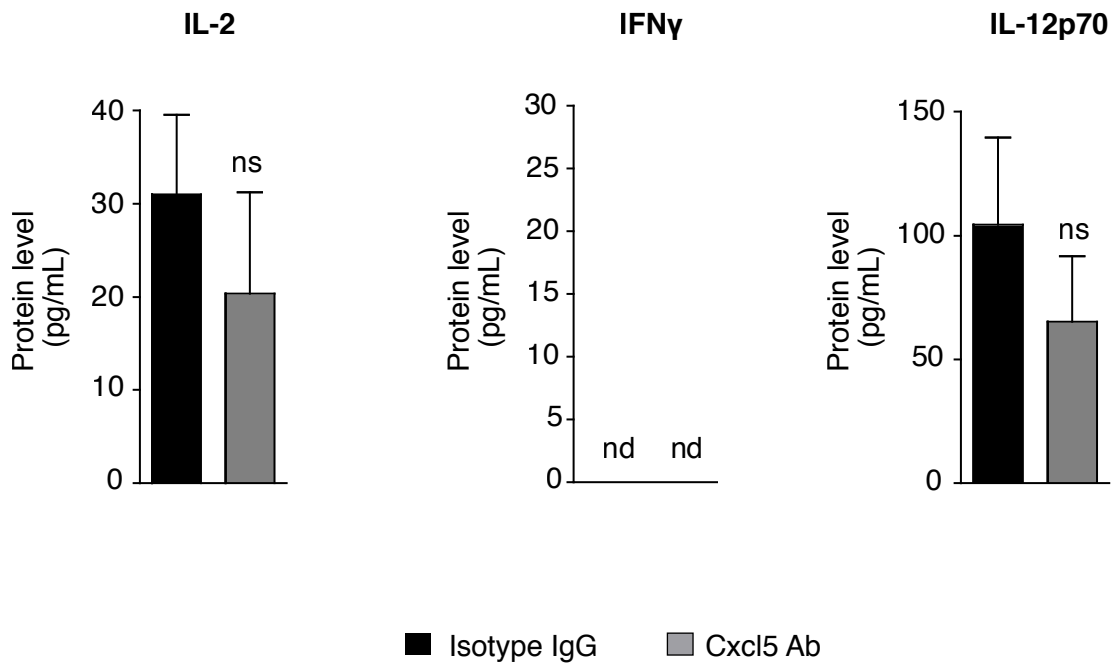
Supplemental Figure 5. Blockade of Cxcl5 does not affect plasma cytokine levels.
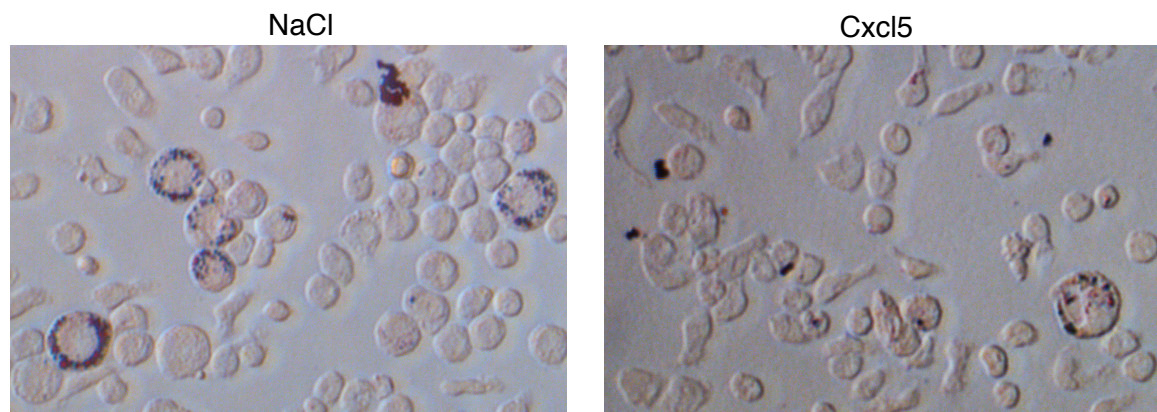ApoE$^{-/-}$ mice were fed a WD for 12wks and treated with either IgG isotype control (IgG) or anti-Cxcl5 Ab (Cxcl5 Ab). Selected plasma cytokines were analysed using Multiplex technology. Data represent mean ± SEM. n=7-8. ns: not significant; nd: not determined (below the limit of detection).
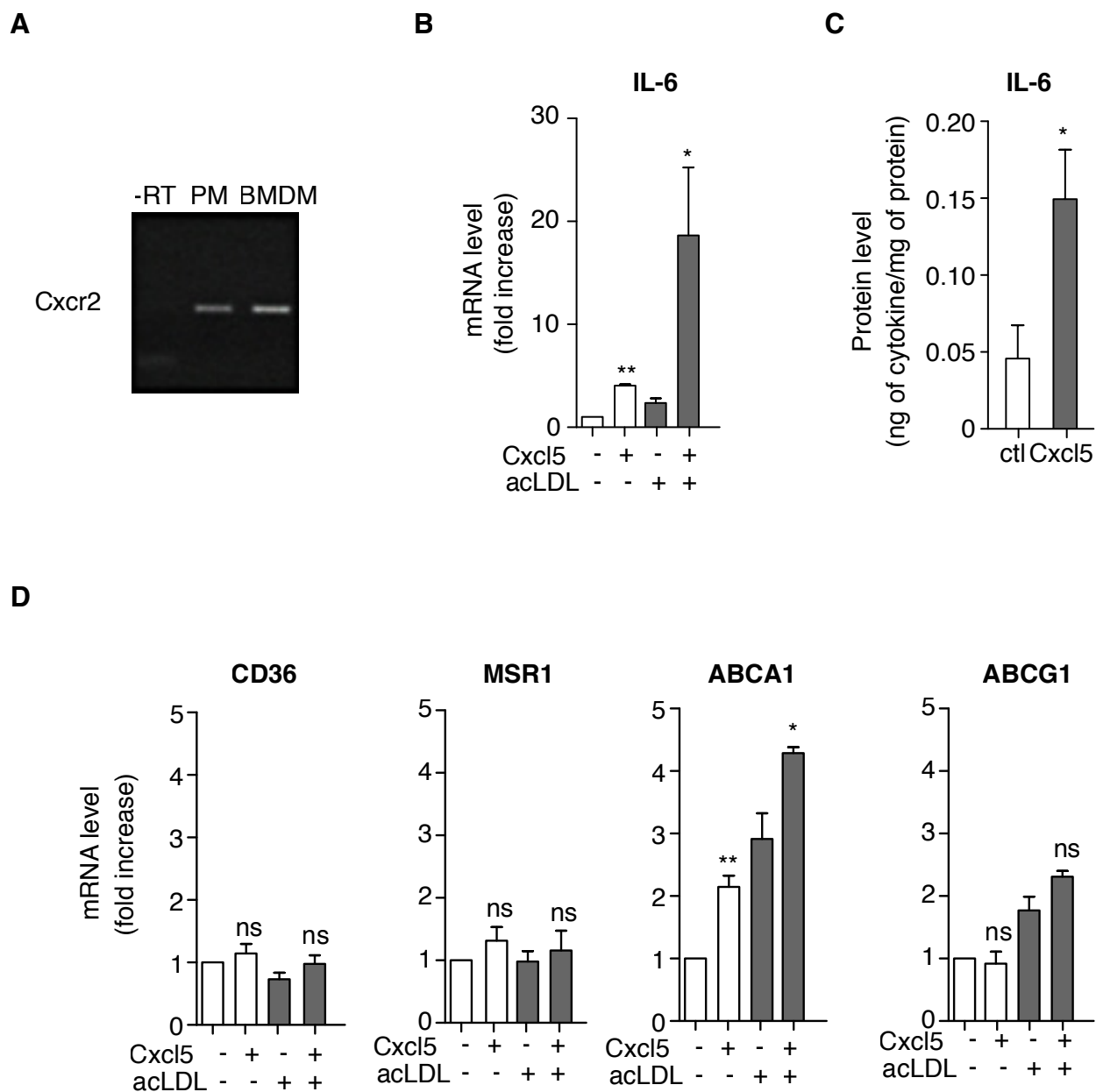
Supplemental Figure 6. Cxcl5 induces IL-6 and ABCA1 expression in peritoneal macrophages in vitro.
(A) Cxcr2 mRNA expression was determined by RT-PCR in BMDM and PM. Minus RT (-RT) serves as a negative control. (B-D) PM were cholesterol-loaded or not with acLDL and treated with or without Cxcl5. Macrophage activation was determined by IL-6 expression (B) at mRNA level using qPCR and (C) protein release in the medium using ELISA. (D) Expression of genes involved in cholesterol trafficking was measured by qPCR in PM. Data are mean ± SEM. n=5-8. **P<0.01, *P<0.05. ns, not significant.
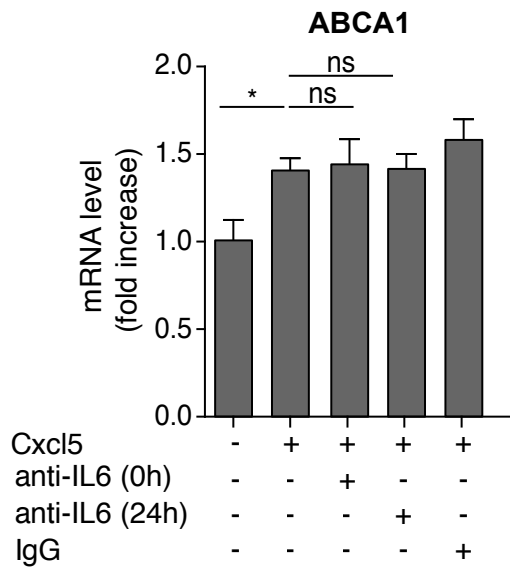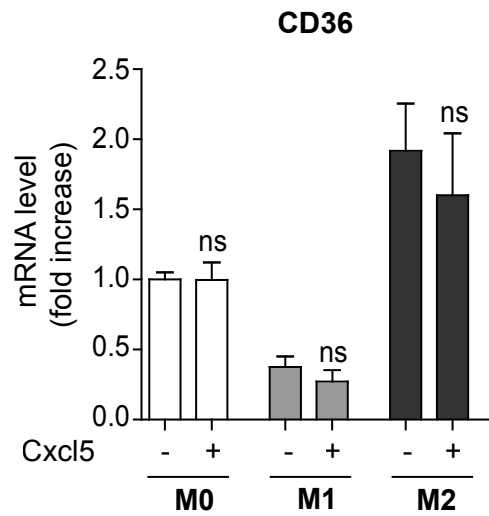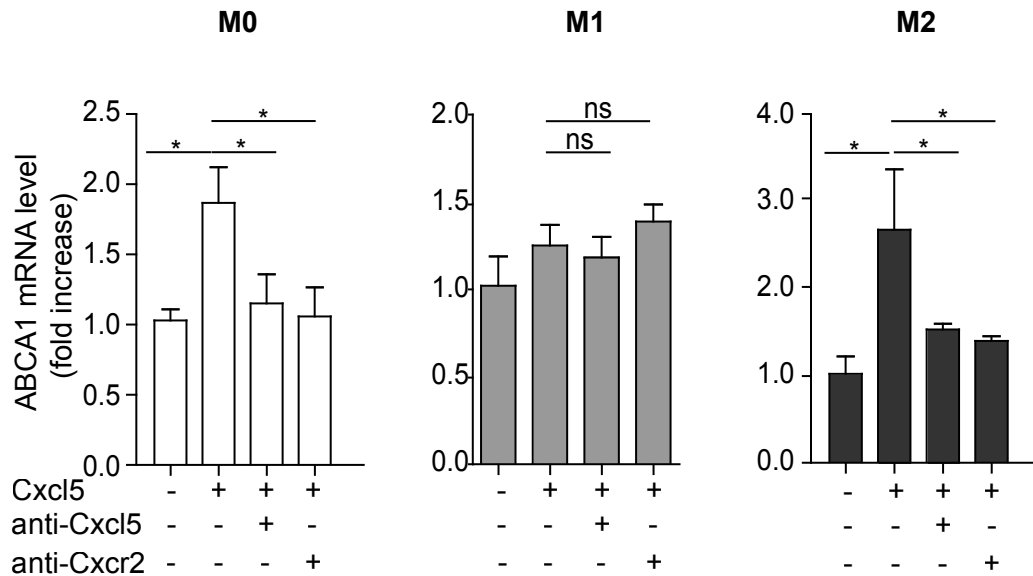
Supplemental Figure 7. Stimulation of Cxcl5-Cxcr2 axis induces expression of ABCA1 but not CD36 in M0 and M2 macrophages and is independent of IL-6 pathway.
(A) Cholesterol-loaded BMDM with acLDL were treated with anti-IL-6 Ab 20min prior to (0h) or 24h after Cxcl5 stimulation. ABCA1 mRNA expression was measured by qPCR at t=48h. (B-C) BMDM were treated with Cxcl5 (M0) or in combination with INFγ (M1) or IL-4 (M2) for 4h. Antibodies against Cxcl5 and Cxcr2 were added 20min prior to Cxcl5, INFγ and IL-4 treatments. CD36 (B) and ABCA1 (C) mRNA expression in naive (M0), classically-activated (M1) and alternatively-activated (M2) macrophage was determined by qPCR. Data are mean ± SEM. n=6. *P<0.05. ns, not significant.

Supplemental Table 1. List of genes significantly correlated to Cxcl5

Rank	Probeset	EntrezGeneID	Symbol	Correlation (R value)
1	1419728_at	20311	Cxcl5	1.0000
2	1440173_x_at	20344	Selp	0.9135
3	1422412_x_at	53876	Ear3	0.8930
4	1424415_s_at	233744	Spon1	0.8897
5	1421977_at	58223	Mmp19	0.8787
6	1418508_a_at	14784	Grb2	0.8732
7	1451537_at	12654	Chi3l1	0.8572
8	1438676_at	100702	Gbp6	0.8520
9	1418675_at	18414	Osmr	0.8507
10	1417721_s_at	16792	Laptm5	0.8500
11	1423878_at	71683	Gypc	0.8472
12	1444242_at	24059	Slco2a1	0.8453
13	1427747_a_at	16819	Lcn2	0.8408
14	1439015_at	14585	Gfra1	0.8407
15	1450826_a_at	20210	Saa3	0.8395
16	1426594_at	232288	Frmd4b	0.8392
17	1419209_at	14825	Cxcl1	0.8386
18	1450430_at	17533	Mrc1	0.8375
19	1420249_s_at	20305	Ccl6	0.8339
20	1442599_at	83704	Slc12a9	0.8336
21	1415804_at	20312	Cx3cl1	0.8300
22	1420498_a_at	13132	Dab2	0.8285
23	1426246_at	19128	Pros1	0.8282
24	1457539_at	52701	D10Ertd709e	0.8280
25	1450822_at	17110	Lyz1	0.8266
26	1448566_at	53945	Slc40a1	0.8259
27	1436987_at	319909	Ism1	0.8197
28	1423632_at	80290	Gpr146	0.8197
29	1417495_x_at	12870	Cp	0.8196
30	1423140_at	16889	Lipa	0.8190
31	1417019_a_at	23834	Cdc6	0.8187
32	1437046_x_at	75007	Fam63a	0.8176
33	1419417_at	22341	Vegfc	0.8159
34	1456620_at	432486	Gnptab	0.8149
35	1450020_at	13051	Cx3cr1	0.8087
36	1439518_at	105450	Mmrn2	0.8083
37	1424125_at	217826	Kcnk13	0.8083
38	1451680_at	76650	Srxn1	0.8074
39	1417523_at	56193	Plek	0.8066
40	1430124_x_at	58810	Akr1a4	0.8046
41	1436963_x_at	67706	Tmem179b	0.8008
42	1440759_at	100038499	Gm10672	0.8001
43	1443698_at	327959	Xaf1	0.8001
44	1449193_at	11801	Cd5l	0.7993
45	1426604_at	24014	Rnasel	0.7977
46	1435135_at	320024	Nceh1	0.7973
47	1451359_at	210992	Lpcat1	0.7948
48	1435143_at	13713	Elk3	0.7941
49	1436003_at	22329	Vcam1	0.7936
50	1449153_at	17381	Mmp12	0.7936
51	1418580_at	67775	Rtp4	0.7934

52	1419043_a_at	60440	Iigp1	0.7931
53	1421138_a_at	18768	Pkib	0.7929
54	1424616_s_at	233575	Pgap2	0.7929
55	1452948_at	69769	Tnfaip8l2	0.7927
56	1426385_x_at	22627	Ywhae	0.7927
57	1422243_at	14178	Fgf7	0.7925
58	1430704_at	73914	Irak3	0.7922
59	1453196_a_at	23962	Oasl2	0.7918
60	1444176_at	242341	Atp6v0d2	0.7915
61	1437726_x_at	12260	C1qb	0.7907
62	1434783_at	380967	Tmem106c	0.7905
63	1448668_a_at	16179	Irak1	0.7905
64	1449516_a_at	50780	Rgs3	0.7902
65	1427348_at	230738	Zc3h12a	0.7891
66	1427994_at	246746	Cd300lf	0.7886
67	1417793_at	54396	Irgm2	0.7882
68	1456111_at	244853	Fam55d	0.7874
69	1449025_at	15959	Ifit3	0.7858
70	1419100_at	20716	Serpina3n	0.7850
71	1417009_at	50909	C1ra	0.7834
72	1418090_at	84094	Plvap	0.7834
73	1449256_a_at	53869	Rab11a	0.7832
74	1421424_a_at	16790	Anpep	0.7831
75	1434380_at	229900	Gbp7	0.7820
76	1421034_a_at	16190	Il4ra	0.7805
77	1419463_at	80797	Clca2	0.7803
78	1433588_at	28006	D6Wsu116e	0.7796
79	**1421839_at**	**11303**	**Abca1**	**0.7795**
80	1425133_s_at	74760	Rab3il1	0.7793
81	1420699_at	56644	Clec7a	0.7790
82	1418626_a_at	12759	Clu	0.7789
83	1419932_s_at	83924	Gpr137b	0.7788
84	1433488_x_at	75612	Gns	0.7788
85	1418021_at	12268	C4b	0.7785
86	1448424_at	20378	Frzb	0.7783
87	1448303_at	93695	Gpnmb	0.7782
88	1448929_at	74145	F13a1	0.7782
89	1425823_at	545366	Cfhr2	0.7780
90	1424603_at	58911	Sumf1	0.7776
91	1449254_at	20750	Spp1	0.7772
92	1434784_s_at	380967	Tmem106c	0.7772
93	1435732_x_at	11984	Atp6v0c	0.7769
94	1451715_at	16658	Mafb	0.7762
95	1429527_a_at	22038	Plscr1	0.7754
96	1428777_at	114715	Spred1	0.7752
97	1435627_x_at	17357	Marcksl1	0.7750
98	1426808_at	16854	Lgals3	0.7748
99	1435133_at	22234	Ugcg	0.7746
100	1423547_at	17105	Lyz2	0.7737
101	1455204_at	71795	Pitpnc1	0.7736
102	1456424_s_at	18830	Pltp	0.7733
103	1451784_x_at	14964	H2-D1	0.7732
104	1429321_at	67702	Rnf149	0.7725
105	1425639_at	216991	Adap2	0.7723
106	1439454_x_at	69742	Tm2d2	0.7720
107	1417040_a_at	51800	Bok	0.7720
108	1420562_at	57277	Slurp1	0.7718
109	1452647_a_at	67728	Dph2	0.7717

110	1448380_at	19039	Lgals3bp	0.7717
111	1451651_at	278180	Vsig4	0.7714
112	1415983_at	18826	Lcp1	0.7714
113	1419449_a_at	14678	Gnai2	0.7712
114	1418133_at	12051	Bcl3	0.7711
115	1451931_x_at	14980	H2-L	0.7684
116	1417492_at	13030	Ctsb	0.7682
117	1426774_at	243771	Parp12	0.7681
118	1448591_at	13040	Ctss	0.7680
119	1436333_a_at	104015	Synj1	0.7680
120	1441216_at	20442	St3gal1	0.7677
121	1454783_at	16164	Il13ra1	0.7676
122	1422062_at	20288	Msr1	0.7672
123	1418318_at	66889	Rnf128	0.7669
124	1427076_at	17476	Mpeg1	0.7667
125	1418736_at	26879	B3galnt1	0.7664
126	1451243_at	215615	Rnpep	0.7661
127	1437760_at	230145	Galnt12	0.7660
128	1422645_at	15216	Hfe	0.7657
129	1451866_a_at	15234	Hgf	0.7656
130	1421172_at	11489	Adam12	0.7656
131	1454086_a_at	16909	Lmo2	0.7650
132	1423593_a_at	12978	Csf1r	0.7649
133	1422978_at	13058	Cybb	0.7648
134	1456212_x_at	12702	Socs3	0.7648
135	1422868_s_at	14544	Gda	0.7645
136	1436589_x_at	101540	Prkd2	0.7632
137	1427103_at	102595	Plekho2	0.7630
138	1433500_at	209773	Dennd2a	0.7619
139	1455357_x_at	67952	Tomm20	0.7618
140	1444052_at	14257	Flt4	0.7609
141	1427327_at	231805	Pilra	0.7607
142	1450764_at	27052	Aoah	0.7601
143	1448163_at	26384	Gnpda1	0.7598
144	1451191_at	12904	Crabp2	0.7595
145	1420196_s_at	100855	Tbc1d14	0.7594
146	1427682_a_at	13654	Egr2	0.7591
147	**1450297_at**	**16193**	**Il6**	**0.7590**
148	1422572_at	56212	Rhog	0.7589
149	1424523_at	140580	Elmo1	0.7583
150	1460619_at	211798	Mfsd9	0.7583
151	1416022_at	16592	Fabp5	0.7582
152	1420697_at	65221	Slc15a3	0.7581
153	1442082_at	12267	C3ar1	0.7579
154	1418539_a_at	19267	Ptpre	0.7572
155	1450678_at	16414	Itgb2	0.7570
156	1438633_x_at	16796	Lasp1	0.7567
157	1455221_at	11307	Abcg1	0.7565
158	1455476_a_at	382034	Gse1	0.7562
159	1449370_at	20677	Sox4	0.7561
160	1436838_x_at	72042	Cotl1	0.7560
161	1430700_a_at	27226	Pla2g7	0.7559
162	1419194_s_at	63986	Gmfg	0.7558
163	1452117_a_at	23880	Fyb	0.7553
164	1424727_at	12774	Ccr5	0.7548
165	1426528_at	18187	Nrp2	0.7544
166	1455660_at	12983	Csf2rb	0.7541
167	1420703_at	12982	Csf2ra	0.7538

168	1428758_at	67893	Tmem86a	0.7535
169	1425546_a_at	22041	Trf	0.7534
170	1423776_s_at	223754	Tbc1d22a	0.7533
171	1415686_at	68365	Rab14	0.7531
172	1434308_at	215113	Slc43a2	0.7527
173	1452068_at	67111	Naaa	0.7523
174	1453055_at	214968	Sema6d	0.7519
175	1460273_a_at	17948	Naip2	0.7518
176	1449824_at	96875	Prg4	0.7514
177	1439256_x_at	664862	Gpr137b-ps	0.7509
178	1449360_at	12984	Csf2rb2	0.7507
179	1416094_at	11502	Adam9	0.7507
180	1424470_a_at	223864	Rapgef3	0.7506
181	1424126_at	11655	Alas1	0.7502
182	1460437_at	72318	Cyth4	0.7500
183	1417648_s_at	69178	Snx5	0.7498
184	1426623_a_at	70497	Arhgap17	0.7498
185	1424265_at	74091	Npl	0.7494
186	1434376_at	12505	Cd44	0.7494
187	1455741_a_at	230857	Ece1	0.7494
188	1425797_a_at	20963	Sykb	0.7489
189	1419128_at	16411	Itgax	0.7489
190	1451821_a_at	20684	Sp100	0.7489
191	1456581_x_at	14569	Gdi2	0.7487
192	1449164_at	12514	Cd68	0.7486
193	1421322_a_at	16391	Irf9	0.7484
194	1423722_at	75909	Vmp1	0.7483
195	1425789_s_at	11752	Anxa8	0.7481
196	1436530_at	100034251	Gm11428	0.7478
197	1435449_at	12125	Bcl2l11	0.7474
198	1419609_at	12768	Ccr1	0.7474
199	1449429_at	14226	Fkbp1b	0.7474
200	1422631_at	11622	Ahr	0.7469
201	1419883_s_at	11966	Atp6v1b2	0.7469
202	1428187_at	16423	Cd47	0.7468
203	1448118_a_at	13033	Ctsd	0.7465
204	1452279_at	18636	Cfp	0.7464
205	1419534_at	108078	Olr1	0.7461
206	1442798_x_at	212032	Hk3	0.7460
207	1427691_a_at	15976	Ifnar2	0.7460
208	1457035_at	226691	AI607873	0.7456
209	1438561_x_at	75146	Tmem180	0.7453
210	1436223_at	320910	Itgb8	0.7452
211	1451363_a_at	72121	Dennd2d	0.7449
212	1448550_at	16803	Lbp	0.7442
213	1449156_at	17085	Ly9	0.7437
214	1422648_at	11988	Slc7a2	0.7436
215	1419605_at	17312	Clec10a	0.7434
216	1423571_at	13609	S1pr1	0.7434
217	1449280_at	71690	Esm1	0.7432
218	1421187_at	12772	Ccr2	0.7430
219	1417381_at	12259	C1qa	0.7426
220	1419598_at	68774	Ms4a6d	0.7426
221	1450686_at	330260	Pon2	0.7424
222	1435416_x_at	14755	Pigq	0.7422
223	1419589_at	17064	Cd93	0.7418
224	1417073_a_at	19317	Qk	0.7417
225	1448620_at	14131	Fcgr3	0.7416

226	1460430_at	72065	Rap2c	0.7414
227	1424595_at	16456	F11r	0.7413
228	1443783_x_at	14960	H2-Aa	0.7412
229	1448595_a_at	19716	Bex1	0.7409
230	1442849_at	16971	Lrp1	0.7405
231	1415947_at	433375	Creg1	0.7398
232	1449846_at	13587	Ear2	0.7397
233	1439069_a_at	66776	Pisd-ps3	0.7395
234	1434731_x_at	18477	Prdx1	0.7388
235	1416046_a_at	66848	Fuca2	0.7384
236	1449454_at	12182	Bst1	0.7383
237	1449519_at	13197	Gadd45a	0.7383
238	1459740_s_at	22228	Ucp2	0.7380
239	1424302_at	18733	Lilrb3	0.7380
240	1450424_a_at	16068	Il18bp	0.7378
241	1416968_a_at	101502	Hsd3b7	0.7376
242	1439440_x_at	23999	Twf2	0.7376
243	1416013_at	18807	Pld3	0.7376
244	1437347_at	13618	Ednrb	0.7375
245	1460235_at	12492	Scarb2	0.7374
246	1448313_at	12751	Tpp1	0.7373
247	1415687_a_at	19156	Psap	0.7373
248	1441281_s_at	18081	Ninj1	0.7368
249	1418738_at	20266	Scn1b	0.7368
250	1450241_a_at	14017	Evi2a	0.7365
251	1433741_at	12494	Cd38	0.7364
252	1427020_at	219151	Scara3	0.7360
253	1449033_at	18383	Tnfrsf11b	0.7360
254	1418446_at	20502	Slc16a2	0.7355
255	1438138_a_at	224824	Pex6	0.7354
256	1419042_at	60440	Iigp1	0.7352
257	1446951_at	320452	P4ha3	0.7349
258	1437454_a_at	66958	Tmx2	0.7348
259	1426441_at	18174	Slc11a2	0.7347
260	1448576_at	16197	Il7r	0.7346
261	1448919_at	66205	Cd302	0.7344
262	1424067_at	15894	Icam1	0.7333
263	1451310_a_at	13039	Ctsl	0.7331
264	1418340_at	14127	Fcer1g	0.7329
265	1425733_a_at	13860	Eps8	0.7328
266	1448617_at	12508	Cd53	0.7328
267	1457753_at	279572	Tlr13	0.7325

Supplemental Table 2. List of the Biological Functions of genes coregulated with Cxcl5 generated by PANTHER Classification System.

Biological Process	amount	expected	P value
immune system process	82	17.54	2.55E-33
response to stimulus	55	14.49	9.00E-18
immune response	29	5.19	1.29E-13
cytokine-mediated signaling pathway	19	2.61	3.25E-11
signal transduction	78	37.09	4.17E-11
cell communication	80	38.76	5.27E-11
cellular process	96	56.16	8.41E-09
macrophage activation	**12**	**1.65**	**1.47E-07**
cell surface receptor linked signal transduction	43	18.96	3.97E-07

Supplemental Table 3. List of primers

Gene	Species	Forward	Reverse
Cxcl1	mouse	TGAGCTGCGCTGTCAGTGCCT	AGAAGCCAGCGTTCACCAGA
Cxcl2	mouse	GAGCTTGAGTGTGACGCCCCCAGG	GTTAGCCTTGCCTTTGTTCAGTATC
Cxcl5	mouse	GCATTTCTGTTGCTGTTCACGCTG	CCTCCTTCTGGTTTTTCAGTTTAGC
Cxcr2	mouse	ATGCCCTCTATTCTGCCAGAT	GTGCTCCGGTTGTATAAGATGAC
IL-6	mouse	CTGCAAGAGACTTCCATCCAGTT	GAAGTAGGGAAGGCCGTGG
CD36	mouse	TTTCCTCTGACATTTGCAGGTCTA	AAAGGCATTGGCTGGAAGAA
MSR1	mouse	TGAACGAGAGGATGCTGACTG	TGTCATTGAACGTGCGTCAAA
ABCA1	mouse	CCCAGAGCAAAAAGCGACTC	GGTCATCATCACTTTGGTCCTTG
ABCG1	mouse	ATCTGAGGGATCTGGGTCTGA	CCTGATGCCACTTCCATGA
HPRT	mouse	GTAATGATCAGTCAACGGGGGAC	CCAGCAAGCTTGCAACCTTAACCA
β-actin	mouse	GAAATCGTGCGTGACATCAAAG	TGTAGTTTCATGGATGCCACAG
CXCL8	human	GAATGGGTTTGCTAGAATGTGATA	CAGACTAGGGTTGCCAGATTTAAC
CXCL6	human	GGTCCTGTCTCTGCTGTGC	GGGAGGCTACCACTTCCA
GAPDH	human	CATGTTCGTCATGGGTGTGAA	ATGGACTGTGGTCATGAGTCCTT

6.4   Atypical chemokine receptor 1 on nucleated erythroid cells regulates hematopoiesis.

Duchene J, Novitzky-Basso I, Thiriot A, Casanova-Acebes M, Bianchini M, Etheridge SL, Hub E, Nitz K, Artinger K, Eller K, Caamaño J, Rülicke T, Moss P, Megens RTA, von Andrian UH, Hidalgo A, Weber C, Rot A.

Atypical chemokine receptor 1 on nucleated erythroid cells regulates hematopoiesis

Johan Duchene[1,14], Igor Novitzky-Basso[2,14], Aude Thiriot[3,4], Maria Casanova-Acebes[5], Mariaelvy Bianchini[1], S Leah Etheridge[6], Elin Hub[6], Katrin Nitz[1,7], Katharina Artinger[6,8], Kathrin Eller[8], Jorge Caamaño[9] , Thomas Rülicke[10] , Paul Moss[9], Remco T A Megens[1,11], Ulrich H von Andrian[3,4], Andres Hidalgo[1,5] , Christian Weber[1,11] & Antal Rot[1,6,12,13]

Healthy individuals of African ancestry have neutropenia that has been linked with the variant rs2814778(G) of the gene encoding atypical chemokine receptor 1 (*ACKR1*). This polymorphism selectively abolishes the expression of ACKR1 in erythroid cells, causing a Duffy-negative phenotype. Here we describe an unexpected fundamental role for ACKR1 in hematopoiesis and provide the mechanism that links its absence with neutropenia. Nucleated erythroid cells had high expression of ACKR1, which facilitated their direct contact with hematopoietic stem cells. The absence of erythroid ACKR1 altered mouse hematopoiesis including stem and progenitor cells, which ultimately gave rise to phenotypically distinct neutrophils that readily left the circulation, causing neutropenia. Individuals with a Duffy-negative phenotype developed a distinct profile of neutrophil effector molecules that closely reflected the one observed in the ACKR1-deficient mice. Thus, alternative physiological patterns of hematopoiesis and bone marrow cell outputs depend on the expression of ACKR1 in the erythroid lineage, findings with major implications for the selection advantages that have resulted in the paramount fixation of the *ACKR1* rs2814778(G) polymorphism in Africa.

Chemokines comprise a family of structurally homologous, intercellular molecular signals that induce migration and other cellular responses, including adhesion, activation, differentiation, proliferation and survival[1–4]. Chemokine effects are mediated by classical G-protein-coupled receptors (GPCRs)[1,2]. Additionally, chemokines ligate atypical chemokine receptors (ACKRs)[5,6]. ACKRs are structurally similar to GPCRs but do not couple to G proteins and therefore fail to induce the full spectrum of downstream intracellular signals that characterize GPCRs[7,8]. However ACKRs may transport, present or scavenge chemokines and thus, by different means, effectively regulate chemokine availability in tissue microenvironments[9–12]. ACKR1, also known as Duffy antigen receptor for chemokines (or DARC), binds more than 20 different CC and CXC chemokines[13,14], and has been ascribed a unique cell expression profile in cerebellar neurons, venular endothelial cells and erythrocytes[13,14]. In endothelial cells, ACKR1 transports and presents chemokines[9]. ACKR1 on erythrocytes has been shown to regulate chemokine concentrations in plasma by functioning as both a chemokine sink and a reservoir[15–17], and to bind

Plasmodium vivax and *Plasmodium knowlesi,* thus allowing these parasites to invade the erythrocytes[18,19].

Divergent paths of human evolution and adaptations to geographically restricted microbial pathogens have resulted in the development of distinctive functions of the immune system that characterize people of different ethnicities[20,21]. Under physiological conditions, individuals of African ancestry have low blood neutrophil counts[22]. Such 'ethnic neutropenia' has been directly linked with the allelic variant rs2814778(G) of *ACKR1*, which is hugely prevalent in Africa, but the mechanism underlying this association remained unexplored[23]. Individuals of African ancestry who are homozygous for the rs2814778(G) allele of *ACKR1* do not express ACKR1 on erythrocytes[24,25]. This 'Duffy-negative' phenotype is caused by a 1-nt substitution within the promoter sequence of *ACKR1*, which disrupts the binding site for the erythroid transcription factor GATA-1 and leads to the selective loss of ACKR1 expression in erythrocytes but not in endothelium[26,27]. Because erythrocytes are terminally differentiated anuclear cells with no transcription and limited translation[28], the expression of ACKR1 might first occur during the earlier stages of
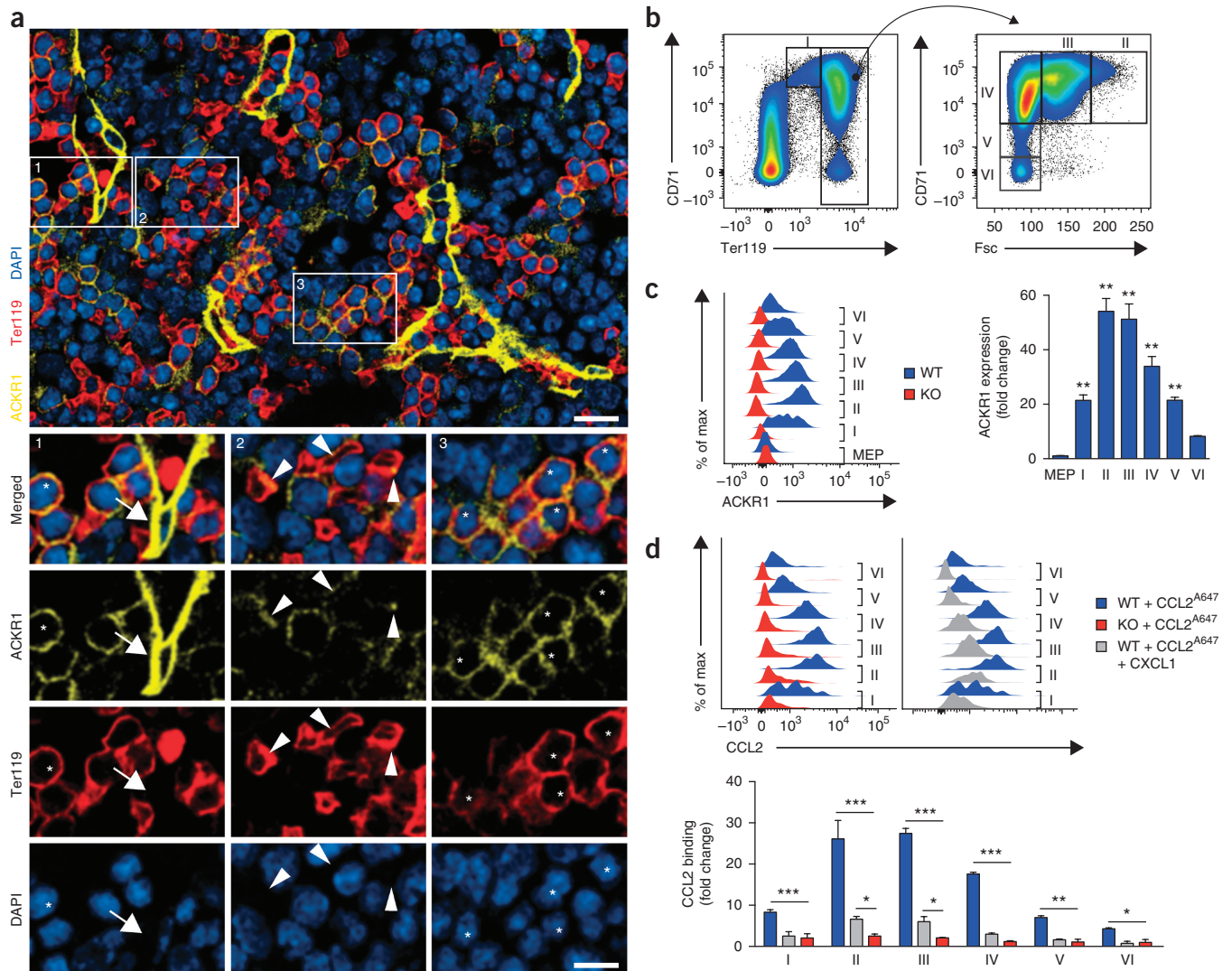
erythroid cell development in the bone marrow (BM). We therefore sought to determine ACKR1 expression in the BM, to investigate its effect on hematopoiesis and to explore the mechanism leading in the absence of erythroid ACKR1 to neutropenia.

RESULTS

ACKR1 is highly expressed by nucleated erythroid cells

We used a new monoclonal antibody specific for mouse ACKR1 (ref. 29) to map ACKR1 expression in mouse BM. Besides its expression

in endothelial cells (ECs), which line BM sinusoids, ACKR1 was detected on erythroid cells but not on any other hematopoietic population (**Fig. 1a–c** and **Supplementary Figs. 1** and **2**). We found that ACKR1 was expressed in nucleated erythroid cells (NECs)—ACKR1 expression was detected initially in pro-erythroblasts, found to peak in early normoblasts and to gradually decline to the lowest amounts in mature erythrocytes (**Fig. 1c** and **Supplementary Fig. 2b**). ACKR1 on NECs was functional, as fluorescently labeled CCL2, an ACKR1-cognate chemokine, bound to NEC subpopulations proportionately to the
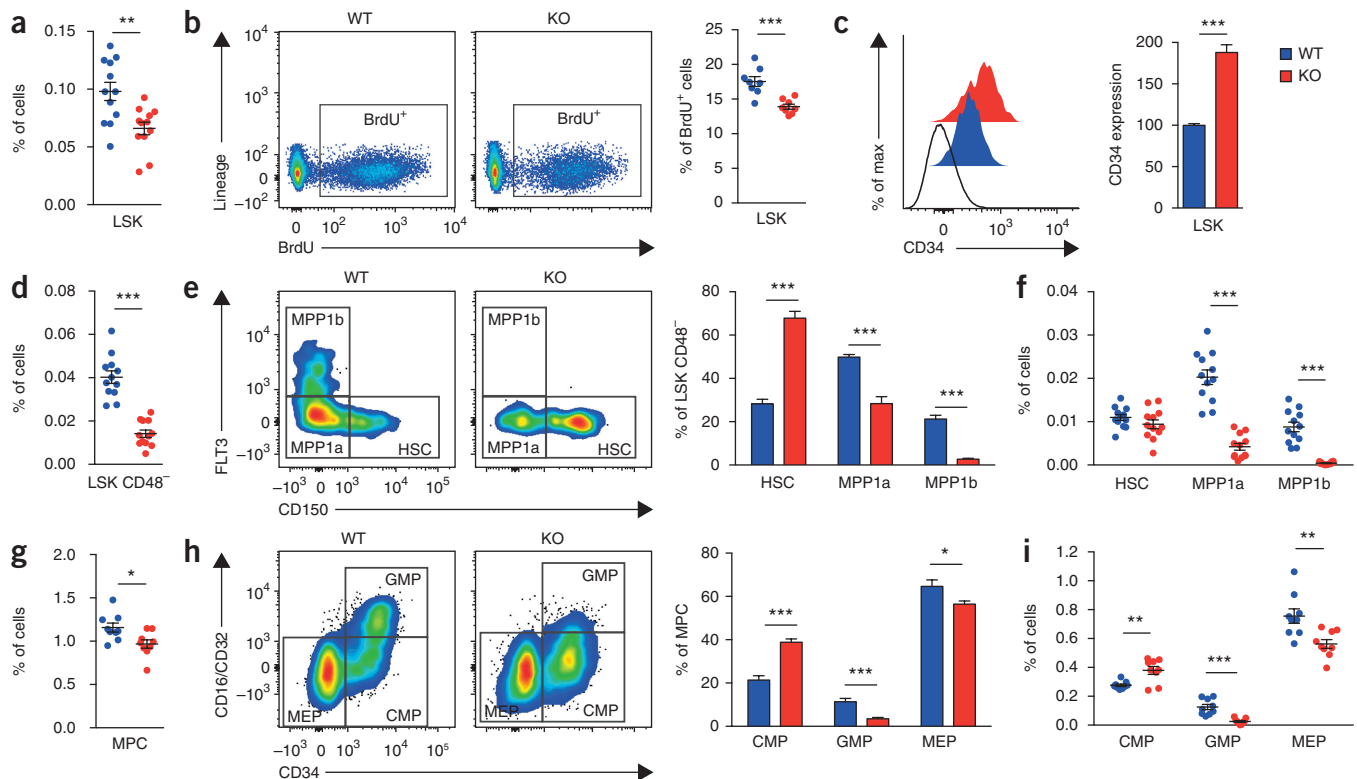
Figure 1 ACKR1 is expressed in the bone marrow by ECs and NECs. (**a**) Representative immunofluorescence micrograph of BM from wild-type (WT) mice after staining with antibodies to ACKR1 (yellow) and the erythroid cell marker Ly76 (also known as Ter119; red) and with DAPI (blue; nuclei) (top). Regions labeled 1–3 are magnified on the bottom. Insets, representative images (of at least 20 taken) showing ACKR1 immunoreactivity in sinusoidal ECs (arrows), anuclear mature erythrocytes (arrowheads) and NECs (asterisks). Scale bars, 30 μm (top) and 15 μm (inset). (**b**) Representative flow cytometry analysis of BM from WT mice ($n = 6$) to identify the stages of erythroid maturation: pro-erythroblasts (population I), early normoblasts (population II), intermediate normoblasts (population III), late normoblasts (population IV), reticulocytes (population V) and mature red cells (population VI), which were gated on the basis of CD71 and Ter119 expression and on forward scatter (Fsc). (**c**) ACKR1 expression on megakaryocytic-erythroid progenitor (MEP) cells and erythroid cells (populations I–VI) in BM from WT (blue) and ACKR1-deficient (KO; red) mice. Left, representative flow cytometry histogram analysis; right, quantification of MEP and erythroid cell populations, expressed as fold change relative to MEP ($n = 6$ mice per group). (**d**) Representative flow cytometry analyses for binding of AF647-conjugated CCL2 to erythroid cells (populations I–VI) that were isolated from the BM of WT (blue) and KO (red) mice (top left) and for competition of AF647-conjugated CCL2 binding to WT erythroid cells by subsequent addition of unlabeled CXCL1 (top right). Bottom, quantification of AF647-conjugated CCL2 binding, expressed as fold change relative to the amount bound to ACKR1-deficient erythrocytes ($n = 2$ mice per group). *$P < 0.05$, **$P < 0.01$ and ***$P < 0.001$ (one-way analysis of variance (ANOVA) (**c**) or two-way ANOVA (**d**)). Data are representative of at least two independent experiments (**a,b,c** (left),**d** (bottom)) or are from two independent experiments (**c,d**). Mean ± s.e.m. (**c**) or mean ± s.d. (**d**).

Figure 2 ACKR1 deficiency alters HSPC populations. (**a–c**) Frequency of LSK cells in the BM from WT (blue; $n = 12$ mice) and ACKR1-deficient (KO; red; $n = 12$ mice) mice (**a**), and flow cytometry analysis of BrdU incorporation ($n = 8$ mice per group) (**b**) and CD34 expression (WT, $n = 12$ mice per group) (**c**) in LSK cells. Each circle represents an individual mouse. (**d,e**) Frequency of LSK CD48⁻ cells (**d**) and relative distribution of their HSC, MPP1a and MPP1b subpopulations (**e**) ($n = 12$ mice per group). (**f**) Frequencies of HSCs and of MPP1a and MPP1b cells in the BM of WT ($n = 12$) and KO ($n = 12$) mice. (**g,h**) Frequency of MPCs (**g**) and distribution of their CMP, GMP and MEP subpopulations (**h**) ($n = 9$ mice per group). (**i**) Frequencies of CMP, GMP and MEP cells in the BM of WT and KO mice ($n = 9$ mice per group). *$P < 0.05$, **$P < 0.01$ and ***$P < 0.001$ (two-tailed Student's t-test). Data are from four (**a,c–f**), two (**b**) or three (**g–i**) independent experiments. Mean ± s.e.m.

levels of their ACKR1 expression (**Fig. 1d**). ACKR1 is the only chemokine receptor that binds both CCL2 and a heterologous chemokine CXCL1. We found that even after extended pre-incubation of NECs with CCL2, almost all of the NEC-bound CCL2 could be displaced by the addition of CXCL1 (**Fig. 1d**). This result suggests that ACKR1 on NECs did not internalize chemokines, which remained available on the cell surface. In summary, our data unequivocally showed that, among hematopoietic BM cells, ACKR1 was expressed only in cells of the erythroid lineage. The high level of ACKR1 expression and chemokine binding by NECs, as compared to those in mature erythrocytes, suggested that ACKR1 might have an important physiological role in the BM.

ACKR1 deficiency alters early hematopoiesis

To evaluate the contribution of ACKR1 expression to BM homeostasis, we compared parameters of hematopoiesis in ACKR1-deficient[30] and wild-type mice. We found no effect of ACKR1 expression on overall BM cellularity, number of erythroid cells, relative proportions of their individual subpopulations or any of the erythrocyte parameters in blood (**Supplementary Fig. 3**). However, ACKR1 expression had cell-extrinsic effects on the BM hematopoietic stem and progenitor cells (HSPCs). In the absence of ACKR1, the size of the lineage-negative (Lin⁻) Sca-1⁺c-Kit⁺ (LSK) cell population decreased (**Fig. 2a**). This was accompanied by their reduced proliferation (**Fig. 2b**) and an increase in the cell surface expression of CD34 (**Fig. 2c**). A major reduction was seen in the CD48⁻ subpopulation of LSKs, characterized by their self-renewing capacity

(**Fig. 2d**). Furthermore, we observed shifts in the proportions of individual LSK CD48⁻ subpopulations in ACKR1-deficient mice, as compared to their wild-type littermates (**Fig. 2e,f**). These included an increase in the relative proportion of hematopoietic stem cells (HSCs; **Fig. 2e**), although their overall numbers remained unaltered (**Fig. 2f**), as well as a relative and an absolute decrease of the CD150⁻Flt3⁻ and CD150⁻Flt3⁺ multipotent progenitor (MPP) 1a and MPP1b subpopulations (**Fig. 2e,f**). Furthermore, the size of the Lin⁻Sca-1⁻c-Kit⁺ myeloid progenitor cell (MPC) population was less in the BM from ACKR1-deficient mice than in the BM from wild-type mice (**Fig. 2g**) due to decreases in populations of CD34⁺CD16/CD32⁺ granulocytic–monocytic progenitor (GMP) and CD34⁻CD16/CD32⁻ megakaryocytic–erythroid progenitor (MEP) cells (**Fig. 2h,i**). Conversely, the proportions of CD34⁺CD16/CD32⁻ common myeloid progenitor (CMP) cells and LSK CD48⁺Flt3⁻ (MMP2) cells were greater in the BM from ACKR1-deficient mice than in the BM from wild-type mice (**Fig. 2h,i** and **Supplementary Fig. 4b–d**), whereas the numbers of LSK CD48⁺ cells, lineage-restricted progenitor (LRP) cells and common lymphoid progenitor (CLP) cells remained unchanged (**Supplementary Fig. 4b,d,e**). Thus, the absence of ACKR1 resulted in numeric changes and shifts in equilibria of HSPC subpopulations and led to characteristic changes in the expression of effector molecules on their cell surface.

ACKR1 deficiency changes the HSPC transcriptome

Next we asked whether ACKR1 expression also affected the transcriptional make-up of HSPCs. To this end, LSK and GMP cells from
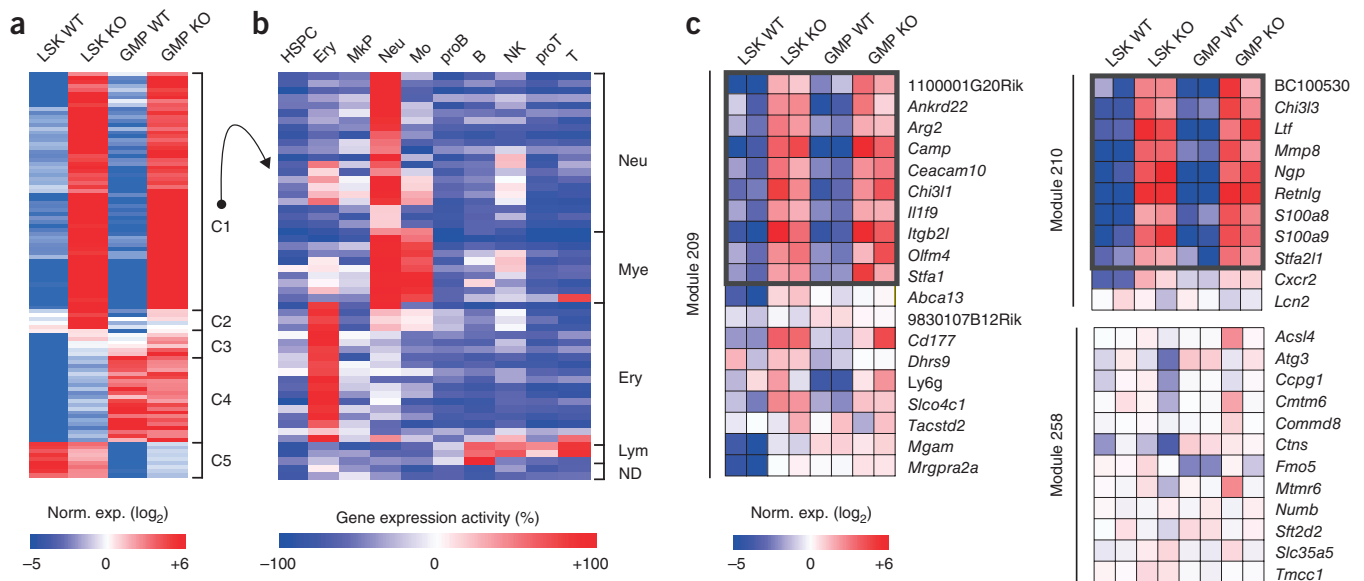
Figure 3 ACKR1 deficiency changes HSPC transcriptomes. (**a**) Microarray analysis of gene expression in LSK and GMP cell populations from the BM of WT and ACKR1-deficient (KO) mice ($n = 2$ samples per group). Colored bar shows normalized expression values. C, cluster. (**b**) Genes from cluster 1 were analyzed for their expression activity in different BM cell types. Ery, erythroid cells; MkP, megakaryocyte progenitors; Neu, neutrophils; Mo, monocytes; proB, B cell progenitors; B, mature B cells; NK, natural killer; proT, T cell progenitors; T, T cells; Mye, myeloid cells; Lym, lymphocytes; ND, not determined. (**c**) Heat maps showing gene expression in three specific neutrophil-enriched modules. Black boxes indicate genes that were significantly (false discovery rate (FDR) < 5%) upregulated in HSPC from AKCR1-deficient as compared to WT cells. Data are from one experiment (**a–c**).

ACKR1-deficient and their wild-type littermates were sorted by flow cytometry, and their transcriptomes were compared using a gene expression microarray. The expression for the overwhelming majority of genes were indistinguishable in corresponding cell populations from the ACKR1-deficient and wild-type mice (**Supplementary Fig. 5a,b**). Significant differences primarily included the upregulation of the same set of genes in both LSK and GMP cells from ACKR1-deficient mice (**Fig. 3a** and **Supplementary Fig. 5c**), with the majority of these transcripts ascribed to be neutrophil or myeloid specific (**Fig. 3b** and **Supplementary Fig. 5d**). Some of the transcripts of genes encoding neutrophil-specific effector molecules, including those encoding cathelicidin, neutrophil granule protein and resistin-like molecule γ, were increased 1,000-fold or more in GMPs from the BM of ACKR1-deficient mice (**Supplementary Fig. 5b**), although the transcripts from the upregulated genes represented only a part of the characteristic neutrophil transcriptome and excluded some classical neutrophil markers (**Fig. 3c**). Thus, the absence of ACKR1 led to an upregulation of a subset of neutrophil and other mature-cell-specific transcripts in HSPCs, findings that were consistent with the altered differentiation of HSPCs. Together with the observed numeric and surface molecule changes in HSPC subsets, these data indicated that ACKR1 expression massively affected the balanced BM homeostasis of HSPCs.

ACKR1 on bone marrow NECs affects HSPCs

In the BM, ACKR1 is expressed by sinusoidal ECs and NECs. Vessels in the BM serve as a HSPC niche[31–33], whereas NECs have not previously been shown to affect HSPC homeostasis. To explore whether the HSPC changes observed in ACKR1-deficient mice were due to the lack of ACKR1 expression in ECs, NECs or both, HSPC parameters were recorded in reciprocal irradiation BM chimeric wild-type and ACKR1-deficient mice. Mice in individual groups expressed ACKR1 in the hematopoietic or stromal compartment, or in both, or either were globally deficient in ACKR1 expression (**Supplementary Fig. 6a–c**). The characteristic for the ACKR1-deficient mice shifts in the HSPC

populations and changes in the expression of CD34 on LSK cells were observed in chimeric mice, which lacked ACKR1 expression in the hematopoietic but not stromal compartment (**Fig. 4a–c** and **Supplementary Fig. 6d**). These data clearly pinpointed ACKR1 expression in erythroid cells as a regulator of HSPC homeostasis.

Next we asked whether the ACKR1 expressed by circulating erythrocytes or by BM NECs might have an effect on HSPCs. To this end, we created parabiotic wild-type and ACKR1-deficient mouse pairs, which shared a common blood circulation but maintained their distinct tissue microenvironments, including those in the BM (**Supplementary Fig. 6e**). ACKR1 on wild-type erythrocytes present within the common circulation restored the plasma concentrations of cognate chemokines in ACKR1-deficient parabionts (**Supplementary Fig. 6f**) but failed to affect the characteristic overexpression of CD34 and the disbalance of HSPC populations in the BM of ACKR1-deficient parabionts (**Fig. 5a–c** and **Supplementary Fig. 6g**). Collectively, our data on ACKR1 expression in BM together with the findings in the reciprocal BM chimeric and parabiotic mice showed that ACKR1 expressed on BM NECs regulated in *trans*–geometry the homeostasis of HSPCs.

ACKR1 on NECs promotes their direct interactions with HSCs

NECs are ubiquitous BM cells that might interact directly with HSCs and thus affect their behavior. Two-photon microscopy analysis of whole-mount BM preparations allowed the unequivocal detection of NECs and HSCs (**Supplementary Fig. 7a,b**) and showed that the NECs formed immediate contacts with the majority of the HSCs present in the BM from wild-type mice (**Fig. 6a**). ACKR1 facilitated the establishment of these close cell encounters, as only a third of all HSCs directly interacted with NECs in BM from ACKR1-deficient mice (**Fig. 6b**), whereas the majority were localized at some distance from the NECs (**Fig. 6c** and **Supplementary Fig. 7c**). The direct interactions between the HSCs and NECs were sufficiently avid to register as cell duplets in flow cytometry analyses, which also revealed that there was a higher proportion of NEC–HSC duplets in the BM from wild-type
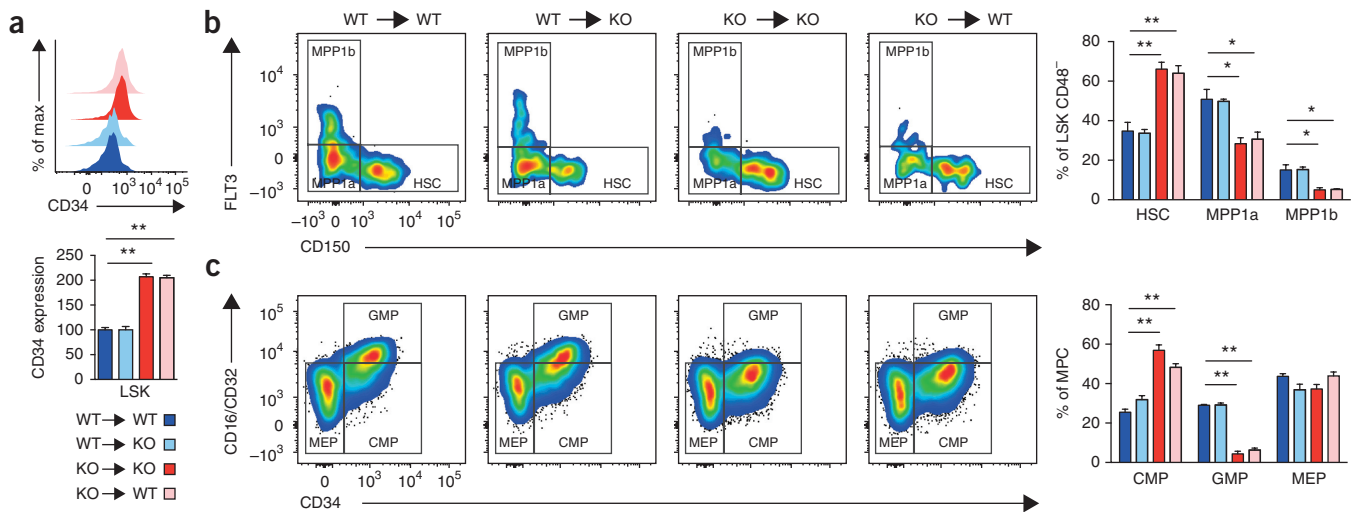
Figure 4 ACKR1 on erythroid cells but not on ECs regulates HSPCs. (**a**) Representative flow cytometry analysis (top) and quantification (bottom) of CD34 expression in LSK cells from the BM chimeric mice: BM from WT mice reconstituted into WT mice (blue), BM from WT mice reconstituted into ACKR1-deficient (KO) mice (light blue), BM from KO mice reconstituted into KO mice (red) and BM from KO mice reconstituted into WT mice (pink) (*n* = 4 per group). (**b,c**) Representative flow cytometry plots (left) and quantification (right) of the proportions of HSC, MPP1a and MPP1b subpopulations of LSK CD48⁻ cells (**b**) and of CMP, GMP and MEP subpopulations of MPCs (**c**) in BM chimeric mice (*n* = 4 mice per group). *$P < 0.01$ and **$P < 0.001$ (one-way ANOVA). Data are representative of two independent experiments (**a** (top),**b,c** (left)) or are from two independent experiments (**a** (bottom),**b,c** (right)). Mean ± s.e.m.

mice than that in the BM from ACKR1-deficient mice (**Fig. 6d**). Flow cytometry analyses showed that MMP1, MPP2 and LRP cells also formed direct contacts with NECs; however, only MMP1 and LRP cells, but not MPP2 cells required the presence of ACKR1 on NECs to establish the direct cell contacts (**Supplementary Fig. 7d**). These data described a previously unknown direct interaction between NECs and HSPCs and uncovered the unexpected role that ACKR1 has in their formation. Taken together with the observed effect of the ACKR1 deficiency on HSPCs, our data suggest that NECs are directly involved in regulating the early stages of hematopoiesis and that an ACKR1 deficiency in the erythroid lineage can broadly affect the phenotypes of BM-derived cells.

ACKR1 deficiency alters neutrophil phenotype

We used ACKR1-deficient mice to explore how the absence of ACKR1 in the erythroid lineage might affect HSPC-derived cells. Neutrophils that developed from the altered HSPCs in the BM of ACKR1-deficient mice carried a characteristic molecular signature, which notably included overexpression of Fcγ receptors (FcγRs; CD16/CD32), key molecules involved in neutrophil antimicrobial defenses[34], and CD45, a molecule that amplifies FcγR function[35], but not several other membrane receptors (**Fig. 7a** and **Supplementary Fig. 8a,b**). A similar phenotype—overexpression of FcγRIIIb (CD16) and CD45—characterized neutrophils from healthy Duffy-negative individuals homozygous for the rs2814778(G) *ACKR1* allele (**Fig. 7b**),
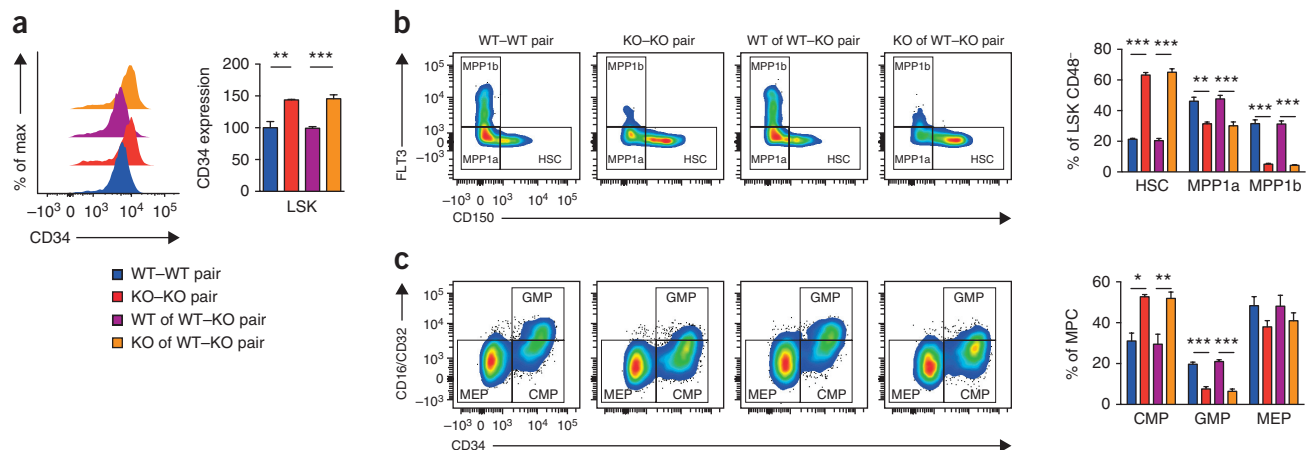

Figure 5 ACKR1 on BM erythroid cells regulates HSPCs. (**a**) Representative flow cytometry analysis (left) and quantification (right) of CD34 expression on LSK cells in parabiotic mice: WT with WT (blue), KO with KO (red), BM from WT mice in WT with KO parabiotic pairs (purple) and BM from KO mice in WT with KO parabiotic pairs (orange) (*n* = 4 per group). (**b,c**) Representative dot plots and quantification of the proportions of HSC, MPP1a and MPP1b subpopulations of LSK CD48⁻ cells (**b**) and of CMP, GMP and MEP subpopulations of MPCs (**c**) in the BM of parabiotic mice (*n* = 4 mice per group) from two independent experiments. *$P < 0.05$, **$P < 0.01$ and ***$P < 0.001$ (one-way ANOVA). Data are representative of two independent experiments (**a–c** (left)) or are from two independent experiments (**a–c** (right)). Mean ± s.e.m.
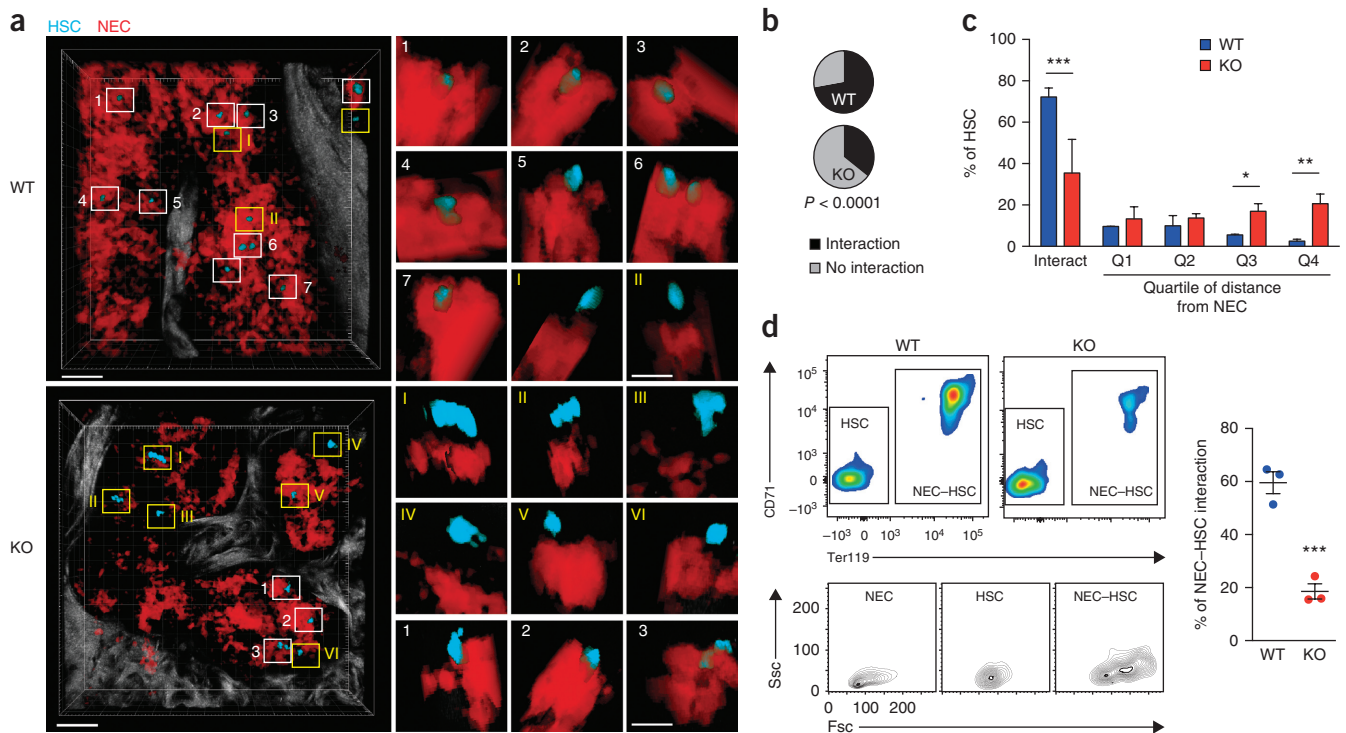
Figure 6 ACKR1 on NECs promotes direct cell interactions with HSCs. (**a**) BM localization of HSCs (blue) and NECs (red) in representative three-dimensionally recontructed images from whole-mounted femurs of WT and ACKR1-deficient (KO) mice, as assessed by two-photon microscopy. White squares with Arabic numerals mark cell contacts between a HSC and NECs; yellow squares with Roman numerals indicate HSCs that do not interact with NECs. Scale bars, 50 μm (left) and 25 μm (numbered inset images). (**b**) Proportions of NEC-interacting and non-interacting HSCs. $P < 0.0001$ (χ^2 test). (**c**) Distance between HSCs and NECs in BM from WT (blue) and KO (red) mice. Among non-interacting HSCs, distribution quartiles were defined as: Q1, <2.56 μm, Q2, <4.96 μm, Q3, <8.30 μm and Q4, <19.82 μm. In **b**,**c**, $n = 145$ HSCs (WT) and $n = 144$ HSCs (KO), as assessed by two-photon microscopy. (**d**) Representative dot plots and quantification of HSC interactions with NECs (NEC–HSC), as assessed by flow cytometry, in the BM from WT and ACKR1-KO mice ($n = 3$ mice per group). Ssc, side scatter. $*P < 0.05$, $**P < 0.01$ and $***P < 0.001$ (one-way ANOVA (**c**) or two-tailed Student's t-test (**d**)). Data are representative of one (**d**, left) and two (**a**) independent experiments or are from one (**d**, right) and two (**b**,**c**) independent experiments. Mean ± s.d. (**c**) or mean ± s.e.m. (**d**).

as compared to that in neutrophils from individuals with a Duffy-positive phenotype. Moreover, neutrophils from both ACKR1-deficient mice and Duffy-negative individuals selectively overexpressed CCR2 (**Fig. 7c,d** and **Supplementary Fig. 8c,d**), a key inflammatory chemokine receptor that characterizes monocytes rather than neutrophils[1]. Thus, HSPCs that were altered in the absence of the erythroid ACKR1 gave rise to phenotypically distinct neutrophils that overexpressed a set of membrane molecules involved in host defenses. The same set of membrane effector molecules was upregulated on neutrophils of Duffy-negative individuals, suggesting that the absence of erythroid ACKR1 due to rs2814778(G) *ACKR1* allele might change BM homeostasis by the same mechanism as that observed in ACKR1-deficient mice.

ACKR1 regulates neutrophil counts in blood

Healthy Duffy-negative individuals of African ancestry have low blood neutrophil counts[22]. In contrast, ACKR1-deficient mice had normal neutrophil counts in blood (**Fig. 8a**) and BM (**Supplementary Fig. 8e**). Thus, the numeric reductions in the LSK subsets and GMP cells that were observed in the ACKR1-deficient mice did not directly lead to neutropenia. Also, ACKR1-deficient mice had normal numbers of all other circulating cell types, despite some numerical changes in the BM (**Supplementary Fig. 8e–g**). Notably, Duffy-negative individuals who were homozygous for the rs2814778(G) *ACKR1* allele lack ACKR1 on erythroid cells only but still express ACKR1 on ECs.

To explore whether such a pattern of ACKR1 expression might lead to neutropenia, we studied blood neutrophils in reciprocal wild-type and ACKR1-deficient BM chimeric mice. Wild-type mice that were reconstituted with BM from ACKR1-deficient mice had characteristically altered neutrophils (**Supplementary Fig. 8h**) and were indeed neutropenic (**Fig. 8b**). This finding suggests that the expression of ACKR1 in the venular compartment may contribute to neutropenia, consistent with its established function in ECs[9,36], by facilitating neutrophil exit into the tissues. We explored this hypothesis and asked which tissues might clear the phenotypically altered neutrophils that develop in the absence of NEC-expressed ACKR1. Parabiotic wild-type and ACKR1-deficient mice allowed us to directly compare, in one artificially created organism, the homing of neutrophils from wild-type or ACKR1-deficient mice into individual ACKR1-sufficient or ACKR1-deficient tissues. Neutrophils that developed in the ACKR1-deficient BM preferentially homed into the spleens—but not other organs tested, including the BM, liver and lungs—of the wild-type parabionts (**Fig. 8c**). In mice, spleen ECs of the red pulp sinusoids expressed ACKR1 (**Fig. 8d**), in direct accord with the expression of ACKR1 in human spleens (**Supplementary Fig. 8i**), including in Duffy-negative individuals[27]. It is not clear whether the altered neutrophils that migrated into the spleen could persist there and contribute to the splenic host defenses. Alternatively, the migration of neutrophils into the spleen that was dependent on EC-expressed ACKR1 might be part of their clearance from the
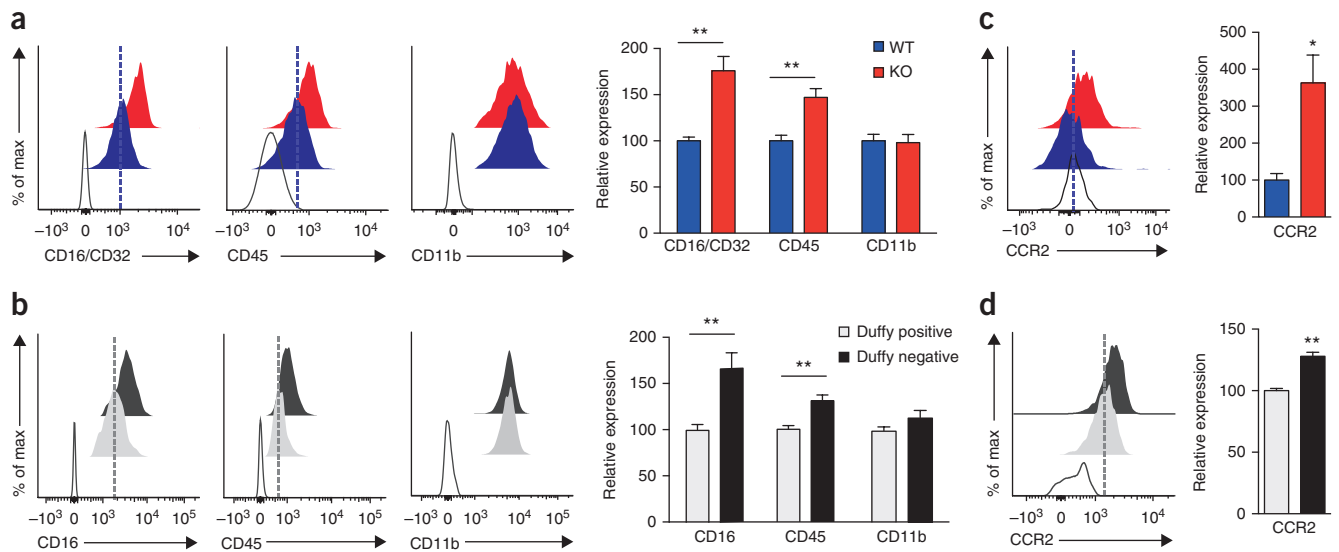
Figure 7 Lack of ACKR1 affects neutrophil phenotype. (**a**) Expression of CD16/CD32, CD45 and CD11b on neutrophils from the blood of WT (blue) and ACKR1-deficient (KO; red) mice ($n = 9$ mice per group). (**b**) CD16, CD45 and CD11b expression on human neutrophils from the blood of healthy Duffy-positive (gray; $n = 14$) and Duffy-negative (black; $n = 7$) individuals. (**c**) Expression of CCR2 on the neutrophils from the blood of WT (blue) and KO (red) mice ($n = 9$ mice per group). (**d**) Expression of CCR2 on human neutrophils from the blood of Duffy-positive (gray; $n = 11$) and Duffy-negative (black; $n = 4$) individuals. *$P < 0.01$ and **$P < 0.001$ (two-tailed Student's t-test). Data are representative of at least three independent experiments (**a**–**c**,**d** (left)) or are from three (**a**,**b**,**d** (right)) and four (**c** (right)) independent experiments. Mean ± s.e.m.

circulation, akin to the mechanism described for neutrophils homing into the BM[37]. Thus, we showed that altered neutrophils, which developed in the absence of ACKR1 on NECs, left the circulation thereby causing neutropenia; however, this occurred only when ACKR1 was expressed by venular ECs, a pattern of ACKR1 expression that was mirrored in individuals of African ancestry who were homozygous for the rs2814778(G) *ACKR1* allele.

DISCUSSION

Hematopoiesis is a robust process controlled by multiple molecular and cellular cues that maintain HSPCs and regulate their differentiation and proliferation for consistent BM cell outputs[32,33]. Here we show that the ACKR1 expressed by NECs, the most ubiquitous BM cells, regulates the homeostasis of HSPCs and modifies downstream hematopoiesis. The absence of ACKR1 led to altered numbers of HSPCs,
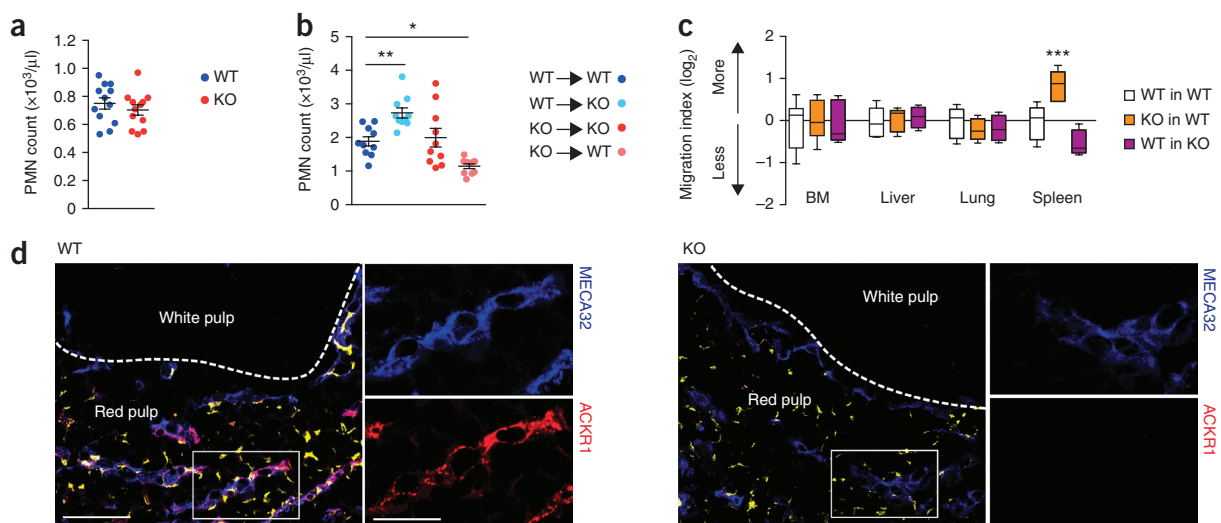

Figure 8 Lack of ACKR1 on NECs together with its expression in ECs causes neutropenia. (**a**) Blood neutrophil counts in WT (blue) and ACKR1-deficient (KO, red) mice ($n = 12$ mice per group). (**b**) Blood neutrophil counts in reciprocal BM chimeric mice ($n = 10$ mice per group). (**c**) Reciprocal homing of neutrophils from WT (purple) and KO (orange) mice into the BM, liver, lungs and spleen of their respective KO and WT parabionts ($n = 5$ pairs), as compared to homing of neutrophils from WT mice into the organs of WT parabionts (white; $n = 8$ pairs). In the box plots, center lines represent the median, limits represent the quartiles, and whiskers represent the minimum and maximum values. (**d**) Representative immunofluorescence micrographs of spleen samples from WT ($n = 3$) and KO ($n = 3$) mice after staining for ACKR1 (red), MECA32 (blue; to visualize ECs) and Ter119 (yellow; to visualize erythrocytes). Insets show ACKR1 immunoreactivity in sinusoidal ECs. Scale bars, 50 μm (main images) and 25 μm (insets). *$P < 0.05$, **$P < 0.01$ and ***$P < 0.001$ (two-tailed Student's t-test (**a**) or one-way ANOVA (**b**,**c**)). Data are from three (**a**) or two (**b**,**c**) independent experiments (mean ± s.e.m.) or are representative of three independent experiments (**d**).

which was due, in part, to their decreased proliferation. It also resulted in shifts in proportions of individual HSPC subpopulations, changes in HSPC transcriptomes and altered expression of their functional surface molecules. The overall BM cellularity was not affected by ACKR1, and the numeric changes in the individual subpopulations of HSPCs seemed discordant. The number of HSCs, the BM's 'reserve' population[38,39], was not affected. However, the immediate downstream population, MPP1a cells, was reduced, and MPP1b cells were practically absent from the BM of ACKR1-deficient mice. This was accompanied by an increase in CMP cells, a population downstream of MPP1 cells, which might have resulted from accelerated differentiation of MPP1 cells to CMP cells. Alternatively, the numerically increased CMP cells may have derived from MPP2 populations, which were also increased in the BM of ACKR1-deficient mice, suggesting either a potential contribution of alternative progenitor clones present in the BM[40] or pathway plasticity of early HSPC differentiation[41]. It is possible that changes in the expression of the molecular markers that were used to define the HSPC subpopulations might have contributed to the numeric differences observed in the BM from ACKR1-deficient mice.

Experiments in ACKR1-deficient chimeric and parabiotic mice unequivocally established that HSPCs were affected by ACKR1 expression on NECs but not by ACKR1 expression on ECs or circulating erythrocytes. Furthermore, the expression of ACKR1 by NECs increased direct cell contacts between HSPC populations and NECs. These data suggest that ACKR1 determines the function of a HSPC niche that is associated with NECs, the existence of which has not been recognized previously. Currently it is not clear whether ACKR1 only mediates the interaction of NECs and HSPCs, whereas another putative NEC molecule signals to HSPCs. Alternatively, ACKR1 might directly signal to HSPCs, for example, by involving the tetraspanin family member CD82, which has been suggested to bind ACKR1 in *trans* geometry[42]. Recently, CD82 on HSCs has been implicated in maintaining their quiescence through interaction with ACKR1, which was detected spuriously on BM macrophages using a nonvalidated antibody to ACKR1 (ref. 43). Indeed, high concentrations of this antibody stained BM macrophages, albeit equally well in WT and ACKR1-deficient mice. On the basis of immunostaining studies using a specific antibody and a transcriptomic analysis, ACKR1 is not expressed on macrophages in the BM or in other tissues[29]. Nevertheless, it is possible that CD82, either in *trans* on HSPCs or through a *cis* interaction in NECs, might contribute to the effects of ACKR1 on HSPCs. Alternatively, the ACKR1-dependent signal to HSPCs involves one or several of more than 20 chemokine ligands for ACKR1 (ref. 13). We showed that ACKR1 on NECs binds, but does not scavenge, cognate chemokines, and it may thus function as a BM reservoir and a universal immobilization template for cognate chemokines. Such function might enable the retention of ACKR1 ligands in NEC-rich microenvironments, thus allowing these chemokines to signal via GPCRs to HSPCs and other BM cells. The chemokine presentation template, ACKR1 on NECs, remains constant, but the signals to HSPCs might change depending on the individual chemokines immobilized and their endless potential combinations that characterize different physiological and pathological conditions. Several of the ACKR1-cognate chemokines have been shown to affect HSPCs and hematopoiesis[44], although CXCL12, which has a key role in HSPC homeostasis[45], does not bind ACKR1 (ref. 46).

The absence of ACKR1 caused a shift in the HSPC transcriptome that resulted in a massive overexpression of a subset of neutrophil- and myeloid-specific genes. This is consistent with an altered differentiation pattern of HSPCs toward the myeloid lineage and suggests

that the characteristic molecular signature of neutrophils that is observed in the context of an ACKR1 deficiency might already be imprinted during the early steps of hematopoiesis. The signature changes in neutrophils that originated in the BM from ACKR1-deficient mice were required, but not sufficient alone, to cause neutropenia. The BM chimeric mice showed that neutropenia developed only when the absence of ACKR1 in the BM was combined with the expression of ACKR1 in the venular ECs. Mechanistically this is consistent with the known contribution of ACKR1 on ECs to optimal chemokine-driven neutrophil egress into tissues[9], and it explains why mice with a global ACKR1 deficiency, despite having altered neutrophils, were not neutropenic. Accordingly, in parabiosis experiments the emigration of the phenotypically altered neutrophils of the ACKR1-deficient parabionts took place preferentially into the spleens of wild-type mice. In addition to the spleen, venular ECs in several other organs and tissues, including the skin and the gut, but not the liver or the lungs, express ACKR1 (ref. 29). Thus, neutrophils that develop in the absence of ACKR1 on NECs might also exit the circulation into the skin, gut and other tissues. Although BM sinusoids expressed ACKR1, they did not support the preferential homing of altered neutrophils. This might be explained by findings that neutrophils use an alternative chemokine pathway for their homing to the BM, involving CXCR4 and its ligand CXCL12 (ref. 37), which is not an ACKR1-cognate chemokine[46].

Our findings on the peculiarities of hematopoiesis that take place in the absence of ACKR1 on NECs are highly relevant for human health, as Duffy-negative individuals of African ancestry selectively lack ACKR1 expression in the cells of the erythroid lineage only, whereas ACKR1 is expressed in ECs[25]. Neutrophils of the Duffy-negative individuals mirror the distinct molecular signature of neutrophils in ACKR1-deficient mice. We suggest that these altered neutrophils in humans also readily leave circulation, thus leading to neutropenia that is associated with the *ACKR1* rs2814778(G) polymorphism[23]. It is conceivable that the differential signature pattern of molecular effectors on neutrophils has provided Duffy-negative individuals with a natural selective advantage for superior innate responses to microbial pathogens. Selective pressure by a broad range of infectious agents, together with the known partial resistance of Duffy-negative individuals to *P. vivax* malaria[47,48], may have contributed to the selection and fixation of the *ACKR1* rs2814778(G) polymorphism in almost the entire population of sub-Saharan Africa[25].

In summary, we show that the absence of ACKR1 on cells of the erythroid lineage changes steady-state hematopoiesis, and alternative physiological patterns of hematopoiesis exist depending on ACKR1 expression in the erythroid lineage. It will be intriguing to elucidate how ACKR1 expression by NECs affects emergency hematopoiesis and BM responses in infection, inflammation, injury and cancer.

METHODS

Methods, including statements of data availability and any associated accession codes and references, are available in the online version of the paper.

Note: Any Supplementary Information and Source Data files are available in the online version of the paper.

AUTHOR CONTRIBUTIONS

COMPETING FINANCIAL INTERESTS
The authors declare no competing financial interests.

Reprints and permissions information is available online at http://www.nature.com/reprints/index.html. Publisher's note: Springer Nature remains neutral with regard to jurisdictional claims in published maps and institutional affiliations.

1. Rot, A. & von Andrian, U.H. Chemokines in innate and adaptive host defense: basic chemokinese grammar for immune cells. *Annu. Rev. Immunol.* **22**, 891–928 (2004).
2. Griffith, J.W., Sokol, C.L. & Luster, A.D. Chemokines and chemokine receptors: positioning cells for host defense and immunity. *Annu. Rev. Immunol.* **32**, 659–702 (2014).
3. Luther, S.A. & Cyster, J.G. Chemokines as regulators of T cell differentiation. *Nat. Immunol.* **2**, 102–107 (2001).
4. Krathwohl, M.D. & Kaiser, J.L. Chemokines promote quiescence and survival of human neural progenitor cells. *Stem Cells* **22**, 109–118 (2004).
5. Ulvmar, M.H., Hub, E. & Rot, A. Atypical chemokine receptors. *Exp. Cell Res.* **317**, 556–568 (2011).
6. Bachelerie, F. *et al.* New nomenclature for atypical chemokine receptors. *Nat. Immunol.* **15**, 207–208 (2014).
7. Nibbs, R.J.B. & Graham, G.J. Immune regulation by atypical chemokine receptors. *Nat. Rev. Immunol.* **13**, 815–829 (2013).
8. Bachelerie, F. *et al.* Update on the extended family of chemokine receptors and introducing a new nomenclature for atypical chemokine receptors. *Pharmacol. Rev.* **66**, 1–79 (2013).
9. Pruenster, M. *et al.* The Duffy antigen receptor for chemokines transports chemokines and supports their pro-migratory activity. *Nat. Immunol.* **10**, 101–108 (2009).
10. Ulvmar, M.H. *et al.* The atypical chemokine receptor CCRL1 shapes functional CCL21 gradients in lymph nodes. *Nat. Immunol.* **15**, 623–630 (2014).
11. Lee, K.M. *et al.* The chemokine receptors ACKR2 and CCR2 reciprocally regulate lymphatic vessel density. *EMBO J.* **33**, 2564–2580 (2014).
12. Cruz-Orengo, L. *et al.* CXCR7 influences leukocyte entry into the CNS parenchyma by controlling abluminal CXCL12 abundance during autoimmunity. *J. Exp. Med.* **208**, 327–339 (2011).
13. Novitzky-Basso, I. & Rot, A. Duffy antigen receptor for chemokines and its involvement in patterning and control of inflammatory chemokines. *Front. Immunol.* **3**, 266 (2012).
14. Rot, A. Contribution of Duffy antigen to chemokine function. *Cytokine Growth Factor Rev.* **16**, 687–694 (2005).
15. Mei, J. *et al.* CXCL5 regulates chemokine scavenging and pulmonary host defense to bacterial infection. *Immunity* **33**, 106–117 (2010).
16. Schnabel, R.B. *et al.* Duffy antigen receptor for chemokines (*Darc*) polymorphism regulates circulating concentrations of monocyte chemoattractant protein 1 and other inflammatory mediators. *Blood* **115**, 5289–5299 (2010).
17. Reutershan, J., Harry, B., Chang, D., Bagby, G.J. & Ley, K. DARC on RBC limits lung injury by balancing compartmental distribution of CXC chemokines. *Eur. J. Immunol.* **39**, 1597–1607 (2009).
18. Miller, L.H., Mason, S.J., Dvorak, J.A., McGinniss, M.H. & Rothman, I.K. Erythrocyte receptors for (*Plasmodium knowlesi*) malaria: Duffy blood group determinants. *Science* **189**, 561–563 (1975).
19. Horuk, R. *et al.* A receptor for the malarial parasite *Plasmodium vivax*: the erythrocyte chemokine receptor. *Science* **261**, 1182–1184 (1993).
20. Nedelec, Y. *et al.* Genetic ancestry and natural selection drive population differences in immune responses to pathogens. *Cell* **167**, 657–669 (2016).
21. Quach, H. *et al.* Genetic adaptation and neandertal admixture shaped the immune system of human populations. *Cell* **167**, 643–656 (2016).
22. Thobakgale, C.F. & Ndung'u, T. Neutrophil counts in persons of African origin. *Curr. Opin. Hematol.* **21**, 50–57 (2014).
23. Reich, D. *et al.* Reduced neutrophil count in people of African descent is due to a regulatory variant in the Duffy antigen receptor for chemokines gene. *PLoS Genet.* **5**, e1000360 (2009).
24. Sanger, R., Race, R.R. & Jack, J. The Duffy blood groups of New York negroes: the phenotype Fy (a–b–). *Br. J. Haematol.* **1**, 370–374 (1955).
25. Howes, R.E. *et al.* The global distribution of the Duffy blood group. *Nat. Commun.* **2**, 266 (2011).
26. Tournamille, C., Colin, Y., Cartron, J.P. & Le Van Kim, C. Disruption of a GATA motif in the Duffy gene promoter abolishes erythroid gene expression in Duffy-negative individuals. *Nat. Genet.* **10**, 224–228 (1995).
27. Peiper, S.C. *et al.* The Duffy antigen/receptor for chemokines (DARC) is expressed in endothelial cells of Duffy-negative individuals who lack the erythrocyte receptor. *J. Exp. Med.* **181**, 1311–1317 (1995).
28. Doss, J.F. *et al.* A comprehensive joint analysis of the long and short RNA transcriptomes of human erythrocytes. *BMC Genomics* **16**, 952 (2015).
29. Thiriot, A. *et al.* Differential immunostaining of DARC (ACKR1) distinguishes venular from nonvenular endothelial cells in murine tissues. *BMC Biol.* **15**, 45 (2017).
30. Dawson, T.C. *et al.* Exaggerated response to endotoxin in mice lacking the Duffy antigen/receptor for chemokines (DARC). *Blood* **96**, 1681–1684 (2000).
31. Itkin, T. *et al.* Distinct bone marrow blood vessels differentially regulate hematopoiesis. *Nature* **532**, 323–328 (2016).
32. Morrison, S.J. & Scadden, D.T. The bone marrow niche for hematopoietic stem cells. *Nature* **505**, 327–334 (2014).
33. Mendelson, A. & Frenette, P.S. Hematopoietic stem cell niche maintenance during homeostasis and regeneration. *Nat. Med.* **20**, 833–846 (2014).
34. Fossati, G., Moots, R.J., Bucknall, R.C. & Edwards, S.W. Differential role of neutrophil Fcγ receptor IIIB (CD16) in phagocytosis, bacterial killing and responses to immune complexes. *Arthritis Rheum.* **46**, 1351–1361 (2002).
35. Gao, H., Henderson, A., Flynn, D.C., Landreth, K.S. & Ericson, S.G. Effects of the protein tyrosine phosphatase CD45 on FcγRIIa signaling and neutrophil function. *Exp. Hematol.* **28**, 1062–1070 (2000).
36. Minten, C. *et al.* DARC shuttles inflammatory chemokines across the blood–brain barrier during autoimmune central nervous system inflammation. *Brain* **137**, 1454–1469 (2014).
37. Martin, C. *et al.* Chemokines acting via CXCR2 and CXCR4 control the release of neutrophils from the bone marrow and their return following senescence. *Immunity* **19**, 583–593 (2003).
38. Busch, K. *et al.* Fundamental properties of unperturbed hematopoiesis from stem cells *in vivo*. *Nature* **518**, 542–546 (2015).
39. Yu, V.W. *et al.* Epigenetic memory underlies cell-autonomous heterogeneous behavior of hematopoietic stem cells. *Cell* **167**, 1310–1322 e1317 (2016).
40. Sun, J. *et al.* Clonal dynamics of native hematopoiesis. *Nature* **514**, 322–327 (2014).
41. Pietras, E.M. *et al.* Functionally distinct subsets of lineage-biased multipotent progenitors control blood production in normal and regenerative conditions. *Cell Stem Cell* **17**, 35–46 (2015).
42. Bandyopadhyay, S. *et al.* Interaction of KAI1 on tumor cells with DARC on vascular endothelium leads to metastasis suppression. *Nat. Med.* **12**, 933–938 (2006).
43. Hur, J. *et al.* CD82 (KAI1) maintains the dormancy of long-term hematopoietic stem cells through interaction with DARC-expressing macrophages. *Cell Stem Cell* **18**, 508–521 (2016).
44. Youn, B.S., Mantel, C. & Broxmeyer, H.E. Chemokines, chemokine receptors and hematopoiesis. *Immunol. Rev.* **177**, 150–174 (2000).
45. Sugiyama, T., Kohara, H., Noda, M. & Nagasawa, T. Maintenance of the hematopoietic stem cell pool by CXCL12–CXCR4 chemokine signaling in bone marrow stromal cell niches. *Immunity* **25**, 977–988 (2006).
46. Gardner, L., Patterson, A.M., Ashton, B.A., Stone, M.A. & Middleton, J. The human Duffy antigen binds selected inflammatory but not homeostatic chemokines. *Biochem. Biophys. Res. Commun.* **321**, 306–312 (2004).
47. Ménard, D. *et al.* Plasmodium vivax clinical malaria is commonly observed in Duffy-negative Malagasy people. *Proc. Natl. Acad. Sci. USA* **107**, 5967–5971 (2010).
48. Miller, L.H., Mason, S.J., Clyde, D.F. & McGinniss, M.H. The resistance factor to *Plasmodium vivax* in blacks. The Duffy-blood-group genotype, FyFy. *N. Engl. J. Med.* **295**, 302–304 (1976).

ONLINE METHODS

Mice. ACKR1-deficient mice[30] were backcrossed for more than 12 generations onto a C57BL/6J background and maintained as a heterozygous breed. WT and ACKR1-deficient littermates were used for comparative studies. Mice were housed in specific-pathogen-free facilities at the University of Birmingham and the University of York in the UK, LMU, Munich in Germany, Austrian Federal Ministry of Science and Research in Austria and CNIC in Madrid, Spain. All experimental procedures were performed with 8- to 12-week-old female mice, as approved by the respective Institutional Ethics and Animal Welfare Committees, the Home Office, UK, or the Regierung von Oberbayern, Munich, Germany, and were compliant with UK, German, Spanish, Austrian and European Union guidelines.

Immunofluorescence staining and detection of ACKR1. Femurs were collected and cleaned, and both ends were cut off to facilitate the fixation in paraformaldehyde (PFA; 4%) overnight at 4 °C. Bones were washed and decalcified in PBS with EDTA (10%) for 3 d, washed and incubated in 20% sucrose PBS overnight at 4 °C, and finally embedded in Optical Cutting Temperature (OCT) compound (Fischer) and stored at −80 °C. Sections (7 μm) were cut and blocked in 20% goat serum plus 0.5% Triton X-100 in PBS for 30 min at 20 °C. After washing, sections were stained with rat anti-mouse-CD31 antibody in PBS with 0.1% BSA before addition of the AF488-conjugated goat anti-rat-IgG secondary antibody. Finally, sections were stained with AF647-conjugated anti-mouse-Ter119 and AF546-conjugated anti-mouse-ACKR1 for 1 h and washed with PBS. Slides were mounted in ProLong Gold anti-fade with DAPI (Fischer) for imaging. Evaluation was performed using a LSM880 microscope (Zeiss). Details regarding the antibodies used for immunofluorescence analysis are provided in **Supplementary Table 1**.

Spleens were frozen in OCT on dry ice, and 7-μm sections were cut using a cryomicrotome. Before staining, slides were air-dried for 30 min and fixed in acetone for 10 min. Slides were washed in PBS and subsequently blocked with 20% goat serum in PBS with 0.1% BSA. Antibodies to DARC (AF546-conjugated), MECA-32 (AF647-conjugated) and Ter119 (fluorescein isothiocyanate (FITC)-conjugated) were diluted in 0.1% BSA in PBS and incubated on the slides for 60 min. After three washes in PBS, the slides were dipped in distilled water, mounted with Prolong Gold with DAPI and evaluated using a LSM880 microscope (Zeiss).

Flow cytometry. To obtain BM cells, femurs were flushed with PBS, and cells were washed with FACS buffer (PBS with 0.5% BSA). Fc receptors were blocked using a rat antibody to mouse CD16/CD32 (2.4G2; BD Bioscience), where appropriate. In all of the experiments, antibody staining was performed at 4 °C for 60 min. Cells were counted using CountBright Absolute Counting Beads (Life Technologies) and analyzed using a FACS CANTOII or LSR Fortessa flow cytometer (BD Biosciences) and FlowJo software (TreeStar). Details regarding the antibodies used in flow cytometry analyses are provided in **Supplementary Table 1**.

ACKR1 expression in bone marrow cells. NECs were stained with antibodies to CD71 and Ter119. Stages of erythropoiesis were defined as follows: $CD71^{hi}Ter119^{int}$ (population I, proerythroblasts), $CD71^{hi}Ter119^{hi}Fsc^{hi}$ (population II, early normoblasts), $CD71^{hi}Ter119^{hi}Fsc^{int/lo}$ (intermediate normoblasts), $CD71^{hi/int}Ter119^{hi}Fsc^{lo}$ (population IV, late normoblasts), $CD71^{int}Ter119^{hi}Fsc^{lo}$ (population V, reticulocytes) and $CD71^{lo}Ter119^{hi}Fsc^{lo}$ (population VI, mature erythrocytes). **Figure 1b** provides details of the gating strategy. In addition, BM leukocytes were gated as lineage (Lin; CD11b, Gr1, CD3, B220)$^{+}CD71^{-}Ter119^{-}$ cells. HSPCs were stained as described below. Expression of ACKR1 in NECs, leukocytes and HSPCs was determined using the monoclonal antibody to mouse ACKR1 (**Supplementary Table 1**). ACKR1 expression was calculated in each erythoid cell population as specific delta mean fluorescence intensity (ΔMFI) = MFI in WT mouse minus average MFI in the KO group. Data were then normalized to the ΔMFI for MEPs.

HSPC analysis. For HSPC analysis, BM cells were stained with combinations of antibodies to the following surface markers: c-Kit, Sca-1, CD150, CD48, Flt3, CD34, CD16/CD32, IL-7rα and the lineage markers Ter119, B220, CD3, CD11b and Gr1. HSPCs were defined as follows: HSC (Lin^{-}Sca1^{+}c-Kit^{+}CD48^{-}CD150^{+}Flt3^{-}), MPP1a (Lin^{-}Sca1^{+}c-Kit^{+}CD48^{-}CD150^{-}Flt3^{-}), MPP1b (Lin^{-}Sca1^{+}c-Kit^{+}CD48^{-}CD150^{-}Flt3^{+}), MPP2 (Lin^{-}Sca1^{+}c-Kit^{+}

CD48^{+}CD150^{+}Flt3^{-}), LRP1 (Lin^{-}Sca1^{+}c-Kit^{+}CD48^{+}CD150^{-}Flt3^{-}), LRP2 (Lin^{-}Sca1^{+}c-Kit^{+}CD48^{+}CD150^{-}Flt3^{+}), CMP (Lin^{-}Sca1^{-}c-Kit^{+}CD34^{+}CD16/CD32^{-}), GMP (Lin^{-}Sca1^{-}c-Kit^{+}CD34^{+}CD16/CD32^{+}), MEP (Lin^{-}Sca1^{-}c-Kit^{+}CD34^{-}CD16/CD32^{-}) and CLP (Lin^{-}Sca1^{lo}c-Kit^{lo}IL-7rα^{+}Flt3^{+}) cells. Details regarding the antibodies are provided in **Supplementary Table 1**.

Neutrophil analysis. For surface marker and chemokine receptor expression analysis on neutrophils, BM cells were collected as described in the flow cytometry subsection, and blood cells were obtained by cardiac puncture using EDTA as an anticoagulant. Erythrocytes were lysed using ACK lysing buffer (155 mM NH_4Cl, 10 mM $KHCO_3$, and 0.1 mM EDTA; all from Sigma) and cells washed with FACS buffer (PBS with 0.5% BSA; Sigma). Cells were incubated with antibodies to CD45, CD11b, Ly6G, CD16/CD32, CD62L, CD11a, CXCR2, CCR1, CCR2, CCR3 and CCR5 (details regarding the antibodies are provided in **Supplementary Table 1**).

Chemokine binding assay. BM cells were incubated with AF647-conjugated CCL2 (10 nM, Almac) for 1 h at 37 °C, and some cells were subsequently incubated either with an excess of CXCL1 (1 μM) in PBS for 1 h to displace CCL2 or with PBS alone. Cells were washed, stained for NEC markers using antibodies to CD71 and Ter119, and analyzed by flow cytometry. Specific binding of CCL2 was calculated for individual erythroid cell populations as ΔMFI of A647-conjugated CCL2 in the WT and KO groups, normalized for that in the mature erythrocyte population (population VI) in ACKR1-deficient (KO) mice and expressed as fold change.

Analysis of HSC–NEC interactions by flow cytometry. For observations of HSC–NEC interactions, mice were euthanized and perfused with PFA via the cardiac route to fix the cells *in situ* and preserve their interactions. BM cells were collected and stained with an antibody panel to the following proteins: c-Kit, Sca-1, CD150, CD48, CD71 and Ter119, and the lineage markers B220, CD3, CD11b and Gr1. The HSCs (LSK CD48^{-}CD150^{+}), MPP1 (LSK CD48^{-}CD150^{-}), MPP2 (LSK CD48^{+}CD150^{+}) and LRP (LSK CD48^{+}CD150^{-}) cells were gated, and their interaction with NECs was assessed by the presence of co-staining with CD71 and Ter119 on the duplets.

Blood erythrocyte and bone marrow NEC parameters. Blood was taken by cardiac puncture, and erythrocyte counts, hematocrit and hemoglobin concentration were determined by using an automated ABX Pentra 60 blood counter (HORIBA ABX S.A.S.). For BM analysis, mice were culled and flushed with PBS to remove the erythrocytes present within the blood vessels. BM was harvested, and cells at different stages of erythropoiesis were analyzed as described above.

Cell parameters in bone marrow and blood. For BM leukocyte analysis, the cells were stained with combinations of antibodies to the following surface markers: CD11b, Ly6G, CD115, CD19 and B220. Leukocyte populations were defined as follows: neutrophils (CD11b^{+}Ly6G^{+}), monocytes (CD11b^{+}Ly6G^{-}CD115^{+}) and B lineage cells (B220^{+}CD19^{+}).

Blood was taken by cardiac puncture, and platelet counts were determined with an automated ABX Pentra 60 blood counter (HORIBA ABX S.A.S.). In addition, erythrocytes were lysed using ACK lysis buffer, and the remaining cells were washed with FACS buffer. Cells were reacted with antibodies to CD45, CD11b, Ly6G, CD115, CD3 and B220. Leucocyte populations were defined as follows: neutrophils (CD11b^{+}Ly6G^{+}), monocytes (CD11b^{+}Ly6G^{-}CD115^{+}) and lymphoid cells (B220^{+} CD3^{+}).

Cell proliferation. To assess the proliferation of BM cell populations, the APC BrdU flow kit (BD Bioscience) was used as per the manufacturer's instructions. Briefly, 5-bromo-2′deoxyuridine (BrdU) was injected intraperitoneally (1 mg) into WT and ACKR1-deficient mice. After 2 h, the mice were euthanized, and the BM was collected and labeled with a cocktail of biotinylated lineage-specific antibodies, followed by labeling with Anti-Biotin MicroBeads (Miltenyi Biotec) as per the manufacturer's instructions. Lin^{+} BM cells were depleted, and Lin^{-} BM cells were incubated with streptavidin (e450, eBioscience) and with fluorescently labeled antibodies to c-Kit and Sca-1 (**Supplementary Table 1**) for 1 h on ice. Cells were washed, fixed, permeabilized, stained with the anti-BrdU antibody in the kit and analyzed by flow cytometry.

Reciprocal irradiation BM chimeric mice. BM cells from either C57BL/6 (WT) or ACKR1-deficient (KO) mice were harvested and transplanted into lethally irradiated (9 Gy) WT or ACKR1-deficient recipients by tail vein injection of 10^7 cells in 200 µl PBS, thus creating four experimental groups. Recipients received prophylactic endofloxacin (Baytril, Bayer AG) for 1 week before and also after irradiation. Eight weeks after the BM transfer, the recipients were culled. BM and blood cells were collected, washed and stained to identify HSPCs and PMNs, respectively, as described above. The degree of donor chimerism was established by measuring the expression of ACKR1 on BM NECs and blood erythrocytes with an antibody to mouse ACKR1 (**Supplementary Table 1**). In addition, CD45.1 and CD45.2 staining showed that all of the BM HSPCs and blood PMNs in the irradiated recipients were replaced by donor cells.

Parabiosis. To generate parabiotic pairs, we followed published protocols[49]. Briefly, anesthetized mice were shaved at the corresponding lateral aspects, matching skin incisions were made from the olecranon to the knee joint of each mouse, and the subcutaneous fascia was bluntly dissected to create about 0.5 cm of free skin. The olecranon and knee joints were attached by a single 5-0 polypropylene suture and tie, and the dorsal and ventral skins were approximated by continuous suture. A single dose of flunixin meglumine (Schering-Plough) was injected subcutaneously in each partner at the end of the surgical procedure (1 mg per kg body weight). WT–WT, KO–KO and WT–KO pairs were created. One month after surgery, blood and BM were obtained from each of the partners for analysis of the hematopoietic progenitors.

In another experiment in which the homing of neutrophils was studied, different parabiotic pairs were used: WT–WT pairs (CD45.1 and CD45.2) and WT–KO pairs (CD45.1 and CD45.2, respectively). One month after surgery, blood, BM, spleen, lung and liver samples were obtained from each of the partners for analysis of neutrophils. The percentage of neutrophils from partner parabionts (percentage chimerism) was defined on gated neutrophils in blood, BM, lung, liver and spleen. Migration indices were calculated for each tissue as the percentage chimerism in a specific tissue divided by the percentage chimerism in blood, and these were normalized by using the values obtained in the WT–WT control pairs.

Cell sorting. The BM of WT or ACKR1-deficient mice was flushed; cells were pooled from three mice and stained for lineage markers, CD34, CD16/CD32, cKit and Sca-1 in 500 µl buffer, for 1 h on ice. Cells were sorted on a Mo-flow MultiLaser flow cytometer (Beckman Coulter). First, an enrichment step was performed, with gates set based on forward- and side-scatter characteristics for lineage-negative and either GMP cells or LSK cells. The GMP and LSK populations then underwent a second sorting step using the same gating profiles. The twice-sorted GMP and LSK populations, which were determined to be more than 97% pure, were snap-frozen on dry ice for storage at −80 °C until use.

Microarray and analysis. RNA was extracted from sorted GMP and LSK populations using Trizol (Life Technologies) as per the manufacturer's directions. An RNA sample (25 ng) was labeled with the Cy3 dye as per the protocol detailed in the Low Input Quick Amp Labeling Kit (Agilent Technologies). A specific activity of >6.0 was confirmed by A_{260nm} and A_{550nm} measurements using a NanoDrop ND-1000 spectrophotometer. Labeled RNA (600 ng) was hybridized to Agilent SurePrint G3 mouse 8 × 60K microarray slides for 16 h. Slides were washed and scanned with a High-Resolution C Scanner (Agilent Technologies), using a scan resolution of 3 µm. Feature extraction was performed using Agilent Feature Extraction software, with no background subtraction. Scanned microarray images were analyzed using Agilent's Feature Extraction software. Feature intensities were background-subtracted according to the normal–exponential convolution model and normalized using 75th percentile normalization. Differentially expressed genes were identified using the significant analysis of microarrays (SAM) method with a false discovery rate (FDR) <0.05 using Multiexperiment Viewer (MeV) software (http://www.tm4.org/mev.html). Hierarchical clustering was obtained using Gene Cluster 3.0 software.

To ascribe characteristic profiles to the set of genes that were differentially expressed in the microarray analysis, the specificity of genes upregulated in both LSK and GMP cells from KO mice, which was defined as cluster 1,

was determined based on their annotation in Gene Expression Commons (GEXC)[50]. Briefly, the gene expression activity files of all of the BM cells were downloaded from GEXC (https://gexc.riken.jp), aligned with those of the 69 genes of cluster 1 that were retrieved, and the heat maps of their expression activity were created for individual cell populations. The analysis showed enrichment primarily in PMN-specific genes. To determine whether such enrichment was selective for a subset or PMN-specific genes, the expression of all genes that were annotated as being PMN specific in the Immgen database (http://www.immgen.org/) was assessed in the microarray. Briefly, among 334 defined cell-specific clusters in the Immgen "Modules and Regulators" tool, three modules (209, 210 and 258) have been assigned as PMN-specific and encompass 54 genes in total (22, 11 and 12 genes, respectively). The expression of these genes was verified in the microarray and presented for individual modules as heat maps.

Two-photon laser scanning microscopy (TPLSM) of the whole-mounted bone marrow. Mice were euthanized and perfused via cardiac puncture with 3 ml cold PBS followed by 3 ml cold 4% PFA. Femurs were harvested, carefully cleaned from the surrounding tissue and post-fixed in 4% PFA at 4 °C overnight. After fixation, bones were briefly washed with PBS and cryopreserved in 15% sucrose at 4 °C for 2 h, followed by incubation in 30% sucrose at 4 °C overnight. Bones were embedded in OCT and flash-frozen. Samples were longitudinally shaved with a Leica CM3050S cryostat to expose the BM along the full length of the femur, OCT residue was washed away with PBS and nonspecific antigens were blocked by a PBS solution containing 20% normal goat serum and CD16/CD32 Fc-block (final concentration 0.5 µg/ml) for 2 h at 20 °C. Bones were incubated overnight in the dark at 20 °C with directly conjugated antibodies to the following markers: CD150, CD71 and lineage (CD3, B22, Gr1, CD11b, CD48, CD41). After incubation, the bones were washed several times with PBS and embedded into PBS-based 1.5% agarose gel before imaging. Further details regarding imaging reagents are provided in **Supplementary Table 1**.

Four-color TPLSM microscopy was performed on a Leica SP5IIMP that was equipped with a 20× NA1.00 WD objective (Leica) and a pre-chirped MaiTai Ti:Sa pulsed laser (Spectra-Physics) tuned at 800 nm to maximize dye emission. Optical zoom was applied where applicable. To allow for the simultaneous collection of all spectra while minimizing color spillover, the collection channels of Hybrid diode detectors were determined as follows: 380–415 nm for bone-collagen-derived second harmonic generation (SHG) signal, 420–470 nm for Pacific Blue, 500–550 nm for AF488 and 600–650 nm for phycoerythrin (PE). z-stacks (1-µm step size) of 1024 × 1024 pixel xy images (f.o.v. 356 × 356 µm²) were collected up to a depth of 100–150 µm. z-stacks were three dimensionally reconstructed using the Imaris software (Bitplane). HSCs were identified as CD150⁺Lin⁻CD7⁻ cells, and NECs as CD71⁺Lin⁻CD150⁻ cells. Both stains were rendered as isosurface, and distances between HSCs and the closest NECs were determined using the software's measurement tools.

Human blood samples. Blood was collected from healthy individuals as approved by the ethical committee of LMU, Munich following written consent. To determine the expression of Duffy antigen on erythrocytes, whole blood was stained with mouse monoclonal anti-ACKR1 (Fy6, gift from Dr. M. Uchikawa), washed and stained with a FITC-conjugated secondary antibody (**Supplementary Table 1**). For staining of neutrophil surface markers, erythrocytes were lysed using ACK lysing buffer, and the remaining cells were washed with FACS buffer. Cells were incubated with antibodies to CD45, CD11b, CD16, CXCR1, CXCR2 and CCR2 and analyzed using a FACS CANTO II flow cytometer.

Statistical analysis. Multiple independent experiments were performed to verify the reproducibility of the experimental findings. When suitable, sample sizes were estimated based on results of explorative experiments to provide adequate power. No randomization or blinding was used for any of the experiments. Mice were excluded from experiments if they showed any signs of sickness. Differences in two-group comparisons were assessed by an unpaired Student's *t*-test, with Welch's correction when appropriate. Comparisons between three or more groups were performed by one-way or two-way ANOVA as appropriate, followed by a Tukey's *post hoc* test.

Differences in proportions were assessed by a χ^2 test with Fisher's correction, when appropriate. Statistical significance is represented by asterisks and the corresponding *P* values, as indicated in the legends. Data are expressed as mean ± s.e.m. or mean ± s.d. Biological replicates are stated in the legends for each figure. Statistical analysis was performed with G-Power[51] and Prism6 (GraphPad) software.

Data availability. The data that support the findings of this study are available from the corresponding author upon request. The complete microarray data set is deposited in the Gene Expression Omnibus (GEO) database (http://www.ncbi.nlm.nih.gov/geo) under accession number GSE86349.

49. Wright, D.E., Wagers, A.J., Gulati, A.P., Johnson, F.L. & Weissman, I.L. Physiological migration of hematopoietic stem and progenitor cells. *Science* **294**, 1933–1936 (2001).
50. Seita, J. *et al.* Gene Expression Commons: an open platform for absolute gene expression profiling. *PLoS One* **7**, e40321 (2012).
51. Faul, F., Erdfelder, E., Lang, A.-G. & Buchner, A. G*Power 3: a flexible statistical power analysis program for the social, behavioral and biomedical sciences. *Behav. Res. Methods* **39**, 175–191 (2007).
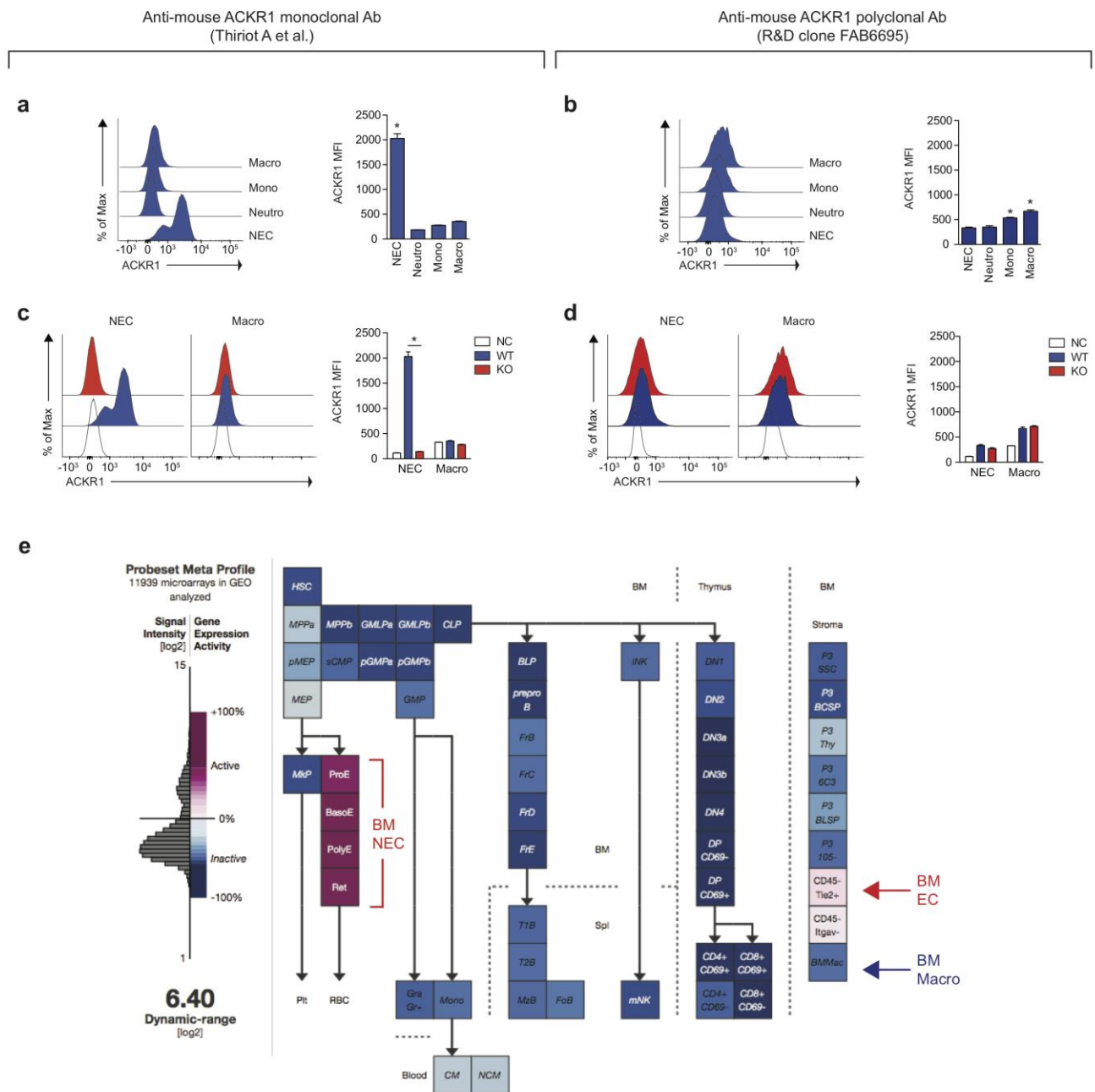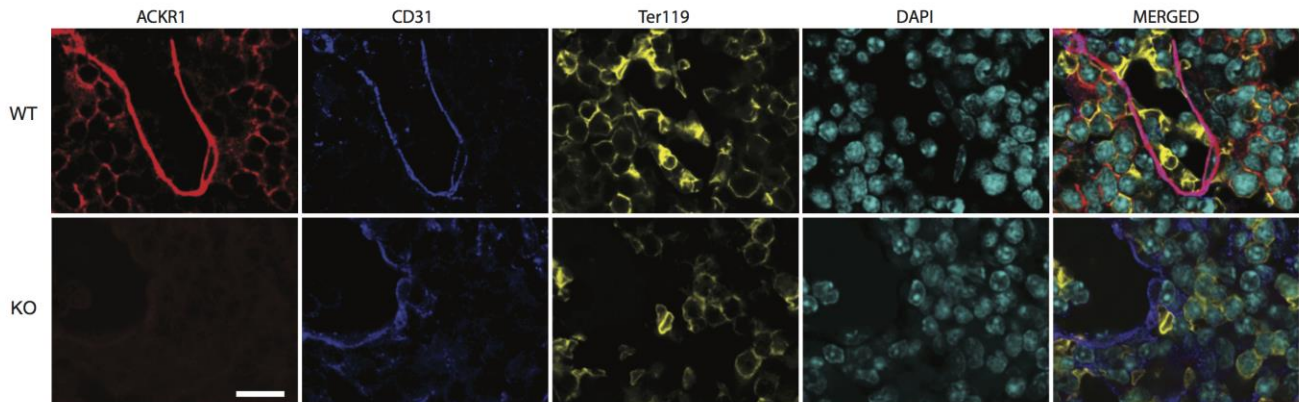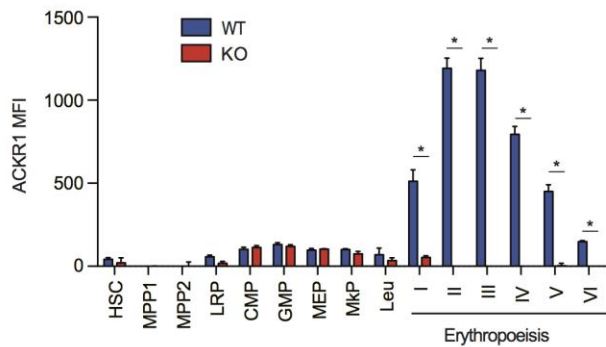
Supplementary Figure 1

Validation of the monoclonal antibody to mouse ACKR1 and expression of ACKR1 by BM hematopoietic cells.

(**a** to **d**) Comparison of immunostaining of BM cells by anti-mouse ACKR1 antibodies: new validated monoclonal (**a** and **c**, Thiriot A et al Ref. 29) and non-validated polyclonal (**b** and **d**, FAB6695P from R&D Systems used by Hur et al., Ref. 43, to report ACKR1 expression in BM macrophages). (**a** and **b**) ACKR1 immunoreactivity in nucleated erythroid cells (NECs; CD71$^+$Ter119$^+$), neutrophils (Neutro; CD11b$^+$CD115$^-$F4/80$^-$Ly6G$^+$), monocytes (Mono; CD11b$^+$ CD115$^+$F4/80$^-$Ly6G$^-$) and macrophages (Macro; CD11b$^+$CD115$^-$ F4/80$^+$Ly6G$^-$) in BM of wild-type (WT) mice. Left, representative flow cytometry histogram plots; right, quantitative analysis. n=3. (**c** and **d**) ACKR1 immunoreactivity and negative control staining (NC) in NECs and macrophages (Macro) in BM of WT (blue) and ACKR1-deficient (KO, red) mice. Left, representative flow cytometry histogram plots; right, quantitative analysis. n=3. BM immunostaining using validated monoclonal antibody (**a** and **c**) show that ACKR1 is expressed in the BM by erythroid cells only but not by macrophages. Polyclonal non-validated antibody failed to immunoreact with NECs but at high concentration stained BM macrophages, (**b**) however

non-specifically as (**d**) to the same extent in WT and KO mice. All data are Mean±SEM. One-Way ANOVA (**a** and **b**). Two-Way ANOVA (**c** and **d**). *P<0.001. (**e**) Relative expression of ACKR1 in hematopoietic and stromal populations as determined by microarray analysis based on the data in the BM cells transcriptome database (https://gexc.riken.jp/models). Microarray dataset of adult definitive murine erythroblasts were retrieved from ArrayExpress (https://www.ebi.ac.uk/arrayexpress; E-MTAB-1035) and implemented in Gene Expression Commons database (link to this model https://gexc.riken.jp/models/1649). Proerythroblasts (ProE), early normoblasts (BasoE), late normoblasts (PolyE), reticulocytes (Ret) and Endothelial cells (BM EC) in BM express ACKR1 whereas BM macrophages (BM Macro) do not.
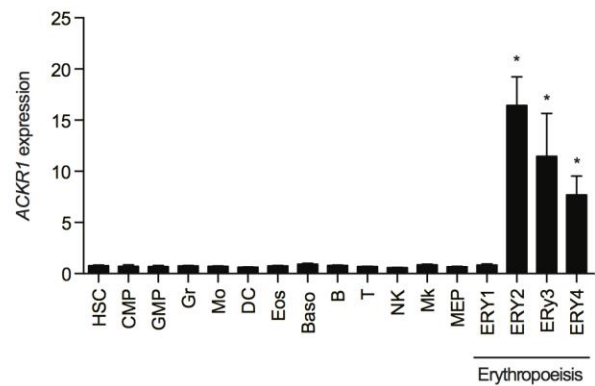
Supplementary Figure 2

ACKR1 is expressed by endothelial cells and nucleated erythroid cells in the BM but not by other hematopoietic cells.
(**a**) Immunofluorescence micrographs of wild-type (WT) and ACKR1-deficient (KO) BM stained with anti-ACKR1 (red), anti-CD31 (endothelial cells, blue), anti-Ter119 (erythroid cells, yellow) antibodies and DAPI (nuclei, turquoise). (**b**) ACKR1 expression (MFI) on HSPCs, megakaryocyte progenitors (MkP) and leukocytes (Leu) as compared to the subpopulations of erythroid cells at different stages of development (I-VI) in WT (red) and KO (blue) BM (Mean±SEM; n=3). Scale bar, 30 μm (**c**) Human ACKR1 mRNA BM expression data retrieved from DMAP (http://portals.broadinstitute.org/dmap/home). Subpopulations of erythroid cells (ERY1-4) were defined as follows: CD71^{hi} GlyA$^-$(Ery1), CD71^{hi} GlyA$^+$(Ery2), CD71^{lo} GlyA$^+$(Ery3) and CD71$^-$GlyA$^+$(Ery4). Mean±SEM, One-Way ANOVA; *P < 0.001.
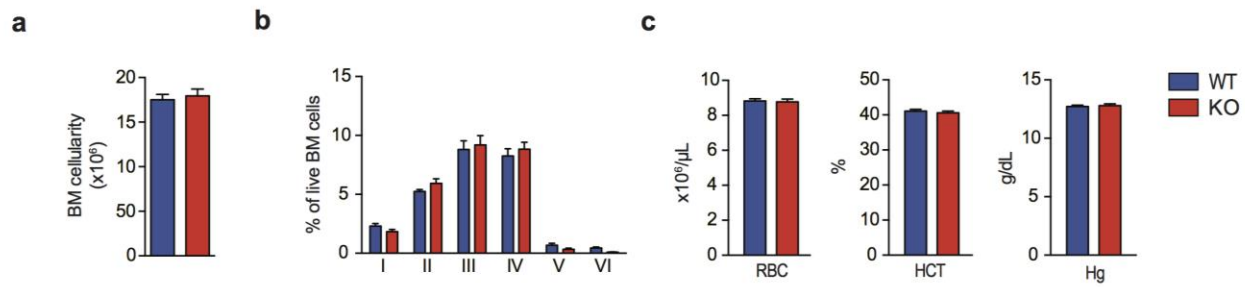
Supplementary Figure 3

ACKR1 deficiency does not affect erythroid parameters in BM and blood.

(**a**) BM cellularity in in WT (blue) and ACKR1-deficient (KO; red) mice (Mean±SEM; n=9). (**b**) Percentage of proerythroblasts (I), early normoblasts (II), intermediate normoblasts (III), late normoblasts (IV), reticulocytes (V) and mature red cells (VI) in BM of WT and KO mice (Mean±SEM; n=3). (**c**) Erythrocyte parameters in blood. RBC: Red blood cell counts; HCT: Haematocrit; Hb: haemoglobin. (Mean±SEM; n=9).
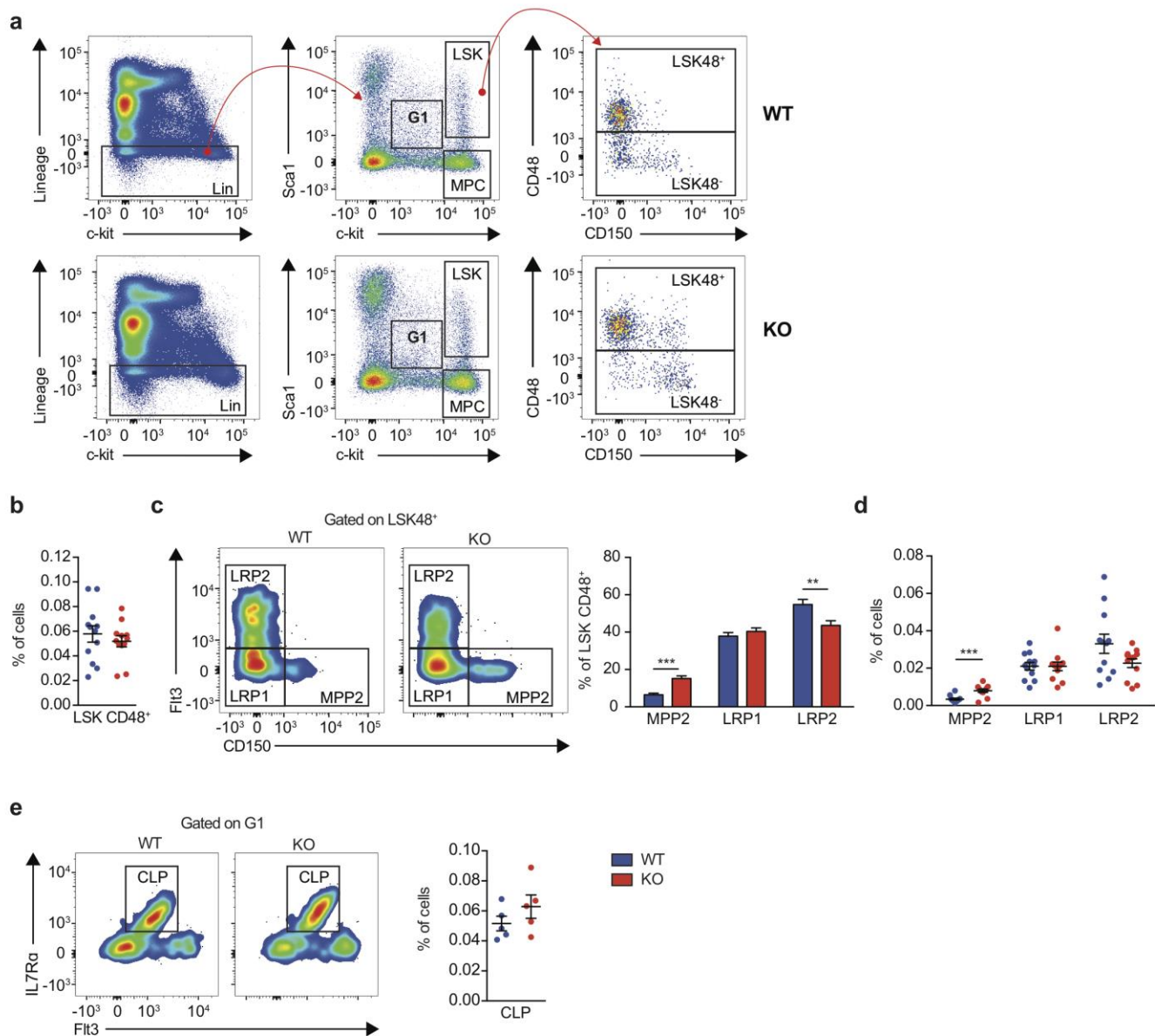
Supplementary Figure 4

Flow cytometry analysis of HSPCs, CD48$^+$ subpopulations of LSK cells and CLP cells.

(**a**) Gating strategy to identify HSPC populations. LSK, defined as Lin$^-$Sca-1$^+$c-Kit$^+$ were subdivided into LSK CD48$^+$ and LSK CD48$^+$. Myeloid progenitor cells (MPC) were defined as Lin$^-$Sca-1$^-$c-Kit$^+$. (**b**) Frequency of LSK CD48$^+$ cells in in WT (blue) and ACKR1-deficient (KO, red) BM. (**c**) Relative distribution of their MPP2, and lineage-restricted progenitor (LRP) 1 and LRP2 sub-populations. Representative dot plots, left; quantitative analysis, right. (**d**) Frequency of MPP2, LRP1 and LRP2 in the BM of WT and KO mice. (**e**) Frequency of common lymphoid progenitors (CLP) defined as Lin$^-$Sca-1^{lo}c-Kit^{lo} (G1 gate in **a**) and IL7Rα$^+$Ftl3$^+$. Representative dot plots, left; quantitative analysis, right. (**b-d**) n=12 in four independent experiments. (**f**) n=5 in two independent experiments. All data show Mean±SEM. Two-tailed Student's t-test; ***p < 0.001.
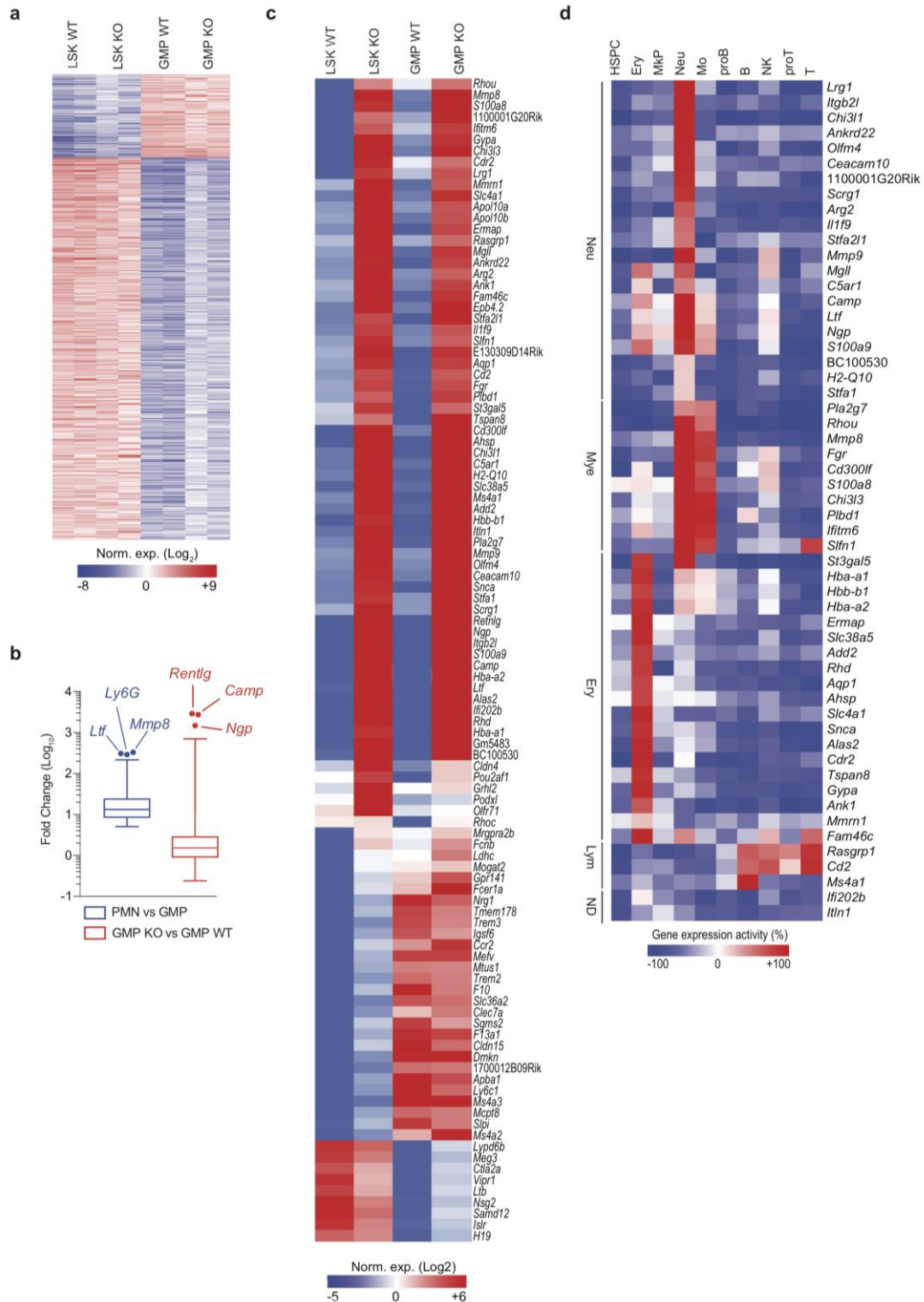
Supplementary Figure 5

Gene expression in LSKs and GMPs from WT and ACKR1-deficient mice.

(**a**) Microarray heatmap of genes expressed in LSKs and GMPs from wild-type (WT) and ACKR1-deficient (KO) BMs. Each row represents a gene and columns show individual cell populations, in duplicates. Two clusters defined by hierarchical clustering analysis

reflect specific gene expression in LSK and GMP. The levels of expression of specific LSK and GMP enriched genes were similar in WT and KO BM. (**b**) Left, blue: Comparative gene expression in neutrophils (PMNs) and GMPs from Immgen dataset (www.immgen.org). The expression of the 444 genes was higher in PMNs vs. GMPs on average >10 times. Three genes with the highest increase, *Ltf*, *Ly6G* and *Mmp8*, were expressed ca. 100 times more in PMN, than in GMP. Right, red: comparative gene expression in GMPs from WT vs. KO BM expressed as fold change. The level of expression of the overwhelming majority of genes was the same in GMPs from WT and KO BMs (mean fold change 1) but some were expressed orders of magnitude higher in KO GMPs. The transcripts for three most overexpressed genes *Rentlg*, *Camp* and *Ngp*, were in excess of 1000 times higher in KO vs. WT GMPs. These genes were not highly upregulated during the differentiation of GMPs towards PMNs (left panel, blue). This excluded a potential contamination of the GMP with PMNs and was consistent with the induction of a specific transcriptional program of a subset of neutrophil specific genes (also see **Fig. 3c**) in GMPs rather than only their conventional differentiation to PMNs. (**c**) Microarray heatmap from Fig. 3a with the list of genes. (**d**) Microarray heatmap from Fig. 3b with the list of genes.
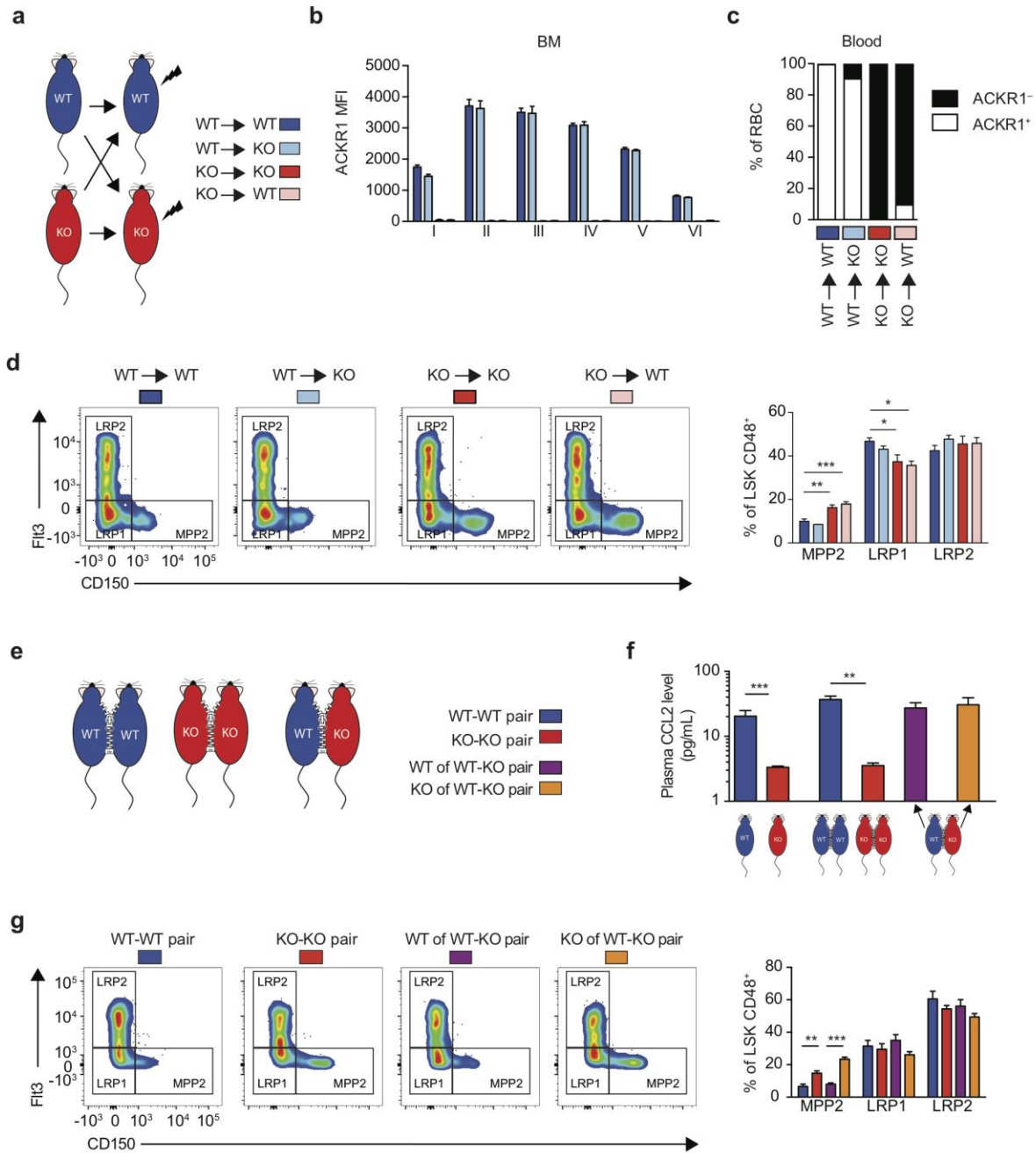
Supplementary Figure 6

BM and blood cell parameters in reciprocal irradiation BM chimeric and parabiotic wild-type and ACKR1-deficient mice.

(**a**) Schematic representation of experimental groups of irradiation BM chimeric mice. (**b,c**) Confirmation of successful BM chimerism by flow cytometric measurement of ACKR1 expression on erythroid cells in BM and in blood. (**b**) Quantitative analysis of ACKR1 expression on subpopulations of erythroid cells (I-VI) in BM. (**c**) Percentages of ACKR1^{+} and ACKR1^{−} RBC in peripheral blood. (**d**) Relative distribution of MPP2, LRP1 and LRP2 subpopulation of LSK CD48^{+} in irradiation BM chimeric mice: wild-type (WT) BM cells reconstituted into WT mice (blue), WT BM cells reconstituted into ACKR1-deficient (KO) mice (light blue), KO BM cells reconstituted into KO mice (red) and KO BM cells reconstituted into WT mice (pink); right, representative dot plots; left, quantitative analysis. (**e**) Schematic representation of experimental groups in parabiosis experiments. (**f**) Confirmation of shared circulation in parabiosis by measurement of plasma CCL2 levels in individual naïve and parabiotic mice. WT with WT parabionts (blue), KO with KO parabionts

(red), WT parabiont in WT with KO pair (purple) and KO parabiont in WT with KO pair (orange) (**g**) Relative distribution of MPP2, LRP1 and LRP2 subpopulation of LSK CD48^{+}, right, representative dot plots; left, quantitative analysis. All data are n=4 from two independent experiments, Mean±SEM. One-way ANOVA; *P < 0.05, **P < 0.01 and ***P < 0.001.

a

b

Lineage HSC NEC

NEC HSC   Lineage HSC   Lineage NEC

c

d
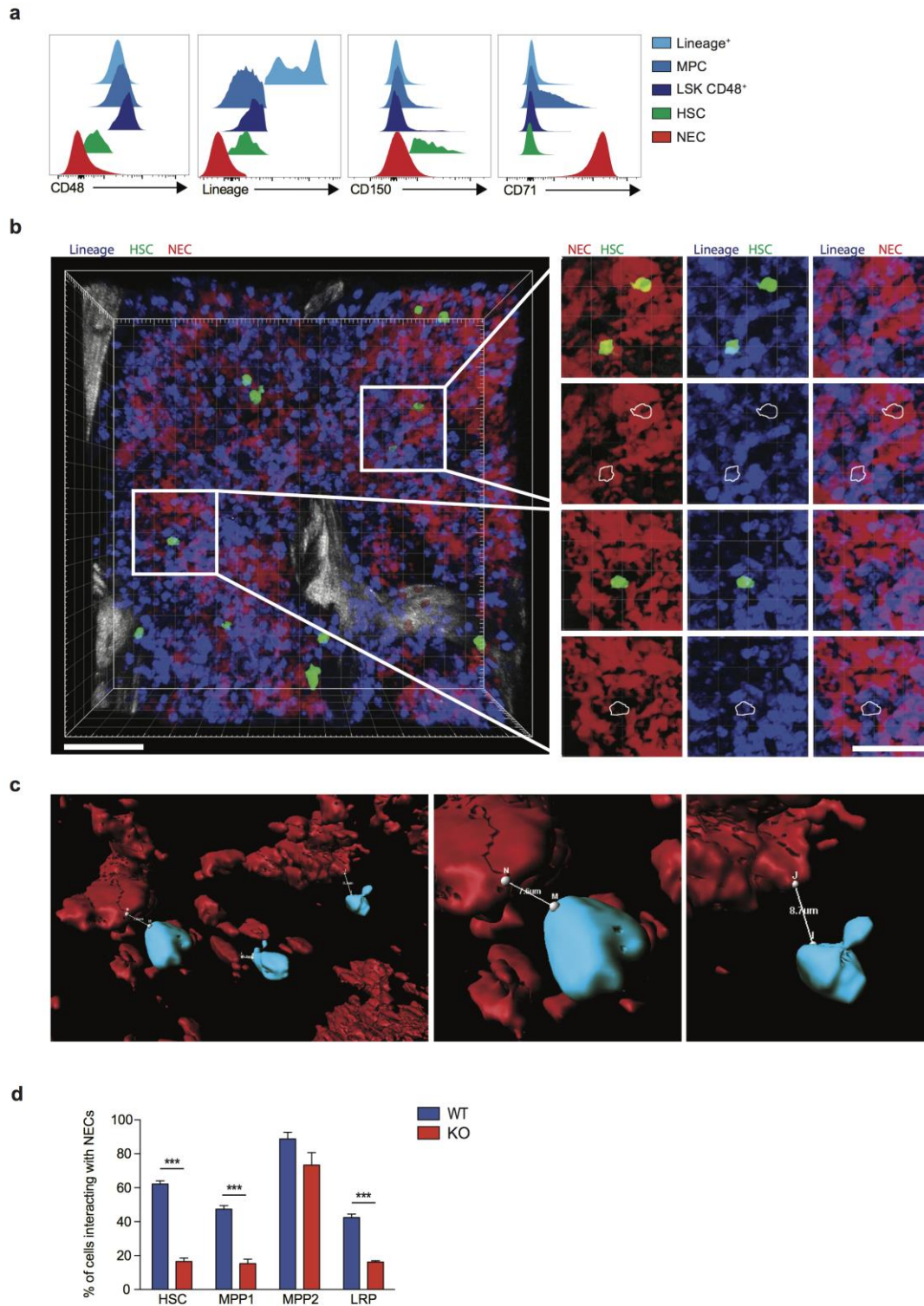
Supplementary Figure 7

Interactions of HSCs and nucleated erythroid cells in the BM.

(**a**) Representative flow cytometry histograms showing staining by antibodies against CD48, Lineage (Lin; B220, CD3, CD11b, Gr1), CD150 and CD71 used for identification of HSCs and nucleated erythroid cells (NECs). The HSCs (LSK CD150$^+$ CD48$^-$) are

distinguished as Lin$^-$ CD150$^+$CD48$^-$CD71$^-$; the NECs (CD71$^+$ Ter119$^+$) are CD71$^+$Lin$^-$CD150$^-$CD48$^-$; the MPCs and CD48$^+$LSK subset are Lin$^-$CD48$^+$ CD150$^-$CD71$^-$ and the lineage cells are Lin$^+$CD48$^+$. (**b**) Application of the above combination of antibodies to the two-photon microscopy of the whole-mounted femur. HSCs (Lin$^-$CD150$^+$CD71$^-$; green) and NECs (Lin$^-$CD150$^-$ CD71$^+$; red) appear clearly distinct. HSCs (in the upper rows of magnification insets, green; in lower rows of insets, only outlined in white) did not stain for lineage or CD71. Scale bars, 50 μm and 40 μm (**c**) Representative two photon microscopy images of the whole-mounted femurs from ACKR1-deficient mice used for the measurements of the distance between NECs and HSCs. (**d**) Quantitative analysis of HSC, MMP1, MPP2 and LRP populations interacting with NECs assessed by flow cytometry. Wild-type (WT, blue) and ACKR1-deficient (KO, red). Two-tailed Student's t-test, (n=3). All numeric data are Mean±SEM. ***$P < 0.001$.
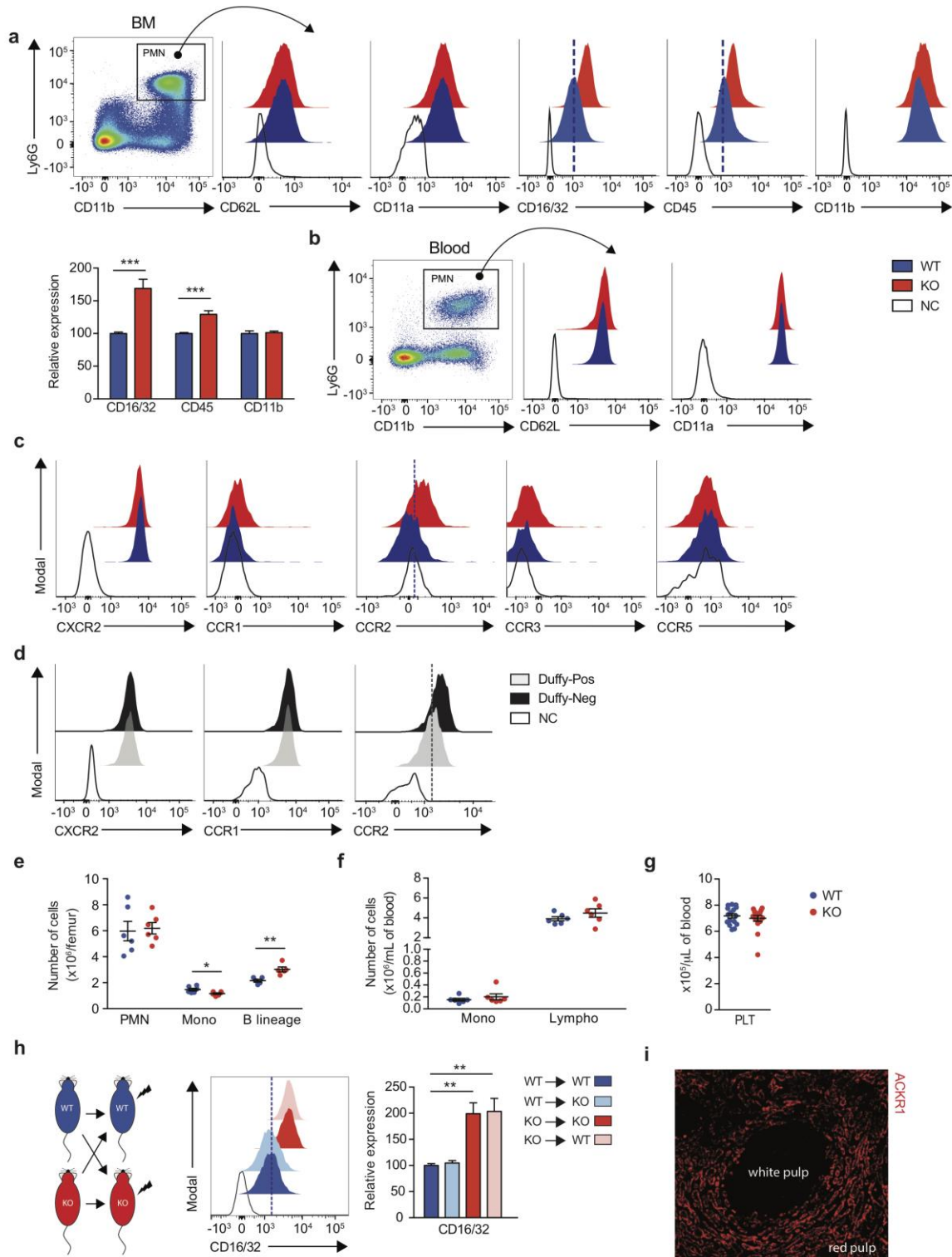
Supplementary Figure 8

Effect of ACKR1 on the expression of cell surface markers and cell numbers in BM and blood.

(**a**) CD62L, CD11a, CD16/32, CD45 and CD11b expression in BM neutrophils (CD11b^{+}Ly6G^{+}) from wild-type (WT, blue) and ACKR1-deficient (KO, red) mice; NC (white), negative control staining. Top, representative flow cytometry histograms; bottom, quantitative

analysis. (**b**) Representative flow cytometry histograms of staining blood neutrophils (CD11b$^+$Ly6G$^+$) from WT and KO mice with antibodies against CD62L and CD11a and (**c**) antibodies against CXCR2, CCR1, CCR2, CCR3 and CCR5. (**d**) Representative flow cytometry histograms of CXCR1, CXCR2 and CCR2 antibodies staining of blood neutrophils from Duffy-positive and Duffy-negative individuals, grey and black histograms, respectively, negative control staining, NC (white). (**e**) PMN (CD11b$^+$Ly6G$^+$CD115$^-$), monocyte (CD11b$^+$Ly6G$^-$CD115$^+$) and B lineage cell (B220$^+$CD19$^+$) counts in BM of WT and ACKR1-deficient mice (n=6). (**f**) Monocyte (CD45$^+$CD11b$^+$Ly6G$^-$ CD115$^+$) and lymphoid cell (CD45$^+$ and B220$^+$ or CD3$^+$) counts in blood of WT and ACKR1-deficient mice (n=6). (**g**) Platelet counts in blood of WT and ACKR1-deficient mice (n=16). (**h**) Expression of CD16/32 on blood neutrophils (CD11b$^+$Ly6G$^+$CD115$^-$) in reciprocal BM chimeric mice; WT BM cells reconstituted into WT mice (blue), WT BM cells reconstituted into KO mice (light blue), KO BM cells reconstituted into KO mice (red) and KO BM cells reconstituted into WT mice (pink); n=4 from two independent experiments. (**i**) Representative immunofluorescence micrograph of human spleen stained with monoclonal anti-ACKR1 (Fy6, red) antibody. All data show Mean±SEM. (**a** and **e**-**g**) two-tailed Student's t-test; *P < 0.05, **P < 0.01. (**h**) one-way ANOVA; **P < 0.01.

Supplementary Table 1
List of antibodies

Mouse antibodies					
Antibody	**Clone**	**Conjugation**	**Provider**	**FACS**	**Imaging**
ACKR1		A647	Ref. 29	x	
ACKR1		A488	Ref. 29	x	
ACKR1		A546	Ref. 29		x
ACKR1	FAB6695P	PE	R&D	x	
B220	RA3-6B2	Pacific Blue	BioLegend	x	x
c-Kit	2B8	PE-Cy7	BioLegend	x	
c-Kit	2B8	APC-Cy7	eBioscience	x	
CD115	AFS98	APC	Biolegend	x	
CD11a	M17/4	PE	BioLegend	x	
CD11b	M1/70	Pacific Blue	BioLegend	x	
CD11b	M1/70	PE-Cy7	BioLegend	x	
CD11b	M1/70	PerCP-Cy5.5	eBioscience	x	
CD11b	M1/70	FITC	eBioscience	x	
CD11b	M1/70	APC-Cy7	Biolegend	x	
CD150	TC15-12F12.2	PerCP-Cy5.5	BioLegend	x	
CD150	TC15-12F12.2	A488	BioLegend		x
CD16/32	93	APC-Cy7	BioLegend	x	
CD19	1D3	PE	eBioscience	x	
CD3	17A2	Pacific Blue	BioLegend	x	x
CD31	MFC13.3	–	BD-Biosciences		x
CD34	RAM34	FITC	eBioscience	x	
CD41	MWReg30	Pacific Blue	BioLegend		x
CD45	30-F11	PE-Cy7	BioLegend	x	
CD45	30-F11	FITC	BioLegend	x	
CD48	HM48-1	BV510	BD-Biosciences	x	
CD48	HM48-1	Pacific Blue	BioLegend	x	x
CD62L	MEL-14	APC-Cy7	BioLegend	x	
CD71	RI7217	FITC	BioLegend	x	
CD71	RI7217	PE	BioLegend	x	x
CCR1	FAB5986P	PE	R&D	x	
CCR2	MC-21	PE	Ref. 52	x	
CCR3	JO73E5	PE	BioLegend	x	
CCR5	HM-CCR5	PE	BioLegend	x	
CXCR2	SA044G4	PerCP-Cy5.5	Biolegend	x	
F4/80	BM8	FITC	BioLegend	x	
F4/80	BM8	PerCP-Cy5.5	BioLegend	x	

Flt3	A2F10	PE	BioLegend	x	
GR1	RB6-8C5	Pacific Blue	BioLegend	x	x
Il-7Rα	A7R34	BV510	BioLegend	x	
Ly6G	1A8	FITC	BioLegend	x	
Ly6G	1A8	BV510	BioLegend	x	
MECA-32	MECA-32	A647	Biorad		x
Sca-1	D7	APC-Cy7	BioLegend	x	
Sca-1	D7	PE-Cy7	eBioscience	x	
Goat anti-rat	A-11006	A488	Life Technologies		x
Ter119	TER-119	Pacific Blue	BioLegend	x	
Ter119	TER-119	A647	BioLegend	x	x
Ter119	TER-119	FITC	BioLegend		x

Human Antibodies					
Antibody	**Clone**	**Conjugation**	**Provider**	**FACS**	**Imaging**
CD16	3G8	PerCP-Cy5.5	BioLegend	x	
CD45	HI30	APC	BioLegend	x	
CD11b	M1/70	APC-Cy7	BioLegend	x	
CXCR1	320606	FITC	BioLegend	x	
CXCR2	5E8/CXCR2	PE	BioLegend	x	
CCR2	FAB151A	APC	R&D	x	
ACKR1	Fy6	–	Ref. 9		x
Goat anti-mouse	F0257	FITC	Sigma	x	

52. Mack, M *et al.* Expression and characterization of the chemokine receptors CCR2 and CCR5 in mice. *J. Immunol.* **166**, 4697-4704 (2001).

6.5 Murine bone marrow macrophages and human monocytes do not express atypical chemokine receptor 1.

Rot A, Gutjahr JC, Biswas A, Aslani M, Hub E, Thiriot A, von Andrian UH, Megens RTA, Weber C, **Duchene J**.

Letter

Murine bone marrow macrophages and human monocytes do not express atypical chemokine receptor 1

Antal Rot,[1,2,3,*] Julia C. Gutjahr,[1] Aindrila Biswas,[3] Maria Aslani,[3] Elin Hub,[1,2] Aude Thiriot,[4,5] Ulrich H. von Andrian,[4,5] Remco T.A. Megens,[3,6] Christian Weber,[3,6,7,8] and Johan Duchene[3,7,*]

[1]Centre for Microvascular Research, William Harvey Research Institute, Barts and The London School of Medicine and Dentistry, Queen Mary University of London, Charterhouse Square, London EC1M 6BQ, UK
[2]Centre for Inflammation and Therapeutic Innovation, Barts and The London School of Medicine and Dentistry, Queen Mary University of London, Charterhouse Square, EC1M 6BQ London, UK
[3]Institute for Cardiovascular Prevention, Ludwig-Maximilians University, Pettenkoferstrasse 8a & 9, 80336 Munich, Germany
[4]Department of Immunology & HMS Center for Immune Imaging, Harvard Medical School, Boston, MA 02115, USA
[5]Ragon Institute of MGH, MIT and Harvard, Cambridge, MA USA
[6]Cardiovascular Research Institute Maastricht, University of Maastricht, P. Debeyelaan, 6229HX Maastricht, the Netherlands
[7]German Center for Cardiovascular Research (DZHK), partner site Munich Heart Alliance, Pettenkoferstrasse 8a & 9, 80336 Munich, Germany
[8]Munich Cluster for Systems Neurology (SyNergy), Pettenkoferstrasse 8a & 9, 80336 Munich, Germany
*Correspondence: a.rot@qmul.ac.uk (A.R.), johan.duchene@med.uni-muenchen.de (J.D.)
https://doi.org/10.1016/j.stem.2021.11.010

The atypical chemokine receptor 1 (ACKR1) was discovered on erythrocytes as the Duffy blood group antigen (Cutbush et al., 1950), also called Duffy-antigen/receptor for chemokines, or DARC (Novitzky-Basso and Rot, 2012). Erythrocytes are terminally differentiated anuclear cells with no transcription and limited translation. Accordingly, within the erythroid lineage ACKR1 expression occurs first and is the highest in erythroblasts (Duchene et al., 2017). Additionally, ACKR1 expression characterizes venular endothelial cells (ECs) (Pruenster et al., 2009; Thiriot et al., 2017), including those lining bone marrow (BM) sinusoids (Duchene et al., 2017). This well-established, distinctive pattern of cell expression has been directly challenged by a publication purporting ACKR1 expression in mouse BM by macrophages, but not erythroblasts and ECs, suggesting that macrophage ACKR1 engages its non-cognate ligand CD82 on hematopoietic stem cells (HSCs) to maintain their quiescence (Hur et al., 2016). In light of the extensive literature, these findings have been particularly provocative, as this was the first description of ACKR1 expression by any leukocyte type and, if correct, would change current concepts of ACKR1 involvement in pathophysiology. The reported ACKR1 expression by macrophages in Hur et al. relied on using commercial anti-ACKR1 antibody FAB6695, which has neither been validated by the manufacturer nor by the authors. This

prompted us to investigate the specificity of FAB6695 and scrutinize the apparent ACKR1 expression in BM macrophages.

According to a comprehensive murine BM transcriptome database (https://gexc.riken.jp/), ACKR1 mRNA accumulates in nucleated erythroid cells (NECs), whereas all non-erythroid nucleated cells (NENCs) are devoid of it (Figure S1A). First, we used flow cytometry to probe FAB6695 staining of these two populations. Whereas ACKR1-specific antibody 6B7 (Duchene et al., 2017; Thiriot et al., 2017) accurately discriminated between NECs and NENCs, FAB6695 stained both cell populations almost equally (Figure S1B), as also revealed by their respective staining indices (Figure S1C). Additionally, in contrast to 6B7, FAB6695 immunostained NECs of both wild-type (WT) and ACKR1-deficient (KO) mice (Figure S1D), as reflected by the antibodies' specificity indices (Figure S1E). Next, we compared the staining properties of FAB6695 and 6B7 using an unbiased t-SNE analysis of all BM cells of WT and KO mice. It confirmed that, in contrast to control 6B7, FAB6695 marked NECs and other BM cells equally well and failed to discriminate between WT and ACKR1 KO cells (Figure S1F), corroborating its lack of sensitivity and specificity, respectively. Furthermore, FAB6695 failed to immunodetect ACKR1 on venular ECs in tissue sections (Figure S1G). These data clearly invalidate FAB6695, as it is neither sufficiently sensi-

tive to detect ACKR1 on NECs and ECs nor specific, as it recognizes unrelated epitope(s) present in ACKR1-deficient cells.

Uncovering the unspecific nature of FAB6695 undermined the assertion of ACKR1 expression in BM macrophages and prompted us to address this question directly by staining the whole BM with ACKR1-specific 6B7, co-staining with a broad set of markers and visualizing the results by t-SNE. Unexpectedly, in addition to all NECs, 6B7 marked a subset of F4/80[pos] macrophages, separating them into two subpopulations (Figure S1H). One, F4/80[pos]ACKR1^{neg}, co-expressed myeloid markers, CD11b, Ly6C, and CEACAM1, while another, F4/80[pos]ACKR1^{pos}, did not, though it co-expressed erythroid-specific Ter119 and CD71. Gating on F4/80^{pos} BM cells confirmed that ACKR1^{pos} cells also expressed erythroid-specific markers CD71 and Ter119 (Figure S1I). Moreover, gating on all ACKR1^{pos} cells retrieved only cells with a complete erythroid signature (Figure S1J). Together these data suggested that either a subset of F4/80[pos] macrophages expressed erythroid-specific surface markers, or, vice versa, a subset of NECs expressed F4/80. To clarify the nature of the F4/80[pos]ACKR1^{pos} cells, we visualized them by imaging flow cytometry, thus revealing that they were not individual cells but cell aggregates comprising at least one ACKR1^{pos}CD71^{pos}Ter119^{pos} NEC and one F4/80^{pos}CD11b^{neg} macrophage

(Figure S1K, Lanes 1–4). NECs and macrophages are spatially and functionally interconnected within the BM erythroblastic islets, each of which comprises a F4/80^{pos}CD11b^{neg} macrophage (Li et al., 2019) surrounded by several adherent NECs (Chasis and Mohandas, 2008). The tight bonds between these cells evidently persist also *ex vivo*, upon their isolation. Conversely, F4/80^{pos}CD11b^{pos} macrophages did not form complexes with NECs and were completely devoid of membrane ACKR1 immunoreactivity (Figure S1K, Lane 5), but few emitted a faint intracellular signal (Figure S1K, Lane 6) that is entirely consistent with an autofluorescence or a spillover from the CD11b channel. The F4/80^{pos}CD11b^{pos} macrophages in the BM, spleen, and peritoneum are known to produce autofluorescent signals. Egregious examples misinterpreting macrophage autofluorescence as immunoreactivity include, e.g., alleging macrophage expression of FoxP3 (Li et al., 2012). Another well-documented artefact associated with immunostaining macrophages results from a non-specific antibody binding via Fc-receptors, necessitating the use of Fc-block and careful analysis versus appropriate controls.

In conjunction, we used a specific antibody 6B7 to establish that BM macrophages themselves do not express ACKR1. However, macrophages form aggregates with ACKR1^{pos} NECs, which, in conventional flow cytometry, despite stringently set doublet-exclusion gates, are detected as singlets, potentially causing artifactual attribution of ACKR1 expression to macrophages, which can also stem from misinterpreting autofluorescence, fluorescence channel spillover, or antibody binding via Fc-receptors. It is plausible that the flow cytometry phenomenon of NEC/macrophage doublets effectively masquerading as single cells is also mirrored in single-cell transcriptomics. However, this was not the case as a comprehensive hematopoietic single-cell transcriptome database (https://tabula-muris.ds.czbiohub.org/) correctly ascribed the ACKR1 mRNA expression to NECs only (Figure S1L).

Our studies provide evidence that BM macrophages do not express ACKR1. However, it remains possible that the described phenotype of HSC dormancy maintained via CD82 (Hur et al., 2016) still depends on ACKR1, albeit expressed by NECs. NECs and macrophages are also spatially and functionally interconnected within the erythroblastic islets of the BM, each comprising a macrophage surrounded by a number of adherent NECs (Chasis and Mohandas, 2008). Because of this functional nexus, it is possible that macrophage depletion by clodronate, which abolished HSC quiescence (Hur et al., 2016), indirectly affected the erythroid lineage and disrupted ACKR1-mediated direct interactions of NECs with HSCs, shown by us to depend on ACKR1 expression by NECs (Duchene et al., 2017). Therefore, it is possible that the ACKR1-dependent *in vitro* effects on HSC proliferation ascribed to BM macrophages (Hur et al., 2016) were actually induced by the ACKR1^{pos} erythroblasts inconspicuously carried into the *in vitro* experimental setups in complex with the isolated macrophages. If CD82 on HSCs indeed engages ACKR1, it would involve NECs, by far the most prevalent BM cell population with all NECs expressing ACKR1.

Paralleling findings in mouse, Hur et al. used an anti-human antibody FAB4139 to ascribe ACKR1 expression to human blood monocytes. We set out to determine the specificity of FAB4139 by comparing its immunoreactivity with erythrocytes of Duffy-positive and Duffy-negative individuals, controlled by a validated anti-ACKR1 antibody 2C3. In contrast to 2C3, which efficiently distinguished Duffy-positive and Duffy-negative erythrocytes, FAB4139 only weakly immunoreacted with Duffy-positive erythrocytes at the highest concentration tested (Figure S1M) and with negligible specificity (Figure S1N). Instead, FAB4139 strongly marked CD45$^+$ leukocytes of both Duffy-positive and Duffy-negative individuals, whereas 2C3 labeled leukocytes of Duffy-positive donors only (Figure S1O). Strong immunoreactivity with leukocytes of Duffy-negative donors combined with low sensitivity for erythrocyte ACKR1 suggests that FAB4139 cross-reacts with an epitope unrelated to ACKR1. Because the ACKR1-specific 2C3 also immunoreacted with CD14$^+$ monocytes (Figure S1P), we investigated whether this might be due to the formation of cell complexes between erythrocytes and leukocytes. Indeed, imaging flow cytometry confirmed that this was the case, as each CD14$^+$ACKR1$^+$ event corresponded to a cell complex of a monocyte and an erythrocyte (Figure S1Q).

Antibodies are indispensable research tools but many, like FAB6695 and FAB4139, are not fit-for-purpose, because they are not specific for their antigens. It is imperative that all antibodies are validated prior to their use. Currently all commercial anti-mouse ACKR1 antibodies, including sc-27817 (Santa Cruz), also used by Hur et al., remain non-validated, completely undermining the credibility of any results obtained using these reagents. Curiously, due to the propensity of myeloid cells to complex with ACKR1^{pos} erythroid cells, staining with specific anti-ACKR1 antibodies might also lead to an erroneous ascription of ACKR1 immunoreactivity to cells devoid of it. Imaging flow cytometry was required to unmask such cell complexes and unequivocally show that myeloid cells themselves neither express ACKR1 nor acquire ACKR1 immunoreactivity through phagocytosis of ACKR1-expressing cells. Other examples of heterologous cell aggregation causing false attribution of cell-specific immunomarkers include complexes between follicular helper T cells and B cells in mouse lymph nodes (Reinhardt et al., 2009) as well as those between T cells and monocytes (Burel et al., 2019) or B cells (Burel et al., 2020) in human blood. It is likely that phenomena of heterologous cell complexes appearing in the singlet gate and masquerading as unusual cell types are even more widespread, necessitating confirmation by imaging whenever new cell types are described solely based on flow cytometry profiles.

In summary, we show that commercial antibodies FAB6695 and FAB4139 are unspecific and unsuitable for detecting mouse and human ACKR1, respectively. We conclude that BM macrophages do not express ACKR1 and therefore cannot maintain the dormancy of HSCs through the ACKR1-CD82 pathway. The human correlate of this molecular pathway is also unsubstantiated, as monocytes do not express ACKR1.

Cell Stem Cell
Letter

CellPress

REFERENCES

Burel, J.G., Pomaznoy, M., Lindestam Arlehamn, C.S., Weiskopf, D., da Silva Antunes, R., Jung, Y., Babor, M., Schulten, V., Seumois, G., Greenbaum, J.A., et al. (2019). Circulating T cell-monocyte complexes are markers of immune perturbations. eLife 8, e46045.

Burel, J.G., Pomaznoy, M., Lindestam Arlehamn, C.S., Seumois, G., Vijayanand, P., Sette, A., and Peters, B. (2020). The Challenge of Distinguishing Cell-Cell Complexes from Singlet Cells in Non-Imaging Flow Cytometry and Single-Cell Sorting. Cytometry A 97, 1127–1135.

Chasis, J.A., and Mohandas, N. (2008). Erythroblastic islands: niches for erythropoiesis. Blood 112, 470–478.

Cutbush, M., Mollison, P.L., and Parkin, D.M. (1950). A New Human Blood Group. Nature 165, 188–189.

Duchene, J., Novitzky-Basso, I., Thiriot, A., Casanova-Acebes, M., Bianchini, M., Etheridge, S.L., Hub, E., Nitz, K., Artinger, K., Eller, K., et al. (2017). Atypical chemokine receptor 1 on nucleated erythroid cells regulates hematopoiesis. Nat. Immunol. 18, 753–761.

Hur, J., Choi, J.I., Lee, H., Nham, P., Kim, T.W., Chae, C.W., Yun, J.Y., Kang, J.A., Kang, J., Lee, S.E., et al. (2016). CD82/KAI1 Maintains the Dormancy of Long-Term Hematopoietic Stem Cells through Interaction with DARC-Expressing Macrophages. Cell Stem Cell 18, 508–521.

Li, W., Wang, Y., Zhao, H., Zhang, H., Xu, Y., Wang, S., Guo, X., Huang, Y., Zhang, S., Han, Y., et al. (2019). Identification and transcriptome analysis of erythroblastic island macrophages. Blood 134, 480–491.

Li, F., Yang, M., Wang, L., Williamson, I., Tian, F., Qin, M., Shah, P.K., and Sharifi, B.G. (2012). Autofluorescence contributes to false-positive intracellular Foxp3 staining in macrophages: A lesson learned from flow cytometry. J Immunol. Methods 386, 101–107.

Novitzky-Basso, I., and Rot, A. (2012). Duffy antigen receptor for chemokines and its involvement in patterning and control of inflammatory chemokines. Front. Immunol. 3, 266.

Pruenster, M., Mudde, L., Bombosi, P., Dimitrova, S., Zsak, M., Middleton, J., Richmond, A., Graham, G.J., Segerer, S., Nibbs, R.J., and Rot, A. (2009). The Duffy antigen receptor for chemokines transports chemokines and supports their promigratory activity. Nat. Immunol. 10, 101–108.

Reinhardt, R.L., Liang, H.E., and Locksley, R.M. (2009). Cytokine-secreting follicular T cells shape the antibody repertoire. Nat. Immunol. 10, 385–393.

Thiriot, A., Perdomo, C., Cheng, G., Novitzky-Basso, I., McArdle, S., Kishimoto, J.K., Barreiro, O., Mazo, I., Triboulet, R., Ley, K., et al. (2017). Differential DARC/ACKR1 expression distinguishes venular from non-venular endothelial cells in murine tissues. BMC Biol. 15, 45.

Supplemental Information

Murine bone marrow macrophages

and human monocytes do not express

atypical chemokine receptor 1

Antal Rot, Julia C. Gutjahr, Aindrila Biswas, Maria Aslani, Elin Hub, Aude Thiriot, Ulrich H. von Andrian, Remco T.A. Megens, Christian Weber, and Johan Duchene

A

Ackr1

NENCs
- HSC
- MPPs
- CMP
- MEP
- MkP
- GMP
- PMN
- MO
- CLP
- BLP
- ProB
- FrB
- FrC
- FrD
- FrE
- T1B
- T2B
- NK
- MAC

NECs
- ProE
- BasoE
- PolyE
- EC

Expression

B

FAB6695   6B7

NECs
NENCs

% of Max

ACKR1

Concentration (µg/mL)
0.125
0.25
0.5
1
2

C

Staining index

— 6B7
--- FAB6695

Concentration (µg/mL)

D

FAB6695   6B7

WT
KO

Gated on NECs   Gated on NECs

% of Max

ACKR1

Concentration (µg/mL)
0.125
0.25
0.5
1
2

E

Specificity index

— 6B7
--- FAB6695

Concentration (µg/mL)

F

FAB6695   6B7

WT + KO   NECs   NECs
WT
KO
ACKR1
Ter119
CD71

tSNE1
tSNE2

Expression

G

CD31   ACKR1   Merged

FAB6695
6B7

H

ACKR1   Ter119   CD71   CD115   Ly6C   Ly6G
F4/80   CD45   CD11b   MHCII   CEACAM1   B220
                          c-Kit   Fsc   Ssc

tSNE1
tSNE2

Expression

I

Ssc
F4/80⁺
F4/80

CD71
Ter119

% of Max
ACKR1

J

Lineage
ACKR1⁺
ACKR1

WT
KO

CD71
Ter119

K

BF   ACKR1   CD71   Ter119   CD11b   F4/80   Overlay

1
2
3
4
5
6

L

Ackr1

tSNE1
tSNE2

MAC   NEC

Expression

M

FAB4139   2C3

Duffy^Pos
Duffy^Neg

% of Max

ACKR1

Concentration (µg/mL)
0.00   0.00
0.09   0.37
0.28   1.11
0.83   3.33
2.50   10.0

N

Specificity index

--- 2C3
— FAB4139

v/v %

O

FAB4139   2C3

Duffy^Pos   Duffy^Neg   Duffy^Pos   Duffy^Neg

CD45
ACKR1

RBCs   RBCs   RBCs   RBCs

P

CD14
ACKR1

Q

BF   CD14   ACKR1   Overlay

Supplemental Figure 1. Mouse bone marrow macrophages and human blood monocytes do not express ACKR1.

(**A**) Microarray analysis heatmap of *Ackr1* mRNA expression in mouse BM cells: proerythroblasts (ProE), early normoblasts (BasoE), late normoblasts (PolyE), endothelial cells (EC). NECs, nucleated erythroid cells; NENCs, non-erythroid nucleated cells. Source: gexc.riken.jp/models/1649. (**B**) Representative flow cytometry analysis of BM cells of WT mice stained with different concentrations (0.125 – 2µg/mL) of FAB6695 and 6B7. Here and elsewhere NECs were gated as $CD71^{pos}Ter119^{pos}$ and NENCs as $CD71^{neg}Ter119^{neg}$. (**C**) Staining Index curves of FAB6695 and 6B7. Geometric MFI of signals in NECs and NENCs were obtained and used to calculate the Staining Index= $(MFI_{NEC}–MFI_{NENC})/(2xSD_{NENC})$. (**D**) Representative flow cytometry staining of BM NECs from WT and ACKR1-deficient (KO) mice by FAB6695 and 6B7 at 0.125 to 2µg/mL. (**E**) Specificity index curves of FAB6695 and 6B7. Geo MFI values obtained for FAB6695 and 6B7 in WT and KO NECs were used to calculate the Specificity Index=$(MFI_{WT}–MFI_{KO})/(2xSD_{KO})$. (**F**) BM cells of WT (red) and KO (blue) mice combined in t-SNE plots. Expression levels of indicated markers are reflected by a color scale from blue (low expression) to red (high expression). ACKR1 stained by FAB6695 or 6B7. Arrows indicate NECs. (**G**) Representative immunofluorescence micrographs of omentum of WT and KO mice, as assessed by confocal microscopy after staining for CD31 (red) and for AKCR1 with either FAB6695 or 6B7 (blue). Scale bar: 100 µm. (**H**) BM cells of WT mice in t-SNE dimensional reduction based on the expression of 13 immunomarkers. Expression levels are color mapped from blue (low expression) to red (high expression). ACKR1 stained by 6B7. (**I**) *Top*: Representative flow cytometry plot showing the gating strategy based on the F4/80 staining of the whole BM. *Bottom left*: Fraction of NECs (red) from the parental gate. *Bottom right*: Expression of ACKR1 (stained by 6B7) in NECs (red) and remaining NENCs (grey). (**J**) *Top*: Representative flow cytometry plot showing the gating strategy of the whole WT (red) and KO (blue) BM based on ACKR1 expression stained with 6B7. Lineage cocktail contained B220, CD3, CD11b and Gr1 antibodies. *Bottom*: Fraction of NECs from the parental gate. (**K**) Gallery of representative images of $F4/80^{pos}ACKR1^{pos}$ events visualized by imaging flow cytometry; ACKR1 stained by 6B7. BF, Brightfield. (**L**) tSNE graph of mRNA expression of *Ackr1* determined by single cell RNA sequencing of mouse BM cells. NECs and macrophages (MAC) are indicated by arrows. Source: tabula-muris.ds.czbiohub.org. (**M**) Representative flow cytometry analysis of FAB41139 and 2C3 binding at different concentrations to red blood cells (RBCs) from healthy Duffy-positive and Duffy-negative individuals. (**N**) Specificity index curves of FAB41139 and 2C3. Geo MFI values obtained for FAB41139 and 2C3 in Duffy-positive and Duffy-negative RBCs were used to calculate the Specificity Index=$(MFI_{Duffy-pos}–MFI_{Duffy-neg})/(2xSD_{Duffy-neg})$. Red dots represent antibody concentrations recommended as optimal by the providers. (**O**) Representative flow cytometry analysis for binding of FAB41139 and 2C3 to white blood cells (WBCs) from Duffy-positive and Duffy-negative individuals. WBCs were gated as $CD45^{pos}$ cells. (**P**) Representative flow cytometry plot of $CD14^{pos}ACKR1^{pos}$ events from Duffy-positive donor blood reacted with 2C3. (**Q**) Gallery of representative images of $CD14^{pos}ACKR1^{pos}$ events visualized by imaging flow cytometry, ACKR1 stained by 2C3. BF, brightfield.

THE END